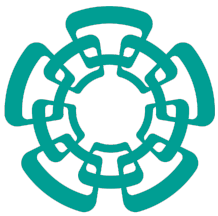

CENTRO DE INVESTIGACIÓN Y DE ESTUDIOS AVANZADOS
DEL INSTITUTO POLITÉCNICO NACIONAL

UNIDAD ZACATENCO
DEPARTAMENTO DE QUÏMICA

Segundas Derivadas Analíticas en la Teoría del Funcional de la Densidad Auxiliar

T E S I S

Que presenta

Rogelio Isaac Delgado Venegas

Para obtener el grado de

Doctor en Ciencias

En la especialidad de

Ciencias Químicas

Directores de tesis: Prof. Dr. Patrizia Calaminici

Prof. Dr. Andreas M. Köster

Ciudad de México Junio, 2018

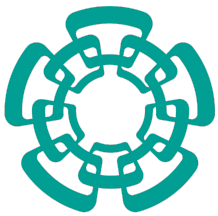

CENTER FOR RESEARCH AND ADVANCED STUDIES
OF THE NATIONAL POLYTECHNIC INSTITUTE

ZACATENCO CAMPUS
CHEMISTRY DEPARTMENT

Analytic Second Derivatives in Auxiliary Density Functional Theory

T H E S I S

Submitted by

Rogelio Isaac Delgado Venegas

In order to obtain the

Doctor in Science

In the specialty of

Chemistry Science

Advisors: Prof. Dr. Patrizia Calaminici

Prof. Dr. Andreas M. Köster

Mexico City June, 2018

El presente trabajo se realizó en el Departamento de Química del Centro de Investigación y de Estudios Avanzados del Instituto Politécnico Nacional (Cinvestav-IPN), bajo la dirección de la Prof. Dra. Patrizia Calaminici y del Prof. Dr. Andreas M. Köster; y con el apoyo de la beca No. 347383, otorgada por el Consejo Nacional de Ciencia y Tecnología (CONACyT).

Acknowledgments

I gratefully acknowledge Dr. Patrizia Calaminici and Dr. Andreas Köster for their guidance through the difficult but extraordinary path of scientific research. Your advices, valuable discussions, and support have helped me a lot during the development of this work and of myself.

Many thanks to Dr. Alberto Vela, Dr. Gerald Geudtner and the theoretical chemistry group in Cinvestav. It was a privilege to share valuable discussions, funny moments and a great workplace with all of you.

I gratefully acknowledge the guidance and help of former members of the theoretical chemistry group in Cinvestav. They taught me with great dedication and patience my first (and many times not-so-first) understandings of the quantum realm. Thanks to Dr. Aurelio Álvarez Ibarra, Dr. Victor Daniel Domínguez Soria, Dr. Gabriel Ulises Gamboa Martínez, Dr. Daniel Mejía Rodríguez and Dr. Bernardo Antonio Zuñiga Gutiérrez.

The very valuable suggestions and corrections of the professors in the commission are also acknowledged, thanks to Dr. Mark E. Casida, Dr. Felipe de Jesús González Bravo, Dr. Lars G. M. Pettersson, Dr. Omar Solorza Feria, and Dr. Alberto Vela Amieva,

Thanks to the Department of Chemistry at Cinvestav. It is an honor to receive classes from this excellent group of professors.

Financial support from the CONACyT Ph.D. Fellowship No. 347383 is gratefully acknowledged.

DEDICATORIA

- A toda mi familia: Mis padres, Rosa Elena Venegas Acosta y Rogelio Delgado López; mis abuelas, Elena Acosta Montes y Ángela López Tapia; mi hermano Jorge Alberto Delgado Venegas; mi tía Martha Zita Venegas Acosta y mi primo-hermano José Gerardo Cruz Venegas. Gracias por guiarme, inspirarme y mostrarme el camino correcto. Gracias por ayudarme a convertirme en quién soy ahora.

- A Elayne Rosas Grajeda. Juntos hemos recorrido caminos increíbles. Tu compañia cambió mi vida, la cambió para bien. Gracias por siempre estar en los momentos que más te necesito.

- A mis profesores: Patrizia Calaminici, Gerald Geudtner y Andreas Köster. Gracias por su dedicación, por sus esfuerzos y paciencia conmigo. Siempre tendré en cuenta sus enseñanzas y consejos.

- A mis viejos amigos: Axel Alcántara, Carlos Alonso, David Gracia, Victor Melo, Aldo Paredes, y Fernán Roa; y a mis nuevos amigos: Ángel Albavera, Alberto Caballero, Antonio Delesma, Ulises Galindo. Ignacio Hernándes, Filiberto Herrera, Adrian Martínez, Arturo Obregón, Naín Pedroza, Sara Pérez, Diego Samaniego y Luis Sosa. La riqueza del humano se mide en la cantidad de amigos que se tiene. Gracias por su amistad.

Contents

List of Figures

List of Tables

Related Work

The following publications contain complementary information and additional applications of some of the algorithms described in this thesis:

- D. Mejía-Rodríguez, **R. I. Delgado-Venegas**, P. Calaminici and A. M. Köster,
  Robust and efficient auxiliary density perturbation theory calculations,
  J. Chem. Theory Comput. **11**, 1493 (2015).

- **R. I. Delgado-Venegas**, D. Mejía-Rodríguez, R. Flores-Moreno, P. Calaminici and A. M. Köster,
  Analytic Second-Derivatives from Auxiliary Density Perturbation Theory,
  J. Chem. Phys. **145**, 224103 (2016).

- J. N. Pedroza-Montero, F. A. Delesma, **R. I. Delgado-Venegas**, P. Calaminici and A. M. Köster,
  Static and dynamic polarizabilities of oligothiophenes,
  Theor. Chem. Acc. **135**, 230 (2016).

- S. E. Pérez-Figueroa, **R. I. Delgado-Venegas**, G. Geudtner, A. A. Martínez-Carranza, P. Calaminici and A. M. Köster,
  Structure and dynamics of $U_2@C_{80}$: An auxiliary density functional theory study,
  In preparation.

I have presented parts of this Ph.D. thesis as oral or poster contributions at the following national and international scientific conferences:

- Poster: Segundas derivadas analíticas en la Teoría del Funcional de la Densidad.
  R. I. Delgado-Venegas, R. Flores-Moreno, P. Calaminici and A. M. Köster.
  XII Reunión Mexicana de Fisicoquímica Teórica.
  Noviembre 13-16, 2013, Juriquilla, Querétaro, México.

- Talk: Analytic Second-Derivatives in Auxiliary Density Functional Theory: Implementation in deMon2k and Perspectives.
  R. I. Delgado-Venegas, R. Flores-Moreno, P. Calaminici and A. M. Köster
  14^{th} deMon Developers Workshop.
  Abril 27-30, 2014, Los Cabos, Baja California Sur, México.

- Talk: Segundas Derivadas Analíticas en la Teoría del Funcional de la Densidad Auxiliar: Implementación y Perspectivas.
  R. I. Delgado-Venegas, R. Flores-Moreno, P. Calaminici and A. M. Köster
  XIII Reunión Mexicana de Fisicoquímica Teórica.
  Noviembre 5-8, 2014, Morelia, Michoacán, México.

- Talk: Analytic Second-Derivatives in Auxiliary Density Functional Theory: Road to ab-initio Calculations and Modeling of Nanomaterials
  R. I. Delgado-Venegas, R. Flores-Moreno, P. Calaminici and A. M. Köster
  15^{th} deMon Developers Workshop.
  Abril 28-31, 2015, Sofia, Bulgaria.

- Talk: Analytic Second-Derivatives in Auxiliary Density Functional Theory: A Guide for the Future User

  R. I. Delgado-Venegas, R. Flores-Moreno, P. Calaminici and A. M. Köster

  17^{th} deMon Developers Workshop.

  Mayo 10-15, 2017, Calgary, Canada.

Notations

$\mathbf{A}$ ..... Coulomb response matrix

a_x, a_y, a_z ..... Angular momentum index of a Gaussian-type orbital

$\mathbf{b}^{(\lambda)}$ ..... Perturbation vector

$\mathbf{c}$ ..... Molecular orbital coefficient matrix

$\check{\mathbf{c}}$ ..... Orthogonalized molecular orbital coefficient matrix

d_{ak} ..... Basis set contraction coefficients

E ..... Electronic energy

$\mathcal{E}_2$ ..... Error of the variational fitting of the Coulomb potential

$E_{xc}[\rho]$ ..... Exchange-correlation energy

$\mathbf{E}$ ..... Identity matrix

$\mathbf{F}$ ..... Exchange-correlation kernel matrix

$F[\rho]$ ..... Hohenberg-Kohn functional

$f_{xc}[\tilde{\rho}]$ ..... Exchange-correlation kernel

G ..... Number of grid points

$\mathbf{G}$ ..... Coulomb matrix

$\hat{H}$ ..... Hamilton operator

$\mathbf{H}$ ..... Monoelectronic contribution to the Kohn-Sham matrix

$\mathscr{H}$ ..... Hessian matrix

$\mathcal{H}$ ..... Molecular orbital representation of $\mathbf{H}$

$\mathbf{J}$ ..... Coulomb vector

$J[\rho]$ ..... Coulomb interaction energy

$\bar{k}(\mathbf{r}), \bar{l}(\mathbf{r}), \bar{m}(\mathbf{r}), \bar{n}(\mathbf{r})$ ..... Hermite-Gaussian auxiliary-functions

Abbreviations

ADFT ..... Auxiliary density functional theory

ADPT ..... Auxiliary density perturbation theory

AO ..... Atomic orbital

aug-cc-pVTZ ..... Dunning augmented correlation-consistent triple-zeta basis set

a.u. ..... Atomic units

BLAS ..... Basic linear algebra subprograms

CPKS ..... Coupled-perturbed Kohn-Sham

Con-EN ..... Conventional Eirola-Nevanlinna

CPSCF ..... Coupled-perturbed self-consistent-field

deMon2k ..... 21^{st} century computational chemistry code density of Montréal

Dir-EN ..... Direct Eirola-Nevanlinna

DFT ..... Density functional theory

DZVP ..... Double-zeta valence polarized basis set

EN ..... Eirola-Nevanlinna

ERI ..... Electron repulsion integral

GEN-An ..... Automatically-generated auxiliary-function set

GGA ..... Generalized gradient approximation

GTO ..... Gaussian-type orbital

HGTO ..... Hermite-Gaussian-type orbital

IR ..... Infrared

KS ..... Kohn-Sham

LAPACK ..... Linear algebra package

LCGTO ..... Linear combination of Gaussian-type orbitals

LDA ..... Local density approximation

MAD ..... Mean absolute deviation

MaxAD ..... Maximum absolute deviation

MO ..... Molecular orbital

PES ..... Potential-energy surface

SCF ..... Self-consistent-field

SCP ..... Self-consistent perturbation

SVD ..... Singular value decomposition

Abstract

This thesis presents the derivation and implementation of analytic second-order electronic energy-derivatives employing perturbation methodologies with efficient scaling with respect to the number of atoms in the framework of auxiliary density functional theory (ADFT). This development and implementation enables the calculation of harmonic IR vibrational spectra with remarkable speed-ups compared to the standard finite-difference methodology. The calculated analytic ADFT frequencies and IR intensities are in excellent quantitative agreement with results obtained from four-center integral approaches, albeit with a fraction of computational time.

For the low-order perturbation approach we implemented an iterative solver for the response equation system of auxiliary density perturbation theory (ADPT). In this work the iterative ADPT solver was further extended to the case of perturbation-dependent basis and auxiliary-functions. This iterative methodology overcomes the speed and memory bottleneck of ADPT calculations, enabling the computation of molecular response properties for nanometric systems in very reasonable times on moderately parallel computational architectures.

Finally, we present a semi-numerical approach for the calculation of third-order energy-derivatives, employing a finite-difference method on top of analytically calculated second-order energy-derivatives. It permits numerically stable calculations of vibrational Raman spectra in the double harmonic approximation. In particular the numerical instabilities inherent to previous high-order finite-difference methods employing only analytical first-order derivatives are avoided. This permits the calculation of Raman spectra of large complex molecules. The application of the developed methodologies to selected molecular systems of current chemical interest demonstrates the potentiality of the low-order scaling method presented here for the calculation of analytic second- and higher-order energy-derivatives.

Resumen

Esta tesis presenta la derivación e implementación de las derivadas analíticas de la energía electrónica de segundo orden empleando metodologías perturbativas con bajo escalamiento en términos del número de átomos en el marco de la teoría funcional de la densidad auxiliar (ADFT por sus siglas en inglés). El presente desarrollo e implementación permite el cálculo de espectros IR armónicos con aceleraciones notables en comparación con la metodología estándar de diferencias finitas. Las frecuencias analíticas calculadas con ADFT, así como las intensidades IR están en excelente acuerdo cuantitativo con los resultados de aproximaciones que emplean integrales de cuatro centros, obtenidos en una fracción del tiempo computacional requerido.

Para la aproximación perturbativa de bajo orden de escalamiento hemos implementado un solucionador iterativo para el sistema de ecuaciones de respuesta de la teoría de perturbaciones de la densidad auxiliar (ADPT por sus siglas en inglés). En este trabajo el solucionador iterativo ADPT fue extendido para el caso de bases y funciones auxiliares dependientes del parámetro de perturbación. Esta metodología iterativa supera los cuellos de botella de la velocidad y memoria de los cálculos de ADPT, lo que permite el cálculo de propiedades de respuesta molecular en sistemas a nanométricos en tiempos razonables en modestas arquitecturas computacionales paralelas.

Finalmente, presentamos una aproximación semi-numérica para el cálculo de derivadas de la energía de tercer orden, mediante un método de diferencias finitas donde se emplean segundas derivadas analíticas. Esto permite cálculos numéricamente estables de espectros vibracionales Raman dentro de la doble aproximación armónica. En lo particular, las inestabilidades numéricas inherentes al anterior método de diferencias finitas de orden superior que solo emplean las derivadas analíticas de primer orden, son evitadas. Esto permite el calculo de espectros Raman de moléculas complejas de gran tamaño. La aplicación de las metodologías desarrolladas a sistemas moleculares seleccionados con actual interés químico demuestran la capacidad de los métodos de bajo orden de escalamiento para el cálculo de segundas derivadas analíticas y de orden superior.

Chapter 1

INTRODUCTION AND OBJECTIVES

Vibrational spectroscopy is a valuable tool in modern chemistry for molecular structure elucidation, reaction monitoring and quality control. The two most common variants are the infrared (IR) and Raman spectroscopy. These are nondestructive techniques which measure vibrational energy levels associated with the chemical structure in a sample. The IR spectrum provides information about how much electromagnetic radiation is absorbed by a sample as function of wavelength, commonly reported in wavenumbers, while the Raman spectrum provides information about how much electromagnetic radiation is inelastically scattered as function of frequency shift, also reported in wavenumbers.

Vibrational spectroscopy can also provide insight into the nature of chemical bonds and intramolecular forces acting between the atoms in a molecule. To extract such information it is necessary to assign vibrational motions to each peak in a spectrum. However even for an experienced chemist, a vibrational mode assignment can be a rather challenging task, in particular when the spectrum is composed of many overlapping bands which can mask valuable information. It is here where first-principle calculations can offer a valuable quantum-chemical analysis of vibrational spectra. Unfortunately, for wave function approaches the calculation of vibrational spectra is an exceptionally time-consuming task. As a result, only small molecules can be treated by these methodologies. For larger systems, density functional theory (DFT) [1] is a promising alternative.

The basic idea of DFT is to describe a microscopic system by means of the electron density —a physical observable, as opposed to the wave functions which are a purely mathematical construct. Thus, for a system with N electrons, the $3N$ spatial degrees of freedom of the wave function are reduced to only three spatial coordinates. This tremendous reduction of complexity allows DFT calculations on large systems with hundreds, or even *thousands* of atoms [2]. Simultaneously, the Kohn-Sham approach to density functional theory (KS-DFT) [3] achieves a fairly good compromise between accuracy and efficiency and is one of the most widely used electronic structure theories today.

Vibrational analyses performed with quantum mechanical methodologies require the calculation of the Hessian matrix, obtained as the second-order energy-derivatives with respect to nuclear displacements. The dimensionality of the Hessian matrix is $3M \times 3M$, with M being the number of atoms in the system. Although the first-order electronic energy derivatives are relatively easy to calculate, second-order derivatives are not. The simplest way to calculate second-order derivatives is to follow a finite-difference method where typically two first-order derivatives are required for each atomic coordinate. This method is easily implemented, but it requires significant computational resources and is prone to numerical instabilities. Thus, an analytic second-order energy derivative formulation is very desirable.

In the framework of KS-DFT the analytic calculation of the Hessian matrix usually involves the solution of the coupled-perturbed Kohn-Sham (CPKS) [4–6] equations. Iterative solvers are employed due to the large dimensionality of the corresponding CPKS equation systems. This also renders analytical Hessian calculations rather time consuming because a CPKS equation system has to be solved for each nuclear displacement[7, 8]. As a consequence, analytic Hessian calculations in the framework of KS-DFT are still formidable tasks even for systems with less than hundred atoms.

An alternative approach to CPKS was developed in the framework of auxiliary density functional theory (ADFT). Due to a dramatic reduction in dimensionality it permits the direct solution of the perturbation equation system. This so-called auxiliary density perturbation theory (ADPT), has been already successfully used to calculate static and dynamic polarizabilities [9–11] as well as spin-spin coupling constants [12] and Fukui functions [13].

Here we present the extension of ADPT for the calculation of second-order electronic energy derivatives with respect to nuclear displacements. As a result, an efficient route for the calculation of IR and Raman spectra in the framework of ADFT becomes available through ADPT. We also show how this methodology improves time and memory consumption compared to the finite-difference method. In the presented applications vibrational spectra simulations are used for the characterization of complex molecular systems.

The thesis is organized in the following way. In Chapter 2 the Kohn-Sham method is briefly outlined. Chapter 3 describes the linear combination of Gaussian-type orbital (LCGTO) approximation for the solution of the Kohn-Sham equations and the foundation of ADFT. In Chapter 4 the derivation of the analytic second-order electronic derivatives in the framework of ADFT, as well as the corresponding semi-numerical third-order derivatives are discussed in detail. The explicit formulas for the calculation of the perturbed density and Kohn-Sham matrices employing McWeeny's self-consistent perturbation (SCP) theory and the implementation of ADPT as an alternative to the CPKS equations is reviewed in the next chapter. This chapter also addresses the adaptation of the iterative Eirola-Nevanlinna algorithms for the solution of the ADPT response equation system. Chapter 5 finishes with the discussion of the different parallelization schemes implemented for large-scale analytic second-order energy-derivative calculations. Chapter 6 describe common algorithmic applications for the developed analytical and semi-numerical energy derivatives. The detailed discussion of such algorithmic implementations focuses on the calculation of IR and Raman spectra in the double harmonic approximation. In Chapter 7 applications of the new algorithms to problems of current interest in our research groups are presented. Conclusions and perspectives of this work are given in the last chapter. The first appendix describes the generic working equations for the calculation of specific ADFT-GGA exchange-correlation integrals for the case of perturbation-dependent auxiliary-functions. These formulas are the basic ingredients for the analytical calculation of second-order ADFT-energy derivatives. The second appendix describes an alternative for the calculation of the perturbed energy-weighted density matrix which avoids the inversion of the overlap matrix. The last two appendices extend the SCP theory and the ADPT response equations to open-shell systems.

The main objective of this work is the development and application of efficient auxiliary-function methods that push the limits of current first-principle molecular property calculations. This methodology should allow the computation of larger systems in reasonable time frames. In order to achieve this goal, we proposed the following specific objectives:

1. Development and implementation of analytic second-order energy-derivatives in the framework of ADFT.
   (a) Theoretical development of analytic second-order energy-derivatives.
   (b) Serial and parallel implementation of the analytic second-order energy-derivatives.
   (c) Implementation of the developed analytical and semi-numerical energy-derivatives.
   (d) Validation, benchmarking and applications of the presented implementation.

Chapter 2

KOHN-SHAM DENSITY FUNCTIONAL THEORY

2.1 The Schrödinger Equation

A central aim of *ab-initio* electronic structure theory methods is to be reliable and predictive within chemical accuracy by combining theoretical physics and chemistry with computer science and mathematics. To do so, molecular electronic structure theory focuses extensively on the solution of the Schrödinger equation [14–18]. In order to simplify the problem, the electronic and nuclear wave functions are separated by the Born-Oppenheimer approximation [19]. The resulting electronic Schrödinger equation is cast in the following form:

$$\hat{H}\Psi\left(\mathbf{r};\mathbf{R}\right) = E\Psi\left(\mathbf{r};\mathbf{R}\right). \tag{2.1}$$

Here, Ψ denotes the electronic wave function—a function that depends explicitly on the electronic coordinates $\mathbf{r}$ and parametrically on the nuclear coordinates $\mathbf{R}$. From now on we will omit the parametric dependence on the nuclear coordinates in order to avoid cluttering of the notation. Thus, for an isolated molecular system, the electronic Hamilton operator $\hat{H}$

has the following form:

$$\hat{H} = -\frac{1}{2}\sum_{i}^{N}\nabla_i^2 - \sum_{i}^{N}\sum_{A}^{M}\frac{Z_A}{|\mathbf{r}_i - \mathbf{R}_A|} + \sum_{i>j}^{N}\frac{1}{|\mathbf{r}_i - \mathbf{r}_j|}. \tag{2.2}$$

We will use atomic units as in Eq. (2.2) throughout this work. The upper sum limits N and M denote the number of electrons and nuclei, respectively. The corresponding position vectors are given by $\mathbf{r}_i$, $\mathbf{r}_j$ and $\mathbf{R}_A$. This Hamilton operator is uniquely determined by the number of electrons, the nuclear coordinates and the nuclear charges of the molecular system. Apart from a small subset of physical systems, mainly one-electron systems, the electronic Schrödinger equation can not be analytically solved. Thus, for most quantum chemical systems approximate solutions of the electronic Schrödinger equation are needed. The most successful approximations rely on the variational principle [20], which may be stated as: *The expectation value of a Hamilton operator $\hat{H}$, calculated using a properly normalized trial wave function $\tilde{\Psi}(\mathbf{r})$ (with $\langle\tilde{\Psi}|\tilde{\Psi}\rangle = 1$), consistent with all the boundary conditions of the problem, is never lower than the true ground state energy E_0, which is the expectation value of $\hat{H}$ calculated using the true ground state wave function $\Psi_0(\mathbf{r})$* [21, 22]:

$$E[\tilde{\Psi}] = \left\langle \tilde{\Psi} \middle| \hat{H} \middle| \tilde{\Psi} \right\rangle \geq E_0. \tag{2.3}$$

This principle guarantees that any approximation to the exact wave function lies above the exact energy of the system and that further improvements to the trial wave function will lower the system energy closer to its exact energy.

2.2 The Hohenberg-Kohn Theorems

One of the fundamental postulates of quantum mechanics [23] establishes that the wave function determines the state of a quantum mechanical system. However, this wave function *per se* has no physical meaning. In 1926 Max Born gave a statistical interpretation [24] of the wave function for a one-electron system, which states that the probability of finding a

particle, bounded between $\mathbf{r}$ and $\mathbf{r} + d\mathbf{r}$, is given by the modulus of the wave function

$$P(\mathbf{r})d\mathbf{r} = \Psi^*(\mathbf{r})\Psi(\mathbf{r})d\mathbf{r} = |\Psi(\mathbf{r})|^2 d\mathbf{r}. \tag{2.4}$$

In the particular case of an one-electron system, this corresponds to the electron density $\rho(\mathbf{r})$ between $\mathbf{r}$ and $\mathbf{r} + d\mathbf{r}$. For a system with N electrons, the wave function will contain $3N$ variables, while the electron density is just a three-dimensional scalar field, no matter how many electrons are in the molecular system. According to the statistical interpretation of Born, the single-particle electron density of a many electron system can be calculated by the following expression:

$$\rho(\mathbf{r}) = N \int ... \int ... |\Psi(\mathbf{r}, \mathbf{r}_2, ..., \mathbf{r}_N)|^2 d\mathbf{r}_2 ... d\mathbf{r}_N. \tag{2.5}$$

Thus, $\rho(\mathbf{r})\ d\mathbf{r}$ is the number of electrons in a volume element $d\mathbf{r}$. Following Born's interpretation, Eq. (2.5) represents the probability of finding an electron at position $\mathbf{r}$ while the other $N-1$ electrons are at arbitrary positions. In addition to being a much simpler mathematical entity, the electron density $\rho(\mathbf{r})$ is an observable, unlike the wave function $\Psi(\mathbf{r})$ which is a purely mathematical construct[1]. This enormous simplification was a main motivation for the development of density functional models [28, 29], like the one from Thomas and Fermi [30–32], in which the electron density substitutes the wave function as basic quantity. However, it was not before the pioneering work of Pierre Hohenberg and Walter Kohn in 1964 [1] that a theory based on density functionals could be formulated. This so-called *Density Functional Theory* (DFT) is based on two theorems, named the Hohenberg-Kohn theorems. The first of these theorems can be stated as: *For a system of N interacting electrons in a non-degenerate ground state, the external potential $v(\mathbf{r})$ is determined, within a trivial additive constant, by the electron density $\rho(\mathbf{r})$, except where $\rho(\mathbf{r}) = 0$.*

Proof: Let us assume that two different external potentials $v(\mathbf{r})$ and $v'(\mathbf{r})$ lead to the same electronic density $\rho(\mathbf{r})$ of a non-degenerate ground state. This implies the existence of

[1]Interestingly, the wave function may be reconstructed by performing a large set of experimental measurements. We refer the interested reader to Refs. 25, 26 and 27.

two different Hamilton operators, $\hat{H}$ and $\hat{H}'$, with different ground state wave functions $\Psi(\mathbf{r})$ and $\Psi'(\mathbf{r})$, that yield the same ground state density $\rho(\mathbf{r})$. By using the variational principle, Eq. (2.3), and taking $\Psi'(\mathbf{r})$ as trial wave function for the Hamilton operator $\hat{H}$ we find,

$$E_0 = \left\langle \Psi \right| \hat{H} \left| \Psi \right\rangle < \left\langle \Psi' \right| \hat{H} \left| \Psi' \right\rangle . \tag{2.6}$$

To proceed we now separate the Hamilton operator as,

$$\hat{H} = \hat{F} + v(\mathbf{r}), \tag{2.7}$$

where,

$$\hat{F} = -\frac{1}{2}\sum_{i}^{N} \nabla_i^2 + \sum_{i>j}^{N} \frac{1}{|\mathbf{r}_i - \mathbf{r}_j|} \tag{2.8}$$

collects the kinetic energy operators of the electrons and their Coulomb repulsion. Thus, it is the same for both Hamilton operators $\hat{H}$ and $\hat{H}'$. As a consequence, $\hat{H}$ and $\hat{H}'$ differ only in their external potentials that are, by construction $v(\mathbf{r})$ and $v'(\mathbf{r})$. Therefore, Eq. (2.6) can be rewritten as,

$$\begin{aligned}
E_0 &< \left\langle \Psi' \right| \hat{H}' \left| \Psi' \right\rangle + \left\langle \Psi' \right| \hat{H} - \hat{H}' \left| \Psi' \right\rangle = \left\langle \Psi' \right| \hat{H} \left| \Psi' \right\rangle , \\
\implies E_0 &< E_0' + \left\langle \Psi' \right| \hat{H} - \hat{H}' \left| \Psi' \right\rangle , \\
\implies E_0 &< E_0' + \left\langle \Psi' \right| v - v' \left| \Psi' \right\rangle , \\
\implies E_0 &< E_0' + \int \left[v(\mathbf{r}) - v'(\mathbf{r}) \right] \rho(\mathbf{r}) \, d\mathbf{r}.
\end{aligned} \tag{2.9}$$

Analogously to Eq. (2.9), taking $\Psi(\mathbf{r})$ as a trial wave function for the Hamilton operator $\hat{H}'$ yields:

$$\begin{aligned}
E_0' &< \left\langle \Psi \right| \hat{H} \left| \Psi \right\rangle + \left\langle \Psi \right| \hat{H}' - \hat{H} \left| \Psi \right\rangle = \left\langle \Psi \right| \hat{H}' \left| \Psi \right\rangle , \\
\implies E_0' &< E_0 + \left\langle \Psi \right| \hat{H}' - \hat{H} \left| \Psi \right\rangle ,
\end{aligned}$$

$$\begin{aligned} \Longrightarrow\ E_0' &< E_0 + \langle \Psi | \, v' - v \, | \Psi \rangle \ > \ E_0', \\ \Longrightarrow\ E_0' &< E_0 + \int [v'(\mathbf{r}) - v(\mathbf{r})] \, \rho(\mathbf{r}) \, d\mathbf{r}. \end{aligned} \tag{2.10}$$

By adding (2.9) to (2.10) we obtain:

$$E_0 + E_0' < E_0' + E_0. \tag{2.11}$$

Obviously Eq. (2.11) is a contradiction. Therefore, the ground state density $\rho(\mathbf{r})$ uniquely determines the corresponding external potential $v(\mathbf{r})$. The unique determination of the external potential by the density implies also the unique determination of the Hamilton operator by the density (up to an arbitrary additive constant), and this is seen from the basic form of the molecular electronic Hamilton operator (2.2), which depends only on the number of electrons, N, and the position of the nuclei and their nuclear charges, Z_A. The knowledge of the external potential $v(\mathbf{r})$ determines the positions and charges of the nuclei. The unknown number of electrons can be determined by integrating Eq. (2.5):

$$\int \rho(\mathbf{r}) \, d\mathbf{r} = N. \tag{2.12}$$

Therefore, the following mapping can be established:

$$\rho(\mathbf{r}) \leftrightarrow N, v(\mathbf{r}) \rightarrow \hat{H} \rightarrow \Psi[\rho] \rightarrow E[\rho]. \tag{2.13}$$

As a consequence, the resulting wave function is also defined up to an arbitrary phase factor by the electronic density $\rho(\mathbf{r})$. Given the fact that the wave function is a functional of the ground state density, the expectation value O of any operator $\hat{O}$ is also a unique functional of this density:

$$\left\langle \hat{O} \right\rangle = \left\langle \Psi[\rho] \middle| \, \hat{O} \, \middle| \Psi[\rho] \right\rangle = O[\rho]. \tag{2.14}$$

Therefore, also all ground state electronic properties are determined by the non-degenerate

ground state density [1]. Further extensions have shown that the first Hohenberg-Kohn theorem also holds for degenerate ground states and excited states, provided that certain symmetry requirements are fulfilled [33]. Note that the above proof only shows the existence of $\Psi[\rho]$ and $E[\rho]$. It does not provide any insight into the functional dependencies.

The second Hohenberg-Kohn theorem can be stated as: *The ground state density $\rho(\mathbf{r})$ can be determined from the ground state energy functional $E[\rho]$ via the variational energy principle.*

Proof: To a trial density $\rho'(\mathbf{r})$, such as $\int \rho'(\mathbf{r})d\mathbf{r} = N$ and $\rho'(\mathbf{r}) \geq 0 \; \forall \; \mathbf{r}$, corresponds according to the mapping of Eq. (2.13) a trial wave function $\Psi'[\rho']$ [2]. From the variational principle (2.3), it follows that,

$$E[\rho'] = \left\langle \Psi' \middle| \hat{H} \middle| \Psi' \right\rangle \geq E[\rho]. \tag{2.15}$$

The equality $E[\rho'] = E[\rho]$ holds if $\rho'(\mathbf{r}) = \rho(\mathbf{r})$. Eq. (2.15) is the analog to the variational principle for wave functions. Thus, the ground state energy and density $\rho(\mathbf{r})$ can be obtained by minimization of the functional $E[\rho]$ with respect to the density, employing the above normalization restriction.

2.3 The Kohn-Sham Methodology

As shown in the proof of the first Hohenberg-Kohn theorem the functional $F[\rho]$ is independent of the external potential $v(\mathbf{r})$ and holds for any number of particles. For this reason it is called the universal (and unknown[3]) Hohenberg-Kohn functional. The terms that define $F[\rho]$ are the electron kinetic energy $T[\rho]$ and the electron-electron interaction energy contributions

[2]The trial density must be restricted to v-representable densities, i.e., an electron density, for which an associated static external potential, $v(\mathbf{r})$, exists.

[3]When we talk about the unknown density functional, we usually mean that we do not know how to write the universal functional as a simple and explicit functional of the density, without any reference to the wave function. A review on methods for constructing the exact density functional mathematically and computationally can be found on Ref. 34.

$V_{ee}[\rho]$:

$$F[\rho] = T[\rho] + V_{ee}[\rho]. \tag{2.16}$$

The electron-electron interaction energy contribution $V_{ee}[\rho]$ can be further divided into the classical Coulomb interaction, $J[\rho]$, and the non-classical (quantum-mechanical) electronic interactions, $V_{nc}[\rho]$. Thus, we find:

$$V_{ee}[\rho] = J[\rho] + V_{nc}[\rho]. \tag{2.17}$$

The only term that has an explicit expression is $J[\rho]$. The expressions for $T[\rho]$ and $V_{nc}[\rho]$ are unknown. But in 1965, Walter Kohn and Lu Jeu Sham devised an ingenious way to overcome this limitation with a trade-off between simplicity and accuracy [3]. They proposed to introduce orbitals for a non-interacting fictitious reference system from which the major part of the kinetic energy can be computed with good accuracy. The resulting residual, $T_c[\rho]$, must be corrected separately:

$$T[\rho] = T_s[\rho] + T_c[\rho]. \tag{2.18}$$

In Eq. (2.18) the subscript s stands for *single-particle* and c stands for *correlation* [35]. In a non-interacting system, the total kinetic energy, $T_s[\rho]$, is the sum of all single-particle kinetic energies:

$$T_s[\rho] = \left\langle \Psi_s[\rho] \middle| \hat{T} \middle| \Psi_s[\rho] \right\rangle = -\frac{1}{2} \sum_i^N \left\langle \psi_i \middle| \nabla^2 \middle| \psi_i \right\rangle. \tag{2.19}$$

Here, $\Psi_s[\rho]$ denotes the wave function of the non-interacting system. It is expressed by a single Slater determinant [36] that forms the density $\rho(\mathbf{r})$. The $\psi_i(\mathbf{r})$ are the single-particle Kohn-Sham orbitals of the non-interacting system. The fictitious non-interacting system is connected to the real system by the constraint that the occupied Kohn-Sham orbitals generate

the ground state density of the real system according to

$$\rho(\mathbf{r}) = \sum_{i}^{N} |\psi_i(\mathbf{r})|^2 . \tag{2.20}$$

Using Eq.(2.16), (2.17) and (2.18), the universal functional $F[\rho]$ can be expressed as,

$$F[\rho] = T_s[\rho] + J[\rho] + E_{xc}[\rho], \tag{2.21}$$

with,

$$E_{xc}[\rho] = T_c[\rho] + V_{nc}[\rho]. \tag{2.22}$$

Here, $E_{xc}[\rho]$ is known as the exchange-correlation functional, which collects the difference of the kinetic energies between the real interacting and fictitious non-interacting system, $T_c[\rho]$, and the non-classical electronic interactions $V_{nc}[\rho]$. By enforcing the identity of the densities between the fictitious non-interacting Kohn-Sham system and the real system, an explicit expression for the Coulomb interaction becomes available. Thus, we obtain as Kohn-Sham energy:

$$E[\rho] = -\frac{1}{2}\sum_{i}^{N} \langle \psi_i | \nabla^2 | \psi_i \rangle + \int \rho(\mathbf{r}) v(\mathbf{r}) d\mathbf{r} + \frac{1}{2} \iint \frac{\rho(\mathbf{r})\rho(\mathbf{r}')}{|\mathbf{r} - \mathbf{r}'|} \, d\mathbf{r} d\mathbf{r}' + E_{xc}[\rho]. \tag{2.23}$$

Since $F[\rho]$ has a universal nature, $E_{xc}[\rho]$ must be universal, too, i.e., it must have the same form for atoms, molecules and solids. However, the actual form of $E_{xc}[\rho]$ is still unsettled. Thus, we must introduce approximate functionals based on the electron density to describe this term. Once such a functional is chosen, the minimization of Eq. (2.23) with respect to the Kohn-Sham orbitals, ψ_i, subject to the orthonormality constraint,

$$\langle \psi_i | \psi_j \rangle = \delta_{ij}, \tag{2.24}$$

yields the single-particle Kohn-Sham equations:

$$\left(-\frac{1}{2}\nabla^2 + v[\rho] + \int \frac{\rho(\mathbf{r}')}{|\mathbf{r}-\mathbf{r}'|}d\mathbf{r}' + v_{xc}[\rho]\right)\psi_i(\mathbf{r}) = \varepsilon_i\psi_i(\mathbf{r}) \;\forall\; i. \tag{2.25}$$

Here ε_i is a Lagrange multiplier, and $v_{xc}[\rho]$ is known as the exchange-correlation potential, which is defined as the functional derivative of the exchange-correlation energy with respect to the density $\rho(\mathbf{r})$,

$$v_{xc}[\rho](\mathbf{r}) \equiv \frac{\delta E_{xc}[\rho]}{\delta\rho(\mathbf{r})}. \tag{2.26}$$

The above Kohn-Sham equations must be solved by an iterative, self-consistent procedure. Although Eq. (2.25) eliminates the unknown kinetic energy functional by introducing orbitals of a fictitious non-interacting reference system, the exchange-correlation energy functional is still unknown. In fact, the quality of a density functional calculation critically depends on the quality of the $E_{xc}[\rho]$ approximation [37]. At this point it is important to note that $E_{xc}[\rho]$ is at least two orders of magnitude smaller than the sum of the other energetic contributions in Eq. (2.23). Nevertheless, an explicit form of $E_{xc}[\rho]$ is necessary to specify the Kohn-Sham equations. The search for an accurate approximation to $E_{xc}[\rho]$ is far from simple, and is one of the greatest challenges in DFT. There is a wide variety of exchange-correlation functionals, leading the way from the "Hartree world" to the "Heaven of Chemical Accuracy", illustrated by Perdew and Schmidt [38, 39] using the "Jacob's ladder" metaphor. In this metaphor, functionals may be grouped according to their formulation, each rung of the ladder adds a refinement to the approximation of the exchange-correlation energy.

The *first-rung functionals* are only dependent upon the density $\rho(\mathbf{r})$ and are known as local density approximation (LDA). The most notable example is the approximation in which the Dirac exchange [32] is combined with a fit to the homogeneous electron gas correlation, like the one proposed by Vosko, Wilk and Nusair (VWN) [40]. The LDA is often surprisingly good at calculating geometries, namely bond lengths and angles to within a few percent. But the corresponding bond energies are very poor and far from chemical accuracy.

Second-rung functionals utilize in addition the gradient of the density, $\nabla\rho(\mathbf{r})$, in their formulation, known as generalized gradient approximation (GGA). Popular GGAs were proposed by Becke, Lee, Yang and Parr (BLYP) [41–44], and Perdew, Burke and Ernzerhof (PBE) [45], to name a few.

Third-rung functionals are known as meta-GGAs. They include the Laplacian of the density $\nabla^2\rho(\mathbf{r})$ as a natural extension of GGAs that include only the density and its first derivatives. More recently developed meta-GGAs like TPSS [46] or SCAN [47] use the kinetic energy density, $\tau(\mathbf{r})$, instead of $\nabla^2\rho(\mathbf{r})$. This is motivated by the fact that more exact conditions for the electron gas can be fulfilled with $\tau(\mathbf{r})$ than $\nabla^2\rho(\mathbf{r})$. However, in the context of our discussion it should be noted that $\tau(\mathbf{r})$ depending meta-GGAs cannot be used with the ADFT framework due to their intrinsic orbital dependency [48].

Fourth-rung functionals are a class of approximations that combine conventional DFT exchange with Hartree-Fock exchange. This hybrid exchange is augmented by conventional DFT correlation. They are known as hybrid-GGAs. The exact exchange energy functional is expressed in terms of the Kohn-Sham orbitals rather than the density. For this reason it is termed as an implicit density functional [49]. One of the most commonly used versions is the global-hybrid B3LYP [50], which stands for Becke, 3-parameter, Lee-Yang-Parr, as well as their range-separated corrected CAM-B3LYP [51, 52] Note that both hybrid functionals, due to the variational fitting of Fock exchange [53], are available within the ADFT framework. In fact ADFT hybrid functional calculations can be computationally less demanding than corresponding Kohn-Sham meta-GGA calculations.

Fifth-rung functionals are explicitly dependent on the occupied and virtual Kohn-Sham orbitals via perturbation theory. They are known as double-hybrid functionals [54, 55]. Although most current implementations are fundamentally semiempirical [56], there are efforts to obtain parameter-free double-hybrid functionals [57–60].

The developments of these, and many other, highly accurate density functional approximations have enabled an exponentially growing application of DFT to the point where Kohn-Sham DFT has become the standard tool for first-principle electronic structure theory calculations [22].

Chapter 3

AUXILIARY DENSITY FUNCTIONAL THEORY

3.1 The LCGTO Approximation

For simplicity, we consider only closed-shell systems in which we have $2N$ electrons occupying N doubly occupied spatial orbitals. The corresponding equations for open-shell systems are, as seen from the surface, a straightforward extension to the closed-shell case [61–63]. In the *linear combination of Gaussian-type orbital* (LCGTO) approximation the Kohn-Sham orbitals are expanded in atomic orbitals,

$$\psi_i(\mathbf{r}) = \sum_{\mu} c_{\mu i}\mu(\mathbf{r}). \tag{3.1}$$

In Eq. (3.1) $\mu(\mathbf{r})$ represents an atomic orbital (AO) or basis function and $c_{\mu i}$ denotes the corresponding molecular orbital (MO) coefficient. Throughout the text, the basis functions will be denoted with Greek letters. The sum in Eq. (3.1) runs over all atomic orbitals used in the calculation. Typically, these orbitals are expressed in terms of contracted Cartesian

Gaussian type orbital (GTO) functions. A (unnormalized) contracted GTO is given by [64]:

$$\mu(\mathbf{r}) = (x - A_x)^{a_x}(y - A_y)^{a_y}(z - A_z)^{a_z} \sum_{k}^{K_a} d_{ak} e^{-\zeta_{ak}(\mathbf{r}-\mathbf{R}_A)^2}. \tag{3.2}$$

The above GTO is defined by its atomic center $\mathbf{A}$, its angular momentum index $\mathbf{a} = (a_x, a_y, a_z)$, its contraction degree K_a, the contraction coefficients d_{ak} and the orbital exponents ζ_{ak}. It is worth noting that the contraction coefficients remain unaltered in electronic structure calculations. By using the LCGTO approximation, we find for the closed-shell electron density (2.20),

$$\rho(\mathbf{r}) = 2\sum_{i}^{occ} |\psi_i(\mathbf{r})|^2 = 2\sum_{i}^{occ}\sum_{\mu,\nu} c_{\mu i} c_{\nu i} \mu(\mathbf{r})\nu(\mathbf{r}) = \sum_{\mu,\nu} P_{\mu\nu}\mu(\mathbf{r})\nu(\mathbf{r}), \tag{3.3}$$

where $P_{\mu\nu}$ is a closed-shell density matrix element,

$$P_{\mu\nu} = 2\sum_{i}^{occ} c_{\mu i} c_{\nu i}. \tag{3.4}$$

Taking into account the LCGTO expansion of the electron density, the Kohn-Sham energy expression (2.23) can be written as,

$$E = \sum_{\mu,\nu} P_{\mu\nu} H_{\mu\nu} + \frac{1}{2}\sum_{\mu,\nu}\sum_{\sigma,\tau} P_{\mu\nu} P_{\sigma\tau} \langle \mu\nu \,\|\, \sigma\tau \rangle + E_{xc}[\rho]. \tag{3.5}$$

The first term in Eq. (3.5) is known as the core energy. The element $H_{\mu\nu}$ contains all one-electron energy contributions, namely the kinetic energy and the nuclear attraction energy of the electrons,

$$H_{\mu\nu} = -\frac{1}{2}\langle \mu | \nabla^2 | \nu \rangle - \sum_{A}^{M} \left\langle \mu \left| \frac{Z_A}{|\mathbf{r} - \mathbf{R}_A|} \right| \nu \right\rangle. \tag{3.6}$$

The second term in Eq. (3.5) is the two-electron Coulomb repulsion energy. The short-hand notation used here for the four-center electron repulsion integrals (ERIs) has the form,

$$\langle \mu\nu \,\|\, \sigma\tau \rangle = \iint \frac{\mu(\mathbf{r})\nu(\mathbf{r})\sigma(\mathbf{r}')\tau(\mathbf{r}')}{|\mathbf{r}-\mathbf{r}'|}\, d\mathbf{r}d\mathbf{r}'. \tag{3.7}$$

In this ERI notation [65] the symbol $\|$ denotes the two-electron Coulomb operator, $1/|\mathbf{r}-\mathbf{r}'|$. It also separates functions of electron 1, on the left side (bra), from those of electron 2, on the right (ket). The same notation will be used for two-center and three-center ERIs that will appear in the following sections.

The derivation of the LCGTO Kohn-Sham equations follows those of the Roothaan-Hall equations in Hartree-Fock [66, 67], except for the exchange-correlation energy functional which is absent in the Hartree-Fock methods. To be more precise, the correlation energy is not included in the Roothaan-Hall equations. However, in Hartree-Fock the Coulomb self-interaction energy cancels exactly with the corresponding exchange energy. This is usually not the case in practical Kohn-Sham calculations where a Coulomb self-interaction error may remain to a certain extent depending on the approximation used for the exchange-correlation energy functional.

The derivation of the Kohn-Sham equations starts with the minimization of the corresponding energy expression, Eq. (3.5), applying the constraint for the molecular orbital orthonormality (2.24) within the LCGTO expansion,

$$\langle \psi_i | \psi_j \rangle = \sum_{\mu,\nu} c_{\mu i} S_{\mu\nu} c_{\nu j} = \delta_{ij}. \tag{3.8}$$

Here $S_{\mu\nu}$ denote the overlap matrix elements. The resulting Lagrange function for the energy minimization is given by,

$$L(\mathbf{c}) = E[\rho] - 2\sum_{i,j}^{all} \lambda_{ij} \left\{ \sum_{\mu,\nu} c_{\mu i} S_{\mu\nu} c_{\nu j} - \delta_{ij} \right\}. \tag{3.9}$$

The variation of (3.9) with respect to the MO coefficients yields,

$$\frac{\partial L(\mathbf{c})}{\partial c_{\mu i}} = 4\sum_{\nu}\left(H_{\mu\nu} + \sum_{\sigma,\tau} P_{\sigma\tau}\left\langle \mu\nu \,\|\, \sigma\tau\right\rangle + \left\langle \mu\right| v_{xc}[\rho]\left|\nu\right\rangle\right) c_{\nu i} - 4\sum_{j}^{all}\sum_{\nu} S_{\mu\nu}c_{\nu j}\lambda_{ji}. \quad (3.10)$$

For the variation of $E_{xc}[\rho]$, assuming a local exchange-correlation functional, the following chain rule was applied:

$$\frac{\partial E_{xc}[\rho]}{\partial c_{\mu i}} = \int \frac{\delta E_{xc}[\rho]}{\delta\rho(\mathbf{r})}\frac{\partial\rho(\mathbf{r})}{\partial c_{\mu i}}d\mathbf{r} = 4\sum_{\nu}\left\langle \mu\right| v_{xc}[\rho]\left|\nu\right\rangle c_{\nu i}. \quad (3.11)$$

At this point it is convenient to introduce the Kohn-Sham matrix, which corresponds to the differentiation of the Kohn-Sham energy with respect to a density matrix element,

$$K_{\mu\nu} \equiv \frac{\partial E_{xc}[\rho]}{\partial P_{\mu\nu}} = H_{\mu\nu} + \sum_{\sigma,\tau} P_{\sigma\tau}\left\langle \mu\nu \,\|\, \sigma\tau\right\rangle + \left\langle \mu\right| v_{xc}[\rho]\left|\nu\right\rangle. \quad (3.12)$$

Combining Eq. (3.10) with (3.12) yields,

$$\sum_{\nu} K_{\mu\nu}c_{\nu i} = \sum_{j}^{all}\sum_{\nu} S_{\mu\nu}c_{\nu j}\lambda_{ji}, \quad (3.13)$$

or in matrix notation,

$$\mathbf{Kc} = \mathbf{Sc}\boldsymbol{\lambda}. \quad (3.14)$$

This set of equations has a significant resemblance to the Roothaan-Hall equations [66, 67]. Because the electronic density is invariant under unitary transformations of the occupied molecular orbitals, it is possible (and convenient) to choose a set of molecular orbitals for which the off-diagonal undefined Lagrange multipliers, λ_{ij}, are zero. Thus, we can use a molecular orbital representation $\mathbf{cU}$, where $\mathbf{U}$ is an orthogonal transformation matrix, such

that $\mathbf{U}\boldsymbol{\lambda}\mathbf{U}^{\mathrm{T}}$ becomes a diagonal matrix:

$$\mathbf{KcU} = \mathbf{ScU}\underbrace{\mathbf{U}^{\mathrm{T}}\boldsymbol{\lambda}\mathbf{U}}_{\boldsymbol{\varepsilon}}. \tag{3.15}$$

These transformed molecular orbitals are called *canonical*, and they are solutions of the canonical Kohn-Sham equations,

$$\mathbf{Kc} = \mathbf{Sc}\boldsymbol{\varepsilon}. \tag{3.16}$$

Throughout the following discussion we will assume canonical Kohn-Sham molecular orbital unless otherwise stated. As Eq. (3.5) shows, the formal scaling of the core energy is $\mathcal{O}(N_{bas}^2)$, whereas the two-electron Coulomb repulsion energy scales as $\mathcal{O}(N_{bas}^4)$. For the calculation of the exchange-correlation contribution a numerical integration has to be performed. This calculation scales formally as $\mathcal{O}(N_{bas}^2 \times G)$, where G is the number of grid points necessary to perform the numerical integration. Further reduction to this scaling can be achieved by exploiting the localized nature of the exchange-correlation potential and by employing the integral prescreening technique [68, 69] with negligible loss of accuracy. From this analysis follows that the computationally most demanding step is the calculation of the four-center ERIs, which tends to become a serious bottleneck as the system grows in size. The scaling for the Coulomb integrals can be reduced by taking into account the permutational symmetry of the four-center ERIs. Nevertheless, the calculation of the Coulomb contribution rapidly becomes the computationally most demanding part as the system size increases. Thus, techniques are needed that reduce the computational work associated to the four-center ERI calculations.

3.2 Variational Fitting of the Coulomb Potential

A very popular technique to reduce the formal scaling of computing the Coulomb potential is the so-called variational fitting approximation. This technique was introduced by Dunlap and co-workers [70–73], inspired by a former work of Sambe and Felton [74]. It is equivalent

to the application of the resolution of the identity (RI) [75, 76] for Coulomb integrals used in programs like TURBOMOLE [77] or GAUSSIAN [78]. The similarities and differences between the variational Coulomb energy fitting and the RI technique are discussed in great detail in a review by Dunlap, Rösch, and Trickey [79]. In this review it is stated that "the RI arguments yield expressions which formally are identical to variational results but the arguments themselves contain no suggestion of variational stability". For this reason we use in this work the terms variational density fitting or variational fitting of the Coulomb potential. Note that this approach not only delivers a variational energy expression but also the corresponding energy derivatives. The variational approximation of the Coulomb potential, as implemented in deMon2k [80], is based on the minimization of the following self-interaction term [81, 82],

$$\mathcal{E}_2 = \frac{1}{2} \iint \frac{[\rho(\mathbf{r}) - \tilde{\rho}(\mathbf{r})][\rho(\mathbf{r}') - \tilde{\rho}(\mathbf{r}')]}{|\mathbf{r} - \mathbf{r}'|} \, d\mathbf{r} d\mathbf{r}' \geq 0. \tag{3.17}$$

The approximate density $\tilde{\rho}(\mathbf{r})$, which is commonly called auxiliary density is calculated in deMon2k as a linear combination of primitive Hermite-Gaussian functions [81], which are centered at the atoms,

$$\tilde{\rho}(\mathbf{r}) = \sum_{\bar{k}} x_{\bar{k}} \bar{k}(\mathbf{r}). \tag{3.18}$$

From now on, these auxiliary-functions are denoted by small Latin letters with a bar over them. An unnormalized auxiliary-function, $\bar{k}(\mathbf{r})$, centered at atom $\mathbf{K}$ with exponent ζ_k has the form:

$$\bar{k}(\mathbf{r}) = \left(\frac{\partial}{\partial K_x}\right)^{\bar{k}_x} \left(\frac{\partial}{\partial K_y}\right)^{\bar{k}_y} \left(\frac{\partial}{\partial K_z}\right)^{\bar{k}_z} e^{-\zeta_k(\mathbf{r}-\mathbf{R_K})^2}. \tag{3.19}$$

The auxiliary-functions are normalized with respect to the Coulomb norm in deMon2k. Because the auxiliary-functions are used to fit the electron density they are grouped in *s*, *spd*, and *spdfg* sets. The exponents are shared within each of these sets [80, 83]. Therefore, the auxiliary-function notation (3,2,2) describes 3 *s* sets with a total of 3 functions, 2 *spd* sets

with a total of 20 functions and 2 *spdfg* sets with a total of 70 functions. For the analytic molecular integral calculations with these auxiliary-functions, specially developed integral recurrence relations are used [81, 84], ensuring high computational performance. Expanding $\rho(\mathbf{r})$ and $\tilde{\rho}(\mathbf{r})$ in Eq. (3.17) according to Eq. (3.3) and (3.18) yields:

$$\begin{aligned}\mathcal{E}_2 &= \frac{1}{2}\iint \frac{\rho(\mathbf{r})\rho(\mathbf{r}')}{|\mathbf{r}-\mathbf{r}'|}\, d\mathbf{r}d\mathbf{r}' - \iint \frac{\rho(\mathbf{r}')\tilde{\rho}(\mathbf{r})}{|\mathbf{r}-\mathbf{r}'|}\, d\mathbf{r}d\mathbf{r}' + \frac{1}{2}\iint \frac{\tilde{\rho}(\mathbf{r})\tilde{\rho}(\mathbf{r}')}{|\mathbf{r}-\mathbf{r}'|}\, d\mathbf{r}d\mathbf{r}' \\ &= \frac{1}{2}\sum_{\mu,\nu}\sum_{\sigma,\tau} P_{\mu\nu}P_{\sigma\tau}\left\langle \mu\nu \,\|\, \sigma\tau\right\rangle - \sum_{\mu,\nu}\sum_{\bar{k}} P_{\mu\nu}\left\langle \mu\nu \,\|\, \bar{k}\right\rangle x_{\bar{k}} + \frac{1}{2}\sum_{\bar{k},\bar{l}} x_{\bar{k}}x_{\bar{l}}\left\langle \bar{k} \,\|\, \bar{l}\right\rangle . \end{aligned} \tag{3.20}$$

Since $\mathcal{E}_2$ is positive semi-definite [82], Eq. (3.17), it follows,

$$\frac{1}{2}\sum_{\mu,\nu}\sum_{\sigma,\tau} P_{\mu\nu}P_{\sigma\tau}\left\langle \mu\nu \,\|\, \sigma\tau\right\rangle \geq \sum_{\mu,\nu}\sum_{\bar{k}} P_{\mu\nu}\left\langle \mu\nu \,\|\, \bar{k}\right\rangle x_{\bar{k}} - \frac{1}{2}\sum_{\bar{k},\bar{l}} x_{\bar{k}}x_{\bar{l}}\left\langle \bar{k} \,\|\, \bar{l}\right\rangle . \tag{3.21}$$

Note that the equality holds only when $\rho(\mathbf{r}) = \tilde{\rho}(\mathbf{r})$. Any approximate density will provide a lower bound to the Coulomb repulsion energy. By combining Eq. (3.5) with (3.21) an approximation to the Kohn-Sham SCF energy is obtained:

$$E = \sum_{\mu,\nu} P_{\mu\nu}H_{\mu\nu} + \sum_{\mu,\nu}\sum_{\bar{k}} P_{\mu\nu}\left\langle \mu\nu \,\|\, \bar{k}\right\rangle x_{\bar{k}} - \frac{1}{2}\sum_{\bar{k},\bar{l}} x_{\bar{k}}x_{\bar{l}}\left\langle \bar{k} \,\|\, \bar{l}\right\rangle + E_{xc}[\rho], \tag{3.22}$$

where the fitting coefficients, $x_{\bar{k}}$, are obtained by minimizing $\mathcal{E}_2$, keeping the density matrix constant:

$$\left(\frac{\partial \mathcal{E}_2}{\partial x_{\bar{k}}}\right)_{\mathbf{P}} = -\sum_{\mu,\nu} P_{\mu\nu}\left\langle \mu\nu \,\|\, \bar{k}\right\rangle + \sum_{\bar{l}} x_{\bar{l}}\left\langle \bar{k} \,\|\, \bar{l}\right\rangle = 0. \tag{3.23}$$

In the context of deMon2k calculations, the energy expression of Eq. (3.22) is often called the *BASIS* approach because the basis set density, $\rho(\mathbf{r})$, is used for the calculation of the exchange-correlation energy. At this point it is convenient to introduce the Coulomb matrix,

defined as,

$$\mathbf{G} = \begin{pmatrix} \langle \bar{1} \,\|\, \bar{1} \rangle & \langle \bar{1} \,\|\, \bar{2} \rangle & \cdots & \langle \bar{1} \,\|\, \bar{N}_{aux} \rangle \\ \langle \bar{2} \,\|\, \bar{1} \rangle & \langle \bar{2} \,\|\, \bar{2} \rangle & \cdots & \langle \bar{2} \,\|\, \bar{N}_{aux} \rangle \\ \vdots & \vdots & \ddots & \vdots \\ \langle \bar{N}_{aux} \,\|\, \bar{1} \rangle & \langle \bar{N}_{aux} \,\|\, \bar{2} \rangle & \cdots & \langle \bar{N}_{aux} \,\|\, \bar{N}_{aux} \rangle \end{pmatrix}, \tag{3.24}$$

and the Coulomb vector,

$$\mathbf{J} = \begin{pmatrix} \sum_{\mu,\nu} P_{\mu\nu} \langle \mu\nu \,\|\, \bar{1} \rangle \\ \sum_{\mu,\nu} P_{\mu\nu} \langle \mu\nu \,\|\, \bar{2} \rangle \\ \vdots \\ \sum_{\mu,\nu} P_{\mu\nu} \langle \mu\nu \,\|\, \bar{N}_{aux} \rangle \end{pmatrix}. \tag{3.25}$$

With $\mathbf{G}$ and $\mathbf{J}$ the following inhomogeneous equation system for the determination of the fitting coefficients, collected in $\mathbf{x}$, can be formulated:

$$\mathbf{G}\mathbf{x} = \mathbf{J} \tag{3.26}$$

A straightforward solution is obtained by the inversion of the Coulomb matrix $\mathbf{G}$,

$$\mathbf{x} = \mathbf{G}^{-1}\mathbf{J}. \tag{3.27}$$

In deMon2k, the inverse $\mathbf{G}^{-1}$ for a initial geometric structure is computed by using a singular value decomposition (SVD). Then the fitting coefficients are calculated directly using Eq. (3.27) in each SCF step. In case of geometry optimizations or molecular dynamics simulations, the initial $\mathbf{G}^{-1}$ matrix is a guess for the following molecular structure. In the corresponding SCF iterations, Eq (3.27) is solved iteratively with a quasi-Newton algorithm [85] employing an inverse BFGS update [86–88] for $\mathbf{G}^{-1}$.

Once the fitting equation, (3.27), has been solved, the corresponding Kohn-Sham matrix—for a particular density—can be obtained by varying Eq. (3.22) with respect to the density matrix,

$$K_{\mu\nu} = H_{\mu\nu} + \sum_{\bar{k}} \left\langle \mu\nu \,\|\, \bar{k} \right\rangle x_{\bar{k}} + \left\langle \mu \right| v_{xc}[\rho] \left| \nu \right\rangle . \tag{3.28}$$

As Eq. (3.22) shows, the variational fitting of the Coulomb potential replaces the four-center ERI calculation by the corresponding three-center and two-center ERI calculations. The formal scaling for this approach is $\mathcal{O}(N_{bas}^2 \times N_{aux})$, where N_{aux} is the number of auxiliary-functions. In most calculations $N_{aux} \leq 3N_{bas}$ holds. As a result the scaling for the ERI calculations becomes $\mathcal{O}(N_{bas}^3)$ with a prefactor greater than 1. This prefactor can be reduced by taking into account the permutational symmetry of the three-center ERIs. Integral screening, efficient recurrence relations and asymptotic expansion techniques can further improve considerably the computation of three-center Coulomb integrals achieving a near linear scaling [81, 84, 89]. Note that for very large systems sub-linear scaling has also been reported [89, 90]. This leads to an algorithm where the most time-demanding computational step corresponds to the numerical integration of the exchange-correlation potential.

3.3 Fitting of the Exchange-Correlation Potential

The use of auxiliary-functions for the calculation of the exchange-correlation energy and potential has a long history in DFT. These methods aim to overcome the computational bottleneck associated with the numerical integration of $E_{xc}[\rho]$ and $v_{xc}[\rho]$ integrals [74, 91]. In programs like deMon-KS [92], DGAUSS [65], or GTOFF [93] the exchange-correlation potential is expanded in auxiliary-functions. The expansion coefficients are obtained by a least-squares fit on a grid. Even though these methods usually deliver good energies, neither the fit nor the energy expression itself is variational. As a result, only approximate gradients (and higher-order derivatives) are available [94, 95]. As an alternative to fitting the exchange-correlation potential by auxiliary-functions, the direct use of the auxiliary-function density

from the variational fitting of the Coulomb potential for the calculation of the exchange-correlation potential has been investigated over the last two decades [96–101]. The resulting energy expression, from now on named auxiliary density functional theory (ADFT) [102], is variational and has the form,

$$E = \sum_{\mu,\nu} P_{\mu\nu} H_{\mu\nu} + \sum_{\mu,\nu} \sum_{\bar{k}} P_{\mu\nu} \left\langle \mu\nu \,\|\, \bar{k} \right\rangle x_{\bar{k}} - \frac{1}{2} \sum_{\bar{k},\bar{l}} x_{\bar{k}} x_{\bar{l}} \left\langle \bar{k} \,\|\, \bar{l} \right\rangle + E_{xc}[\tilde{\rho}]. \tag{3.29}$$

In deMon2k [80], this theoretical model is often referred to as the *AUXIS* approach. It is the default method for calculating the exchange-correlation contributions. In this approach, it is fundamental that the auxiliary density $\tilde{\rho}(\mathbf{r})$ has the same properties as the Kohn-Sham density $\rho(\mathbf{r})$, namely $\tilde{\rho}(\mathbf{r}) \geq 0$ and $\int \tilde{\rho}(\mathbf{r}) d\mathbf{r} = N$. The normalization to the number of electrons can be included in the variational fitting of the Coulomb potential by a constraint [98]. Even without such a constraint the approximate density conserves the electron number to a sufficiently good degree. The semi-positive definiteness of $\tilde{\rho}(\mathbf{r})$ cannot be guaranteed with similar constraints. Nevertheless, the construction of the approximate density avoids by itself the accumulation of larger areas with negative densities [103]. As soon as a region accumulates negative fitted density it acts as an attractive potential for the remaining electron density. Because the fitting is variational in the Coulomb self-energy error negative fitted density regions almost never occur. In practice, artificial negative electron densities occur when $\rho(\mathbf{r}) \approx 0$ [104]. They can be eliminated by enlarging the auxiliary-function set. During the numerical integration of the approximate density, grid points with negative density values can be safely screened out without compromising the accuracy of the integrated electron number, if sufficiently large auxiliary-function sets are used [99].

Since the approximate density is a linear combination of auxiliary-functions, the density calculation at each grid point scales linearly. This is a clear advantage to the use of the Kohn-Sham density for which basis function products have to be evaluated at each grid point. Due to the fact that auxiliary-functions with shared exponents are used in deMon2k, the computationally expensive exponential part is shared by all functions of an auxiliary-function set and has only to be calculated once at each grid point. Furthermore, for the

uncontracted unnormalized Hermite-Gaussian functions, Eq. (3.19), the following recurrence relation can be deduced:

$$[\bar{\mathbf{k}} + \bar{\mathbf{1}}_i|(\mathbf{r}) = 2\zeta_k(i - K_i)[\bar{\mathbf{k}}|(\mathbf{r}) \; - \; 2\zeta_k \bar{k}_i[\bar{\mathbf{k}} - \bar{\mathbf{1}}_i|(\mathbf{r}) \; ; \; i = x, y, z. \tag{3.30}$$

The recursion starts with $[\bar{\mathbf{s}}| = e^{-\zeta_k(\mathbf{r}-\mathbf{R}_A)^2}$. All higher angular functions can be generated by Eq. (3.30). Because the approximate density, $\tilde{\rho}(\mathbf{r})$, is a linear combination of auxiliary-functions, a very efficient algorithm for the numerical integration of the approximate exchange-correlation energy and potential can be formulated [99]. As in Kohn-Sham DFT, the ADFT Kohn-Sham matrix elements can be obtained by differentiation of the ADFT energy expression, Eq. (3.29), with respect to the density matrix elements,

$$K_{\mu\nu} = H_{\mu\nu} + \sum_{\bar{k}} \langle \mu\nu \,\|\, \bar{k} \rangle \, x_{\bar{k}} + \frac{\partial E_{xc}[\tilde{\rho}]}{\partial P_{\mu\nu}}. \tag{3.31}$$

The last term of Eq. (3.31), evaluated analogously to Eq. (3.11), is:

$$\frac{\partial E_{xc}[\tilde{\rho}]}{\partial P_{\mu\nu}} = \int \frac{\delta E_{xc}[\tilde{\rho}]}{\delta \tilde{\rho}(\mathbf{r})} \frac{\partial \tilde{\rho}(\mathbf{r})}{\partial P_{\mu\nu}} d\mathbf{r} = \sum_{\bar{l}} \frac{\partial x_{\bar{l}}}{\partial P_{\mu\nu}} \int \bar{l}(\mathbf{r}) v_{xc}\,[\tilde{\rho}](\mathbf{r}) \; d\mathbf{r}, \tag{3.32}$$

where,

$$v_{xc}\,[\tilde{\rho}](\mathbf{r}) \equiv \frac{\delta E_{xc}[\tilde{\rho}]}{\delta \tilde{\rho}(\mathbf{r})}. \tag{3.33}$$

The derivatives of the Coulomb fitting coefficients are obtained using Eq. (3.25) and (3.26) as,

$$\frac{\partial x_{\bar{l}}}{\partial P_{\mu\nu}} = \sum_{\bar{k}} \langle \mu\nu \,\|\, \bar{k} \rangle \, G^{-1}_{\bar{k}\bar{l}}. \tag{3.34}$$

Therefore, we obtain as ADFT Kohn-Sham matrix elements,

$$K_{\mu\nu} = H_{\mu\nu} + \sum_{\bar{k}} \left\langle \mu\nu \,\|\, \bar{k} \right\rangle x_{\bar{k}} + \sum_{\bar{k},\bar{l}} \left\langle \mu\nu \,\|\, \bar{k} \right\rangle G^{-1}_{\bar{k}\bar{l}} \left\langle \bar{l} \right| v_{xc}\left[\tilde{\rho}\right] \left\rangle \right. . \tag{3.35}$$

To simplify notation, we now introduce the exchange-correlation fitting coefficient vector, $\mathbf{z}$, with elements,

$$z_{\bar{k}} \equiv \sum_{\bar{l}} G^{-1}_{\bar{k}\bar{l}} \left\langle \bar{l} \right| v_{xc}\left[\tilde{\rho}\right] \left\rangle \right. . \tag{3.36}$$

Hence, Eq. (3.31) can be rewritten as,

$$K_{\mu\nu} = H_{\mu\nu} + \sum_{\bar{k}} \left\langle \mu\nu \,\|\, \bar{k} \right\rangle \left(x_{\bar{k}} + z_{\bar{k}}\right) . \tag{3.37}$$

It is important to point out that $\mathbf{z}$ is a spin-dependent quantity. Its different values for α and β spin densities determine the differences between α and β Kohn-Sham matrices in open-shell calculations. Similar to Eq. (3.26), an inhomogeneous equation system can be formulated as,

$$\mathbf{G}\mathbf{z} = \mathbf{L}, \tag{3.38}$$

with,

$$\mathbf{L} = \begin{pmatrix} \langle \bar{1} | v_{xc}[\tilde{\rho}] \rangle \\ \langle \bar{2} | v_{xc}[\tilde{\rho}] \rangle \\ \vdots \\ \left\langle \bar{N}_{aux} \right| v_{xc}[\tilde{\rho}] \left\rangle \right. \end{pmatrix} . \tag{3.39}$$

Domínguez-Soria *et al.* [85] proposed an iterative method for solving the inhomogeneous linear equation systems associated with Coulomb and exchange-correlation fitting. For the exchange-correlation fitting they proposed a preconditioned conjugate gradient method with

a preconditioner built by the quasi-Newton solver for the Coulomb fitting. For the implementation it is important to note that $\tilde{\rho}(\mathbf{r})$ has to be used directly for the evaluation of the exchange-correlation potential in order to keep the calculation variational. However, this is not mandatory for the calculation of the Coulomb contribution in the SCF energy expression. As a result, there are two sets of fitting coefficients in deMon2k calculations. The first one refers to the solution to Eq. (3.26), and the other results from SCF acceleration techniques, such as fitting coefficient mixing [102] or direct inversion in the iterative subspace (DIIS) [102, 105, 106], which are used to build the Coulomb part of the Kohn-Sham matrix.

With the above described ADFT approach the bottleneck for the numerical integration becomes negligible. In combination with a sophisticated implementation of the three-center ERI calculations, the computational bottleneck is now shifted to linear algebra operations, mainly the diagonalization and multiplication of matrices. In particular, we can identify two linear algebra tasks that are computationally most demanding. The first one is the diagonalization of the Coulomb matrix, Eq. (3.24), associated with its SVD. Because the Coulomb matrix scales with the number of auxiliary-functions its diagonalization is the single most demanding linear algebra task in deMon2k. The second most demanding linear algebra task represents the solution of the Kohn-Sham equation system, Eq. (3.16), that has to be performed in each SCF step. It consists of the transformation of the general eigenvalue equation system into its special form and the diagonalization of the corresponding Kohn-Sham matrix. Although these operations have a formal scaling of N_{bas}^3, they can be performed in a very efficient manner using optimized computational libraries. Many of these libraries are based on the Basic Linear Algebra Subroutines (BLAS) [107–111] and the Linear Algebra Package (LAPACK) [112]. They are machine-specific optimized libraries. Well-known examples are Intel's Math Kernel Library (MKL) and AMD's Core Math Library (ACML). The current implementation in deMon2k allows routine calculations of systems with up to 10000 basis functions and has been already successfully applied to systems with more than 25000 basis functions.

Chapter 4

ANALYTIC ADFT ENERGY DERIVATIVES

This chapter focuses on the calculation of analytic first- and second-order ADFT-energy derivatives with respect to arbitrary perturbations. For the sake of clarity, only the closed-shell case is depicted in the following sections.

4.1 First-Order Derivatives

Energy derivatives with respect to an external perturbation may have two contributions. The first contribution corresponds to the derivatives of the electronic energy. The second one are the corresponding derivatives of the nuclear repulsion energy. Because these derivatives are straightforward to calculate they will not be discussed here. For the calculation of the electronic energy derivatives we will use Eq. (3.29). In the case where basis and auxiliary-functions are dependent on the perturbation parameter, λ, the derivative of the electronic energy is expressed as,

$$\begin{aligned} E^{(\lambda)} = &\sum_{\mu,\nu} P_{\mu\nu}^{(\lambda)} H_{\mu\nu} + \sum_{\mu,\nu} P_{\mu\nu} H_{\mu\nu}^{(\lambda)} + \sum_{\mu,\nu} \sum_{\bar{k}} P_{\mu\nu}^{(\lambda)} \left\langle \mu\nu \middle|\middle| \bar{k} \right\rangle x_{\bar{k}} + \sum_{\mu,\nu} \sum_{\bar{k}} P_{\mu\nu} \left\langle \mu\nu \middle|\middle| \bar{k} \right\rangle^{(\lambda)} x_{\bar{k}} + \\ &\sum_{\mu,\nu} \sum_{\bar{k}} P_{\mu\nu} \left\langle \mu\nu \middle|\middle| \bar{k} \right\rangle x_{\bar{k}}^{(\lambda)} - \frac{1}{2} \sum_{\bar{k},\bar{l}} \left\langle \bar{k} \middle|\middle| \bar{l} \right\rangle^{(\lambda)} x_{\bar{k}} x_{\bar{l}} - \sum_{\bar{k},\bar{l}} \left\langle \bar{k} \middle|\middle| \bar{l} \right\rangle x_{\bar{k}}^{(\lambda)} x_{\bar{l}} + E_{xc}^{(\lambda)}[\tilde{\rho}]. \end{aligned} \tag{4.1}$$

In order to simplify the notation, we will denote the derivative of a function f with respect to a parameter λ as,

$$\frac{\partial f}{\partial \lambda} = f^{(\lambda)}. \tag{4.2}$$

Because basis and auxiliary-functions are λ-dependent none of the molecular integral derivatives vanishes. To proceed we rewrite Eq. (4.1) as,

$$\begin{aligned} E^{(\lambda)} = &\sum_{\mu,\nu} P_{\mu\nu}^{(\lambda)} \left(H_{\mu\nu} + \sum_{\bar{k}} \left\langle \mu\nu \middle|\middle| \bar{k} \right\rangle x_{\bar{k}} \right) + \sum_{\mu,\nu} P_{\mu\nu} \left(H_{\mu\nu}^{(\lambda)} + \sum_{\bar{k}} \left\langle \mu\nu \middle|\middle| \bar{k} \right\rangle^{(\lambda)} x_{\bar{k}} \right) + \\ &\sum_{\bar{k}} x_{\bar{k}}^{(\lambda)} \underbrace{\left(\sum_{\mu,\nu} P_{\mu\nu} \left\langle \mu\nu \middle|\middle| \bar{k} \right\rangle - \sum_{\bar{l}} \left\langle \bar{k} \middle|\middle| \bar{l} \right\rangle x_{\bar{l}} \right)}_{0} - \frac{1}{2} \sum_{\bar{k},\bar{l}} \left\langle \bar{k} \middle|\middle| \bar{l} \right\rangle^{(\lambda)} x_{\bar{k}} x_{\bar{l}} + E_{xc}^{(\lambda)}[\tilde{\rho}]. \end{aligned} \tag{4.3}$$

Due to the variational fitting of the Coulomb potential, Eq. (3.26), the third term in Eq. (4.3) vanishes. For the exchange-correlation energy-derivative follows:

$$E_{xc}^{(\lambda)}[\tilde{\rho}] = \int \frac{\delta E_{xc}[\tilde{\rho}]}{\delta \tilde{\rho}(\mathbf{r})} \frac{\partial \tilde{\rho}(\mathbf{r})}{\partial \lambda} \, d\mathbf{r}. \tag{4.4}$$

The auxiliary density derivative is given by,

$$\frac{\partial \tilde{\rho}(\mathbf{r})}{\partial \lambda} = \frac{\partial}{\partial \lambda} \sum_{\bar{k}} x_{\bar{k}} \bar{k}(\mathbf{r}) = \sum_{\bar{k}} x_{\bar{k}}^{(\lambda)} \bar{k}(\mathbf{r}) + \sum_{\bar{k}} x_{\bar{k}} \bar{k}^{(\lambda)}(\mathbf{r}). \tag{4.5}$$

Thus, it follows that,

$$E_{xc}^{(\lambda)}[\tilde{\rho}] = \sum_{\bar{k}} x_{\bar{k}}^{(\lambda)} \left\langle \bar{k} \middle| v_{xc}\left[\tilde{\rho}\right] \right\rangle + \sum_{\bar{k}} x_{\bar{k}} \left\langle \bar{k}^{(\lambda)} \middle| v_{xc}\left[\tilde{\rho}\right] \right\rangle. \tag{4.6}$$

The derivative of the density fitting coefficients, $x_{\bar{k}}^{(\lambda)}$, are found by differentiation of Eq. (3.26) with respect to the perturbation λ. This yields:

$$x_{\bar{k}}^{(\lambda)} = \sum_{\bar{l}} G_{\bar{k}\bar{l}}^{-1} \left(\sum_{\mu,\nu} P_{\mu\nu}^{(\lambda)} \left\langle \mu\nu \,\|\, \bar{l} \right\rangle + \sum_{\mu,\nu} P_{\mu\nu} \left\langle \mu\nu \,\|\, \bar{l} \right\rangle^{(\lambda)} - \sum_{\bar{m}} G_{\bar{l}\bar{m}}^{(\lambda)} x_{\bar{m}} \right). \tag{4.7}$$

By substituting Eq. (4.7) and Eq. (3.36) into Eq. (4.6) we find that,

$$\begin{aligned} E_{xc}^{(\lambda)}[\tilde{\rho}] = & \sum_{\bar{k}} z_{\bar{k}} \left(\sum_{\mu,\nu} P_{\mu\nu}^{(\lambda)} \left\langle \mu\nu \,\|\, \bar{k} \right\rangle + \sum_{\mu,\nu} P_{\mu\nu} \left\langle \mu\nu \,\|\, \bar{k} \right\rangle^{(\lambda)} - \sum_{\bar{m}} G_{\bar{k}\bar{m}}^{(\lambda)} x_{\bar{m}} \right) + \\ & \sum_{\bar{k}} x_{\bar{k}} \left\langle \bar{k}^{(\lambda)} \middle| v_{xc}\left[\tilde{\rho}\right] \right\rangle . \end{aligned} \tag{4.8}$$

With this explicit form for the exchange-correlation energy-derivative we find for the first-order ADFT-energy derivative:

$$\begin{aligned} E^{(\lambda)} = & \sum_{\mu,\nu} P_{\mu\nu}^{(\lambda)} K_{\mu\nu} + \sum_{\mu,\nu} P_{\mu\nu} H_{\mu\nu}^{(\lambda)} + \sum_{\mu,\nu} \sum_{\bar{k}} P_{\mu\nu} \left\langle \mu\nu \middle\| \bar{k} \right\rangle^{(\lambda)} \left(x_{\bar{k}} + z_{\bar{k}} \right) + \\ & \sum_{\bar{k}} x_{\bar{k}} \left\langle \bar{k}^{(\lambda)} \middle| v_{xc}\left[\tilde{\rho}\right] \right\rangle - \sum_{\bar{k},\bar{l}} G_{\bar{k}\bar{l}}^{(\lambda)} x_{\bar{l}} \left(\frac{1}{2} x_{\bar{k}} + z_{\bar{k}} \right). \end{aligned} \tag{4.9}$$

The perturbed density matrix derivative follows from Eq. (3.4),

$$P_{\mu\nu}^{(\lambda)} = 2 \sum_{i}^{occ} c_{\mu i}^{(\lambda)} c_{\nu i} + 2 \sum_{i}^{occ} c_{\mu i} c_{\nu i}^{(\lambda)}. \tag{4.10}$$

The explicit differentiation of the molecular orbital coefficients can be avoided because of Wigner's $2n + 1$ theorem for perturbation theory [20, 113]. To exploit this theorem the orthonormality constraint for the molecular orbitals, Eq. (2.24), has to be differentiated. This yields the so-called Pulay relation [114, 115],

$$\begin{aligned} & \sum_{\mu,\nu} c_{\mu i}^{(\lambda)} S_{\mu\nu} c_{\nu i} + \sum_{\mu,\nu} c_{\mu i} S_{\mu\nu} c_{\nu i}^{(\lambda)} + \sum_{\mu,\nu} c_{\mu i} S_{\mu\nu}^{(\lambda)} c_{\nu i} = 0 \\ \Longrightarrow \; & 2 \sum_{\mu,\nu} c_{\nu i} S_{\mu\nu} c_{\mu i}^{(\lambda)} + \sum_{\mu,\nu} c_{\mu i} S_{\mu\nu}^{(\lambda)} c_{\nu i} = 0. \end{aligned} \tag{4.11}$$

By substituting the first term of (4.9) with Eq. (4.10), it follows that,

$$\sum_{\mu,\nu} P^{(\lambda)}_{\mu\nu} K_{\mu\nu} = 2 \sum_{i}^{occ} \sum_{\mu,\nu} \left(c^{(\lambda)}_{\mu i} c_{\nu i} + c_{\mu i} c^{(\lambda)}_{\nu i} \right) K_{\mu\nu}$$

$$\Longrightarrow \sum_{\mu,\nu} P^{(\lambda)}_{\mu\nu} K_{\mu\nu} = 4 \sum_{i}^{occ} \sum_{\mu,\nu} c^{(\lambda)}_{\mu i} K_{\mu\nu} c_{\nu i}. \tag{4.12}$$

Employing the Kohn-Sham equation identity of Eq. (3.16) to Eq. (4.12) yields:

$$\sum_{\mu,\nu} P^{(\lambda)}_{\mu\nu} K_{\mu\nu} = 4 \sum_{i}^{occ} \sum_{\mu,\nu} c^{(\lambda)}_{\mu i} S_{\mu\nu} c_{\nu i} \varepsilon_i. \tag{4.13}$$

With the Pulay relation, Eq. (4.11), the explicit differentiation of the molecular orbital coefficients can then be eliminated from Eq. (4.13). Thus we find:

$$\sum_{\mu,\nu} P^{(\lambda)}_{\mu\nu} K_{\mu\nu} = -2 \sum_{i}^{occ} \sum_{\mu,\nu} c_{\mu i} S^{(\lambda)}_{\mu\nu} c_{\nu i} \varepsilon_i. \tag{4.14}$$

To simplify the notation we now introduce the energy-weighted density matrix,

$$W_{\mu\nu} \equiv 2 \sum_{i}^{occ} \varepsilon_i c_{\mu i} c_{\nu i}. \tag{4.15}$$

Combining Eq. (4.15) and (4.14) with Eq. (4.9) yields the final working equation for the calculation of first-order ADFT-energy derivatives [99]:

$$E^{(\lambda)} = -\sum_{\mu,\nu} W_{\mu\nu} S^{(\lambda)}_{\mu\nu} + \sum_{\mu,\nu} P_{\mu\nu} H^{(\lambda)}_{\mu\nu} + \sum_{\mu,\nu} \sum_{\bar{k}} P_{\mu\nu} \left\langle \mu\nu \middle| \middle| \bar{k} \right\rangle^{(\lambda)} (x_{\bar{k}} + z_{\bar{k}}) +$$
$$\sum_{\bar{k}} x_{\bar{k}} \left\langle \bar{k}^{(\lambda)} \middle| v_{xc}\left[\tilde{\rho}\right] \right\rangle - \sum_{\bar{k},\bar{l}} G^{(\lambda)}_{\bar{k}\bar{l}} x_{\bar{l}} \left(\frac{1}{2} x_{\bar{k}} + z_{\bar{k}} \right). \tag{4.16}$$

4.2 Second-Order Derivatives

Taking the derivative of Eq. (4.16) with respect to a second perturbation parameter, denoted by η, in analogy with the previous discussion, yields the second-order ADFT-energy derivatives:

$$\begin{aligned}
E^{(\lambda\eta)} = & \sum_{\mu,\nu} P_{\mu\nu}^{(\eta)} \left(H_{\mu\nu}^{(\lambda)} + \sum_{\bar{k}} \left\langle \mu\nu \,\|\, \bar{k} \right\rangle^{(\lambda)} \left(x_{\bar{k}} + z_{\bar{k}} \right) \right) + \\
& \sum_{\mu,\nu} P_{\mu\nu} \left(H_{\mu\nu}^{(\lambda\eta)} + \sum_{\bar{k}} \left\langle \mu\nu \,\|\, \bar{k} \right\rangle^{(\lambda\eta)} \left(x_{\bar{k}} + z_{\bar{k}} \right) \right) + \\
& \sum_{\mu,\nu} \sum_{\bar{k}} P_{\mu\nu} \left\langle \mu\nu \,\|\, \bar{k} \right\rangle^{(\lambda)} \left(x_{\bar{k}}^{(\eta)} + z_{\bar{k}}^{(\eta)} \right) + \sum_{\bar{k}} x_{\bar{k}}^{(\eta)} \left\langle \bar{k}^{(\lambda)} \middle| v_{xc} \left[\tilde{\rho} \right] \right\rangle + \\
& \sum_{\bar{k}} x_{\bar{k}} \left\langle \bar{k}^{(\lambda\eta)} \middle| v_{xc} \left[\tilde{\rho} \right] \right\rangle + \sum_{\bar{k}} x_{\bar{k}} \left\langle \bar{k}^{(\lambda)} \middle| v_{xc}^{(\eta)} \left[\tilde{\rho} \right] \right\rangle - \sum_{\mu,\nu} W_{\mu\nu}^{(\eta)} S_{\mu\nu}^{(\lambda)} - \\
& \sum_{\mu,\nu} W_{\mu\nu} S_{\mu\nu}^{(\lambda\eta)} - \sum_{\bar{k},\bar{l}} G_{\bar{k}\bar{l}}^{(\lambda\eta)} x_{\bar{l}} \left(\frac{1}{2} x_{\bar{k}} + z_{\bar{k}} \right) - \sum_{\bar{k},\bar{l}} G_{\bar{k}\bar{l}}^{(\lambda)} x_{\bar{l}}^{(\eta)} \left(x_{\bar{k}} + z_{\bar{k}} \right) - \\
& \sum_{\bar{k},\bar{l}} G_{\bar{k}\bar{l}}^{(\lambda)} x_{\bar{l}} z_{\bar{k}}^{(\eta)}.
\end{aligned} \tag{4.17}$$

Differentiation of the exchange-correlation potential in Eq. (4.17) gives:

$$v_{xc}^{(\eta)} \left[\tilde{\rho} \right] (\mathbf{r}) = \int \frac{\delta v_{xc} \left[\tilde{\rho} \right] (\mathbf{r})}{\delta \tilde{\rho}(\mathbf{r}')} \frac{\partial \tilde{\rho}(\mathbf{r}')}{\partial \eta} \, d\mathbf{r}'. \tag{4.18}$$

In the case of pure density functionals the functional derivative of the exchange-correlation potential defines the corresponding exchange-correlation kernel as [12],

$$\frac{\delta v_{xc} \left[\tilde{\rho} \right] (\mathbf{r})}{\delta \tilde{\rho}(\mathbf{r}')} = \delta(\mathbf{r} - \mathbf{r}') f_{xc}[\tilde{\rho}](\mathbf{r}, \mathbf{r}'). \tag{4.19}$$

Inserting Eq. (4.19) and (4.5) into (4.18) and then in Eq. (4.17) yields for the second-order

ADFT-energy derivatives:

$$
\begin{aligned}
E^{(\lambda\eta)} = & \sum_{\mu,\nu} P_{\mu\nu}^{(\eta)} \left(H_{\mu\nu}^{(\lambda)} + \sum_{\bar{k}} \left\langle \mu\nu \,\|\, \bar{k} \right\rangle^{(\lambda)} \left(x_{\bar{k}} + z_{\bar{k}} \right) \right) + \\
& \sum_{\mu,\nu} P_{\mu\nu} \left(H_{\mu\nu}^{(\lambda\eta)} + \sum_{\bar{k}} \left\langle \mu\nu \,\|\, \bar{k} \right\rangle^{(\lambda\eta)} \left(x_{\bar{k}} + z_{\bar{k}} \right) \right) + \\
& \sum_{\mu,\nu} \sum_{\bar{k}} P_{\mu\nu} \left\langle \mu\nu \,\|\, \bar{k} \right\rangle^{(\lambda)} \left(x_{\bar{k}}^{(\eta)} + z_{\bar{k}}^{(\eta)} \right) + \sum_{\bar{k}} x_{\bar{k}}^{(\eta)} \left\langle \bar{k}^{(\lambda)} \middle| v_{xc} \left[\tilde{\rho} \right] \right\rangle + \\
& \sum_{\bar{k}} x_{\bar{k}} \left\langle \bar{k}^{(\lambda\eta)} \middle| v_{xc} \left[\tilde{\rho} \right] \right\rangle + \sum_{\bar{k},\bar{l}} x_{\bar{k}} \left\langle \bar{k}^{(\lambda)} \middle| f_{xc} \left[\tilde{\rho} \right] \middle| \bar{l} \right\rangle x_{\bar{l}}^{(\eta)} + \\
& \sum_{\bar{k},\bar{l}} x_{\bar{k}} \left\langle \bar{k}^{(\lambda)} \middle| f_{xc} \left[\tilde{\rho} \right] \middle| \bar{l}^{(\eta)} \right\rangle x_{\bar{l}} - \sum_{\mu,\nu} W_{\mu\nu}^{(\eta)} S_{\mu\nu}^{(\lambda)} - \sum_{\mu,\nu} W_{\mu\nu} S_{\mu\nu}^{(\lambda\eta)} - \\
& \sum_{\bar{k},\bar{l}} G_{\bar{k}\bar{l}}^{(\lambda\eta)} x_{\bar{l}} \left(\frac{1}{2} x_{\bar{k}} + z_{\bar{k}} \right) - \sum_{\bar{k},\bar{l}} G_{\bar{k}\bar{l}}^{(\lambda)} x_{\bar{l}}^{(\eta)} \left(x_{\bar{k}} + z_{\bar{k}} \right) - \sum_{\bar{k},\bar{l}} G_{\bar{k}\bar{l}}^{(\lambda)} x_{\bar{l}} z_{\bar{k}}^{(\eta)}.
\end{aligned}
\tag{4.20}
$$

At this point it is convenient to sort the individual terms in Eq. (4.20) according to their dependence on the perturbed matrix or vector elements, namely the perturbed density or energy-weighted density matrix elements and perturbed Coulomb or exchange-correlation fitting coefficients. Based on this sorting, the second-order ADFT-energy derivative is partitioned as,

$$
E^{(\lambda\eta)} = \mathcal{E}^{(\lambda\eta)} + \mathfrak{E}^{(\lambda\eta)}. \tag{4.21}
$$

The first contribution, $\mathcal{E}^{(\lambda\eta)}$, is completely independent of the perturbed matrix and vector elements and has the form:

$$
\begin{aligned}
\mathcal{E}^{(\lambda\eta)} = & \sum_{\mu,\nu} P_{\mu\nu} \left(H_{\mu\nu}^{(\lambda\eta)} + \sum_{\bar{k}} \left\langle \mu\nu \,\|\, \bar{k} \right\rangle^{(\lambda\eta)} \left(x_{\bar{k}} + z_{\bar{k}} \right) \right) + \sum_{\bar{k}} x_{\bar{k}} \left\langle \bar{k}^{(\lambda\eta)} \middle| v_{xc} \left[\tilde{\rho} \right] \right\rangle + \\
& \sum_{\bar{k},\bar{l}} x_{\bar{k}} \left\langle \bar{k}^{(\lambda)} \middle| f_{xc} \left[\tilde{\rho} \right] \middle| \bar{l}^{(\eta)} \right\rangle x_{\bar{l}} - \sum_{\mu,\nu} W_{\mu\nu} S_{\mu\nu}^{(\lambda\eta)} - \sum_{\bar{k},\bar{l}} G_{\bar{k}\bar{l}}^{(\lambda\eta)} x_{\bar{l}} \left(\frac{1}{2} x_{\bar{k}} + z_{\bar{k}} \right).
\end{aligned}
\tag{4.22}
$$

The analytic molecular integral derivatives in Eq. (4.22) can be straightforwardly calculated from the corresponding integral recurrence relations [81, 84]. Similarly, the numerical inte-

grals of the exchange-correlation potential and kernel are evaluated with the same adaptive grid [100, 116] that is used for the SCF. Note that the primitive Hermite-Gaussian function derivatives are simply higher-order functions of the same type. The exchange-correlation kernel is calculated either from analytic expressions for the kernel [12] or by finite-differences if only analytic exchange-correlation potential expressions are available [117]. The density, $P_{\mu\nu}$, and energy-weighted density, $W_{\mu\nu}$, matrix elements are calculated from the converged molecular orbital (MO) coefficients and energies. The fitting coefficients, $x_{\bar{k}}$ and $z_{\bar{k}}$, are also taken directly from the previously converged single-point energy calculation.

Unlike Eq. (4.22), the other contribution to the second-order derivatives of the ADFT energy, $\mathfrak{E}^{(\lambda\eta)}$, contains only terms that depend on the perturbed matrix or vector elements,

$$\begin{aligned}\mathfrak{E}^{(\lambda\eta)} = &\sum_{\mu,\nu} P_{\mu\nu}^{(\eta)} \left(H_{\mu\nu}^{(\lambda)} + \sum_{\bar{k}} \left\langle \mu\nu \,\|\, \bar{k} \right\rangle^{(\lambda)} \left(x_{\bar{k}} + z_{\bar{k}} \right) \right) + \\ &\sum_{\mu,\nu} \sum_{\bar{k}} P_{\mu\nu} \left\langle \mu\nu \,\|\, \bar{k} \right\rangle^{(\lambda)} \left(x_{\bar{k}}^{(\eta)} + z_{\bar{k}}^{(\eta)} \right) + \sum_{\bar{k}} x_{\bar{k}}^{(\eta)} \left\langle \bar{k}^{(\lambda)} \middle| v_{xc}\left[\tilde{\rho}\right] \right\rangle + \\ &\sum_{\bar{k},\bar{l}} x_{\bar{k}} \left\langle \bar{k}^{(\lambda)} \middle| f_{xc}\left[\tilde{\rho}\right] \middle| \bar{l} \right\rangle x_{\bar{l}}^{(\eta)} - \sum_{\mu,\nu} W_{\mu\nu}^{(\eta)} S_{\mu\nu}^{(\lambda)} - \sum_{\bar{k},\bar{l}} G_{\bar{k}\bar{l}}^{(\lambda)} \left(x_{\bar{k}} + z_{\bar{k}} \right) x_{\bar{l}}^{(\eta)} - \\ &\sum_{\bar{k},\bar{l}} G_{\bar{k}\bar{l}}^{(\lambda)} z_{\bar{k}}^{(\eta)} x_{\bar{l}}. \end{aligned} \tag{4.23}$$

Again, the molecular integral derivatives appearing here can be straightforwardly calculated. For the calculation of the perturbed $x_{\bar{k}}^{(\eta)}$ vector elements, we employ ADPT. The actual implementation of second-order ADFT-energy derivatives is presented in the following chapter.

4.3 Mixed Derivatives

There are several cases where molecular properties depend on different perturbations [118], i.e., infrared (IR) intensities which are proportional to second-order derivatives of the energy with respect to the nuclear positions $\mathbf{R}$ and a component of an external electric field $\mathbf{F}$:

$$\text{IR intensities} \propto \frac{\partial^2 E}{\partial R_i \partial F_j} \quad i = A_x, A_y, A_z, \ldots ; \; j = x, y, z. \tag{4.24}$$

In the particular case where the basis and auxiliary-functions are dependent on one perturbation, here R_i, but not on the other, here F_j, the symmetry of the second-order derivatives,

$$\frac{\partial^2 E}{\partial R_i \partial F_j} = \frac{\partial^2 E}{\partial F_j \partial R_i}, \tag{4.25}$$

permits to select two algorithms. If one chooses λ as an electric field component and η as a nuclear coordinate most of the integral derivatives in Eq. (4.22) and Eq. (4.23) will vanish. The corresponding mixed second-order derivative is given as,

$$\frac{\partial^2 E}{\partial R_i \partial F_j} = \sum_{\mu,\nu} P_{\mu\nu} H_{\mu\nu}^{(R_i,F_j)} + \sum_{\mu,\nu} P_{\mu\nu}^{(R_i)} H_{\mu\nu}^{(F_j)}. \tag{4.26}$$

The perturbation operator added to the monoelectronic Hamilton operator for IR intensities is expressed as,

$$\hat{\Gamma} = -\mathbf{F} \cdot \mathbf{r}. \tag{4.27}$$

Thus, we find as explicit expression for the mixed second-order derivatives with respect to an electric field component and a nuclear coordinate:

$$\frac{\partial^2 E}{\partial R_i \partial F_j} = -\sum_{\mu,\nu} P_{\mu\nu} \left\langle \mu \right| j \left| \nu \right\rangle^{(R_i)} - \sum_{\mu,\nu} P_{\mu\nu}^{(R_i)} \left\langle \mu \right| j \left| \nu \right\rangle. \tag{4.28}$$

Note that this approach will require all $3M$ perturbed density matrices, $\mathbf{P}^{(R_i)}$, for the nuclear coordinates. If the IR intensities are calculated within an analytic frequency analysis this disadvantage disappears because the $3M$ $\mathbf{P}^{(R_i)}$ matrices are readily available. Therefore, the extra computational effort for the calculation of IR intensities reduces to the evaluation of dipole integral matrices and their derivatives. Consequently, we use this approach as default for the mixed second-order derivatives associated with the IR intensities. On the other hand, if the perturbed density matrices are not available, e.g. in a frequency restart calculation, where some or all Hessian matrix elements are already evaluated, we can take the nuclear coordinates as first perturbation, λ, and the electric field components as the second, η. This

yields the following expression for the mixed second-order energy-derivatives:

$$\begin{aligned}\frac{\partial^2 E}{\partial F_j \partial R_i} = &- \sum_{\mu,\nu} P_{\mu\nu} \left\langle \mu \right| j \left| \nu \right\rangle^{(R_i)} + \sum_{\mu,\nu} P_{\mu\nu}^{(F_j)} \left(H_{\mu\nu}^{(R_i)} + \sum_{\bar{k}} \left\langle \mu\nu \right\| \bar{k} \right\rangle^{(R_i)} \left(x_{\bar{k}} + z_{\bar{k}} \right) \right) + \\ &\sum_{\mu,\nu} \sum_{\bar{k}} P_{\mu\nu} \left\langle \mu\nu \right\| \bar{k} \right\rangle^{(R_i)} \left(x_{\bar{k}}^{(F_j)} + z_{\bar{k}}^{(F_j)} \right) + \sum_{\bar{k}} x_{\bar{k}}^{(F_j)} \left\langle \bar{k}^{(R_i)} \right| v_{xc} \left[\tilde{\rho} \right] \left\rangle + \right. \\ &\sum_{\bar{k},\bar{l}} x_{\bar{k}} \left\langle \bar{k}^{(R_i)} \right| f_{xc} \left[\tilde{\rho} \right] \left| \bar{l} \right\rangle x_{\bar{l}}^{(F_j)} - \sum_{\mu,\nu} W_{\mu\nu}^{(F_j)} S_{\mu\nu}^{(R_i)} - \sum_{\bar{k},\bar{l}} G_{\bar{k}\bar{l}}^{(R_i)} \left(x_{\bar{k}} + z_{\bar{k}} \right) x_{\bar{l}}^{(F_j)} - \\ &\sum_{\bar{k},\bar{l}} G_{\bar{k}\bar{l}}^{(R_i)} z_{\bar{k}}^{(F_j)} x_{\bar{l}}. \end{aligned} \tag{4.29}$$

The analytic dipole moment derivatives are calculated in a time comparable to one polarizability calculation [11]. The advantages of Eq. (4.29) is that only three perturbed density matrices, $\mathbf{P}^{(F_j)}$, need to be evaluated. On the downside the ERI derivatives with respect to all nuclear coordinates need to be calculated. Nevertheless this is the method of choice if the Hessian matrix elements are available from a restart.

For the evaluation of Raman intensities knowledge of the third-order derivatives of the energy with respect to a nuclear coordinate and two electric external fields is required [119]. In deMon2k, the energy gradient of a molecule in the presence of a small finite external electric field is calculated. Then the second-order derivatives of the gradient with respect to the external field are calculated using a second-order finite-field perturbation method. Although the advantage of the procedure is that the analytic calculation of the gradient vector is computationally very efficient, numerical precision difficulties could arise if a too small external electric field is used. This is particularly critical for second-order finite-field methods due to the quadratic finite-field dependence. Thus, an alternative semi-numerical procedure is presented here to overcome these drawbacks. It is based on the analytic expression for the second-order derivatives of the energy with respect to the nuclear positions $\mathbf{R}_A$ and a component of an external electric field $\mathbf{F}$, Eq. (4.29), and a collinear external electric field $\mathbf{F}'$. Differentiation of Eq. (4.29) with respect to an external electric field is mathematically equivalent to the second-order derivatives of the energy gradient with respect to two external

electric field components discussed above yields:

$$\frac{\partial^3 E}{\partial F'_k \partial F_j \partial R_i} = \frac{\partial^2}{\partial F'_k \partial F_j}\frac{\partial E}{\partial R_i} = \frac{\partial}{\partial F'_k}\frac{\partial^2 E}{\partial F_j \partial R_i}. \tag{4.30}$$

Thus, the semi-numerical third-order derivative necessary for Raman intensities can be calculated by the expression:

$$\frac{\partial^3 E}{\partial F'_k \partial F_j \partial R_i} \approx \frac{1}{2\Delta F'_k}\left[\left(\frac{\partial^2 E}{\partial F_j \partial R_i}\right)_{+\Delta F'_k} - \left(\frac{\partial^2 E}{\partial F_j \partial R_i}\right)_{-\Delta F'_k}\right]. \tag{4.31}$$

The advantage of this semi-numerical approach lies in the fact that the finite-field dependency is linear, which renders this approach numerically more stable, and, therefore, more reliable than the previous second-order finite-field method. The analytic second-order energy-derivatives perturbed by the external $\mathbf{F}'$ finite-field are calculated as,

$$\begin{aligned}\left(\frac{\partial^2 E}{\partial F_j \partial R_i}\right)_{\pm\Delta F'_k} = &-\sum_{\mu,\nu} P_{\mu\nu} \left\langle \mu \right| j \left| \nu \right\rangle^{(R_i)} + \sum_{\mu,\nu} P^{(F_j)}_{\mu\nu}\left(H^{(R_i)}_{\mu\nu} + \sum_{\bar{k}} \left\langle \mu\nu \right\| \bar{k} \right\rangle^{(R_i)} \left(x_{\bar{k}} + z_{\bar{k}}\right)\right) + \\ &\sum_{\mu,\nu}\sum_{\bar{k}} P_{\mu\nu} \left\langle \mu\nu \right\| \bar{k} \right\rangle^{(R_i)} \left(x^{(F_j)}_{\bar{k}} + z^{(F_j)}_{\bar{k}}\right) + \sum_{\bar{k}} x^{(F_j)}_{\bar{k}} \left\langle \bar{k}^{(R_i)} \right| v_{xc}\left[\tilde{\rho}\right] \left\rangle + \right. \\ &\sum_{\bar{k},\bar{l}} x_{\bar{k}} \left\langle \bar{k}^{(R_i)} \right| f_{xc}\left[\tilde{\rho}\right] \left| \bar{l} \right\rangle x^{(F_j)}_{\bar{l}} - \sum_{\mu,\nu} W^{(F_j)}_{\mu\nu} S^{(R_i)}_{\mu\nu} - \sum_{\bar{k},\bar{l}} G^{(R_i)}_{\bar{k}\bar{l}} \left(x_{\bar{k}} + z_{\bar{k}}\right) x^{(F_j)}_{\bar{l}} - \\ &\sum_{\bar{k},\bar{l}} G^{(R_i)}_{\bar{k}\bar{l}} z^{(F_j)}_{\bar{k}} x_{\bar{l}} \pm \Delta F'_k \sum_{\mu,\nu} P^{(F_j)}_{\mu\nu} \left\langle \mu \right| k \left| \nu \right\rangle .\end{aligned} \tag{4.32}$$

The additional quantities that must be calculated are six finite-field SCF calculations and their respective dipole moment derivatives. Thus, for a given molecular system both infrared and Raman intensities can be calculated at a computational cost comparable to that of six single-point SCF calculation and seven polarizability calculations. These working equations are the fundamental pillars for the analytic calculations of harmonic vibrational spectra in the framework of ADFT. The implementation of these equations will be discussed in the following chapters.

Chapter 5

AUXILIARY DENSITY PERTURBATION THEORY

The calculation of the density matrix response, i.e., the derivative of density matrix elements with respect to the perturbation parameter, is mandatory for the evaluation of analytic second-order derivatives. In the literature two principal methods are available. On one side are the methods that are based on the linear response of the molecular orbitals. They yield the so-called Coupled-Perturbed SCF (CPSCF) [4–6, 120–123] equations, which become the Coupled-Perturbed Kohn-Sham (CPKS) equations in the framework of Kohn-Sham DFT. Because of their large dimension they are usually solved iteratively. Therefore, many developments in Kohn-Sham response theory are devoted to the simplification of the CPKS equation system [124–136]. As an alternative to the computationally expensive CPKS method, a non-iterative formulation based on the response of the fitting coefficients has been introduced [137]. This so-called auxiliary density perturbation theory (ADPT) [9, 11, 137–139] represents a specific adaptation of McWeeny's self-consistent perturbation (SCP) theory to ADFT.

5.1 McWeeny's Self-Consistent Perturbation Theory

Self-consistent perturbation theory as proposed by McWeeny [140–144] is based on the use of projection operators that separate the occupied-occupied, virtual-virtual and occupied-virtual subspaces. These projection operators are described by $N_{bas} \times N_{bas}$ matrices. To simplify the algebra orthogonal atomic orbitals (AOs) are used. The MO coefficients are transformed to orthogonal AO representation by $\mathbf{S}^{1/2}$ [145, 146]:

$$\breve{c}_{\mu p} = \sum_{\sigma} S_{\mu\sigma}{}^{1/2} c_{\sigma p} \quad \therefore \quad \sum_{\mu} \breve{c}_{\mu p} \breve{c}_{\mu q} = \delta_{pq}. \tag{5.1}$$

The breve on the transformed MO coefficients indicates the orthogonal AO basis and will be used for all matrices represented in this basis. For the occupied-space projection operator follows that

$$\breve{\mathbf{\Pi}} = \sum_{i}^{occ} \mathbf{S^{1/2}} \mathbf{c}_i \mathbf{c}_i^{\mathrm{T}} \mathbf{S^{1/2}}, \tag{5.2}$$

whereas for the complementary unoccupied-space projection operator we have

$$\breve{\mathbf{U}} = \mathbf{E} - \breve{\mathbf{\Pi}}. \tag{5.3}$$

Here $\mathbf{c}_i$ denotes MO coefficient (column) vectors of non-orthogonal AOs. The operators $\breve{\mathbf{\Pi}}$ and $\breve{\mathbf{U}}$ define a N_{occ}-dimensional occupied subspace $\mathfrak{S}_1$ in the space spanned by the N_{bas} basis functions and a $(N_{bas} - N_{occ})$-dimensional complementary unoccupied subspace $\mathfrak{S}_2$, respectively. The $\mathfrak{S}_1$ and $\mathfrak{S}_2$ subspaces are spanned by the doubly occupied and virtual orbitals, respectively [147]. The projection matrices $\breve{\mathbf{\Pi}}$ and $\breve{\mathbf{U}}$ must be idempotent and self-adjoint. The proofs of these properties are straightforward and are given by the following equations:

$$\breve{\mathbf{\Pi}}^2 = \breve{\mathbf{\Pi}}\breve{\mathbf{\Pi}} = \sum_{i,j}^{occ} \breve{\mathbf{c}}_i \breve{\mathbf{c}}_i^{\mathrm{T}} \breve{\mathbf{c}}_j \breve{\mathbf{c}}_j^{\mathrm{T}} = \sum_{i,j}^{occ} \breve{\mathbf{c}}_i \delta_{ij} \breve{\mathbf{c}}_j^{\mathrm{T}} = \sum_{i}^{occ} \breve{\mathbf{c}}_i \breve{\mathbf{c}}_i^{\mathrm{T}} = \breve{\mathbf{\Pi}}, \tag{5.4}$$

$$\breve{\mathbf{U}}^2 = \breve{\mathbf{U}}\breve{\mathbf{U}} = (\mathbf{E} - \breve{\mathbf{\Pi}})(\mathbf{E} - \breve{\mathbf{\Pi}}) = \mathbf{E} - 2\breve{\mathbf{\Pi}} + \breve{\mathbf{\Pi}}^2 = \mathbf{E} - \breve{\mathbf{\Pi}} = \breve{\mathbf{U}}, \tag{5.5}$$

$$\breve{\mathbf{\Pi}}^{\mathrm{T}} = \sum_{i}^{occ} \left(\breve{\mathbf{c}}_i \breve{\mathbf{c}}_i^{\mathrm{T}}\right)^{\mathrm{T}} = \sum_{i}^{occ} \left(\breve{\mathbf{c}}_i^{\mathrm{T}}\right)^{\mathrm{T}} \breve{\mathbf{c}}_i^{\mathrm{T}} = \sum_{i}^{occ} \breve{\mathbf{c}}_i \breve{\mathbf{c}}_i^{\mathrm{T}} = \breve{\mathbf{\Pi}}, \tag{5.6}$$

$$\breve{\mathbf{U}}^{\mathrm{T}} = \mathbf{E}^{\mathrm{T}} - \breve{\mathbf{\Pi}}^{\mathrm{T}} = \mathbf{E} - \breve{\mathbf{\Pi}} = \breve{\mathbf{U}}. \tag{5.7}$$

Furthermore, $\breve{\mathbf{\Pi}}$ and $\breve{\mathbf{U}}$ are complementary to each other which is expressed by their orthogonality,

$$\breve{\mathbf{\Pi}}\breve{\mathbf{U}} = \breve{\mathbf{\Pi}}(\mathbf{E} - \breve{\mathbf{\Pi}}) = \breve{\mathbf{\Pi}} - \breve{\mathbf{\Pi}} = \mathbf{0}. \tag{5.8}$$

Thus, for any arbitrary $N_{bas} \times N_{bas}$ matrix $\breve{\mathbf{M}}$ the following identity is fulfilled:

$$\breve{\mathbf{M}} = (\breve{\mathbf{\Pi}} + \breve{\mathbf{U}})\breve{\mathbf{M}}(\breve{\mathbf{\Pi}} + \breve{\mathbf{U}}) = \breve{\mathbf{\Pi}}\breve{\mathbf{M}}\breve{\mathbf{\Pi}} + \breve{\mathbf{\Pi}}\breve{\mathbf{M}}\breve{\mathbf{U}} + \breve{\mathbf{U}}\breve{\mathbf{M}}\breve{\mathbf{\Pi}} + \breve{\mathbf{U}}\breve{\mathbf{M}}\breve{\mathbf{U}}, \tag{5.9}$$

$$\breve{\mathbf{M}} = \breve{\mathbf{M}}_{oo} + \breve{\mathbf{M}}_{ou} + \breve{\mathbf{M}}_{uo} + \breve{\mathbf{M}}_{uu}. \tag{5.10}$$

The right hand side of Eq. (5.10) corresponds to the projected components of $\breve{\mathbf{M}}$ onto the $\mathfrak{S}_1$ and $\mathfrak{S}_2$ subspaces ($\breve{\mathbf{M}}_{oo}$ and $\breve{\mathbf{M}}_{uu}$) and their intersections ($\breve{\mathbf{M}}_{ou}$ and $\breve{\mathbf{M}}_{uo}$)[1] [147]. In the SCP method developed by McWeeny [141, 142] the idempotence of the occupied-space projector matrix, Eq. (5.4), and its commutator with the Kohn-Sham matrix,

$$\breve{\mathbf{K}}\breve{\mathbf{\Pi}} = \breve{\mathbf{\Pi}}\breve{\mathbf{K}}, \tag{5.11}$$

are used to derive the corresponding linear response equations. By differentiating Eq. (5.4) and Eq. (5.11), taking into account the perturbation-dependence of the basis functions, we find that

$$\breve{\mathbf{\Pi}}^{(\lambda)} = \breve{\mathbf{\Pi}}^{(\lambda)}\breve{\mathbf{\Pi}} + \breve{\mathbf{\Pi}}\breve{\mathbf{S}}^{(\lambda)}\breve{\mathbf{\Pi}} + \breve{\mathbf{\Pi}}\breve{\mathbf{\Pi}}^{(\lambda)}, \tag{5.12}$$

[1] The notation should not be confused with that for block matrices. All $\breve{\mathbf{M}}$ components are $N_{bas} \times N_{bas}$ matrices.

$$\breve{\mathbf{K}}^{(\lambda)}\breve{\mathbf{\Pi}} + \breve{\mathbf{K}}\breve{\mathbf{\Pi}}^{(\lambda)} + \breve{\mathbf{K}}\breve{\mathbf{\Pi}}\breve{\mathbf{S}}^{(\lambda)} = \breve{\mathbf{S}}^{(\lambda)}\breve{\mathbf{\Pi}}\breve{\mathbf{K}} + \breve{\mathbf{\Pi}}^{(\lambda)}\breve{\mathbf{K}} + \breve{\mathbf{\Pi}}\breve{\mathbf{K}}^{(\lambda)}. \tag{5.13}$$

Note the appearance of $\breve{\mathbf{S}}^{(\lambda)}$ which is the non-vanishing derivative of the orthogonal overlap matrix, i.e., the unit matrix. It is calculated from the non-orthogonal overlap matrix derivative as,

$$\breve{\mathbf{S}}^{(\lambda)} = \mathbf{S}^{-1/2}\mathbf{S}^{(\lambda)}\mathbf{S}^{-1/2}. \tag{5.14}$$

By using the aforementioned method the following projections are obtained from the idempotence relation, Eq. (5.12):

$$\breve{\mathbf{\Pi}}^{(\lambda)}_{oo} = -\breve{\mathbf{S}}^{(\lambda)}_{oo}, \tag{5.15}$$

$$\breve{\mathbf{\Pi}}^{(\lambda)}_{uu} = \mathbf{0}, \tag{5.16}$$

$$\breve{\mathbf{\Pi}}^{(\lambda)}_{ou} = \breve{\mathbf{\Pi}}^{(\lambda)}\breve{\mathbf{U}}, \tag{5.17}$$

$$\breve{\mathbf{\Pi}}^{(\lambda)}_{uo} = \breve{\mathbf{U}}\breve{\mathbf{\Pi}}^{(\lambda)}. \tag{5.18}$$

As an example we show below the derivation of Eq. (5.15) from the projection of Eq. (5.12) on the occupied-occupied subspace:

$$\begin{aligned}
\breve{\mathbf{\Pi}}\left(\breve{\mathbf{\Pi}}^{(\lambda)}\right)\breve{\mathbf{\Pi}} &= \breve{\mathbf{\Pi}}\left(\breve{\mathbf{\Pi}}^{(\lambda)}\breve{\mathbf{\Pi}} + \breve{\mathbf{\Pi}}\breve{\mathbf{S}}^{(\lambda)}\breve{\mathbf{\Pi}} + \breve{\mathbf{\Pi}}\breve{\mathbf{\Pi}}^{(\lambda)}\right)\breve{\mathbf{\Pi}}, \\
\breve{\mathbf{\Pi}}^{(\lambda)}_{oo} &= \breve{\mathbf{\Pi}}\breve{\mathbf{\Pi}}^{(\lambda)}\underbrace{\breve{\mathbf{\Pi}}\breve{\mathbf{\Pi}}}_{\breve{\mathbf{\Pi}}} + \underbrace{\breve{\mathbf{\Pi}}\breve{\mathbf{\Pi}}}_{\breve{\mathbf{\Pi}}}\breve{\mathbf{S}}^{(\lambda)}\underbrace{\breve{\mathbf{\Pi}}\breve{\mathbf{\Pi}}}_{\breve{\mathbf{\Pi}}} + \underbrace{\breve{\mathbf{\Pi}}\breve{\mathbf{\Pi}}}_{\breve{\mathbf{\Pi}}}\breve{\mathbf{\Pi}}^{(\lambda)}\breve{\mathbf{\Pi}}, \\
\breve{\mathbf{\Pi}}^{(\lambda)}_{oo} &= \underbrace{\breve{\mathbf{\Pi}}\breve{\mathbf{\Pi}}^{(\lambda)}\breve{\mathbf{\Pi}}}_{\breve{\mathbf{\Pi}}^{(\lambda)}_{oo}} + \underbrace{\breve{\mathbf{\Pi}}\breve{\mathbf{S}}^{(\lambda)}\breve{\mathbf{\Pi}}}_{\breve{\mathbf{S}}^{(\lambda)}_{oo}} + \underbrace{\breve{\mathbf{\Pi}}\breve{\mathbf{\Pi}}^{(\lambda)}\breve{\mathbf{\Pi}}}_{\breve{\mathbf{\Pi}}^{(\lambda)}_{oo}}, \\
\breve{\mathbf{\Pi}}^{(\lambda)}_{oo} &= -\breve{\mathbf{S}}_{oo}.
\end{aligned} \tag{5.19}$$

Projection of the commutation condition, Eq. (5.13), leads to the following equations:

$$\breve{\mathbf{K}}\breve{\mathbf{\Pi}}^{(\lambda)}_{oo} + \breve{\mathbf{K}}\breve{\mathbf{S}}^{(\lambda)}_{oo} = \breve{\mathbf{S}}^{(\lambda)}_{oo}\breve{\mathbf{K}} + \breve{\mathbf{\Pi}}^{(\lambda)}_{oo}\breve{\mathbf{K}}, \tag{5.20}$$

$$\breve{\mathbf{K}}^{(\lambda)}_{ou} = \breve{\mathbf{K}}\breve{\mathbf{\Pi}}^{(\lambda)}_{ou} - \breve{\mathbf{\Pi}}^{(\lambda)}_{ou}\breve{\mathbf{K}} + \breve{\mathbf{K}}\breve{\mathbf{S}}^{(\lambda)}_{ou}, \tag{5.21}$$

$$-\breve{\mathbf{K}}^{(\lambda)}_{uo} = \breve{\mathbf{K}}\breve{\mathbf{\Pi}}^{(\lambda)}_{uo} - \breve{\mathbf{\Pi}}^{(\lambda)}_{uo}\breve{\mathbf{K}} - \breve{\mathbf{S}}^{(\lambda)}_{uo}\breve{\mathbf{K}}, \tag{5.22}$$

$$\breve{\mathbf{K}}\breve{\mathbf{\Pi}}^{(\lambda)}_{uu} = \breve{\mathbf{\Pi}}^{(\lambda)}_{uu}\breve{\mathbf{K}}. \tag{5.23}$$

Eq. (5.20) and (5.23) are trivially solved because of Eq. (5.15) and (5.16), respectively. Since Eq. (5.22) is just the transposition of Eq. (5.21), Eq. (5.21) alone is sufficient for the determination of the density matrix response. To proceed we expand $\breve{\mathbf{\Pi}}^{(\lambda)}_{ou}$, $\breve{\mathbf{K}}^{(\lambda)}_{ou}$, $\breve{\mathbf{S}}^{(\lambda)}_{ou}$ and $\breve{\mathbf{S}}^{(\lambda)}_{oo}$ into their MO representation:

$$\breve{\mathbf{\Pi}}^{(\lambda)}_{ou} = \sum_{i}^{occ}\sum_{a}^{uno} \breve{\mathbf{c}}_i \Pi^{(\lambda)}_{ia} \breve{\mathbf{c}}^{\mathrm{T}}_a, \tag{5.24}$$

$$\breve{\mathbf{K}}^{(\lambda)}_{ou} = \sum_{i}^{occ}\sum_{a}^{uno} \breve{\mathbf{c}}_i \mathcal{K}^{(\lambda)}_{ia} \breve{\mathbf{c}}^{\mathrm{T}}_a, \tag{5.25}$$

$$\breve{\mathbf{S}}^{(\lambda)}_{ou} = \sum_{i}^{occ}\sum_{a}^{uno} \breve{\mathbf{c}}_i \mathcal{S}^{(\lambda)}_{ia} \breve{\mathbf{c}}^{\mathrm{T}}_a, \tag{5.26}$$

$$\breve{\mathbf{S}}^{(\lambda)}_{oo} = \sum_{i,j}^{occ} \breve{\mathbf{c}}_i \mathcal{S}^{(\lambda)}_{ij} \breve{\mathbf{c}}^{\mathrm{T}}_j. \tag{5.27}$$

The perturbed Kohn-Sham, $\mathcal{K}^{(\lambda)}_{ia}$, and overlap matrix, $\mathcal{S}^{(\lambda)}_{ia}$, elements in MO representation are invariant with respect to the underlying AO basis set, i.e., they can be expressed in terms of the orthogonal or non-orthogonal AO basis. Using the latter we find:

$$\mathcal{K}^{(\lambda)}_{ia} \equiv \sum_{\sigma,\tau} c_{\sigma i} K^{(\lambda)}_{\sigma\tau} c_{\tau a}, \tag{5.28}$$

$$\mathcal{S}^{(\lambda)}_{ia} \equiv \sum_{\sigma,\tau} c_{\sigma i} S^{(\lambda)}_{\sigma\tau} c_{\tau a}. \tag{5.29}$$

By substituting Eqs. (5.24), (5.25) and (5.26) into Eq. (5.21) it follows that

$$\sum_{i}^{occ}\sum_{a}^{uno}\breve{\mathbf{c}}_i\mathcal{K}_{ia}^{(\lambda)}\breve{\mathbf{c}}_a^{\mathrm{T}} = \sum_{i}^{occ}\sum_{a}^{uno}\breve{\mathbf{K}}\breve{\mathbf{c}}_i\Pi_{ia}^{(\lambda)}\breve{\mathbf{c}}_a^{\mathrm{T}} - \sum_{i}^{occ}\sum_{a}^{uno}\breve{\mathbf{c}}_i\Pi_{ia}^{(\lambda)}\breve{\mathbf{c}}_a^{\mathrm{T}}\breve{\mathbf{K}} + \sum_{i}^{occ}\sum_{a}^{uno}\breve{\mathbf{K}}\breve{\mathbf{c}}_i\mathcal{S}_{ia}^{(\lambda)}\breve{\mathbf{c}}_a^{\mathrm{T}}. \tag{5.30}$$

To proceed we now introduce molecular orbital energies, ε_i and ε_a, according to the solutions of the Kohn-Sham equations, i.e., $\breve{\mathbf{K}}\breve{\mathbf{c}}_i = \epsilon_i\breve{\mathbf{c}}_i$, and $\breve{\mathbf{c}}_a^{\mathrm{T}}\breve{\mathbf{K}} = \breve{\mathbf{c}}_a^{\mathrm{T}}\epsilon_a$. This yields:

$$\sum_{i}^{occ}\sum_{a}^{uno}\breve{\mathbf{c}}_i\mathcal{K}_{ia}^{(\lambda)}\breve{\mathbf{c}}_a^{\mathrm{T}} = \sum_{i}^{occ}\sum_{a}^{uno}\breve{\boldsymbol{c}}_{\boldsymbol{i}}\epsilon_i\Pi_{ia}^{(\lambda)}\breve{\mathbf{c}}_a^{\mathrm{T}} - \sum_{i}^{occ}\sum_{a}^{uno}\breve{\mathbf{c}}_i\Pi_{ia}^{(\lambda)}\epsilon_a\breve{\boldsymbol{c}}_{\boldsymbol{a}}^{\ \mathrm{T}} + \sum_{i}^{occ}\sum_{a}^{uno}\breve{\boldsymbol{c}}_{\boldsymbol{i}}\epsilon_i\mathcal{S}_{ia}^{(\lambda)}\breve{\mathbf{c}}_a^{\mathrm{T}}, \tag{5.31}$$

$$\Pi_{ia}^{(\lambda)} = \frac{\mathcal{K}_{ia}^{(\lambda)} - \epsilon_i\mathcal{S}_{ia}^{(\lambda)}}{\epsilon_i - \epsilon_a}. \tag{5.32}$$

With the explicit expression for $\Pi_{ia}^{(\lambda)}$ and Eqs. (5.15), (5.16) and (5.17) we find for the perturbed closed-shell density matrix in the orthogonal basis:

$$\breve{\mathbf{P}}^{(\lambda)} = 2\breve{\mathbf{\Pi}}^{(\lambda)} = 2(\breve{\mathbf{\Pi}}_{ou}^{(\lambda)} + \breve{\mathbf{\Pi}}_{uo}^{(\lambda)} + \breve{\mathbf{\Pi}}_{oo}^{(\lambda)}), \tag{5.33}$$

$$\breve{\mathbf{P}}^{(\lambda)} = 2\left(\sum_{i}^{occ}\sum_{a}^{uno}\breve{\mathbf{c}}_i\frac{\mathcal{K}_{ia}^{(\lambda)} - \epsilon_i\mathcal{S}_{ia}^{(\lambda)}}{\epsilon_i - \epsilon_a}\breve{\mathbf{c}}_a^{\mathrm{T}} + \sum_{i}^{occ}\sum_{a}^{uno}\breve{\mathbf{c}}_a\frac{\mathcal{K}_{ia}^{(\lambda)} - \epsilon_i\mathcal{S}_{ia}^{(\lambda)}}{\epsilon_i - \epsilon_a}\breve{\mathbf{c}}_i^{\mathrm{T}} - \breve{\mathbf{S}}_{oo}^{(\lambda)}\right). \tag{5.34}$$

Back-transformation to the non-orthogonal basis with $\mathbf{P}^{(\lambda)} = \mathbf{S}^{-1/2}\breve{\mathbf{P}}^{(\lambda)}\mathbf{S}^{-1/2}$, yields the perturbed closed-shell density matrix in the non-orthogonal basis:

$$\mathbf{P}^{(\lambda)} = 2\left(\sum_{i}^{occ}\sum_{a}^{uno}\mathbf{c}_i\frac{\mathcal{K}_{ia}^{(\lambda)} - \epsilon_i\mathcal{S}_{ia}^{(\lambda)}}{\epsilon_i - \epsilon_a}\mathbf{c}_a^{\mathrm{T}} + \sum_{i}^{occ}\sum_{a}^{uno}\mathbf{c}_a\frac{\mathcal{K}_{ia}^{(\lambda)} - \epsilon_i\mathcal{S}_{ia}^{(\lambda)}}{\epsilon_i - \epsilon_a}\mathbf{c}_i^{\mathrm{T}} - \frac{1}{2}\mathbf{P}\mathbf{S}^{(\lambda)}\mathbf{P}\right). \tag{5.35}$$

From Eq. (5.35) we find as working equation for the calculation of the perturbed closed-shell density matrix elements:

$$P_{\mu\nu}^{(\lambda)} = 2\sum_{i}^{occ}\sum_{a}^{uno}\frac{\mathcal{K}_{ia}^{(\lambda)} - \epsilon_i\mathcal{S}_{ia}^{(\lambda)}}{\epsilon_i - \epsilon_a}(c_{\mu i}c_{\nu a} + c_{\mu a}c_{\nu i}) - \frac{1}{2}\sum_{\sigma,\tau}P_{\mu\sigma}S_{\sigma\tau}^{(\lambda)}P_{\tau\nu}. \tag{5.36}$$

Because $\mathcal{K}_{ia}^{(\lambda)}$ depends on $P_{\mu\nu}^{(\lambda)}$ a self-consistent approach is needed for the calculation of the perturbed density matrix elements [140]. Note, however, that the explicit response

of the molecular orbitals is never needed in such an approach. Instead the target quantity in McWeeny's SCP approach is the linear response of the density matrix. Thus, the SCP formulation is the method of choice for DFT perturbation calculations employing the electron density and its derivatives as the fundamental ingredients.

5.2 Restricted ADPT Equation System

As Eq. (5.36) shows, the iterative evaluation of the perturbed density matrix can become a serious computational bottleneck if convergence is slow. Thus, a more direct method that is driven by the auxiliary-function density rather than the orbital density is desirable. In such an approach the response of the density matrix elements is substituted by the response of the fitting coefficients. To proceed in this direction we expand the perturbed ADFT Kohn-Sham matrix elements of Eq. (5.36) and Eq. (5.28) as,

$$K_{\mu\nu}^{(\lambda)} = H_{\mu\nu}^{(\lambda)} + \sum_{\bar{k}} \left\langle \mu\nu \,\|\, \bar{k} \right\rangle^{(\lambda)} \left(x_{\bar{k}} + z_{\bar{k}} \right) + \sum_{\bar{k}} \left\langle \mu\nu \,\|\, \bar{k} \right\rangle \left(x_{\bar{k}}^{(\lambda)} + z_{\bar{k}}^{(\lambda)} \right). \tag{5.37}$$

The perturbed Coulomb fitting coefficients appearing here are given by Eq. (4.7). The perturbed exchange-correlation fitting coefficients are as follows:

$$\begin{aligned} z_{\bar{k}}^{(\lambda)} = & \sum_{\bar{l}} G_{\bar{k}\bar{l}}^{-1} \left\langle \bar{l}^{(\lambda)} \middle| v_{xc}\left[\tilde{\rho}\right] \right\rangle - \sum_{\bar{l},\bar{m}} G_{\bar{k}\bar{l}}^{-1} G_{\bar{l}\bar{m}}^{(\lambda)} z_{\bar{m}} + \sum_{\bar{l},\bar{m}} G_{\bar{k}\bar{l}}^{-1} \left\langle \bar{l} \middle| f_{xc}\left[\tilde{\rho}\right] \middle| \bar{m} \right\rangle x_{\bar{m}}^{(\lambda)} + \\ & \sum_{\bar{l},\bar{m}} G_{\bar{k}\bar{l}}^{-1} \left\langle \bar{l} \middle| f_{xc}\left[\tilde{\rho}\right] \middle| \bar{m}^{(\lambda)} \right\rangle x_{\bar{m}}. \end{aligned} \tag{5.38}$$

Thus, in ADFT the response of the Kohn-Sham matrix can be evaluated directly from the response of the auxiliary-function density. As a result, the self-consistent solution of Eq. (5.36) can be substituted by an analytic solution in the space of the auxiliary-functions. To do so we expand the perturbed Kohn-Sham matrix in Eq. (5.36) according to Eq. (5.28),

(5.37) and (5.38). This yields:

$$
\begin{aligned}
P_{\mu\nu}^{(\lambda)} = & 2\sum_{i}^{occ}\sum_{a}^{uno}\frac{\mathcal{H}_{ia}^{(\lambda)}}{\epsilon_i-\epsilon_a}(c_{\mu i}c_{\nu a}+c_{\mu a}c_{\nu i})+ \\
& 2\sum_{i}^{occ}\sum_{a}^{uno}\sum_{\bar{k}}\frac{\left\langle ia\,\|\,\bar{k}\right\rangle^{(\lambda)}x_{\bar{k}}}{\epsilon_i-\epsilon_a}(c_{\mu i}c_{\nu a}+c_{\mu a}c_{\nu i})+ \\
& 2\sum_{i}^{occ}\sum_{a}^{uno}\sum_{\bar{k}}\frac{\left\langle ia\,\|\,\bar{k}\right\rangle^{(\lambda)}z_{\bar{k}}}{\epsilon_i-\epsilon_a}(c_{\mu i}c_{\nu a}+c_{\mu a}c_{\nu i})+ \\
& 2\sum_{i}^{occ}\sum_{a}^{uno}\sum_{\bar{k}}\frac{\left\langle ia\,\|\,\bar{k}\right\rangle x_{\bar{k}}^{(\lambda)}}{\epsilon_i-\epsilon_a}(c_{\mu i}c_{\nu a}+c_{\mu a}c_{\nu i})- \\
& 2\sum_{i}^{occ}\sum_{a}^{uno}\sum_{\bar{k},\bar{l},\bar{m}}\frac{\left\langle ia\,\|\,\bar{k}\right\rangle G_{\bar{k}\bar{l}}^{-1}G_{\bar{l}\bar{m}}^{(\lambda)}z_{\bar{m}}}{\epsilon_i-\epsilon_a}(c_{\mu i}c_{\nu a}+c_{\mu a}c_{\nu i})+ \\
& 2\sum_{i}^{occ}\sum_{a}^{uno}\sum_{\bar{k},\bar{l}}\frac{\left\langle ia\,\|\,\bar{k}\right\rangle G_{\bar{k}\bar{l}}^{-1}\left\langle \bar{l}^{(\lambda)}\right|v_{xc}\left[\tilde{\rho}\right]\rangle}{\epsilon_i-\epsilon_a}(c_{\mu i}c_{\nu a}+c_{\mu a}c_{\nu i})+ \\
& 2\sum_{i}^{occ}\sum_{a}^{uno}\sum_{\bar{k},\bar{l},\bar{m}}\frac{\left\langle ia\,\|\,\bar{k}\right\rangle G_{\bar{k}\bar{l}}^{-1}\left\langle \bar{l}\right|f_{xc}\left[\tilde{\rho}\right]\left|\bar{m}\right\rangle x_{\bar{m}}^{(\lambda)}}{\epsilon_i-\epsilon_a}(c_{\mu i}c_{\nu a}+c_{\mu a}c_{\nu i})+ \\
& 2\sum_{i}^{occ}\sum_{a}^{uno}\sum_{\bar{k},\bar{l},\bar{m}}\frac{\left\langle ia\,\|\,\bar{k}\right\rangle G_{\bar{k}\bar{l}}^{-1}\left\langle \bar{l}\right|f_{xc}\left[\tilde{\rho}\right]\left|\bar{m}^{(\lambda)}\right\rangle x_{\bar{m}}}{\epsilon_i-\epsilon_a}(c_{\mu i}c_{\nu a}+c_{\mu a}c_{\nu i})- \\
& 2\sum_{i}^{occ}\sum_{a}^{uno}\frac{\epsilon_i\mathcal{S}_{ia}^{(\lambda)}}{\epsilon_i-\epsilon_a}(c_{\mu i}c_{\nu a}+c_{\mu a}c_{\nu i})-\frac{1}{2}\sum_{\sigma,\tau}P_{\mu\sigma}S_{\sigma\tau}^{(\lambda)}P_{\tau\nu}.
\end{aligned}
\tag{5.39}
$$

In the above equation $\mathcal{H}_{ia}$ denotes the core Hamilton matrix elements in MO representation:

$$
\mathcal{H}_{ia}^{(\lambda)} \equiv \sum_{\mu,\nu} c_{\mu i}H_{\mu\nu}^{(\lambda)}c_{\nu a}. \tag{5.40}
$$

On the other hand, the differentiation of the fitting equation system given in Eq. (3.26) with respect to the perturbation parameter λ yields:

$$
\sum_{\mu,\nu}P_{\mu\nu}^{(\lambda)}\left\langle \mu\nu\,\|\,\bar{n}\right\rangle = \sum_{\bar{k}}G_{\bar{n}\bar{k}}^{(\lambda)}x_{\bar{k}}+\sum_{\bar{k}}G_{\bar{n}\bar{k}}\,x_{\bar{k}}^{(\lambda)}-\sum_{\mu,\nu}P_{\mu\nu}\left\langle \mu\nu\,\|\,\bar{n}\right\rangle^{(\lambda)}. \tag{5.41}
$$

By multiplying Eq. (5.39) with three-center ERIs and then combining it with Eq. (5.41) an inhomogeneous equation system for the direct calculation of the perturbed Coulomb fitting coefficients, employing perturbation-dependent basis and auxiliary-functions, is obtained:

$$\begin{aligned}
\sum_{\mu,\nu} P^{(\lambda)}_{\mu\nu} \left\langle \mu\nu \,\|\, \bar{n} \right\rangle = {} & 4 \sum_{i}^{occ} \sum_{a}^{uno} \frac{\mathcal{H}^{(\lambda)}_{ia}}{\epsilon_i - \epsilon_a} \left\langle ia \,\|\, \bar{n} \right\rangle + \\
& 4 \sum_{i}^{occ} \sum_{a}^{uno} \sum_{\bar{k}} \frac{\left\langle ia \,\|\, \bar{k} \right\rangle^{(\lambda)} x_{\bar{k}}}{\epsilon_i - \epsilon_a} \left\langle ia \,\|\, \bar{n} \right\rangle + \\
& 4 \sum_{i}^{occ} \sum_{a}^{uno} \sum_{\bar{k}} \frac{\left\langle ia \,\|\, \bar{k} \right\rangle^{(\lambda)} z_{\bar{k}}}{\epsilon_i - \epsilon_a} \left\langle ia \,\|\, \bar{n} \right\rangle + \\
& 4 \sum_{i}^{occ} \sum_{a}^{uno} \sum_{\bar{k}} \frac{\left\langle ia \,\|\, \bar{k} \right\rangle x^{(\lambda)}_{\bar{k}}}{\epsilon_i - \epsilon_a} \left\langle ia \,\|\, \bar{n} \right\rangle - \\
& 4 \sum_{i}^{occ} \sum_{a}^{uno} \sum_{\bar{k},\bar{l},\bar{m}} \frac{\left\langle ia \,\|\, \bar{k} \right\rangle G^{-1}_{\bar{k}\bar{l}} G^{(\lambda)}_{\bar{l}\bar{m}} z_{\bar{m}}}{\epsilon_i - \epsilon_a} \left\langle ia \,\|\, \bar{n} \right\rangle + \\
& 4 \sum_{i}^{occ} \sum_{a}^{uno} \sum_{\bar{k},\bar{l}} \frac{\left\langle ia \,\|\, \bar{k} \right\rangle G^{-1}_{\bar{k}\bar{l}} \left\langle \bar{l}^{(\lambda)} \right| v_{xc}\left[\tilde{\rho}\right] \rangle}{\epsilon_i - \epsilon_a} \left\langle ia \,\|\, \bar{n} \right\rangle + \\
& 4 \sum_{i}^{occ} \sum_{a}^{uno} \sum_{\bar{k},\bar{l},\bar{m}} \frac{\left\langle ia \,\|\, \bar{k} \right\rangle G^{-1}_{\bar{k}\bar{l}} \left\langle \bar{l} \right| f_{xc}\left[\tilde{\rho}\right] \left| \bar{m} \right\rangle x^{(\lambda)}_{\bar{m}}}{\epsilon_i - \epsilon_a} \left\langle ia \,\|\, \bar{n} \right\rangle + \\
& 4 \sum_{i}^{occ} \sum_{a}^{uno} \sum_{\bar{k},\bar{l},\bar{m}} \frac{\left\langle ia \,\|\, \bar{k} \right\rangle G^{-1}_{\bar{k}\bar{l}} \left\langle \bar{l} \right| f_{xc}\left[\tilde{\rho}\right] \left| \bar{m}^{(\lambda)} \right\rangle x_{\bar{m}}}{\epsilon_i - \epsilon_a} \left\langle ia \,\|\, \bar{n} \right\rangle - \\
& 4 \sum_{i}^{occ} \sum_{a}^{uno} \frac{\epsilon_i \mathcal{S}^{(\lambda)}_{ia}}{\epsilon_i - \epsilon_a} \left\langle ia \,\|\, \bar{n} \right\rangle - 2 \sum_{i,j}^{occ} S^{(\lambda)}_{ij} \left\langle ij \,\|\, \bar{n} \right\rangle \\
= {} & \sum_{\bar{k}} G^{(\lambda)}_{\bar{n}\bar{k}} x_{\bar{k}} + \sum_{\bar{k}} G_{\bar{n}\bar{k}} \, x^{(\lambda)}_{\bar{k}} - \sum_{\mu,\nu} P_{\mu\nu} \left\langle \mu\nu \,\|\, \bar{n} \right\rangle^{(\lambda)} . \qquad (5.42)
\end{aligned}$$

At this point it is convenient to introduce the Coulomb response matrix $\mathbf{A}$ with elements,

$$A_{\bar{n}\bar{k}} \equiv \sum_{i}^{occ} \sum_{a}^{uno} \frac{\left\langle \bar{n} \,\|\, ia \right\rangle \left\langle ia \,\|\, \bar{k} \right\rangle}{\epsilon_i - \epsilon_a}, \qquad (5.43)$$

the exchange-correlation kernel matrix $\mathbf{F}$ with elements,

$$F_{\bar{k}\bar{m}} \equiv \sum_{\bar{l}} G^{-1}_{\bar{k}\bar{l}} \left\langle \bar{l} \right| f_{xc}\left[\tilde{\rho}\right] \left| \bar{m} \right\rangle, \tag{5.44}$$

and the perturbation vector $\mathbf{b}^{(\lambda)}$ with elements:

$$\begin{aligned} b^{(\lambda)}_{\bar{n}} = & \sum_{i}^{occ}\sum_{a}^{uno} \frac{\mathcal{H}^{(\lambda)}_{ia}}{\epsilon_i - \epsilon_a} \left\langle ia \,\|\, \bar{n} \right\rangle + \sum_{i}^{occ}\sum_{a}^{uno}\sum_{\bar{k}} \frac{\left\langle \bar{n} \,\|\, ia \right\rangle \left\langle ia \,\|\, \bar{k} \right\rangle^{(\lambda)}}{\epsilon_i - \epsilon_a} x_{\bar{k}} + \\ & \sum_{i}^{occ}\sum_{a}^{uno}\sum_{\bar{k}} \frac{\left\langle \bar{n} \,\|\, ia \right\rangle \left\langle ia \,\|\, \bar{k} \right\rangle^{(\lambda)}}{\epsilon_i - \epsilon_a} z_{\bar{k}} - \sum_{i}^{occ}\sum_{a}^{uno}\sum_{\bar{k},\bar{l},\bar{m}} \frac{\left\langle \bar{n} \,\|\, ia \right\rangle \left\langle ia \,\|\, \bar{k} \right\rangle}{\epsilon_i - \epsilon_a} G^{-1}_{\bar{k}\bar{l}} G^{(\lambda)}_{\bar{l}\bar{m}} z_{\bar{m}} + \\ & \sum_{i}^{occ}\sum_{a}^{uno}\sum_{\bar{k},\bar{l}} \frac{\left\langle \bar{n} \,\|\, ia \right\rangle \left\langle ia \,\|\, \bar{k} \right\rangle}{\epsilon_i - \epsilon_a} G^{-1}_{\bar{k}\bar{l}} \left\langle \bar{l}^{(\lambda)} \right| v_{xc}\left[\tilde{\rho}\right] \left\rangle + \right. \\ & \sum_{i}^{occ}\sum_{a}^{uno}\sum_{\bar{k},\bar{l},\bar{m}} \frac{\left\langle \bar{n} \,\|\, ia \right\rangle \left\langle ia \,\|\, \bar{k} \right\rangle}{\epsilon_i - \epsilon_a} G^{-1}_{\bar{k}\bar{l}} \left\langle \bar{l} \right| f_{xc}\left[\tilde{\rho}\right] \left| \bar{m}^{(\lambda)} \right\rangle x_{\bar{m}} - \\ & \sum_{i}^{occ}\sum_{a}^{uno} \frac{\epsilon_i \mathcal{S}^{(\lambda)}_{ia}}{\epsilon_i - \epsilon_a} \left\langle ia \,\|\, \bar{n} \right\rangle - \frac{1}{2}\sum_{i,j}^{occ} S^{(\lambda)}_{ij} \left\langle ij \,\|\, \bar{n} \right\rangle - \frac{1}{4}\sum_{\bar{k}} G^{(\lambda)}_{\bar{n}\bar{k}} x_{\bar{k}} + \\ & \frac{1}{4}\sum_{\mu,\nu} P_{\mu\nu} \left\langle \mu\nu \,\|\, \bar{n} \right\rangle^{(\lambda)}. \end{aligned} \tag{5.45}$$

It is important to note that the Coulomb response matrix, the exchange correlation response matrix and the perturbation vector are spin-dependent. However, for the sake of simplicity we restrict our discussion here to the restricted closed-shell formulation. For the extension to open-shell see appendix C and D. With these quantities the inhomogeneous equation system, Eq. (5.42), can be written in the following form:

$$\begin{aligned} 4\, b^{(\lambda)}_{\bar{n}} &= \sum_{\bar{k}} G_{\bar{n}\bar{k}} x^{(\lambda)}_{\bar{k}} - 4\sum_{\bar{k}} A_{\bar{n}\bar{k}} x^{(\lambda)}_{\bar{k}} - 4\sum_{\bar{k},\bar{l}} A_{\bar{n}\bar{k}} F_{\bar{k}\bar{l}} x^{(\lambda)}_{\bar{l}}, \\ 4\mathbf{b}^{(\lambda)} &= \left(\mathbf{G} - 4\mathbf{A} - 4\mathbf{A}\mathbf{F}\right)\mathbf{x}^{(\lambda)}. \end{aligned} \tag{5.46}$$

This is the working equation system for auxiliary density perturbation theory (ADPT) with perturbation-dependent basis and auxiliary-functions. It has the same algebraic form as

the ADPT equation system for perturbation-independent basis and auxiliary-functions [137]. The essential difference lies in the calculation of the perturbation vector elements, $b_{\bar{n}}^{(\lambda)}$, which becomes much more complicated if perturbation-dependent basis and auxiliary-functions are used. In this case the calculation of these vector elements can become a computational bottleneck, in particular for second-order energy-derivatives, because they are needed for each individual perturbation. Therefore, we will discuss the efficient calculation of the $b_{\bar{n}}^{(\lambda)}$ elements in the following section.

5.3 Calculation of the Perturbation Vector

For the computationally efficient calculation of the perturbation vector the three-center ERIs in MO representation are expanded as,

$$\left\langle ia \,\|\, \bar{k} \right\rangle = \sum_{\mu,\nu} c_{\mu i} c_{\nu a} \left\langle \mu\nu \,\|\, \bar{k} \right\rangle . \tag{5.47}$$

Inserting Eq. (5.47) into Eq. (5.45) yields the following explicit form for a perturbation vector element:

$$\begin{aligned}
b_{\bar{n}}^{(\lambda)} = & \sum_{i}^{occ} \sum_{a}^{uno} \sum_{\mu,\nu} \sum_{\sigma,\tau} c_{\mu i} c_{\nu a} \frac{H_{\mu\nu}^{(\lambda)}}{\epsilon_i - \epsilon_a} c_{\sigma i} c_{\tau a} \left\langle \sigma\tau \,\|\, \bar{n} \right\rangle + \\
& \sum_{i}^{occ} \sum_{a}^{uno} \sum_{\mu,\nu} \sum_{\sigma,\tau} \sum_{\bar{k}} c_{\mu i} c_{\nu a} \frac{\left\langle \mu\nu \,\|\, \bar{k} \right\rangle^{(\lambda)} x_{\bar{k}}}{\epsilon_i - \epsilon_a} c_{\sigma i} c_{\tau a} \left\langle \sigma\tau \,\|\, \bar{n} \right\rangle + \\
& \sum_{i}^{occ} \sum_{a}^{uno} \sum_{\mu,\nu} \sum_{\sigma,\tau} \sum_{\bar{k}} c_{\mu i} c_{\nu a} \frac{\left\langle \mu\nu \,\|\, \bar{k} \right\rangle^{(\lambda)} z_{\bar{k}}}{\epsilon_i - \epsilon_a} c_{\sigma i} c_{\tau a} \left\langle \sigma\tau \,\|\, \bar{n} \right\rangle + \\
& \sum_{i}^{occ} \sum_{a}^{uno} \sum_{\mu,\nu} \sum_{\sigma,\tau} \sum_{\bar{k},\bar{l},\bar{m}} c_{\mu i} c_{\nu a} \frac{\left\langle \mu\nu \,\|\, \bar{k} \right\rangle G_{\bar{k}\bar{l}}^{-1} G_{\bar{l}\bar{m}}^{(\lambda)} z_{\bar{m}}}{\epsilon_i - \epsilon_a} c_{\sigma i} c_{\tau a} \left\langle \sigma\tau \,\|\, \bar{n} \right\rangle + \\
& \sum_{i}^{occ} \sum_{a}^{uno} \sum_{\mu,\nu} \sum_{\sigma,\tau} \sum_{\bar{k},\bar{l}} c_{\mu i} c_{\nu a} \frac{\left\langle \mu\nu \,\|\, \bar{k} \right\rangle G_{\bar{k}\bar{l}}^{-1} \left\langle \bar{l}^{(\lambda)} \right| v_{xc}\left[\tilde{\rho}\right] \left\rangle \right.}{\epsilon_i - \epsilon_a} c_{\sigma i} c_{\tau a} \left\langle \sigma\tau \,\|\, \bar{n} \right\rangle + \\
& \sum_{i}^{occ} \sum_{a}^{uno} \sum_{\mu,\nu} \sum_{\sigma,\tau} \sum_{\bar{k},\bar{l},\bar{m}} c_{\mu i} c_{\nu a} \frac{\left\langle \mu\nu \,\|\, \bar{k} \right\rangle G_{\bar{k}\bar{l}}^{-1} \left\langle \bar{l} \right| f_{xc}\left[\tilde{\rho}\right] \left| \bar{m}^{(\lambda)} \right\rangle x_{\bar{m}}}{\epsilon_i - \epsilon_a} c_{\sigma i} c_{\tau a} \left\langle \sigma\tau \,\|\, \bar{n} \right\rangle - \\
\end{aligned}$$

$$\sum_{i}^{occ}\sum_{a}^{uno}\sum_{\sigma,\tau}\frac{\epsilon_i \mathcal{S}_{ia}^{(\lambda)}}{\epsilon_i-\epsilon_a}c_{\sigma i}c_{\tau a}\left\langle\sigma\tau\,\|\,\bar{n}\right\rangle-\frac{1}{8}\sum_{\mu,\nu}\sum_{\sigma,\tau}P_{\sigma\mu}S_{\mu\nu}^{(\lambda)}P_{\nu\tau}\left\langle\sigma\tau\,\|\,\bar{n}\right\rangle-$$
$$\frac{1}{4}\sum_{\bar{k}}G_{\bar{n}\bar{k}}^{(\lambda)}x_{\bar{k}}+\frac{1}{4}\sum_{\sigma,\tau}P_{\sigma\tau}\left\langle\sigma\tau\,\|\,\bar{n}\right\rangle^{(\lambda)}. \tag{5.48}$$

The auxiliary-function summations in the fourth, fifth and sixth term of Eq. (5.48),

$$\sum_{\mu,\nu}\sum_{\bar{k},\bar{l},\bar{m}}c_{\mu i}c_{\nu a}\big\langle\mu\nu\,\|\,\bar{k}\big\rangle\,G_{\bar{k}\bar{l}}^{-1}G_{\bar{l}\bar{m}}^{(\lambda)}z_{\bar{m}}+\sum_{\mu,\nu}\sum_{\bar{k},\bar{l}}\sum_{\mu,\nu}c_{\mu i}c_{\nu a}\big\langle\mu\nu\,\|\,\bar{k}\big\rangle\,G_{\bar{k}\bar{l}}^{-1}\left\langle\bar{l}^{(\lambda)}\right|v_{xc}\left[\tilde{\rho}\right]\big\rangle+ \tag{5.49}$$
$$\sum_{\mu,\nu}\sum_{\bar{k},\bar{l},\bar{m}}c_{\mu i}c_{\nu a}\big\langle\mu\nu\,\|\,\bar{k}\big\rangle\,G_{\bar{k}\bar{l}}^{-1}\left\langle\bar{l}\right|f_{xc}\left[\tilde{\rho}\right]\left|\bar{m}^{(\lambda)}\right\rangle x_{\bar{m}},$$

can be grouped together as:

$$\sum_{\mu,\nu}\sum_{\bar{k},\bar{l}}c_{\mu i}c_{\nu a}\left\langle\mu\nu\,\|\,\bar{k}\right\rangle G_{\bar{k}\bar{l}}^{-1}q_{\bar{l}}. \tag{5.50}$$

The elements of the newly introduced vector $\mathbf{q}$ are defined as,

$$q_{\bar{l}}=\sum_{\bar{m}}G_{\bar{l}\bar{m}}^{(\lambda)}z_{\bar{m}}+\left\langle\bar{l}^{(\lambda)}\right|v_{xc}\left[\tilde{\rho}\right]\big\rangle+\sum_{\bar{m}}\left\langle\bar{l}\right|f_{xc}\left[\tilde{\rho}\right]\left|\bar{m}^{(\lambda)}\right\rangle x_{\bar{m}}. \tag{5.51}$$

The first two terms in Eq. (5.51) are calculated analogously to the corresponding contributions to the ADFT gradients [99]. The calculation of the last term in Eq. (5.51) can be significantly simplified by noting that

$$\sum_{\bar{m}}\left\langle\bar{l}\right|f_{xc}\left[\tilde{\rho}\right]\left|\bar{m}^{(\lambda)}\right\rangle x_{\bar{m}}=\left\langle\bar{l}\right|f_{xc}\left[\tilde{\rho}\right]\left|\sigma^{(\lambda)}\right\rangle, \tag{5.52}$$

with,

$$\sigma^{(\lambda)}(\mathbf{r})=\sum_{\bar{m}}x_{\bar{m}}\bar{m}^{(\lambda)}(\mathbf{r}). \tag{5.53}$$

The formal scaling of Eq. (5.53) is $\mathcal{O}(N_{aux}\times G)$, where G denotes the number of grid points for the numerical integration. This scaling can be further reduced by grid screening tech-

niques [81]. This compression allows calculating the exchange-correlation kernel contribution on the grid directly on a vector of dimension N_{aux} instead of performing a matrix-vector multiplication, avoiding the allocation of a full N_{aux}^2 field [117]. Afterwards the $\mathbf{q}$ vector is multiplied with the inverse of the Coulomb $\mathbf{G}$ matrix previously stored on hard disk:

$$q'_{\bar{k}} = \sum_{\bar{l}} G^{-1}_{\bar{k}\bar{l}} q_{\bar{l}}. \tag{5.54}$$

This operation results in a new vector which is multiplied in the same way as the first three terms in Eq. (5.48). For the simultaneous processing, we introduce a N_{bas}^2 matrix $\mathbf{L}$ with elements

$$L_{\mu\nu} = H^{(\lambda)}_{\mu\nu} + \sum_{\bar{k}} \left\langle \mu\nu \,\|\, \bar{k} \right\rangle^{(\lambda)} (x_{\bar{k}} + z_{\bar{k}}) + \sum_{\bar{k}} \left\langle \mu\nu \,\|\, \bar{k} \right\rangle q'_{\bar{k}}. \tag{5.55}$$

The calculation of these matrix elements is analogous to corresponding contributions to the ADFT gradients [99]. Employing integral screening and the double asymptotic expansion for the three-center ERI derivatives [89] a sub-quadratic scaling for the evaluation of these matrix elements can be reached. Once the $\mathbf{L}$ matrix is calculated it is transformed to the MO representation,

$$L_{ia} = \sum_{\mu,\nu} c_{\mu i} L_{\mu\nu} c_{\nu a}. \tag{5.56}$$

This step scales as $\mathcal{O}(n^3)$. However, by employing optimized BLAS routines [107–111] this cubic scaling is efficiently suppressed. The L_{ia} matrix elements are then scaled with the corresponding MO energy differences,

$$L'_{ia} = \frac{L_{ia}}{\epsilon_i - \epsilon_a}, \tag{5.57}$$

and summed together with S'_{ia} matrix elements defined as,

$$S'_{ia} = \frac{\epsilon_i \mathcal{S}^{(\lambda)}_{ia}}{\epsilon_i - \epsilon_a}, \tag{5.58}$$

yielding the **Q** matrix:

$$Q_{ia} = L'_{ia} + S'_{ia}. \tag{5.59}$$

With this **Q** matrix, Eq. (5.48) can be rewritten as,

$$b_{\bar{n}}^{(\lambda)} = \sum_{i}^{occ}\sum_{a}^{uno}\sum_{\sigma,\tau} Q_{ia}c_{\sigma i}c_{\tau a}\left\langle \sigma\tau \,\|\, \bar{n}\right\rangle - \frac{1}{8}\sum_{\mu,\nu}\sum_{\sigma,\tau} P_{\sigma\mu}S^{(\lambda)}_{\mu\nu}P_{\nu\tau}\left\langle \sigma\tau \,\|\, \bar{n}\right\rangle - \frac{1}{4}\sum_{\bar{k}} G^{(\lambda)}_{\bar{n}\bar{k}}x_{\bar{k}} + \frac{1}{4}\sum_{\sigma,\tau} P_{\sigma\tau}\left\langle \sigma\tau \,\|\, \bar{n}\right\rangle^{(\lambda)}. \tag{5.60}$$

Transformation of the **Q** matrix into atomic orbital representation yields:

$$T_{\sigma\tau} = \sum_{i}^{occ}\sum_{a}^{uno} c_{\sigma i}Q_{ia}c_{\tau a}. \tag{5.61}$$

By inserting Eq. (5.61) into Eq. (5.60) we find for the perturbation vector elements,

$$b_{\bar{n}}^{(\lambda)} = \sum_{\sigma,\tau} T_{\sigma\tau}\left\langle \sigma\tau \,\|\, \bar{n}\right\rangle - \frac{1}{8}\sum_{\mu,\nu}\sum_{\sigma,\tau} P_{\sigma\mu}S^{(\lambda)}_{\mu\nu}P_{\nu\tau}\left\langle \sigma\tau \,\|\, \bar{n}\right\rangle - \frac{1}{4}\sum_{\bar{k}} G^{(\lambda)}_{\bar{n}\bar{k}}x_{\bar{k}} + \frac{1}{4}\sum_{\sigma,\tau} P_{\sigma\tau}\left\langle \sigma\tau \,\|\, \bar{n}\right\rangle^{(\lambda)}. \tag{5.62}$$

To proceed we introduce a matrix **V** with elements,

$$V_{\sigma\tau} = T_{\sigma\tau} - \frac{1}{8}\sum_{\sigma,\tau} P_{\sigma\mu}S^{(\lambda)}_{\mu\nu}P_{\nu\tau}. \tag{5.63}$$

All matrix-matrix multiplications in the above equations are performed with BLAS [107–111] routines that suppress their formal cubic scaling for the systems studied here. Once the **V** matrix is collected, Eq. (5.62) reduces to:

$$b_{\bar{n}}^{(\lambda)} = \sum_{\sigma,\tau} V_{\sigma\tau}\left\langle \sigma\tau \,\|\, \bar{n}\right\rangle - \frac{1}{4}\sum_{\bar{k}} G^{(\lambda)}_{\bar{n}\bar{k}}x_{\bar{k}} + \frac{1}{4}\sum_{\sigma,\tau} P_{\sigma\tau}\left\langle \sigma\tau \,\|\, \bar{n}\right\rangle^{(\lambda)}. \tag{5.64}$$

The first term is algebraically identical to the calculation of the **J** vector in the SCF procedure [81]. It possesses a formal scaling of $\mathcal{O}(n^3)$ but shows a sub-quadratic scaling if integral screening and double asymptotic expansions for the three-center ERIs are employed [81, 89]. The second term is calculated analogously to the corresponding contributions to the ADFT gradients [99] and thus the same routines can be used. The third term is calculated through the corresponding integral recurrence relations [81, 84]. After these operations, the perturbation vector is readily available to be used in the corresponding ADPT equation system. The memory requirement of this approach is no more than three N_{bas}^2 matrices and some N_{aux} vectors, which is roughly equivalent to the memory used during the SCF procedure. Therefore, if the SCF energy of a system can be calculated so can its perturbation vectors.

5.4 ADPT Eirola-Nevannlina Algorithm

To solve the ADPT equation system, Eq. (5.46), the inverse of the response matrix, $\mathbf{R} = \mathbf{G} - 4\mathbf{A} - 4\mathbf{AF}$, can be calculated. This is possible because the dimension of the ADPT response matrix ($N_{aux} \times N_{aux}$) is small compared to the ($N_{occ} \times N_{uno}$)$\times$($N_{occ} \times N_{uno}$) CPKS dimension [137]. Also, it is important to keep in mind that **R** is perturbation-independent. This is clearly an advantage, because regardless of the number of perturbations (or perturbation types), **R** remains unaltered. Thus, a single inversion is needed and $\mathbf{R}^{-1}$ can be stored on disk for later purposes. However, as system size grows, the response matrix **R** tends to become ill-conditioned. This leads to numerical instabilities during the matrix inversion. Therefore, a robust and efficient algorithm for large indefinite non-symmetric systems of linear equations is needed [148]. To this end iterative methods for linear equation systems are employed. They have the additional advantage that the time consuming AO to MO transformations associated with the calculation of the **A** matrix,

$$\left\langle i\nu \,\|\, \bar{k} \right\rangle = \sum_{\mu} c_{\mu i} \left\langle \mu\nu \,\|\, \bar{k} \right\rangle \;\; \forall \; \nu, \bar{k} \;\; \wedge \;\; i \in occ, \tag{5.65}$$

and,

$$\left\langle ia \,\|\, \bar{k} \right\rangle = \sum_{\nu} c_{\nu a} \left\langle i\nu \,\|\, \bar{k} \right\rangle \;\; \forall \; i, \bar{k} \;\; \wedge \;\; a \in uno, \tag{5.66}$$

can be avoided. It has been shown in the literature [137] that the $\mathcal{O}(n^4)$ scaling of these transformations with increasing system size becomes the computationally most demanding step in ADPT calculations. As an example, Figure 5.1 depicts computational timings for the calculation of **F** and **A** matrices of linear alkanes from $C_{10}H_{22}$ to $C_{100}H_{202}$. All calculations are performed on a single Intel Xeon X5675 @ 3.07 GHz processor with 2 GB RAM employing the VWN/TZVP/GEN-A2 methodology with the default adaptive grid [100, 116] accuracy of 10^{-5} a.u. in deMon2k. Up to 1 048 auxiliary-functions, the timings for both matrices are roughly the same. Then they split and for the biggest alkane, the time to calculate **A** is about 26 times the time spent to calculate **F**. As a result, even for medium-sized systems the calculation of the Coulomb matrix can become a computational bottleneck.

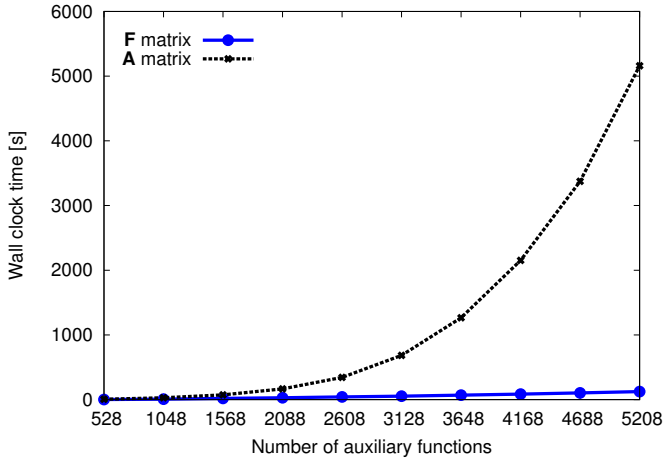

Figure 5.1: Wall clock times for the calculation of the kernel matrix **F** and Coulomb response matrix **A** of linear alkane chains. The VWN/TZVP/GEN-A2 level of theory was used.

To overcome this computational bottleneck and to obtain stable solutions for the ADPT equation system, our method of choice is a variant of the Eirola-Nevanlinna algorithm [149, 150]. Such an approach was implemented for the first time in our laboratory for the calculation of static polarizabilities of giant fullerenes with up to 960 carbon atoms [11, 151]. However, as opposed to polarizability calculations, the evaluation of analytic second-order energy-derivatives requires many individual perturbation calculations, namely three times the number of atoms in the system. For this reason, the perturbation-independence of the Coulomb response matrix **A** and the kernel matrix **F** can be computationally advantageous, despite their unfavorable scaling because they have to be calculated and stored only once. In analogy to the conventional SCF approach we name this implementation for the solution of the ADPT equation systems the conventional Eirola-Nevanlinna (Con-EN) method. A drawback of the Con-EN method is its rather large memory demand. As an example, take the calculation of the Coulomb response matrix for the carbon fullerene C_{540}. Employing the VWN/DZVP/GEN-A2 level of theory with 18 360 auxiliary-functions requires about 2.5 GB of available RAM per processor. To avoid the memory bottleneck of the Con-EN method, a direct variant, named the direct Eirola-Nevanlinna (Dir-EN) [11, 151] method, was implemented in deMon2k, too. It avoids the explicit calculation and storage of the **A** and **F** matrices. Instead it calculates directly the actions of these matrices on trial vectors. Take as an example the second term of Eq. (5.46) in which the Coulomb response matrix **A** is multiplied with perturbed Coulomb fitting coefficients:

$$a_{\bar{n}} = \sum_{\bar{k}} A_{\bar{n}\bar{k}} x_{\bar{k}}^{(\lambda)} = \sum_{\bar{k}} \sum_{i}^{occ} \sum_{a}^{uno} \langle \bar{n} \,\|\, ia \rangle \frac{1}{\epsilon_i - \epsilon_a} \left\langle ia \,\|\, \bar{k} \right\rangle x_{\bar{k}}^{(\lambda)}. \tag{5.67}$$

By expanding the MOs in the three-center ERIs, and rearranging terms, Eq. (5.67) can be rewritten as,

$$a_{\bar{n}} = \sum_{\mu,\nu} \langle \bar{n} \,\|\, \mu\nu \rangle \sum_{i}^{occ} \sum_{a}^{uno} c_{\mu i} c_{\nu a} \frac{1}{\epsilon_i - \epsilon_a} \sum_{\sigma,\tau} c_{\sigma i} c_{\tau a} \sum_{\bar{k}} \left\langle \sigma\tau \,\|\, \bar{k} \right\rangle x_{\bar{k}}^{(\lambda)}. \tag{5.68}$$

To proceed, a matrix $\mathbf{Q}$ is defined as,

$$Q_{\sigma\tau} = \sum_{\bar{k}} \left\langle \sigma\tau \,\|\, \bar{k} \right\rangle x_{\bar{k}}^{(\lambda)}. \tag{5.69}$$

The sum in Eq. (5.69) possesses a resembles the one appearing in the Kohn-Sham matrix construction in the SCF procedure [81], Eq. (3.28). Therefore, integral screening and double asymptotic ERI expansions [89] can be used to obtain an asymptotic $\mathcal{O}(N_{bas})$ scaling for the calculation of the $\mathbf{Q}$ matrix elements. Substituting Eq. (5.69) into (5.68) yields:

$$a_{\bar{n}} = \sum_{\mu,\nu} \langle \bar{n} \,\|\, \mu\nu \rangle \sum_{i}^{occ} \sum_{a}^{uno} c_{\mu i} c_{\nu a} \frac{1}{\epsilon_i - \epsilon_a} \sum_{\sigma,\tau} c_{\sigma i} Q_{\sigma\tau} c_{\tau a}. \tag{5.70}$$

The transformation of $\mathbf{Q}$ into MO representation, similar to Eq. (5.56), yields:

$$Q_{ia} = \sum_{\sigma,\tau} c_{\sigma i} Q_{\sigma\tau} c_{\tau a}. \tag{5.71}$$

The transformation is computationally further accelerated using BLAS [107–111] routines, such that the formal scaling of $\mathcal{O}(N_{bas}^3)$ is efficiently suppressed for the system sizes discussed here. Then, the resulting Q_{ia} elements are scaled with the corresponding MO energy differences,

$$Q'_{ia} = \frac{Q_{ia}}{\epsilon_i - \epsilon_a}. \tag{5.72}$$

Substituting Eq. (5.72) into Eq. (5.70) yields the following expression:

$$a_{\bar{n}} = \sum_{\mu,\nu} \langle \bar{n} \,\|\, \mu\nu \rangle \sum_{i}^{occ} \sum_{a}^{uno} c_{\mu i} Q'_{ia} c_{\nu a}. \tag{5.73}$$

Next, the Q'_{ia} matrix elements are transformed into AO representation,

$$T_{\mu\nu} = \sum_{i}^{occ} \sum_{a}^{uno} c_{\mu i} Q'_{ia} c_{\nu a}. \tag{5.74}$$

By inserting Eq. (5.74) into (5.73), it follows that,

$$a_{\bar{n}} = \sum_{\mu,\nu} \langle \bar{n} \,\|\, \mu\nu \rangle \, T_{\mu\nu}. \tag{5.75}$$

This equation is algebraically identical to the one for the calculation of the Coulomb vector **J**, Eq. (3.25). Integral screening and double asymptotic expansions for the three-center ERIs can be used [81, 89] to reduce the scaling from $\mathcal{O}(N_{bas}^3)$ to well below $\mathcal{O}(N_{bas}^2)$. Similarly, the third term in Eq. (5.46) can be expanded as,

$$\alpha_{\bar{n}} = \sum_{\bar{k},\bar{m}} A_{\bar{n}\bar{k}} G^{-1}_{\bar{k}\bar{m}} \sum_{\bar{l}} \left\langle \bar{m} \right| f_{xc}[\tilde{\rho}] \left| \bar{l} \right\rangle x_{\bar{l}}^{(\lambda)}. \tag{5.76}$$

For the efficient calculation of this term, a vector **q** is defined,

$$q_{\bar{m}} = \sum_{\bar{l}} \left\langle \bar{m} \right| f_{xc} \left[\tilde{\rho}\right] \left| \bar{l} \right\rangle x_{\bar{l}}^{(\lambda)} = \left\langle \bar{m} \right| f_{xc} \left[\tilde{\rho}\right] \left| \sigma \right\rangle. \tag{5.77}$$

with,

$$\sigma(\mathbf{r}) = \sum_{\bar{l}} x_{\bar{l}}^{(\lambda)} \bar{l}(\mathbf{r}). \tag{5.78}$$

Eq. (5.77) and (5.78) have a similar structure to Eq. (5.52) and Eq. (5.53). Thus, the same algorithm can be used for its calculation. Afterwards the **q** vector is multiplied with the inverse of the Coulomb **G** matrix previously stored on hard disk:

$$q'_{\bar{k}} = \sum_{\bar{m}} G^{-1}_{\bar{k}\bar{m}} q_{\bar{m}}. \tag{5.79}$$

Ultimately, by inserting Eq. (5.77), (5.78) and (5.79) into (5.76) we obtain:

$$\alpha_{\bar{n}} = \sum_{\bar{k}} A_{\bar{n}\bar{k}} q'_{\bar{k}}. \tag{5.80}$$

Eq. (5.80) has the same structure as (5.67), and, therefore, it is calculated by the same approach. This reduces the formal scaling for the solution of the ADPT equation system to $\mathcal{O}(N_{bas}^3)$. Even more important, the Dir-EN method has a reduced memory demand. It requires about $2N_{bas}^2$ matrices and a few N_{aux} vectors, compared to the $N_{bas} \times N_{occ} \times N_{uno}$ memory demand for the explicit Coulomb response matrix calculation. This permits ADPT calculations on systems with thousand and more atoms. As in the direct SCF algorithm, the Dir-EN method requires the repetitive calculation of three-center ERIs in each iteration step of the EN algorithm. For many perturbations, as needed for the calculation of analytic second-order energy-derivatives, this repetitive ERI calculation is usually the most demanding computational task in the Dir-EN method. Fortunately, three-center ERI calculation is well developed in deMon2k [81, 84, 89] and also very well parallelized [152].

Once the ADPT equation system is solved and the perturbed fitting coefficients, $x_{\tilde{k}}^{(\lambda)}$, are obtained the calculations of the needed perturbation matrix and vector elements are straightforward. First, the perturbed exchange-correlation fitting coefficients, $z_{\tilde{k}}^{(\lambda)}$, are obtained according to Eq. (5.38). Then, the perturbed Kohn-Sham matrix elements, Eq. (5.37), are calculated with the perturbed Coulomb and exchange-correlation fitting coefficients. Afterwards, the perturbed Kohn-Sham matrix elements are transformed into the MO representation using Eq. (5.28) and the perturbed density matrix is calculated according to Eq. (5.36). Once the perturbed density and Kohn-Sham matrix are available the perturbed energy-weighted density matrix can be calculated as,

$$W_{\mu\nu}^{(\lambda)} = \frac{1}{2} \sum_{\sigma,\tau} \left(P_{\mu\sigma}^{(\lambda)} K_{\sigma\tau} P_{\tau\nu} + P_{\mu\sigma} K_{\sigma\tau}^{(\lambda)} P_{\tau\nu} + P_{\mu\sigma} K_{\sigma\tau} P_{\tau\nu}^{(\lambda)} \right). \tag{5.81}$$

With all the perturbed matrix and vector elements at hand, the corresponding contributions to the Hessian matrix, Eq. (4.23), can be calculated. Figures 5.2 and 5.3 depict the flowcharts of the analytic frequency module in deMon2k employing the Con-EN and Dir-EN method, respectively.

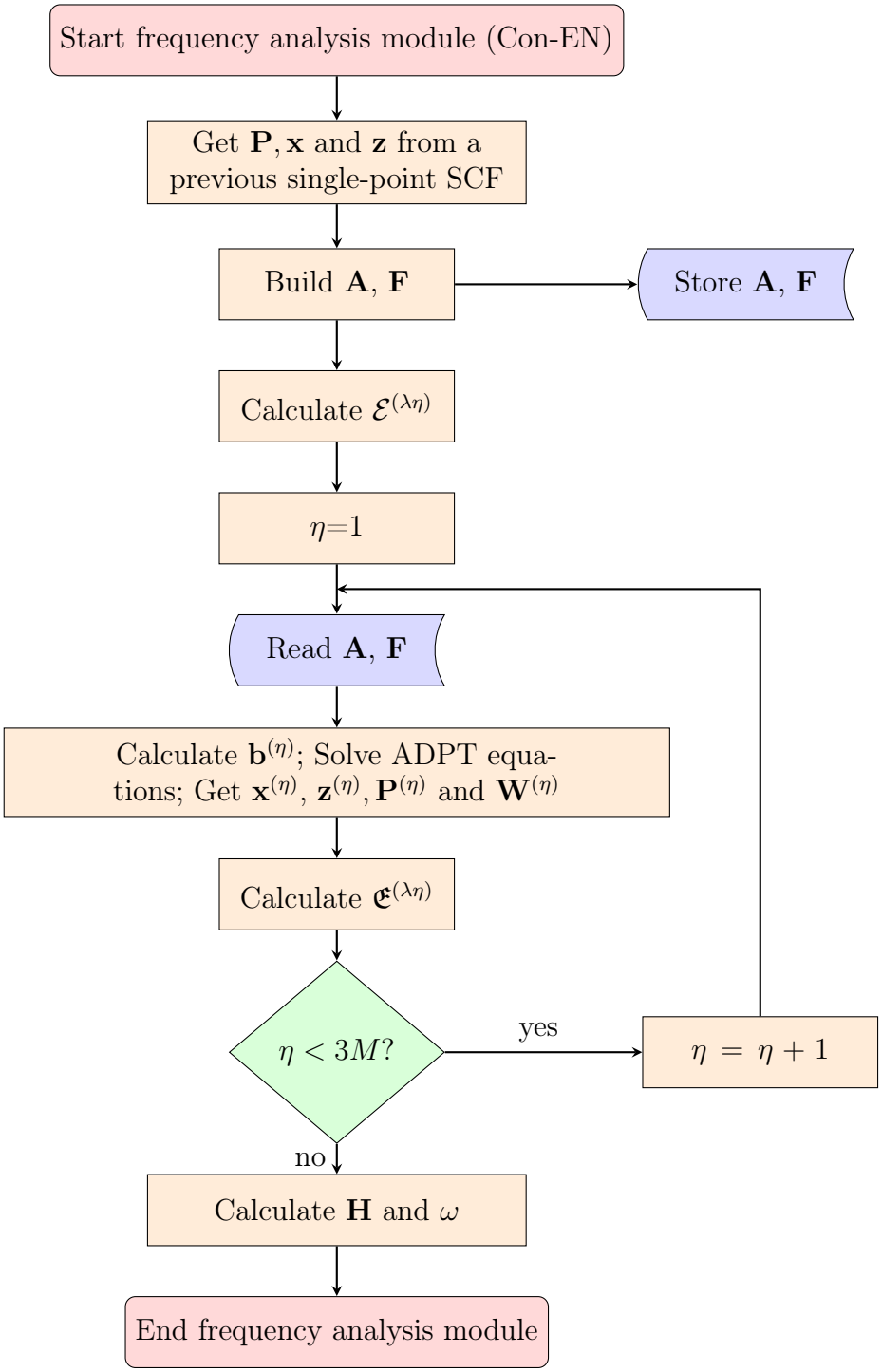

Figure 5.2: Flowchart of the analytic frequency module in deMon2k using the Con-EN method. See text for further details.

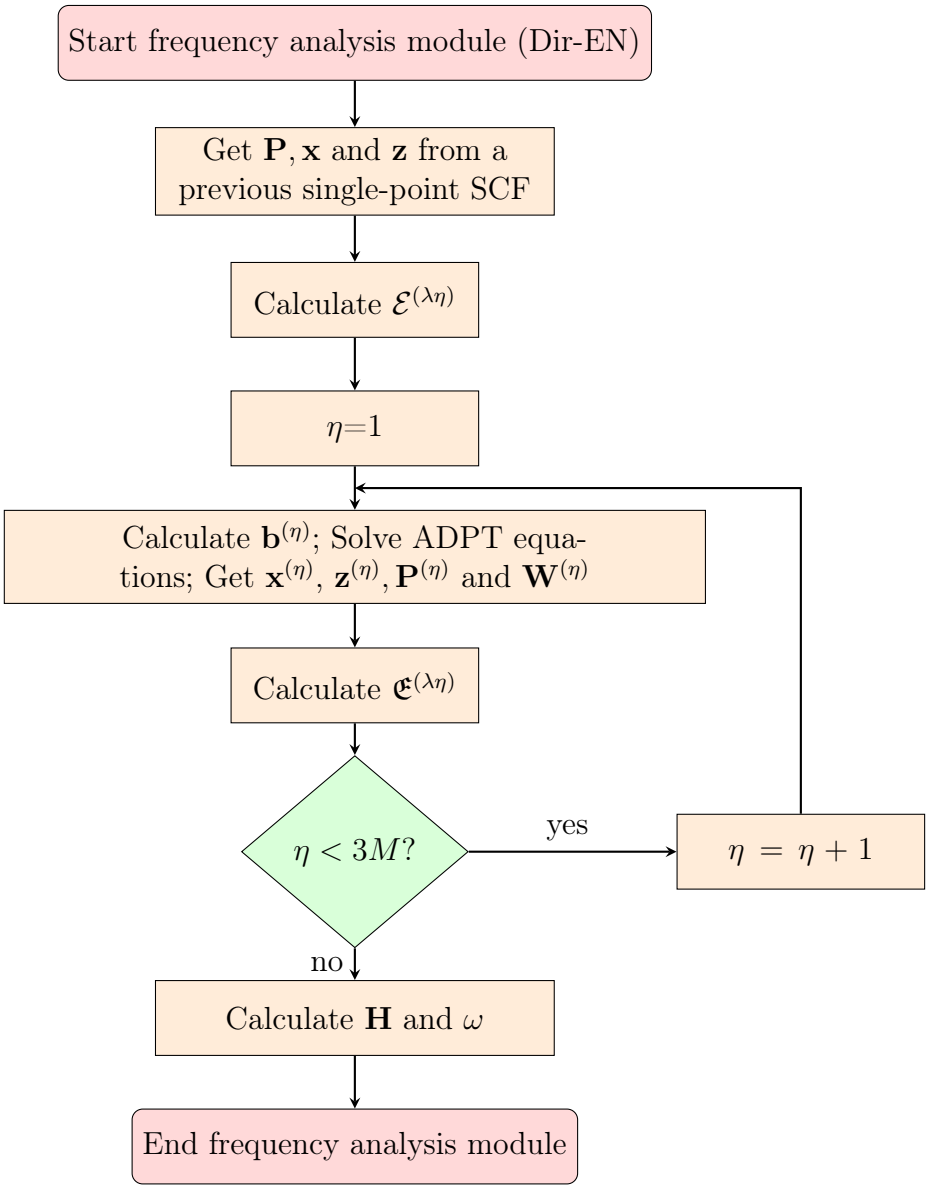

Figure 5.3: Flowchart of the analytic frequency module in deMon2k using the Dir-EN method. Note that the calculation of $\mathbf{A}$ and $\mathbf{F}$ and the corresponding I/O operations are absent. See text for further details.

In order to test the serial computational performance of the second-order ADFT-energy derivatives harmonic vibrational frequencies of alkane chains containing 10 to 100 carbon atoms were calculated on an Intel Xeon X5675 @ 3.07 GHz processor with a maximum of 2 GB of allocatable RAM. In Figure 5.4 the CPU timings for the frequency analysis calculations employing the analytic Con-EN and Dir-EN algorithms are compared to the corresponding timings of the numerical finite-difference (FD-ADFT) method. All calculations were performed using the DFT optimized TZVP basis set [153] in combination with the automatically-generated GEN-A2* auxiliary-function set [83]. The SCF energy convergence criterion [102] and grid tolerance were set to 5×10^{-7} a.u. and 10^{-6} a.u., respectively. These calculations were performed with the local density approximation (LDA) using the Dirac exchange [32] and VWN [40] correlation functionals. The corresponding exchange-correlation kernel was calculated analytically. The structure parameters were optimized prior to the frequency analyses and the default settings of deMon2k are used [154].

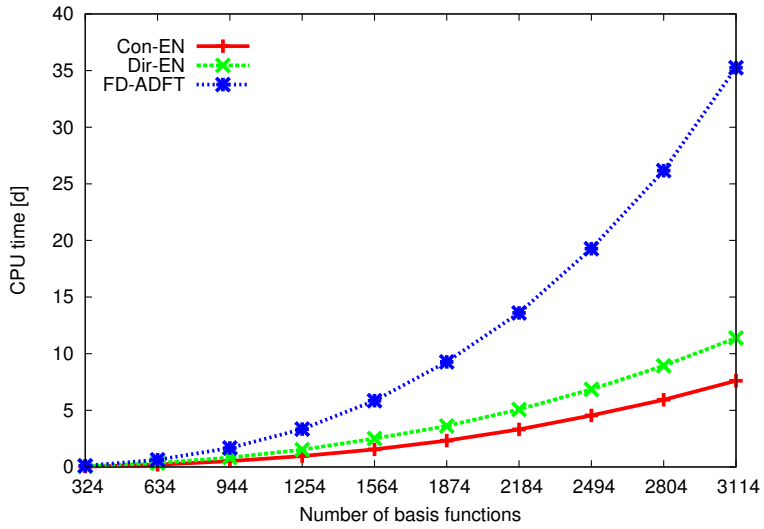

Figure 5.4: CPU time in days for the frequency analysis with the conventional EN (Con-EN), direct EN (Dir-EN) and numerical finite-difference (FD-ADFT) algorithm of linear alkane chains C_nH_{2n+2} with $n = 10, 20, ..., 100$.

For all system sizes the analytic second-order derivative calculations are clearly faster than their numerical counterpart. The difference is even more noticeable with increasing system size. From the two analytic approaches the one that employs the Con-EN algorithm for the

solution of the ADPT equations systems is the computationally most efficient. This indicates that for the one-dimensional systems studied here the higher-order scaling of the explicit **A** matrix calculation, Eq. (5.43), is overcompensated by the increasing vibrational degrees of freedom with system size. As a result, the Con-EN algorithm in which the perturbation-independent **A** matrix is calculated only once outperforms the direct approach. Therefore, the use of the Con-EN algorithm will be bounded by memory, rather than CPU time.

5.5 Parallelization

Because the calculation of $\mathfrak{E}^{(\lambda\eta)}$, Eq. (4.23), is computationally most demanding two different parallelization schemes were implemented in deMon2k. The first one is inspired by the already available parallel finite-difference calculation of second-order energy-derivatives in deMon2k [154] using the Message Passing Interface (MPI) [155]. It distributes the nuclear displacements across a number of processors, where each CPU works independently on a previously assigned set of perturbations. As a result the number of perturbations per processor is given as:

$$\#\text{ of perturbations per processor} \approx \text{Int}\left(\frac{3M}{\#\text{ of processors}}\right). \tag{5.82}$$

The scheme is called *parallelization over the perturbations*, and is triggered in deMon2k by the keyword PARALLEL HXYZ. This is the default for parallel analytic second-order derivative calculations. It is the method of choice for high-performance computing architectures. In this setup, each processor requires a complete set of data, namely the fitting coefficients, $x_{\bar{k}}$ and $z_{\bar{k}}$, the density matrix elements $P_{\mu\nu}$ and, if the Con-EN variant is used, the response matrices **A** and **F** which can reside in RAM or on hard disk. The parallelization over the perturbations minimizes the communication between processors, therefore showing a consistent speed-up with increasing number of processors in a calculation. Figures 5.5 and 5.6 depict the flowcharts of the parallel frequency module in deMon2k employing the Con-EN and Dir-EN method, respectively.

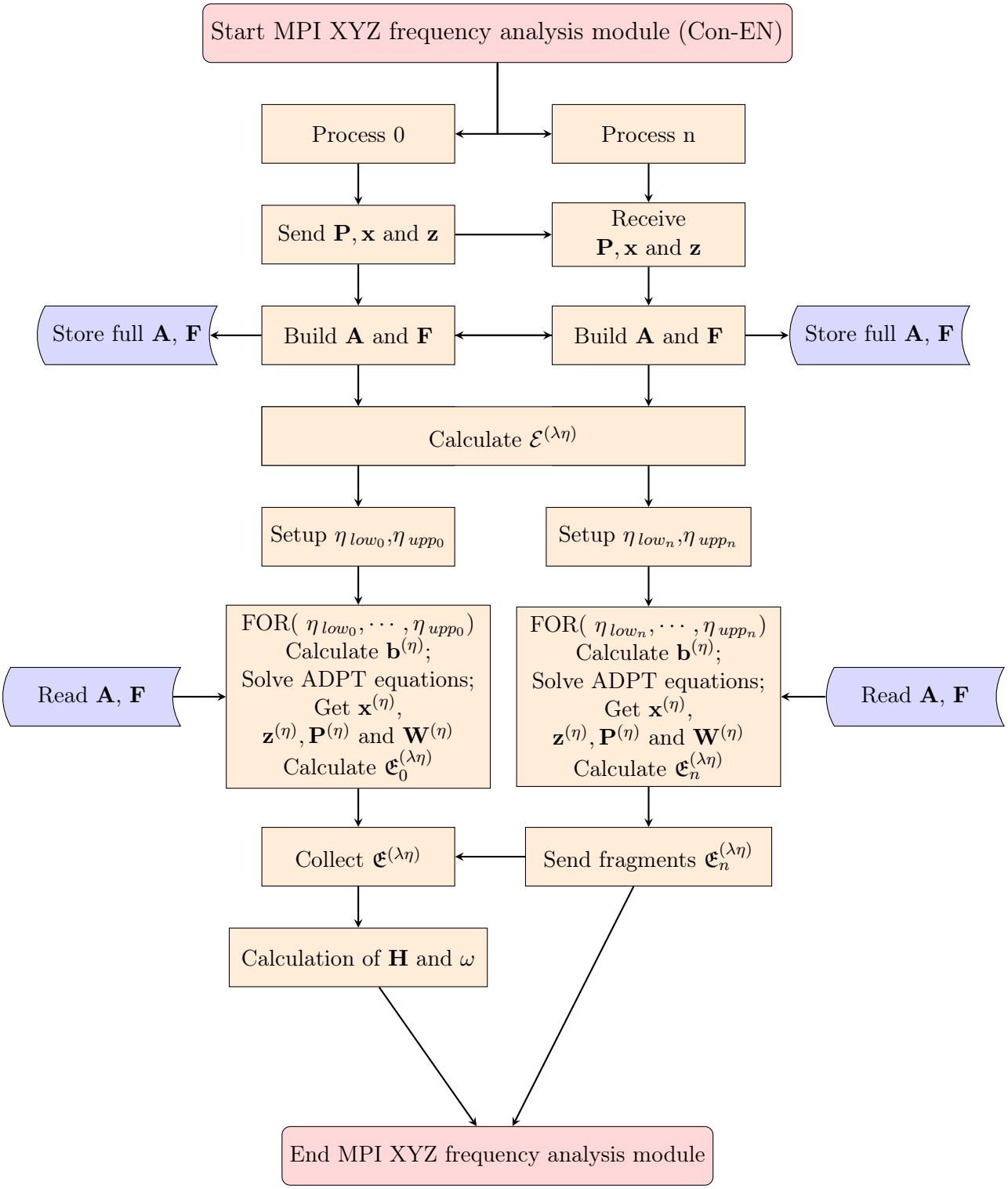

Figure 5.5: Flowchart of XYZ parallel frequency analysis with the Con-EN method.

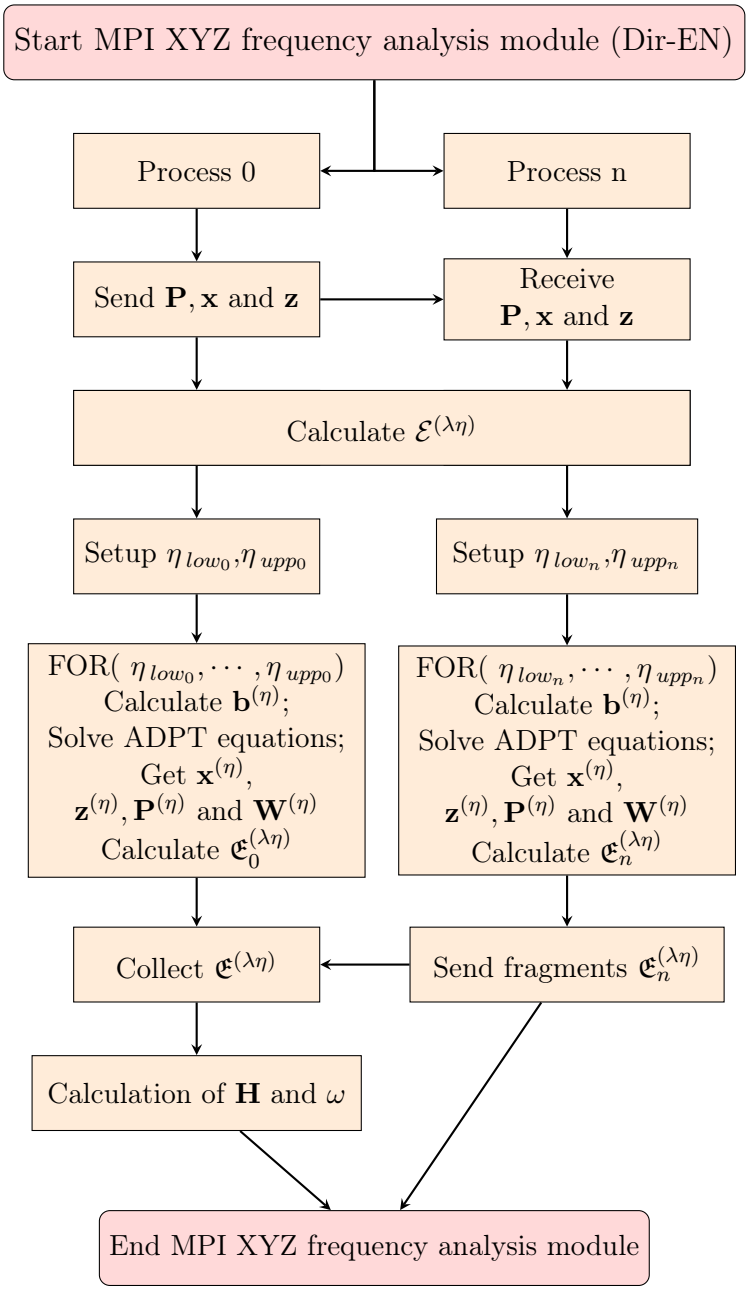

Figure 5.6: Flowchart of XYZ parallel frequency analysis with the Dir-EN method.

As example, the frequency analysis of the C_{240} fullerene was performed on 48, 72, 80, 120, 144, 240, 360 and 720 Intel®Xeon®L5520 @ 2.27GHz processors with 1.5 GB of RAM at the VWN/DZVP/GEN-A2 level of theory. The Dir-EN method was used in order to maintain memory allocation as small as possible. Whereas the frequency calculation performed with 48 processors needed about 3 days to finish, the same calculation employing 720 processors finished in about 8 hours. Figure 5.7 depicts the reciprocal time spent for a parallel run with increasing number of processors.

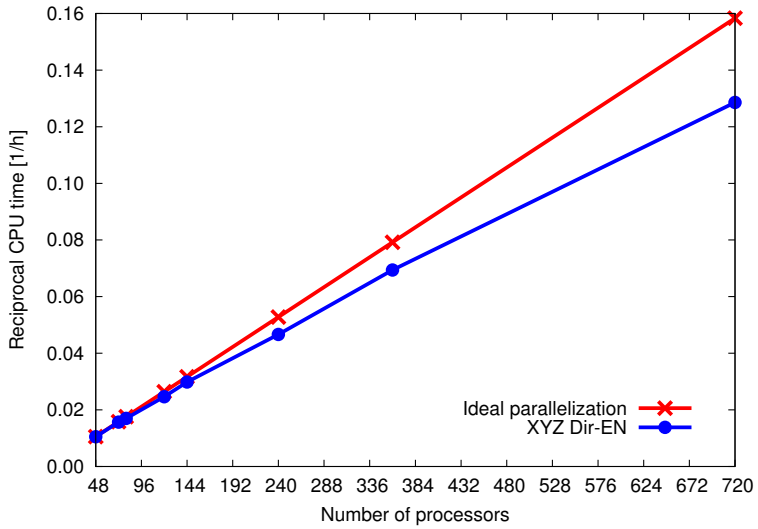

Figure 5.7: Reciprocal CPU time [h^{-1}] for C_{240} frequency analysis as a function of processors used in parallel runs. The actual data points of XYZ Dir-EN calculations are connected by a solid line to guide the eye.

The red line represents the ideal parallelization, where the calculation time is halved as the number of processors is doubled. The blue line connects data points obtained with our parallelization scheme. As the blue line is nearer to the red line, the parallel performance approaches its ideal behavior. As Figure 5.7 shows, our data points behave in a very satisfactory way with increasing number of processors, in the sense that their reciprocal timing is monotonically increasing. A drawback of this parallelization scheme is the existence of an upper limit for the number of processors, namely three times the number of atoms in the system, i.e., one perturbation per processor. In our example, the frequency analysis of the C_{240} fullerene can make use of at most 720 processors. Besides, as the studied systems

increase in size, hard disk intensive I/O saturation and/or RAM memory exhaustion, mainly in the Con-EN method, can hinder the efficiency of this scheme.

To overcome this limitation, the second implemented parallelization scheme focuses on the distribution of data across the processors. In this setup all processors work simultaneously on the same task, i.e., the same nuclear displacement, and the work of the task is parallelized. This is called *parallelization over the SCP* and is triggered in deMon2k by the keyword PARALLEL HSCP. Only one processor hosts the complete set of matrices and files and accesses the hard disk. Figures 5.8 and 5.9 show simplified flowcharts depicting how this parallel scheme works. When a task is declared, i.e., the linear algebra or the integral derivative calculation, the required subsets of data are distributed over all processors and the task itself is executed. As a consequence, if a processor finishes its part of a task earlier than the others, it must wait for them to complete their contributions before the next perturbation cycle, $\eta + 1$, begins. Therefore, this data distribution avoids parallel hard disk I/O and minimizes RAM allocation, but might show a less optimal work load distribution. It is our method of choice for larger system sizes where the parallelization over the perturbation fails due to RAM and/or storage limitations. Note also that the number of processors used in this setup is not bound by the number of perturbations. Table 5.1 compares both parallelization schemes in terms of characteristics that have to be taken into account in order to choose the optimal parallelization according to individual hardware setups.

Table 5.1: Comparison of parallelization schemes.

Parallelization scheme	XYZ	SCP
Maximum number of processors	3M	Unlimited
Cycles performed to calculate $\mathfrak{E}^{(\lambda\eta)}$	$(3M/N_{proc})$	3M
Memory and storage demand	High	Low

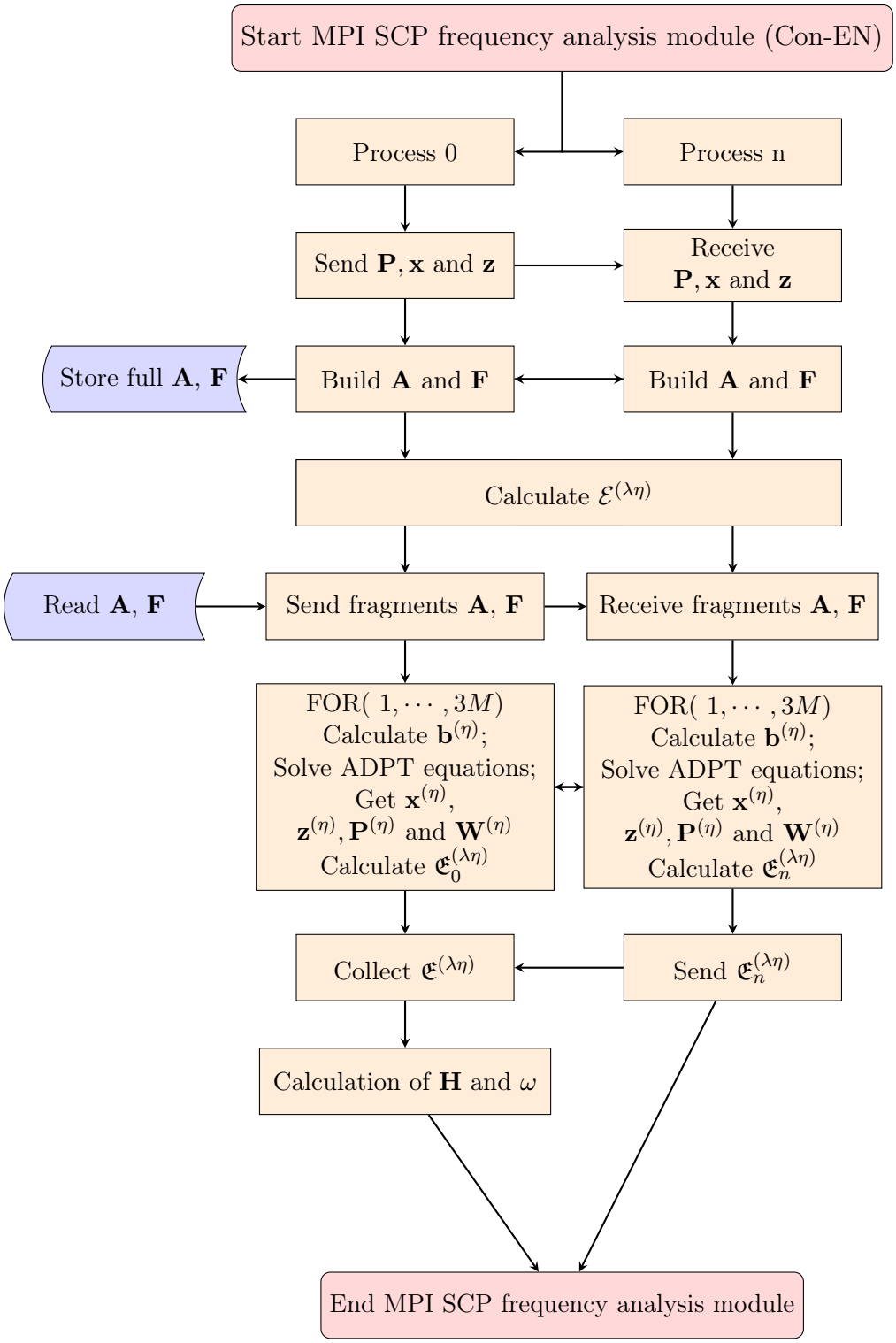

Figure 5.8: Flowchart of SCP parallel frequency analysis with the Con-EN method.

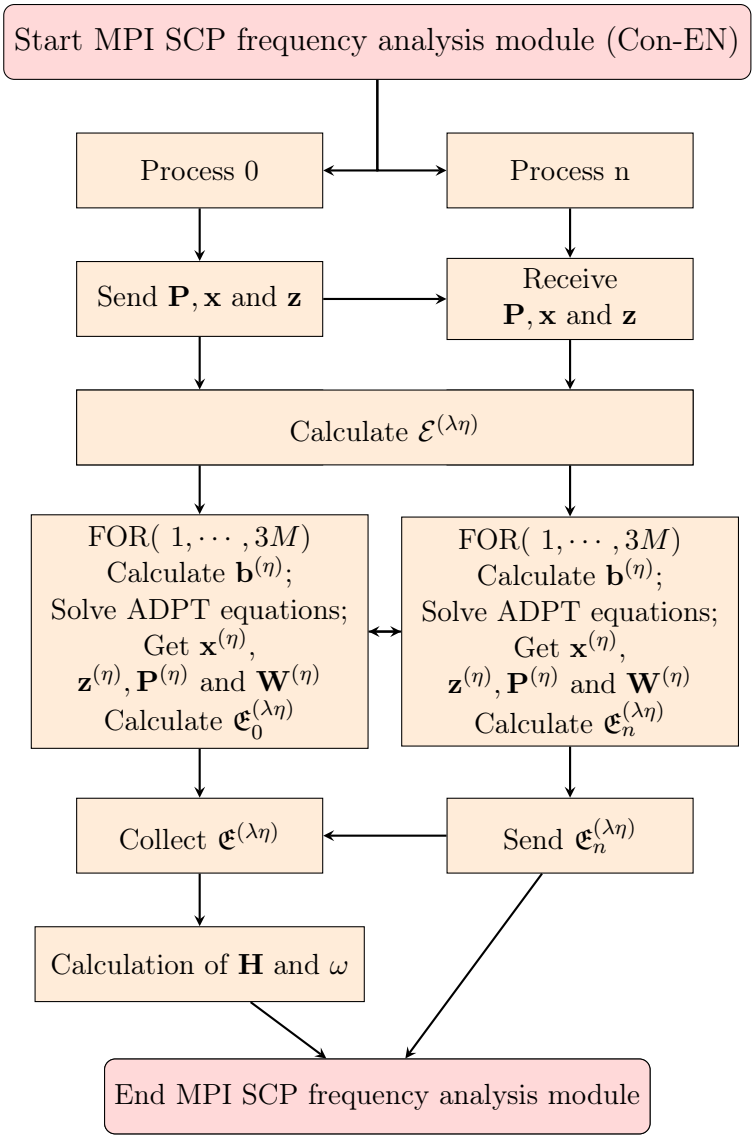

Figure 5.9: Flowchart of SCP parallel frequency analysis with the Dir-EN method.

For the sake of clarity, let us compare the memory allocation of both parallelization schemes for frequency analyses of the C_{540} fullerene that are intended to be performed on 48, 72, 80, 120, 144, 240, 360 and 720 processors at the VWN/DZVP/GEN-A2 level of theory, using the Con-EN method. Employing the XYZ parallelization scheme, the kernel matrix **F**, with an approximate size of 2.5 GB, has to be stored in RAM as many times as threads are requested. The red line in Figure 5.10 illustrates this RAM allocation.

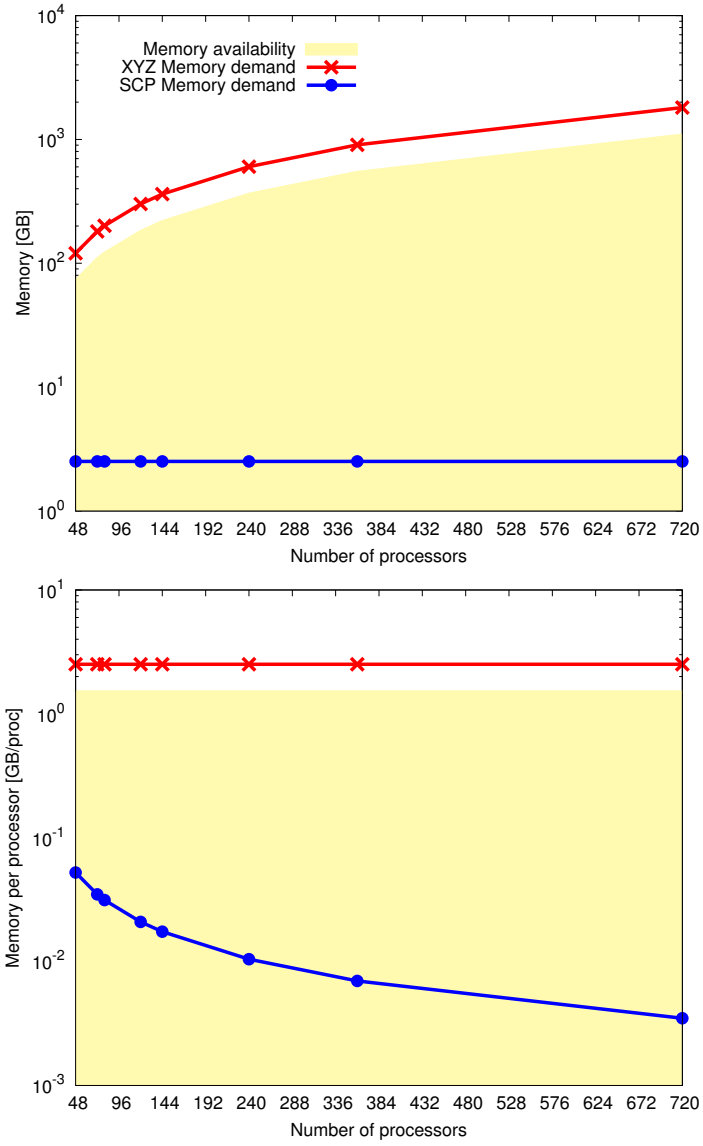

Figure 5.10: RAM demand of different parallelization schemes. On the top the total RAM allocation is depicted whereas on the bottom the allocation per core is displayed.

If the calculation is intended to be performed on processors with 1.5 GB of RAM each, the required memory will surpass the memory available on the system. Thus, a frequency analysis with the XYZ parallel scheme is impossible. On the other hand, the SCP parallelization scheme requires only one **F** matrix which is distributed over all processors. This means that RAM allocation of **F** per processor actually decreases as the number of processors increases. This behavior is shown as the blue line in Figure 5.10. The drawback of this scheme is that as more threads are requested, the processor communication overhead affects severely the parallel performance [156].

Chapter 6

ALGORITHMIC APPLICATIONS OF SECOND DERIVATIVES

6.1 Restricted Step Algorithm for Optimization

The method of choice for local structure optimizations, i.e., minimization or transition state search, is in many quantum chemical programs the restricted-step algorithm from Levenberg and Marquardt [157, 158]. In this method a trust region is defined in which the quadratic expansion of the potential energy surface (PES) is minimized. The corresponding Levenberg-Marquardt step is given by,

$$\Delta\mathbf{r} = -(\mathbf{H} - \lambda\mathbf{E})^{-1}\mathbf{g}. \tag{6.1}$$

Here $\mathbf{g}$ and $\mathbf{H}$ denote the energy gradient vector and Hessian matrix, respectively. The nuclear displacement according to the Levenberg-Marquardt step is given by $\Delta\mathbf{r}$ and λ is an undefined Lagrange multiplier arising from the constraint that the step must reside inside a given trust region. It has been shown by Fletcher [159] that such a sequence of Levenberg-Marquardt steps converges to a local minimum. However, the choice of λ is critical for this convergence to a local minimum and also for the overall performance of the method,

i.e., in how many steps a converged solution is found. For minimizations[1] Nocedal and Wright [161] described a three-case approach that always provides the "best" λ in terms of method performance. This algorithm is implemented in deMon2k [160] and shows superb performance if numerically stable gradients and Hessian matrices are provided. However, because of the computational demand associated with the quantum chemical calculations of the Hessian matrix, restricted-step algorithms for structure optimization are often formulated as quasi-Newton methods [98]. In these methods the explicit calculation of the Hessian matrix is substituted by its successive update with gradient and step vectors [86–88, 162]. For structure minimizations the so-called BFGS update has proven particularly useful because it generates positive-definite approximations of the Hessian matrix. Whereas the BFGS quasi-Newton restricted-step algorithm shows similar performance as its Newton counterpart, i.e., a restricted-step algorithm in which the Hessian matrix is calculated in each step, molecular structure minimization is very sensitive to the choice of the initial Hessian matrix [160, 163]. In particular, more complicated molecular structures usually fail to optimize to a local minimum if the initial Hessian matrix is approximated by a force field [164–166]. Instead they optimize to higher-order critical points on the PES. The initial calculation of the Hessian matrix cures this algorithmic problem in a rather satisfying way. Therefore, the efficient calculation of the Hessian matrix is of great importance for the local minimization of complex molecular structures.

Besides molecular structure optimization, the Hessian matrix must also be calculated for local transition state searches employing an uphill-trust region method [167, 168]. Here the calculation of the initial Hessian matrix is mandatory in order to define the uphill search direction by the Hessian eigenmode with negative curvature. Similarly, for the initial step of a intrinsic reaction coordinate (IRC) [169] calculation the Hessian matrix of the transition state must be calculated in order to determine the "transition mode", i.e., the Hessian eigenmode with negative curvature. Therefore, all the above discussed computational methods benefit from efficient and numerically stable analytical calculation of the Hessian matrix.

[1] For an in-depth discussion of restricted-step algorithm methods for unconstrained and constrained structure optimizations as well as transition state searches we refer the interested reader to Ref. 160.

6.2 Harmonic Vibrational Analysis

Vibrational spectroscopy is one of the most widely used techniques for the determination, identification and characterization of molecular structures. Quantum chemical calculations can be a reliable tool for the qualitative assignment of experimental spectra. This can become particularly important for large molecules with many degrees of freedom where normal modes become too complicated to be anticipated only by chemical intuition. In this section we discuss how IR and Raman spectra can be calculated from second- and third-order analytic ADFT-energy derivatives.

6.2.1 Harmonic IR Spectra Simulation

In the harmonic approximation the potential energy of a polyatomic system near a reference coordinate $\mathbf{R}_0$, is expanded up to the quadratic term as a Taylor series. For sufficiently small amplitudes of vibration, the higher-order terms are neglected [170]:

$$V(\mathbf{R}_0 + \Delta\mathbf{R}) = V(\mathbf{R}_0) + \sum_{i}^{3M} \frac{\partial V}{\partial R_i}\Delta R_i + \sum_{i,j}^{3M} \frac{\partial^2 V}{\partial R_i \partial R_j}\Delta R_i \Delta R_j. \tag{6.2}$$

The constant term V($\mathbf{R}_0$) can be taken as reference and set to zero for the following discussion. If $\mathbf{R}_0$ is assumed to be a stationary point, then the gradient of the potential with respect to the nuclear position will vanish and Eq. (6.2) can be rewritten as,

$$V(\mathbf{R}_0 + \Delta\mathbf{R}) = \sum_{i,j}^{3M} \frac{\partial^2 V}{\partial R_i \partial R_j}\Delta R_i \Delta R_j. \tag{6.3}$$

Eq. (6.3) can be transformed into mass-weighted Cartesian coordinates (MWC) according to the reference coordinates $\mathbf{R}_0$ by:

$$\Delta R_i = \frac{\Delta R'_i}{\sqrt{m_i}} \implies \frac{\partial}{\partial R_i} = \sqrt{m_i}\frac{\partial}{\partial R'_i}, \tag{6.4}$$

where $\sqrt{m_i}$ denotes the square root of the mass of the atom associated with the Cartesian coordinate R_i. The substitution of (6.4) into (6.3) yields:

$$V(\mathbf{R}'_0 + \Delta\mathbf{R}') = \sum_{i,j}^{3M} \frac{\partial^2 V}{\partial R'_i \partial R'_j} \Delta R'_i \Delta R'_j. \tag{6.5}$$

The potential can be transformed to a set of normal coordinates $\mathbf{Q}$ where each one of these coordinates is associated with one mode of motion, be it a rotation, translation or vibration. These coordinates are defined in terms of the MWC by an orthogonal transformation:

$$\Delta Q_k = \sum_{i}^{3M} \Delta R'_i D_{ik}, \tag{6.6}$$

$$\Delta R'_i = \sum_{k}^{3M} \Delta Q_k D_{ki}. \tag{6.7}$$

The D_{ik} matrix elements, which will be calculated later on, are defined by,

$$\sum_{i,j}^{3M} D_{ik} \frac{\partial^2 V}{\partial R'_i \partial R'_j} D_{jl} = \omega_k \delta_{kl}. \tag{6.8}$$

Note that the indices i and j refer to the MWC coordinates, whereas the indices k and l refer to the normal coordinates. By the substitution of (6.7) into (6.5), employing Eq. (6.8), the following expression is obtained:

$$V(\mathbf{Q}_0 + \Delta\mathbf{Q}) = \sum_{k,l}^{3M} \Delta Q_k \omega_k \delta_{kl} \Delta Q_l = \sum_{k}^{3M} \omega_k \Delta Q_k^2. \tag{6.9}$$

Eq. (6.9) has the same form as the potential operator for a multi-dimensional quantum harmonic oscillator [171], which contains the information of its fundamental frequency for a given mode. If we place the origin of Eq. (6.9) in the same point as the minimum point of the potential energy surface $E(\mathbf{Q}_0)$, the lower portion of $V(\mathbf{Q})$ will exactly coincide with the one of $E(\mathbf{Q})$. Thus, the harmonic oscillator force constant ω_k for a given vibrational mode should

coincide with the Hessian matrix transformed to the normal coordinate representation:

$$\omega_k = \frac{\partial^2 E}{\partial Q_k^2} \,. \tag{6.10}$$

For the $3M$ degrees of freedom of a molecule with M atoms, three of them are connected with translational motions as a whole and another three (two for a linear molecule) correspond to the rotation of the molecule as a whole. We will refer to these six (five) motions, depicted in Figure 6.1, as *external degrees of freedom*.

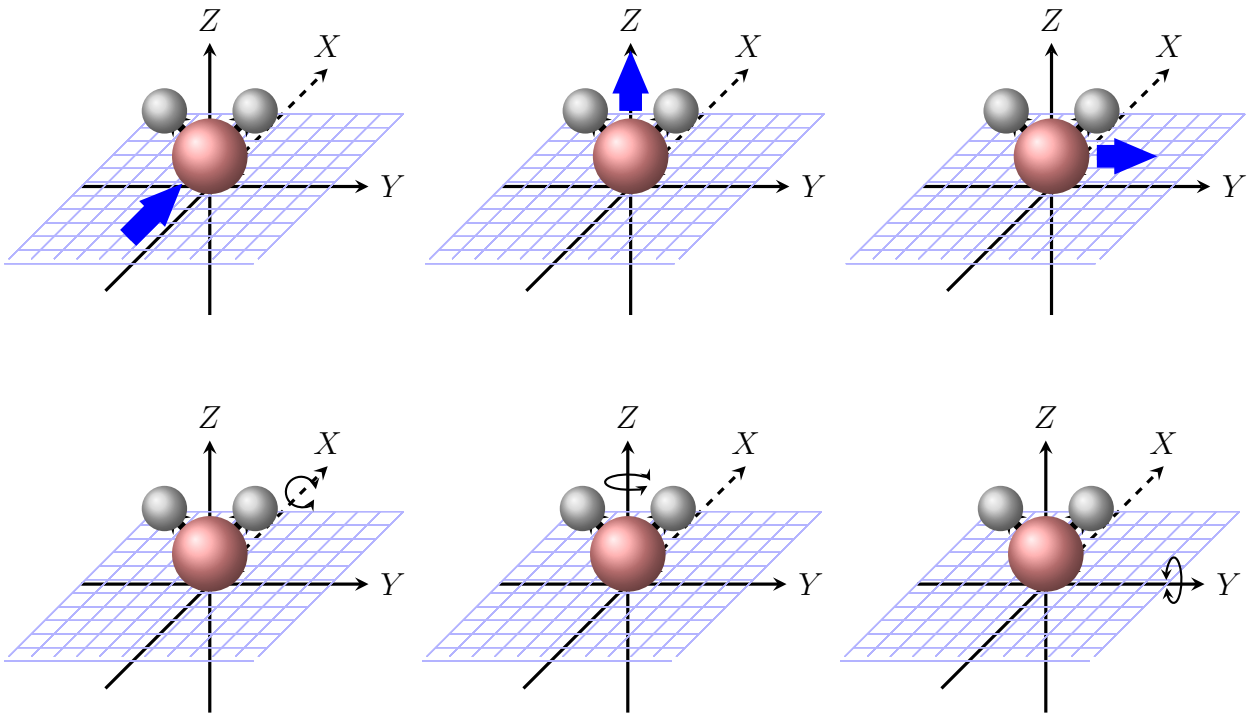

Figure 6.1: External degrees of freedom of a molecule.

In the normal coordinate frame, the external degrees of freedom are expected to have zero frequency. As a consequence, the second-order energy-derivatives with respect to the normal coordinates $\partial^2 E/\partial Q_k^2$ for the corresponding rotation and translation modes vanish. Thus:

$$V(\mathbf{Q}_0 + \Delta\mathbf{Q}) = \sum_k^{3M-6} \omega_k \Delta Q_k^2. \tag{6.11}$$

In order to calculate the remaining $3M-6$ ($3M-5$) fundamental frequencies of the *internal*

degrees of freedom the corresponding $\partial^2 E/\partial Q_k^2$ must be calculated. To do so we assume that the Hessian matrix elements in MWC, $\mathscr{H}_{ij}$, at an equilibrium point are already calculated:

$$\mathscr{H}'_{ij} = \left(\frac{1}{\sqrt{m_i m_j}}\right) \frac{\partial^2 E}{\partial R_i \partial R_j} = \frac{\partial^2 E}{\partial R'_i \partial R'_j}. \tag{6.12}$$

The transformation to a set of coordinates ξ_k is defined by the following orthogonal transformation:

$$\Delta\xi_k = \sum_i^{3M} \Delta R'_i \Gamma_{ik}, \tag{6.13}$$

$$\Delta R'_i = \sum_k^{3M} \Delta\xi_k \Gamma_{ki}. \tag{6.14}$$

The Γ_{ik} matrix elements are calculated in the so-called standard orientation with the center of mass at the origin and the $\mathcal{Z}$ and $\mathcal{Y}$ axes along the first and second principal axes of the tensor of inertia. The transformation into standard orientation is depicted in Figure 6.2.

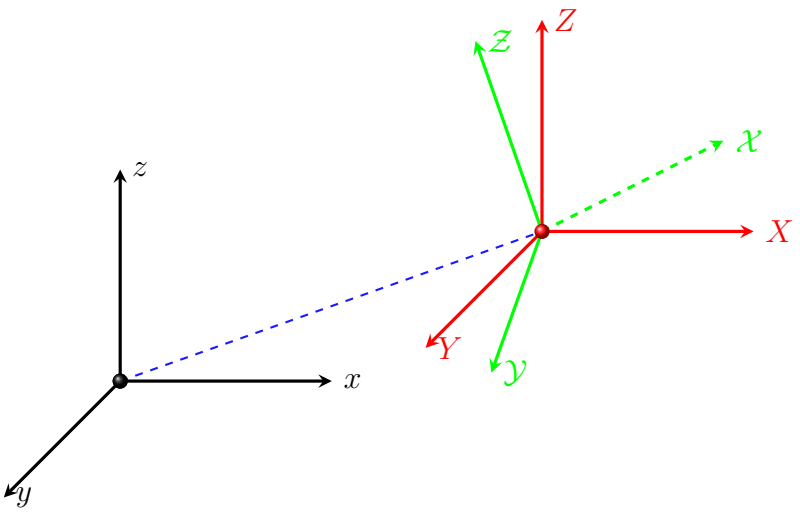

Figure 6.2: Coordinate systems for the transformation into standard orientation. The "xyz" system (black) represents the MWC coordinates. The "XYZ" system is parallel to "xyz", but its origin is now shifted to the center of mass. The "$\mathcal{XYZ}$" system (green) coincides with the principal axes of the tensor of inertia. This coordinate system represents the so-called standard orientation.

The three orthogonal vectors, $\mathbf{\Gamma}^{\text{trans}}$, of length $3M$ correspond to the translational degrees of freedom. Their elements are defined by:

$$[\mathbf{\Gamma}_x^{\text{trans}}]_{\mathbf{A}_i} = \delta_{xi}\sqrt{m_{\mathbf{A}}}, \tag{6.15}$$

$$[\mathbf{\Gamma}_y^{\text{trans}}]_{\mathbf{A}_i} = \delta_{yi}\sqrt{m_{\mathbf{A}}}, \tag{6.16}$$

$$[\mathbf{\Gamma}_z^{\text{trans}}]_{\mathbf{A}_i} = \delta_{zi}\sqrt{m_{\mathbf{A}}}. \tag{6.17}$$

The three orthogonal vectors, $\mathbf{\Gamma}^{\text{rot}}$, represent orthogonal rotations around the principal axes of the tensor of inertia $\mathbf{\Theta}$. These principal axes are obtained by diagonalization, i.e., $\tilde{\mathbf{U}}\mathbf{\Theta}\mathbf{U} = \mathbf{\Theta}_{diag}$. Their elements are calculated as,

$$[\mathbf{\Gamma}_{R_x}^{\text{rot}}]_{\mathbf{A}_i} = \left([P_{\mathbf{A}}]_y U_{iz} - [P_{\mathbf{A}}]_z U_{iy}\right)\sqrt{m_{\mathbf{A}}}, \tag{6.18}$$

$$[\mathbf{\Gamma}_{R_y}^{\text{rot}}]_{\mathbf{A}_i} = \left([P_{\mathbf{A}}]_z U_{ix} - [P_{\mathbf{A}}]_x U_{iz}\right)\sqrt{m_{\mathbf{A}}}, \tag{6.19}$$

$$[\mathbf{\Gamma}_{R_z}^{\text{rot}}]_{\mathbf{A}_i} = \left([P_{\mathbf{A}}]_x U_{iy} - [P_{\mathbf{A}}]_y U_{ix}\right)\sqrt{m_{\mathbf{A}}}, \tag{6.20}$$

where the $[P_{\mathbf{A}}]_j$ components appearing here are defined as,

$$[P_{\mathbf{A}}]_j = \sum_{i=x,y,z} R''_{\mathbf{A}_i} U_{ij}. \tag{6.21}$$

The $\mathbf{R}''_{\mathbf{A}}$ are the Cartesian coordinates of atom $\mathbf{A}$ with respect to the center of mass. If one of these vectors does not correspond to a rotation, namely $\mathbf{\Gamma}_n \cdot \mathbf{\Gamma}_n \approx 0$, the corresponding rotation mode is removed. After these vectors are normalized the remaining Γ_{ik} coefficients are generated by a Gram-Schmidt orthogonalization [172]. This process builds on the previously calculated orthogonal $\mathbf{\Gamma}^{\text{trans}}$ and $\mathbf{\Gamma}^{\text{rot}}$ vectors and generates an orthogonal set of $3M-6$ ($3M-5$ for a linear molecule) $\mathbf{\Gamma}^{\text{vib}}$ vectors, that span the space for the internal degrees of freedom of the molecule. The full $\mathbf{\Gamma}$ transformation matrix is described in Table 6.1.

Table 6.1: Matrix elements for the orthogonal transformation of Eq. (6.13) and (6.14).

	ξ_x^{trans}	ξ_y^{trans}	ξ_z^{trans}	ξ_{Rx}^{rot}	ξ_{Ry}^{rot}	ξ_{Rz}^{rot}	ξ_1^{vib}	$\cdots$	$\xi_{N_{vib}}^{vib}$
R'_1	Γ_{11}	Γ_{12}	Γ_{13}	Γ_{14}	Γ_{15}	Γ_{16}	Γ_{17}	$\cdots$	Γ_{1k}
R'_2	Γ_{21}	Γ_{22}	Γ_{23}	Γ_{24}	Γ_{25}	Γ_{26}	Γ_{27}	$\cdots$	Γ_{2k}
R'_3	Γ_{31}	Γ_{32}	Γ_{33}	Γ_{34}	Γ_{35}	Γ_{36}	Γ_{37}	$\cdots$	Γ_{3k}
R'_4	Γ_{41}	Γ_{42}	Γ_{43}	Γ_{44}	Γ_{45}	Γ_{46}	Γ_{47}	$\cdots$	Γ_{4k}
R'_5	Γ_{51}	Γ_{52}	Γ_{53}	Γ_{54}	Γ_{55}	Γ_{56}	Γ_{57}	$\cdots$	Γ_{5k}
R'_6	Γ_{61}	Γ_{62}	Γ_{63}	Γ_{64}	Γ_{65}	Γ_{66}	Γ_{67}	$\cdots$	Γ_{6k}
R'_7	Γ_{71}	Γ_{72}	Γ_{73}	Γ_{74}	Γ_{75}	Γ_{76}	Γ_{77}	$\cdots$	Γ_{7k}
$\vdots$	$\vdots$	$\vdots$	$\vdots$	$\vdots$	$\vdots$	$\vdots$	$\vdots$	$\ddots$	$\vdots$
R'_i	Γ_{i1}	Γ_{i2}	Γ_{i3}	Γ_{i4}	Γ_{i5}	Γ_{i6}	Γ_{i7}	$\cdots$	Γ_{ik}

As the external motion modes are orthogonal to vibrations, they can be projected out from the Cartesian Hessian matrix. This projection results in a reduced $N_{vib} \times N_{vib}$ Hessian matrix,

$$F_{kl} = \frac{\partial^2 E}{\partial \xi_k \partial \xi_l} = \sum_{i,j}^{3M} \Gamma_{ki}^{vib} \frac{\partial^2 E}{\partial R'_i \partial R'_j} \Gamma_{jl}^{vib} \quad ; \quad l,k = 1,2,\cdots,N_{vib}. \tag{6.22}$$

The F_{ij} are elements of the harmonic force constant matrix that represents a system of N_{vib} harmonic oscillators [170]. After the external degrees of freedom are eliminated the projected Hessian matrix is diagonalized:

$$\boldsymbol{\omega} = \mathbf{L}^{\mathrm{T}}\mathbf{F}\mathbf{L}. \tag{6.23}$$

The resulting diagonal matrix $\boldsymbol{\omega} = [\omega_1, \omega_2, \cdots, \omega_{N_{vib}}]$ contains the force constants $\partial^2 E/\partial Q_k^2 = \omega_k$. The frequency (cycles per unit time) for each vibrational mode is calculated as,

$$\nu_i = \frac{\sqrt{\omega_i}}{2\pi}. \tag{6.24}$$

In spectroscopy, the frequency is usually given indirectly in wavenumbers, $\tilde{\nu}$, which are defined by the number of electromagnetic wavelengths per length unit. Wavenumbers are obtained

by dividing Eq. (6.24) by the speed of light in vacuum, c_0.

$$\tilde{\nu}_i = \frac{\sqrt{\omega_i}}{2\pi c_0}. \tag{6.25}$$

The D_{ik} matrix elements that satisfy Eq. (6.8) and (6.10) are then calculated as,

$$D_{ki} = \sum_{l}^{N_{vib}} L_{kl}\Gamma_{li}. \tag{6.26}$$

As Eq. (6.8) is calculated in terms of MWC, the displacements in terms of Cartesian coordinates for each vibrational mode are obtained with the following expression:

$$D'_{ki} = \frac{D_{ki}}{\sqrt{m_i}}. \tag{6.27}$$

Each set of $3M$ coordinates of a particular vibration must be normalized.

The absolute infrared absorption intensities of a given vibrational mode is proportional to the transition intensity from an initial vibrational state Φ_i to a final vibrational state Φ_f due to the interaction of the dipole moment with the incident light [173]:

$$\mathcal{A} = \int \frac{1}{l} \ln\left(\frac{I_0}{I}\right) d\nu \propto \langle \Phi_i | \, \boldsymbol{\mu} \, | \Phi_f \rangle^2 . \tag{6.28}$$

Here I_0 is the intensity of the incident radiation, I denotes the final intensity of the transmitted radiation traversing a length l of an absorbing gas and $\boldsymbol{\mu} = \left\langle \Psi^{el} \right| \hat{\mu} \left| \Psi^{el} \right\rangle$ is the expectation value of the electronic dipole moment. The vibrational wave function, $|\Phi\rangle$, can be written as the product of N_{vib} harmonic oscillator functions $\left|\varphi^k\right\rangle$ as,

$$|\Phi\rangle = \prod_{k}^{N_{vib}} \left|\varphi^k\right\rangle . \tag{6.29}$$

The integration in Eq. (6.28) is performed over a frequency range which corresponds to a specific absorption band. By omitting translational contributions, and because molecules are randomly oriented in an experimental gas phase setup, a summation over all allowed

rotational states is necessary in order to model the spectrum quantum mechanically. Thus, the following relations apply [174]:

$$\langle \Phi_i | \, \boldsymbol{\mu} \, | \Phi_f \rangle^2 = \langle \Phi_i | \, \mu_x \, | \Phi_f \rangle^2 + \langle \Phi_i | \, \mu_y \, | \Phi_f \rangle^2 + \langle \Phi_i | \, \mu_z \, | \Phi_f \rangle^2 , \tag{6.30}$$

$$\mathcal{A} \propto \left(\langle \Phi_i | \, \mu_x \, | \Phi_f \rangle^2 + \langle \Phi_i | \, \mu_y \, | \Phi_f \rangle^2 + \langle \Phi_i | \, \mu_z \, | \Phi_f \rangle^2 \right) . \tag{6.31}$$

As the change of the expectation value μ with respect to the normal coordinates $\mathbf{Q}$ is unknown, a Taylor series expansion of the dipole integral is used. If this expansion is truncated after the linear term we obtain:

$$\mu_i(\mathbf{Q}_0 + \Delta\mathbf{Q}) = \mu_i(\mathbf{Q}_0) + \sum_k^{N_{vib}} \frac{\partial \mu_i}{\partial Q_k} \Delta Q_k . \tag{6.32}$$

The substitution of Eq. (6.32) into the expectation value of the dipole moment yields:

$$\langle \Phi_i | \, \mu_i \, | \Phi_f \rangle = \mu_i(\mathbf{Q}_0) \, \langle \Phi_i | \Phi_f \rangle + \sum_k^{N_{vib}} \frac{\partial \mu_i}{\partial Q_k} \, \langle \Phi_i | \, \Delta Q_k \, | \Phi_f \rangle . \tag{6.33}$$

The first term on the right-hand side of Eq. (6.33) vanishes unless the initial and final states are the same. Therefore, it has no influence on the transitions of vibrational states. Thus, for an IR active normal mode, a non-zero transition probability is only obtained if the following two conditions are fulfilled due to the second term of Eq. (6.33): First, the derivative of the dipole moment with respect to the normal coordinate, $\partial \mu_i / \partial Q_k$, must be non-zero. This is only true if the dipole moment changes according to the corresponding normal mode motion. Second, the integral $\langle \Phi_i | \, \Delta Q_k \, | \Phi_f \rangle$, must not vanish. For a given normal mode k, this integral is expanded as follows:

$$\langle \Phi_i | \, \Delta Q_k \, | \Phi_f \rangle = \left\langle \varphi_i^1 \middle| \varphi_f^1 \right\rangle \left\langle \varphi_i^2 \middle| \varphi_f^2 \right\rangle \left\langle \varphi_i^3 \middle| \varphi_f^3 \right\rangle \cdots \left\langle \varphi_i^k \middle| \, \Delta Q_k \, \middle| \varphi_f^k \right\rangle . \tag{6.34}$$

The integrals $\langle \varphi_i | \varphi_f \rangle$ will vanish unless $\left| \varphi_i^k \right\rangle = \left| \varphi_f^k \right\rangle$, i.e., the initial and final state remain the same, due to the orthogonality of the functions. This does not apply for $\left\langle \varphi_i^k \middle| \, \Delta Q_k \, \middle| \varphi_f^k \right\rangle$.

This integral will be different from zero only if $\left|\varphi_f^k\right\rangle = \left|\varphi_{i\pm\mathbf{1}}^k\right\rangle$, i.e., if the vibrational quantum numbers of the initial and final state differ by one [171]. This implies that the fundamental transitions for a given normal mode k occur at their frequency $\tilde{\nu}_k$. The absorption for a fundamental transition from $\left|\varphi_0^k\right\rangle \rightarrow \left|\varphi_1^k\right\rangle$, is then given by [174, 175],

$$\langle\Phi_0|\,\mu_i\,|\Phi_1\rangle_k^2 = \frac{\hbar}{8\pi^2 c_0 \tilde{\nu}_k}\left(\frac{\partial\mu_i}{\partial Q_k}\right)^2. \tag{6.35}$$

Thus, the absorption coefficient for a vibrational normal mode can be expressed as,

$$\mathcal{A}_k \propto \frac{\hbar}{8\pi^2 c_0 \tilde{\nu}_k}\sum_{i=x,y,z}\left(\frac{\partial\mu_i}{\partial Q_k}\right)^2. \tag{6.36}$$

The expectation value of the dipole moment can be calculated as the first-order energy-derivative with respect to an electric field [138, 176, 177],

$$\left\langle\Psi^{el}\right|\hat{\mu}_i\left|\Psi^{el}\right\rangle = \frac{\partial E}{\partial F_i} \quad ; \quad i = x, y, z. \tag{6.37}$$

Thus, the final expression for the integrated absorption coefficient for a given normal mode k [174] is given by:

$$\mathcal{A}_k = \frac{1}{4\epsilon_0}\frac{N_A}{3c_0^2}\sum_{i=x,y,z}\left(\frac{\partial^2 E}{\partial F_i \partial Q_k}\right)^2. \tag{6.38}$$

The second-order derivatives of the energy, $\partial^2 E/\partial F_i \partial Q_k$ are obtained from the corresponding mixed Cartesian derivatives by using the transformation matrix of Eq. (6.27):

$$\frac{\partial^2 E}{\partial F_i \partial Q_k} = \sum_j^{3M}\frac{\partial^2 E}{\partial F_i \partial R_j}D'_{jk}. \tag{6.39}$$

Note that the wave function $|\Phi\rangle$ is only a product of the individual harmonic oscillator wave functions for normal modes of the molecule within the harmonic oscillator approximation. Because the Taylor series for μ is truncated after the linear terms, which represents a second-order mixed energy-derivative (electrical harmonicity), the procedure presented here

is usually referred to as the double harmonic approximation.

6.2.2 Harmonic Raman Spectra Simulation

Raman spectroscopy differs from IR spectroscopy in that it is based on photon scattering rather than photon absorption [178–180]. The treatment of Raman intensities is based on Placzek's classical theory of polarizability [181], where the Raman scattering may be thought of as the radiation emitted from an oscillating dipole [175, 182]:

$$I = \frac{16\pi^2\nu_0^4}{3c_0^3}\left(\mu^{ind}\right)^2. \tag{6.40}$$

In Eq. (6.40) ν_0 is the frequency of oscillation and of the emitted light. In order to apply a semi-quantum-mechanical treatment, the hypothesis is made that the classical formulas can be converted to quantum formulas by replacing the induced dipole by its expectation value:

$$I \propto \tilde{\nu}_{in}^4 \left\langle \Omega_i \right| \boldsymbol{\mu}^{ind} \left| \Omega_f \right\rangle^2. \tag{6.41}$$

Here $\tilde{\nu}_{in}$ is the wavenumber of the incident beam, and $|\Omega\rangle$ is the rotational-vibrational wave function that can be factored into a pure vibrational $|\Phi\rangle$ and rotational $|Y\rangle$ wave function,

$$|\Omega\rangle = |\Phi\rangle \cdot |Y\rangle. \tag{6.42}$$

Of course the previous expression is only valid if the rotational-vibrational couplings can be neglected. The induced dipole moment $\boldsymbol{\mu}^{ind}$ is calculated from the polarizability tensor and the electric field vector $\mathbf{F}$ as:

$$\begin{pmatrix} \mu_x^{ind} \\ \mu_y^{ind} \\ \mu_z^{ind} \end{pmatrix} = \begin{pmatrix} \alpha_{xx} & \alpha_{xy} & \alpha_{xz} \\ \alpha_{yx} & \alpha_{yy} & \alpha_{yz} \\ \alpha_{zx} & \alpha_{zy} & \alpha_{zz} \end{pmatrix} \begin{pmatrix} F_x \\ F_y \\ F_z \end{pmatrix}. \tag{6.43}$$

Here $\alpha_{ij} = \left\langle \Psi^{el} \right| \hat{\alpha}_{ij} \left| \Psi^{el} \right\rangle$ is the expectation value of the electronic polarizabilities at coordinates $\mathbf{R}_0$. The intensity of light emitted from a molecule corresponding to a given vibration can then be expressed as,

$$I^{(m)} = K \left\langle \Omega_i \right| \alpha_{mx} F_x + \alpha_{my} F_y + \alpha_{mz} F_z \left| \Omega_f \right\rangle^2 . \tag{6.44}$$

The constant K collects characteristics that depend on the experimental setup [174]. As an example, let us consider the geometry depicted in Figure 6.3, where an incident laser beam, Z-polarized, travels in the X direction to a molecule at the origin. Light is scattered and the Raman effect is observed along the Y axis. The scattered light is observed with intensity $I^{(z)}$ (blue wave) in the plane perpendicular to the XY-plane, whereas the intensity $I^{(x)}$ (red wave) is observed in the plane parallel to the XY-plane.

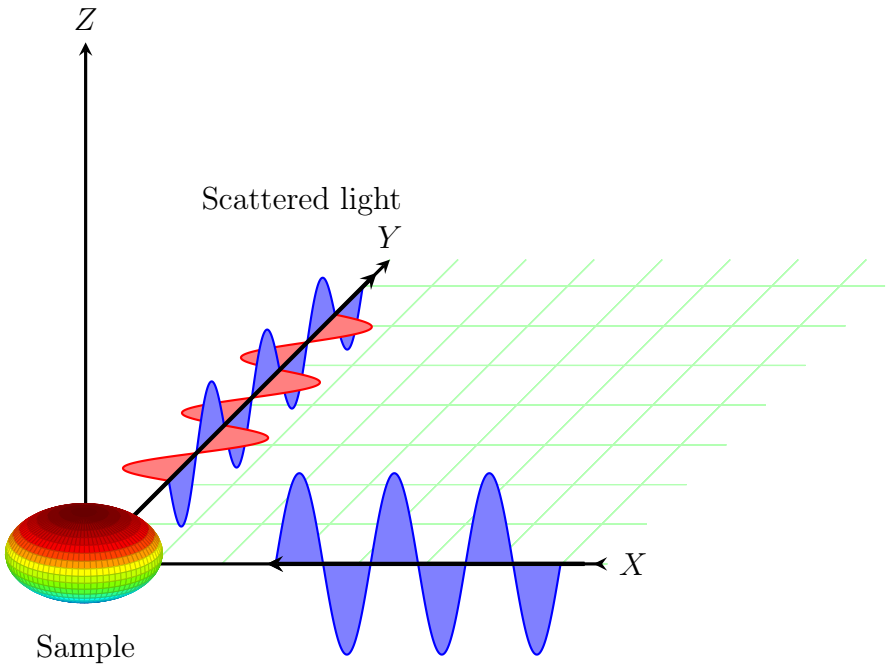

Figure 6.3: Geometrical setup used for the discussion of the Raman effect. The sample is at the origin. The laser is incident in the X-direction and the scattered light is measured in the Y-direction. The laser light is polarized perpendicular to the XY plane. The scattered light perpendicular to the XY plane has an intensity $I^{(z)}$, whereas the scattered light parallel to the XY plane has an intensity $I^{(x)}$.

Under these conditions, where $F_x = F_y = 0$ and $F_z \neq 0$, the intensity components of the scattered light are obtained as,

$$I^{(x)} = K \langle \Omega_i | \alpha_{xz} F_z | \Omega_f \rangle^2 = K F_z^2 \langle \Omega_i | \alpha_{xz} | \Omega_f \rangle^2 , \tag{6.45}$$

$$I^{(z)} = K \langle \Omega_i | \alpha_{zz} F_z | \Omega_f \rangle^2 = K F_z^2 \langle \Omega_i | \alpha_{zz} | \Omega_f \rangle^2 . \tag{6.46}$$

By introducing the irradiance, which connects the intensity of the incident beam with the amplitude of the electric field [175],

$$I_0 = \frac{1}{2} \epsilon_0 c_0 F_z^2, \tag{6.47}$$

Eq. (6.45) and (6.46) take the forms:

$$I^{(x)} = K' I_0, \langle \Omega_i | \alpha_{xz} | \Omega_f \rangle^2 \tag{6.48}$$

$$I^{(z)} = K' I_0 \langle \Omega_i | \alpha_{zz} | \Omega_f \rangle^2 . \tag{6.49}$$

The quantities most frequently observed experimentally are the *depolarization ratios*, ρ, defined as the ratio of the scattered intensity which is polarized parallel to F_z (blue wave), to the intensity perpendicular to F_z (red wave) [175]. When linear polarized incident light (as shown in Figure 6.3) is used, the ratio of intensities is given by:

$$\rho = \frac{I^{(z)}}{I^{(x)}} = \frac{\langle \Omega_i | \alpha_{xz} | \Omega_f \rangle^2}{\langle \Omega_i | \alpha_{zz} | \Omega_f \rangle^2}. \tag{6.50}$$

Thus, in order to obtain the depolarization ratio, the integrals in Eq. (6.50) must be evaluated. The components of the polarizability tensor, α_{ij} depend on the orientation of the molecule in a space-fixed reference frame, but they are related to the principal axes of polarizability. This system is depicted in Figure 6.4. The general formulation that relates the polarizability tensor in a space-fixed orientation in terms of the principal polarizability axes

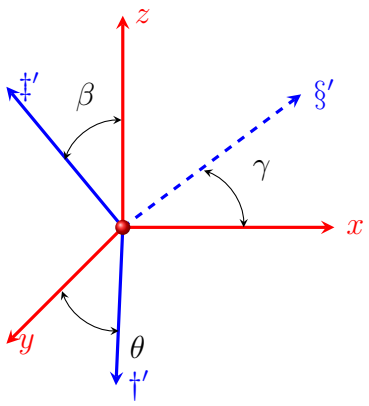

Figure 6.4: Angles that relate a space-fixed Cartesian coordinate (red) and a rotated Cartesian coordinate system (blue) which coincides with the principal axes of inertia.

is expressed as [182],

$$\alpha_{ij} = \sum_{i'=x',y',z'} \alpha_{i'i'} l_{ii'} l_{ji'}. \tag{6.51}$$

The $l_{ij'}$ are matrix elements of a rotation matrix $\mathbf{L}$, called direction cosine matrix [183]. These coefficients are defined as the cosine of the angle between the positive directions of the i and j' axes,

$$\cos\theta = l_{ij'}. \tag{6.52}$$

The geometrical description of these direction cosine elements is analogous to the standard orientation rotation, but instead of coinciding with the principal axes of inertia, the rotated body-fixed molecule orientation, shown in Figure 6.4, will now coincide with the principal polarizability axes of the molecule. The substitution of Eq (6.52) into the transition integral appearing in both Eq. (6.48) and (6.49) yields:

$$\langle \Omega_i | \, \alpha_{ij} \, | \Omega_f \rangle = \left\langle \Omega_i \middle| \sum_{i'=x',y',z'} \alpha_{i'i'} l_{ii'} l_{ji'} \middle| \Omega_f \right\rangle. \tag{6.53}$$

As α_{ij} depends on the orientation of the molecule, the rotational contribution of the total wave

function must be taken into account [174]. The translational contribution is not considered because it does not affect the polarizability tensor. Thus, by the separation of vibrations and rotations in Eq. (6.53) we obtain:

$$\langle \Omega_i | \, \alpha_{ij} \, | \Omega_f \rangle = \sum_{i'=x',y',z'} \langle \Phi_i | \, \alpha_{i'i'} \, | \Phi_f \rangle \, \langle Y_i | \, l_{ii'} l_{ji'} \, | Y_f \rangle \, . \tag{6.54}$$

As the intensities $I^{(x)}$ and $I^{(z)}$ are proportional to the squared transition integrals,

$$\langle \Omega_i | \, \alpha_{ij} \, | \Omega_f \rangle^2 = \left(\sum_{i'=x',y',z'} \langle \Phi_i | \, \alpha_{i'i'} \, | \Phi_f \rangle \, \langle Y_i | \, l_{ii'} l_{ji'} \, | Y_f \rangle \right)^2 , \tag{6.55}$$

the following explicit expression is obtained:

$$\begin{aligned} \langle \Omega_i | \, \alpha_{ij} \, | \Omega_f \rangle^2 = & \sum_{i'=x',y',z'} \langle \Phi_i | \, \alpha_{i'i'} \, | \Phi_f \rangle^2 \, \langle Y_i | \, l_{ii'} \, | Y_f \rangle^2 \, \langle Y_i | \, l_{ji'} \, | Y_f \rangle^2 + \\ & \sum_{i'=x',y',z'} \sum_{j' \neq i'} \langle \Phi_i | \, \alpha_{i'i'} \, | \Phi_f \rangle \, \langle \Phi_i | \, \alpha_{j'j'} \, | \Phi_f \rangle \, \langle Y_i | \, l_{ii'} \, | Y_f \rangle \, \langle Y_i | \, l_{ji'} \, | Y_f \rangle \times \\ & \langle Y_i | \, l_{ij'} \, | Y_f \rangle \, \langle Y_i | \, l_{jj'} \, | Y_f \rangle \, . \end{aligned} \tag{6.56}$$

As an illustrative example we now evaluate $I^{(z)}$, Eq. (6.49), which requires the evaluation of the terms in Eq. (6.56) with the condition $i = j = z$. Thus Eq. (6.56) reduces to,

$$\begin{aligned} \langle \Omega_i | \, \alpha_{zz} \, | \Omega_f \rangle^2 = & \sum_{i'=x',y',z'} \langle \Phi_i | \, \alpha_{i'i'} \, | \Phi_f \rangle^2 \, \langle Y_i | \, l_{zi'} \, | Y_f \rangle^4 + \\ & \sum_{i'=x',y',z'} \sum_{j' \neq i'} \langle \Phi_i | \, \alpha_{i'i'} \, | \Phi_f \rangle \, \langle \Phi_i | \, \alpha_{j'j'} \, | \Phi_f \rangle \, \langle Y_i | \, l_{zi'} \, | Y_f \rangle^2 \, \langle Y_i | \, l_{zj'} \, | Y_f \rangle^2 \, . \end{aligned} \tag{6.57}$$

The integrals $\langle Y_i | \, l_{zi'} \, | Y_f \rangle$ in Eq. (6.57) can be solved by means of the isotropic average [184]. Such averaging is a classical process in which all molecular orientations are assumed to be equally possible [184]. The isotropic average of a product of four identical direction cosines

results in,

$$\langle Y_i|\, l_{zi'}\, |Y_f\rangle^4 = \frac{1}{5}. \tag{6.58}$$

If the four direction cosines consist of products of pairs of identical direction cosines then the average is,

$$\langle Y_i|\, l_{zi'}\, |Y_f\rangle^2 \langle Y_i|\, l_{zj'}\, |Y_f\rangle^2 = \frac{1}{15}. \tag{6.59}$$

It is noteworthy that this procedure gives results which are identical with those obtained by calculating Eq. (6.54) and summing the intensity expressions over the complete set of initial and final rotational states [183]. After the isotropic average is calculated, the substitution of Eq. (6.58) and (6.59) into (6.57) yields:

$$\begin{aligned}\langle \Omega_i|\, \alpha_{zz}\, |\Omega_f\rangle^2 = \frac{1}{5} \sum_{i'=x',y',z'} \langle \Phi_i|\, \alpha_{i'i'}\, |\Phi_f\rangle^2 + \\ \frac{1}{15} \sum_{i'=x',y',z'} \sum_{j'\neq i'} \langle \Phi_i|\, \alpha_{i'i'}\, |\Phi_f\rangle \langle \Phi_i|\, \alpha_{j'j'}\, |\Phi_f\rangle .\end{aligned} \tag{6.60}$$

Eq. (6.60) can be conveniently replaced as function of two invariants of the polarizability tensor. The first one is called mean isotropic polarizability $\bar{\alpha}$, expressed as,

$$\bar{\alpha} = \frac{1}{3} \left(\langle \Phi_i|\, \alpha_{x'x'}\, |\Phi_f\rangle + \langle \Phi_i|\, \alpha_{y'y'}\, |\Phi_f\rangle + \langle \Phi_i|\, \alpha_{z'z'}\, |\Phi_f\rangle \right), \tag{6.61}$$

whereas the second one is the polarizability anisotropy $|\Delta\alpha|^2$,

$$\begin{aligned}|\Delta\alpha|^2 = \frac{1}{2} \big([\langle \Phi_i|\, \alpha_{x'x'}\, |\Phi_f\rangle - \langle \Phi_i|\, \alpha_{y'y'}\, |\Phi_f\rangle]^2 + [\langle \Phi_i|\, \alpha_{y'y'}\, |\Phi_f\rangle - \langle \Phi_i|\, \alpha_{z'z'}\, |\Phi_f\rangle]^2 + \\ [\langle \Phi_i|\, \alpha_{z'z'}\, |\Phi_f\rangle - \langle \Phi_i|\, \alpha_{x'x'}\, |\Phi_f\rangle]^2 \big) - \\ 3 \left(\langle \Phi_i|\, \alpha_{x'y'}\, |\Phi_f\rangle^2 - \langle \Phi_i|\, \alpha_{y'z'}\, |\Phi_f\rangle^2 - \langle \Phi_i|\, \alpha_{z'x'}\, |\Phi_f\rangle^2 \right).\end{aligned} \tag{6.62}$$

For the body-fixed orientation frame (Figure 6.4), $\alpha_{x'y'} = \alpha_{y'z'} = \alpha_{z'x'} = 0$. Thus, the following expression is valid:

$$|\Delta\alpha|^2 = \frac{1}{2}\left(\left[\langle\Phi_i|\,\alpha_{x'x'}\,|\Phi_f\rangle - \langle\Phi_i|\,\alpha_{y'y'}\,|\Phi_f\rangle\right]^2 + \left[\langle\Phi_i|\,\alpha_{y'y'}\,|\Phi_f\rangle - \langle\Phi_i|\,\alpha_{z'z'}\,|\Phi_f\rangle\right]^2 + \left[\langle\Phi_i|\,\alpha_{z'z'}\,|\Phi_f\rangle - \langle\Phi_i|\,\alpha_{x'x'}\,|\Phi_f\rangle\right]^2\right). \tag{6.63}$$

From the definition of Eq. (6.60) and (6.63), Eq. (6.49) takes the form,

$$I^{(z)} = K' I_0 \frac{|\Delta\alpha|^2}{15}. \tag{6.64}$$

With a similar procedure, the expression for $I^{(x)}$, Eq. (6.49) results in,

$$I^{(x)} = K' I_0 \frac{45\bar{\alpha}^2 + 4|\Delta\alpha|^2}{45}. \tag{6.65}$$

Similar to the IR intensity calculations, $\alpha_{i'i'}$ is not known as an explicit function of the normal coordinates $\mathbf{Q}$. Thus, a Taylor series expansion, truncated to first order in the normal coordinates, is used:

$$\alpha_{x'x'}(\mathbf{Q}_0 + \Delta\mathbf{Q}) = \alpha_{x'x'}(\mathbf{Q}_0) + \sum_k^{N_{vib}} \frac{\partial\alpha_{x'x'}}{\partial Q_k}\Delta Q_k. \tag{6.66}$$

Substitution of Eq. (6.66) into the expectation value of the electric polarizability yields:

$$\langle\Phi_i|\,\alpha_{x'x'}\,|\Phi_f\rangle = \alpha_{x'x'}(\mathbf{Q}_0)\,\langle\Phi_i|\Phi_f\rangle + \sum_k^{N_{vib}} \frac{\partial\alpha_{x'x'}}{\partial Q_k}\,\langle\Phi_i|\,\Delta Q_k\,|\Phi_f\rangle\,. \tag{6.67}$$

The very same conditions as for Eq. (6.33) apply to Eq.(6.67). The non-vanishing contributions where $\left|\varphi_i^k\right\rangle = \left|\varphi_f^k\right\rangle$ correspond to the Rayleigh scattering, i.e., the frequency of the scattered light is the same as that of the incident beam, $\tilde{\nu}_{in}$. For Stokes Raman scattering, where $\left|\varphi_0^k\right\rangle \rightarrow \left|\varphi_1^k\right\rangle$, the frequency of the inelastically scattered light is no longer the same as the wavenumber of the incident beam, $\tilde{\nu}_{in}$. This frequency in Eq. (6.41) has to be replaced by $\tilde{\nu}_{in} - \tilde{\nu}_k$ where $\tilde{\nu}_k$ is the wavenumber corresponding to the vibrational transition for normal

mode k. Thus, the Stokes scattering for a fundamental transition from $\left|\varphi_0^k\right\rangle \rightarrow \left|\varphi_1^k\right\rangle$, is given by [174, 175],

$$\langle\Phi_0|\,\alpha_{x'x'}\,|\Phi_1\rangle_k = \sqrt{\frac{\hbar}{8\pi^2 c_0 \tilde{\nu}_k}}\frac{\partial \alpha_{x'x'}}{\partial Q_k}. \tag{6.68}$$

The corresponding intensities for Stokes scattering, Eq. (6.64) and (6.65) take the form:

$$I_k^{(z)} \propto K'' I_0(\tilde{\nu}_{in} - \tilde{\nu}_k)^4 \frac{|\Delta\alpha|_k^2}{15}, \tag{6.69}$$

$$I_k^{(x)} \propto K'' I_0(\tilde{\nu}_{in} - \tilde{\nu}_k)^4 \frac{45\bar{\alpha}_k^2 + 4|\Delta\alpha|_k^2}{45}. \tag{6.70}$$

As the mean isotropic polarizability and the polarizability anisotropy are invariant with respect to rotation of the coordinate system, the following relations for Eq. (6.69) apply:

$$\bar{\alpha}_k = \frac{1}{3}\left(\langle\Phi_0|\,\alpha_{xx}\,|\Phi_1\rangle_k + \langle\Phi_0|\,\alpha_{yy}\,|\Phi_1\rangle_k + \langle\Phi_0|\,\alpha_{zz}\,|\Phi_1\rangle_k\right), \tag{6.71}$$

and,

$$\begin{aligned}|\Delta\alpha|_k^2 = \frac{1}{2}\Big(&\left[\langle\Phi_0|\,\alpha_{xx}\,|\Phi_1\rangle_k - \langle\Phi_0|\,\alpha_{yy}\,|\Phi_1\rangle_k\right]^2 + \left[\langle\Phi_0|\,\alpha_{yy}\,|\Phi_1\rangle_k - \langle\Phi_0|\,\alpha_{zz}\,|\Phi_1\rangle_k\right]^2 + \\ &\left[\langle\Phi_0|\,\alpha_{zz}\,|\Phi_1\rangle_k - \langle\Phi_0|\,\alpha_{xx}\,|\Phi_1\rangle_k\right]^2\Big) - \\ &3\left(\langle\Phi_0|\,\alpha_{xy}\,|\Phi_1\rangle_k^2 - \langle\Phi_0|\,\alpha_{yz}\,|\Phi_1\rangle_k^2 - \langle\Phi_0|\,\alpha_{zx}\,|\Phi_1\rangle_k^2\right),\end{aligned} \tag{6.72}$$

where,

$$\langle\Phi_0|\,\alpha_{ij}\,|\Phi_1\rangle_k = \sqrt{\frac{\hbar}{8\pi^2 c_0 \tilde{\nu}_k}}\frac{\partial \alpha_{ij}}{\partial Q_k} = \sqrt{\frac{\hbar}{8\pi^2 c_0 \tilde{\nu}_k}}\frac{\partial^3 E}{\partial F_i \partial F_j \partial Q_k}. \tag{6.73}$$

The third-order energy-derivative in Eq. (6.73) is transformed into the normal mode coordinate representation by using the transformation matrix of (6.27),

$$\frac{\partial^3 E}{\partial F_i \partial F_j \partial Q_k} = \sum_a^{3M} \frac{\partial^3 E}{\partial F_i \partial F_j \partial R_a} D'_{ak}. \tag{6.74}$$

Thus, the depolarization ratio of the k^{th} vibrational mode [179] is defined as,

$$\rho_k = \frac{I_k^{(z)}}{I_k^{(x)}} = \frac{3|\Delta\alpha|_k^2}{45\bar{\alpha}_k^2 + 4|\Delta\alpha|_k^2}; \quad k = 1, 2, \cdots, N_{vib}. \tag{6.75}$$

The importance of the depolarization ratio lies in the fact that it is a pure molecular property, independent of the experimental setup. Therefore, it contains useful information about the symmetry of the vibrational modes [182]. If the vibration is not totally symmetric, then the trace of the polarizability tensor $\bar{\alpha}_k$ will be zero, and the anisotropy $|\Delta\alpha|_k^2$ will be non-zero. Thus,

$$\rho_k = \frac{3}{4}. \tag{6.76}$$

On the other hand, for totally symmetric vibrations which belong to the point groups of the cubic system (such as O_h and T_d) the anisotropy $|\Delta\alpha|_k^2$ will be zero and, thus, the depolarization ratio will vanish,

$$\rho_k = 0. \tag{6.77}$$

For the remaining vibrations there may be both diagonal and off-diagonal terms in the third-order derivative tensor. The resulting range for these situations is given by,

$$0 \leq \rho_i \leq \frac{3}{4}. \tag{6.78}$$

In order to validate our ADPT approach we present the calculation of the harmonic vibrational frequencies, along with the IR spectra and Raman intensities for the icosahedral fullerene C_{60}, obtained with both ADPT-ADFT and finite-difference methodologies. All calculations were performed on 16 Intel Xeon X5675 @ 3.07 GHz processors with 4 GB of RAM. The comparison is shown in Figure 6.5.

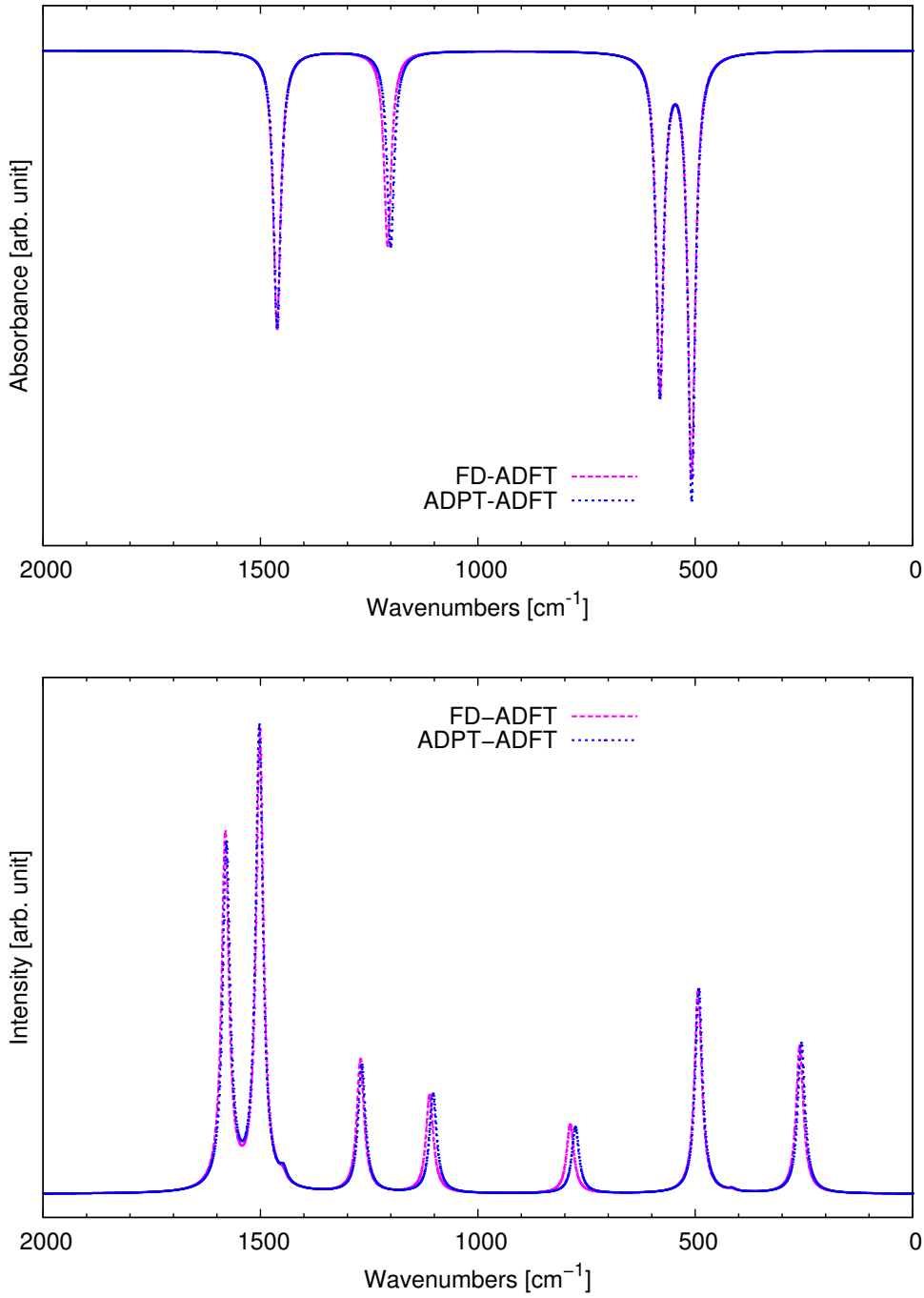

Figure 6.5: Comparison of C_{60} (I_h symmetry) IR (top) and Raman (bottom) spectra calculated from numerical finite-differences and analytical second-order energy-derivatives.

The optimization and frequency analysis was performed using the GGA PBE [45] exchange-correlation functional. The SCF energy convergence criterion [102] was set to 10^{-6} a.u., whereas for the numerical integration an adaptive grid with a tolerance of 10^{-6} a.u. was used. For the density fitting the GEN-A2* auxiliary-function set was automatically generated [83]. The DZVP-GGA basis set [83] was employed. For the finite-difference second-order derivatives the nuclear displacement step size is 0.01 a.u, whereas for Raman intensities a finite electric field strength of 0.01 a.u. is employed. The analytic second-order derivatives are calculated with the Con-EN iterative solver. It is evident that the spectra obtained with the ADPT-ADFT methodology show an excellent agreement compared to those obtained with the finite-difference methodology. Besides its remarkable agreement, the ADPT-ADFT method offers a considerable speed-up, specifically for this system up to four times faster compared to the finite-difference method. Nevertheless it should be remembered that these spectra are calculated within the double harmonic approximation. Thus, for a reliable comparison with experiment anharmonic corrections must be included. They are currently under development in our laboratory.

Chapter 7

APPLICATIONS

7.1 Carbon Fullerenes

Fullerenes are closed carbon-cage molecules which contain only pentagonal and hexagonal rings, the most famous of them is the icosahedral C_{60} [185], composed of twelve pentagonal carbon rings located around the vertices and twenty hexagonal carbon rings at the centers of icosahedral faces. These carbon systems, being known since 1985 [186], have attracted great attention, and consequently, a large number of works, experimental as well as theoretical, are focused on the study of these systems [187–191]. Larger fullerenes that have an icosahedral symmetry can be constructed as well [192, 193]. These carbon clusters, called giant fullerenes can be seen as cut-out of graphene sheets folded into their final shape. These giant icosahedral fullerenes are always formed by twelve pentagonal carbon rings, while the remaining rings have a hexagonal arrangement [185]. To the best of our knowledge, there exists no systematic study on the vibrational spectroscopy of giant fullerenes based on non-symmetry-adapted first-principle calculations. Most certainly this is due to the prohibitive computational demand required for such a study. In this section, we focus on the calculation of the harmonic vibrational frequencies as well as the corresponding IR and Raman intensities for the icosahedral C_{60}, C_{180}, C_{240} and C_{540} fullerenes [194]. We circumvent the computational bottleneck by employing ADFT. The structures of the optimized fullerene

minima are depicted in Figure 7.1.

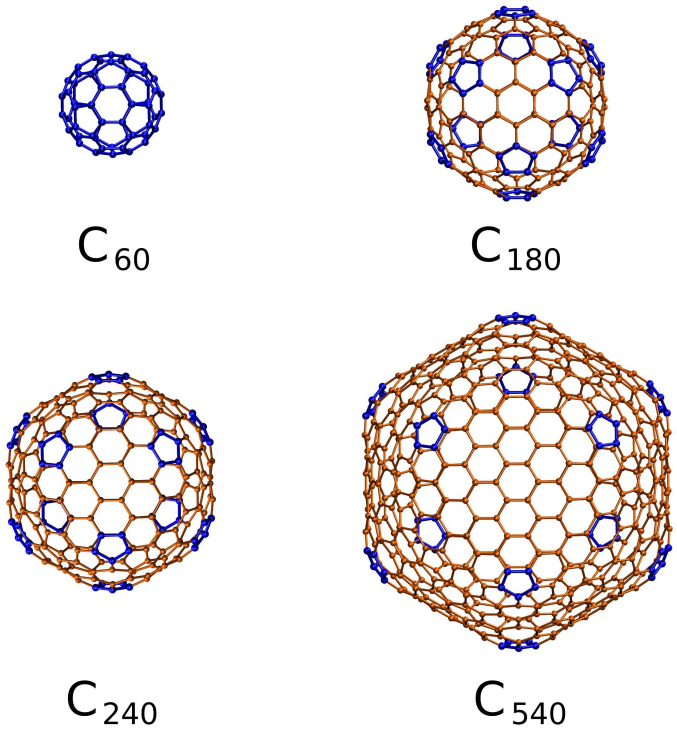

Figure 7.1: Optimized structures of the calculated icosahedral fullerenes. Geometries were optimized at the PBE/DZVP-GGA/GEN-A2+ level of theory without any symmetry constraints. The view is aligned along one of the C_3 axes and all twelve five-membered rings of all the larger fullerenes are colored in blue to facilitate the identification of the vertices of the icosahedron.

As our calculations were performed without simplification due to symmetry, they also indicate that IR and Raman calculations can be performed for other non-symmetric systems of similar size with approximately the same computational efficiency. All calculations were performed on 64 Intel Xeon X5675 @ 3.07 GHz processors with 4 GB of RAM. The optimization and frequency analysis calculations for all fullerenes were performed using both LDA VWN [40] and GGA PBE [45] exchange-correlation functionals. The SCF energy convergence criterion [102] and grid tolerance were set to 10^{-6} a.u. and 10^{-6} a.u., respectively. The DZVP-GGA basis set [83] was employed along with the GEN-A2+ customized auxiliary-function set. This basis and auxiliary-function set combination results in more than 8000 basis functions and 31 000 auxiliary-functions for the C_{540} fullerene. For the Raman intensities a

finite electric field strength of 0.01 atomic units was employed. The HXYZ parallelization scheme was employed, along with the Con-EN algorithm except for C_{540}. For this system the Dir-EN variant was used. All other settings were according to the deMon2k defaults [154]. Our calculations show that the optimized fullerenes possess icosahedral-like structures. The corresponding vibrational analyses confirmed that they are stable local minima on the singlet potential energy surface.

Figure 7.2 depicts the normalized distribution of bond lengths in the optimized systems. The dashed line at 1.42 Å is the graphene bond length obtained from a periodic deMon2k calculation [195].

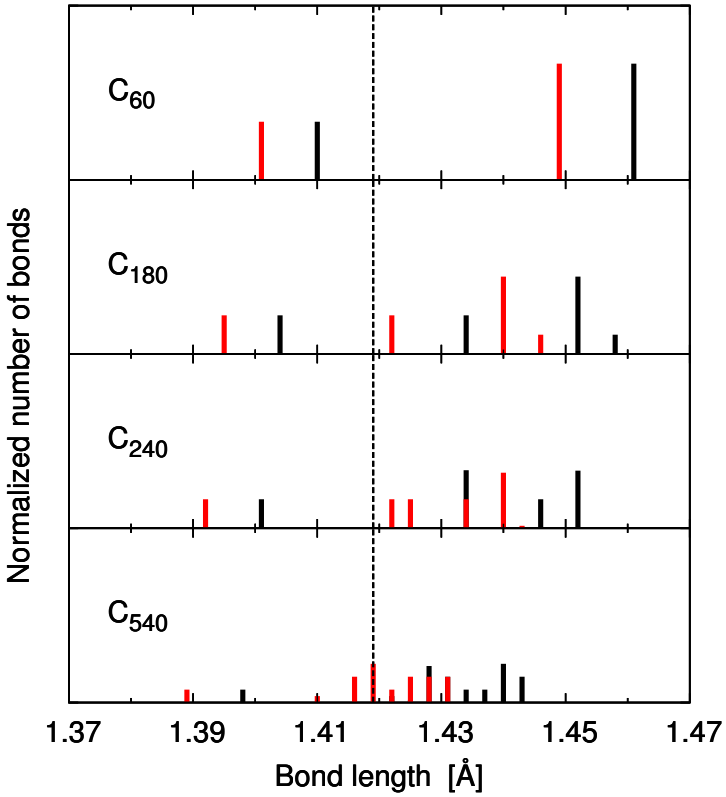

Figure 7.2: Normalized number of bonds for the C_{60}, C_{180}, C_{240} and C_{540} fullerenes versus bond length, calculated with the VWN (red line) and PBE (black line) exchange-correlation functionals.

As Figure 7.2 shows, bond lengths obtained with the VWN functional are shorter than those obtained with the PBE functional. The difference between the shortest and longest C-C bond reaches a maximum in C_{180}, and then decreases until C_{540}. As the fullerenes grow in size, a delocalization over the bonds is observed with a converging behavior near to the graphene bond length value, albeit somewhat slower for the PBE/DZVP-GGA/GEN-A2+ level of theory. Also with growing system size, the faceted surfaces start to resemble the hexagonal arrangement in graphene. This trend is even more pronounced in larger fullerenes, namely the C_{720} and C_{960} fullerenes. These systems were optimized with the VWN/DZVP/GEN-A2 level of theory [139]. This behavior supports the statement that giant fullerenes, starting from the C_{540}, begin to show an enhanced π-system delocalization. Thus, giant fullerenes can be seen as finite size analogs of graphene.

The bonds that fall outside the increasingly narrower distribution around the graphene bond length are the shortest bonds in the fullerenes. They can be assigned to the conjugated double bonds adjacent to the cyclopentadienyl units. Interestingly these shortest bond lengths are longest in C_{60}, decreasing monotonically to around 1.39 Å for the VWN functional and 1.40 Å for the PBE functional when going to C_{540}. This is an indicator that the cyclopentadienyl units are less incorporated into the delocalized π-system of the fullerenes. As the system grows in size, these cyclopentadienyl units are consistently more isolated from the delocalized π-system found in the planar faces of fullerenes. This is consistent with the experimental finding on C_{60} where the hexagons adjacent to the cyclopentadienyl units behave more like cyclohexatrienes rather than benzene rings [196].

In order to compare with experiment the analytic IR and Raman spectra were calculated for the C_{60} fullerene. The obtained results are presented in Figure 7.3. The experimental C_{60} IR and Raman line positions [197] are also depicted in this figure 7.3 as green dashed lines. As can be seen from Figure 7.3, the features of the obtained spectra are very similar, both with the VWN and PBE functionals. Moreover, the analytic IR frequency analysis shows an excellent agreement with the experimental measurement, in particular for the PBE exchange-correlation functional.

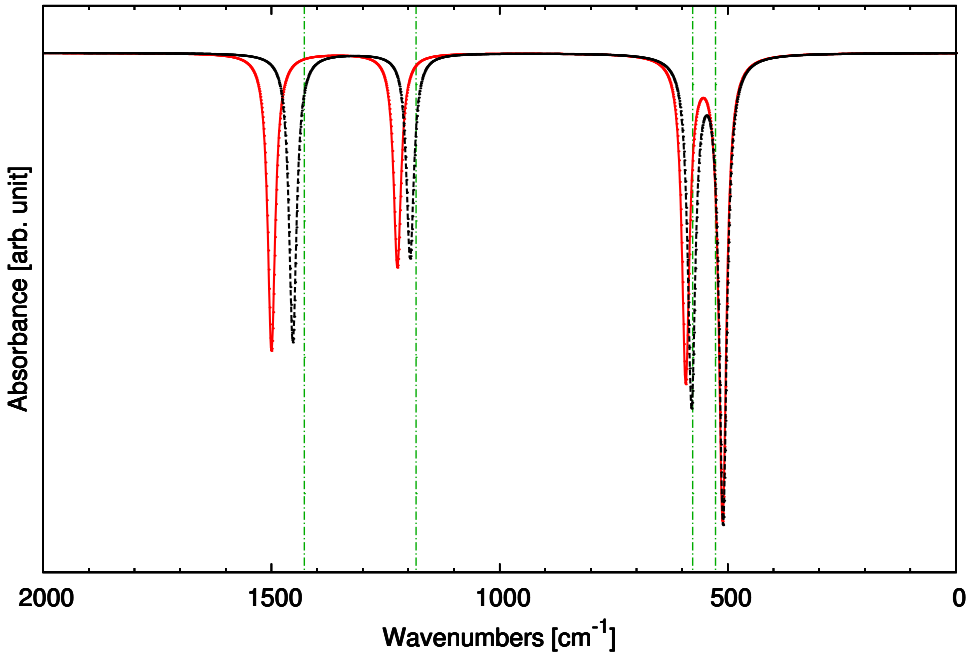

(a)

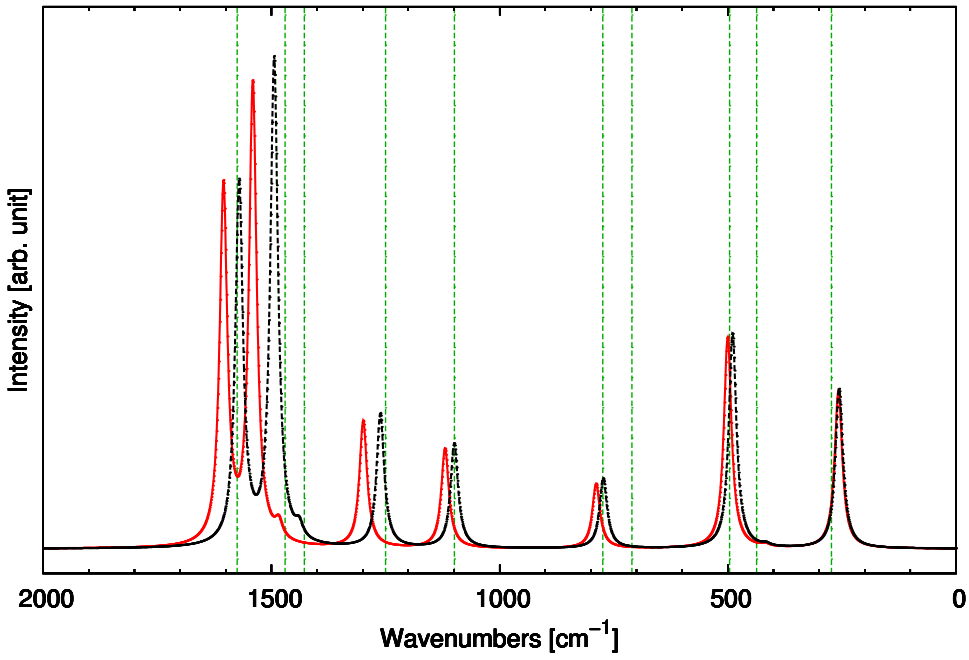

(b)

Figure 7.3: Comparison of the analytically calculated VWN (red) and PBE (black) IR (top) and Raman (bottom) spectra of C_{60}. The green dashed lines indicate experimental data.

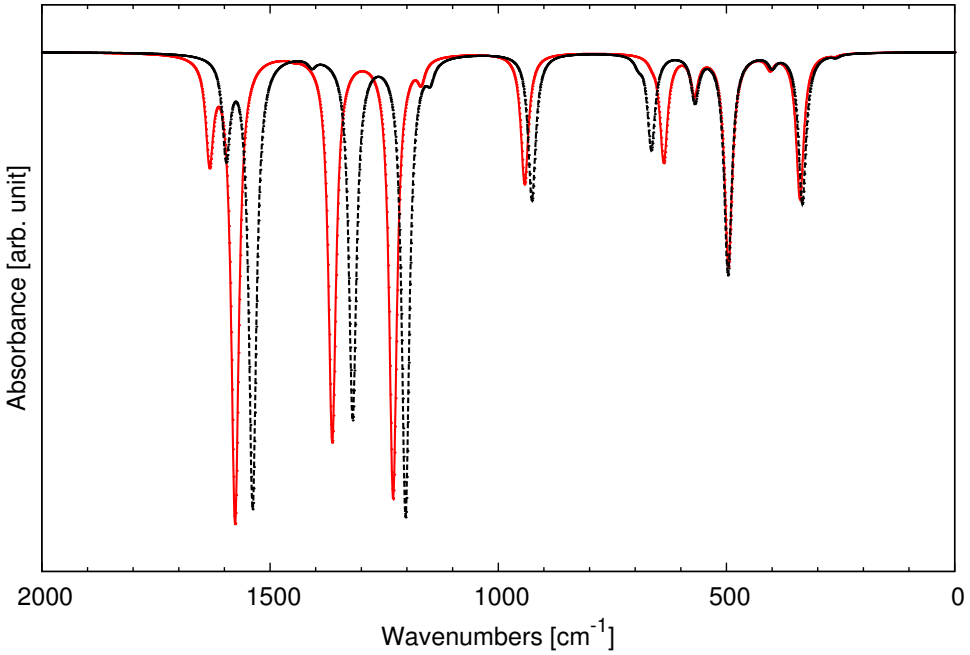

(a)

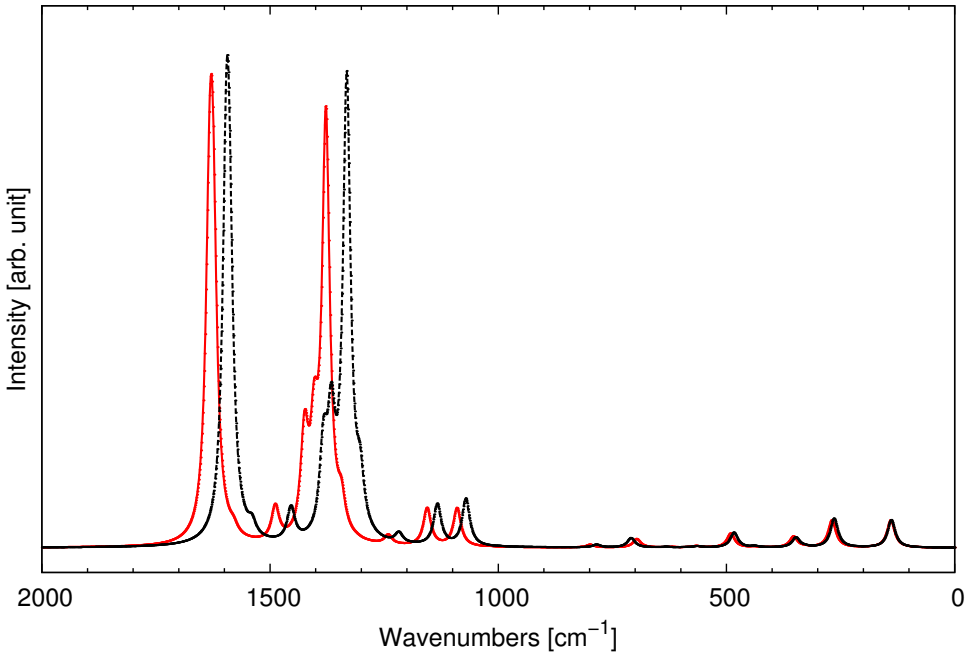

(b)

Figure 7.4: Comparison of the analytically calculated VWN (red) and PBE (black) IR (top) and Raman (bottom) spectra of C_{180}.

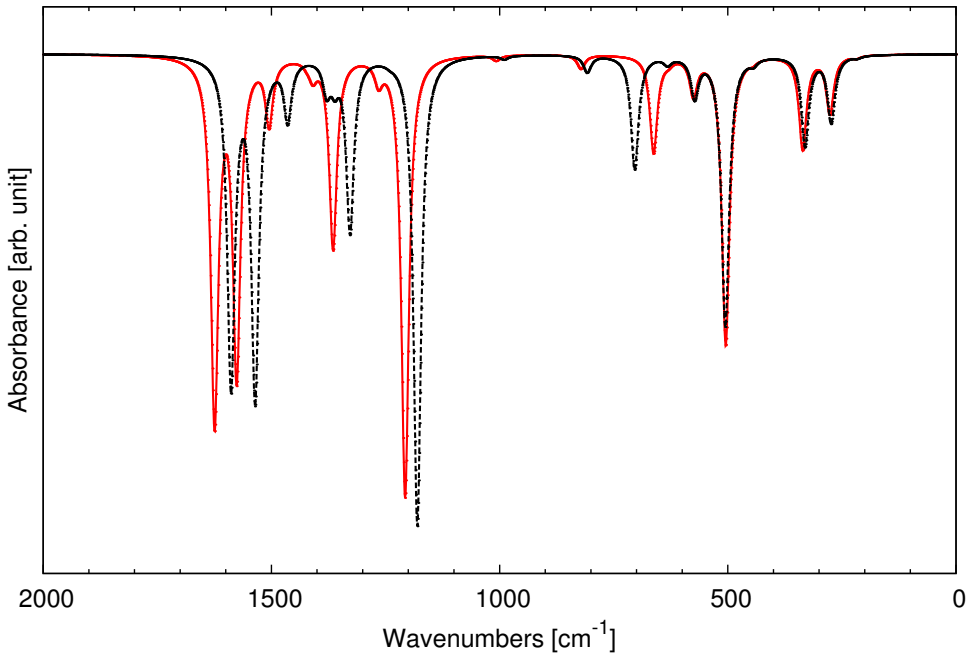

(a)

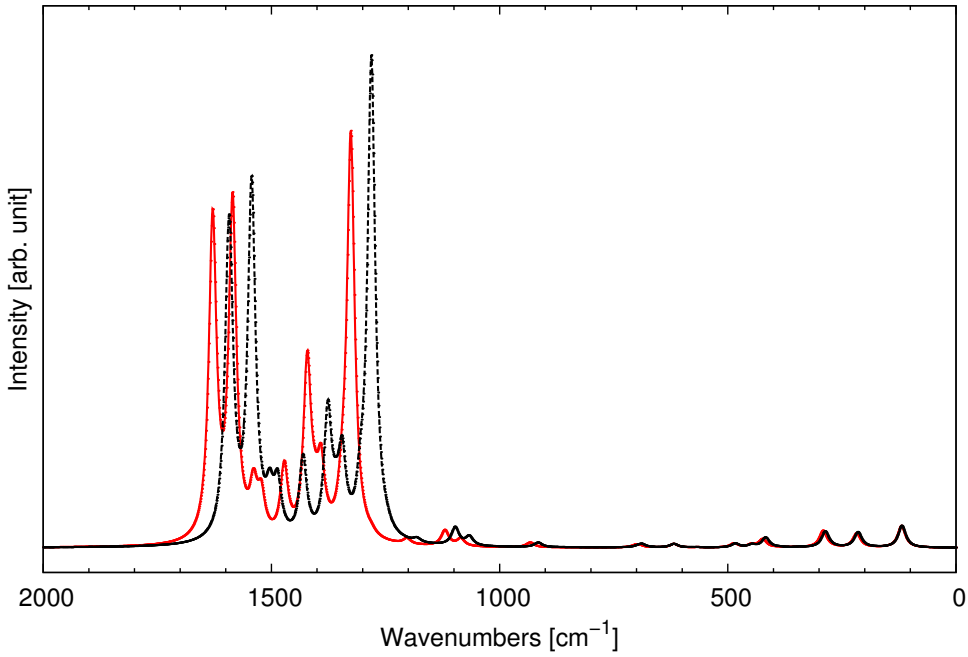

(b)

Figure 7.5: Comparison of the analytically calculated VWN (red) and PBE (black) IR (top) and Raman (bottom) spectra of C_{240}.

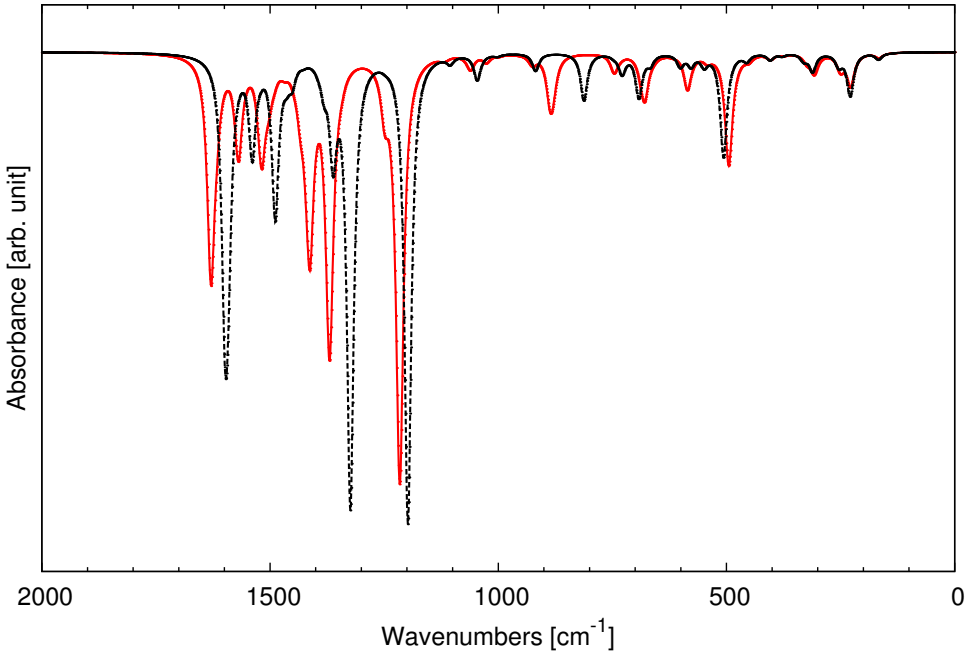

(a)

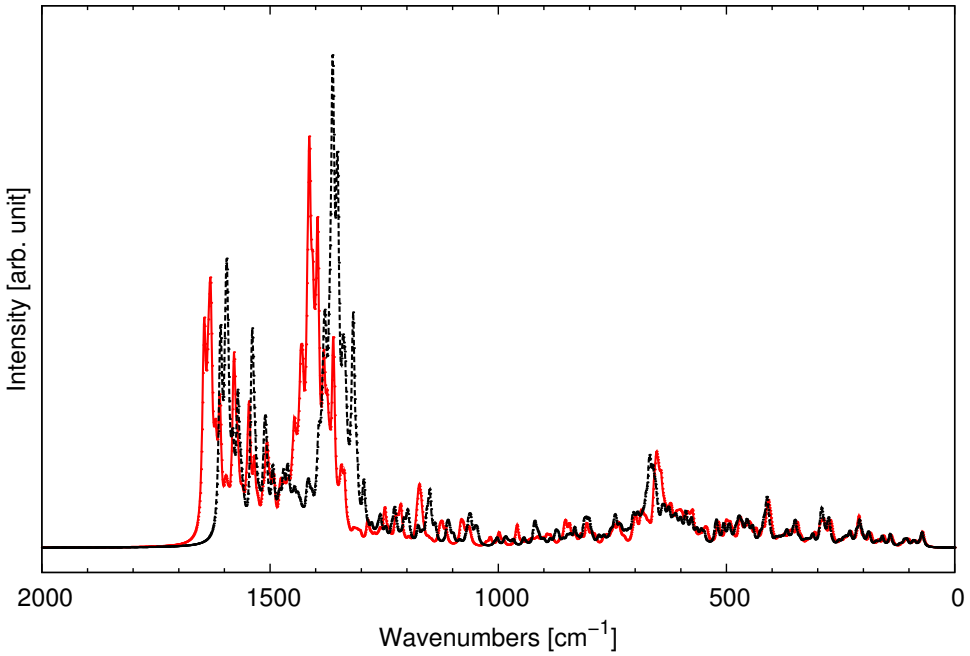

(b)

Figure 7.6: Comparison of the analytically calculated VWN (red) and PBE (black) IR (top) and Raman (bottom) spectra of C_{540}.

Active modes present in C_{60} are also observed in the theoretical spectra obtained for C_{180}, C_{240} and C_{540} although with variable intensity. These spectra are depicted in Figures 7.4 to 7.6. As systems grow in size, more IR- and Raman-active modes appear in both vibrational spectra below 1700 cm^{-1}. The most demanding calculation of the Hessian matrix corresponds to the C_{540} fullerene with the PBE functional and the Dir-EN ADPT algorithm. It took around 9 days to be completed. As the single-point SCF energy calculation for this system needs about 1500 seconds on the same computational setup, an estimated time for a finite-difference Hessian matrix is approximately 70 days. This means that the analytic approach is almost 8 times faster than its finite-difference counterpart. An interesting behavior is observed for the Raman spectra of the studied fullerenes. As systems increase in size, the peak intensity in the region between 1000 and 1700 cm^{-1} grows rapidly. Besides, the Raman spectra for the C_{540} clearly presents some noise. The source of this noise might be connected to the fact that the electric-dipole polarizabilities of giant fullerenes grow very rapidly [11]. This could introduce unexpected numerical instabilities in the semi-numerical methodology presented in Section 4.3. Further numerical tests are necessary to obtain a definitive answer for this unexpected behavior.

7.2 Thiolate-Protected Gold Nanoclusters

Ligand-thiolate-protected gold nanoclusters with the formula $Au_n(S\text{-}R)_m$ and sizes ranging from about ten to a few hundred atoms constitute a special class of nanomaterials [198]. These clusters are unique in the sense that they can be treated as inorganic-organic hybrid compounds. Strong quantum size effects are observed in these systems. As a result specific physicochemical properties such as discrete energy levels, enhanced photoluminescence, catalytic reactivity and nonlinear optical properties [199–205] are found in these clusters. The technological significance of these protected clusters has led to extensive research. In particular, the size-selective production of these clusters without the necessity of cumbersome electrophoretic or chromatographic isolation [206–209] has attracted much attention. The properties of thiolate-protected nanoclusters are controlled by both the ligands and the Au core [210, 211]. These clusters can range in size as small as $Au_{15}(SR)_{13}$ [212], up to hundreds of gold atoms such as $Au_{279}(SR)_{84}$ [213]. Despite the remarkable success in this research area, structure determination of thiolate-protected nanoclusters remains a great challenge for both experiment and theory. Because the large size gold clusters are appealing for practical applications, the understanding of their atomic structures and structure evolution, in particular the surface atom arrangements and gold-thiolate interface, are of paramount importance in order to reveal the nature of their structure-property correlation.

The computational study of these systems is quite complex as they are composed of a core with a specific arrangement of Au atoms, surrounded by ligands which possess many degrees of freedom. One of the main objectives in our research groups is to determine the correlation between different ligand-protectors and the size and geometrical shape of the metallic core. To achieve this goal the availability of the analytic Hessian matrix is very advantageous. An initial Hessian for a geometry optimization calculation can reduce significantly the number of iterations of the structure optimization. If the cost of the Hessian is not too large, its use can significantly reduce the overall time for the structure minimization. Besides, the Hessian matrix calculation is a must in order to determine whether the optimized structure is truly

a local minimum.

To show the advantages of the availability of the analytic Hessian matrix for this research area and to probe the calculation of analytic second-order energy-derivatives on systems which make use of effective core potentials, the optimization of the methylthiolate-protected gold cluster $Au_{20}(S\text{-}CH_3)_{16}$ is presented. We also calculated the harmonic vibrational frequencies along with the IR and Raman intensities. The structure optimization and frequency analysis were performed with the HXYZ parallelization scheme, along with the Con-EN algorithm in parallel on 12 Intel Xeon X5675 @ 3.07 GHz processors with 4 GB of RAM. For the optimization and frequency analysis the LDA VWN [40] exchange-correlation functional was used. The SCF energy convergence criterion [102] was set to 10^{-6} atomic units. For the numerical integration a pruned fixed grid with 99 radial shells and 590 angular points per shell was employed [214]. For the density fitting the GEN-A2 auxiliary-functions were automatically generated. The gold atoms were represented with a Stuttgart-Dresden relativistic effective core potential with 19 valence electrons [215], whereas for the remaining atoms an all-electron DZVP basis set [83] was employed. The methodology was validated previously to match with the experimental Au_2 bond distance [216]. For all other settings the deMon2k defaults are used in these calculations [154]. The optimized geometry of $Au_{20}(S\text{-}CH_3)_{16}$ is depicted in Figure 7.7, where the sulfur atoms are represented by yellow-colored spheres. The inner Au atoms are metallic orange spheres, whereas the carbon and hydrogen atoms are black- and white-colored spheres, respectively.

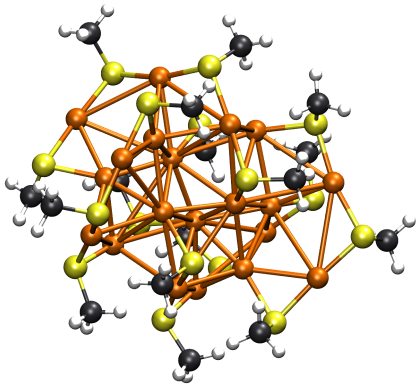

Figure 7.7: Optimized structure of the thiolate-protected $Au_{20}(S\text{-}CH_3)_{16}$.

The resulting size of the cluster is approximately 1.45 nm, with a core size of 0.82 nm. Each sulfur atom is always connected to two superficial gold atoms with an average bond length of 2.32 Å. In Figure 7.8 the analytically calculated IR and Raman spectra of the $Au_{20}(S\text{-}CH_3)_{16}$ cluster are presented. The vibrational analysis confirms that the structure is indeed a local minimum.

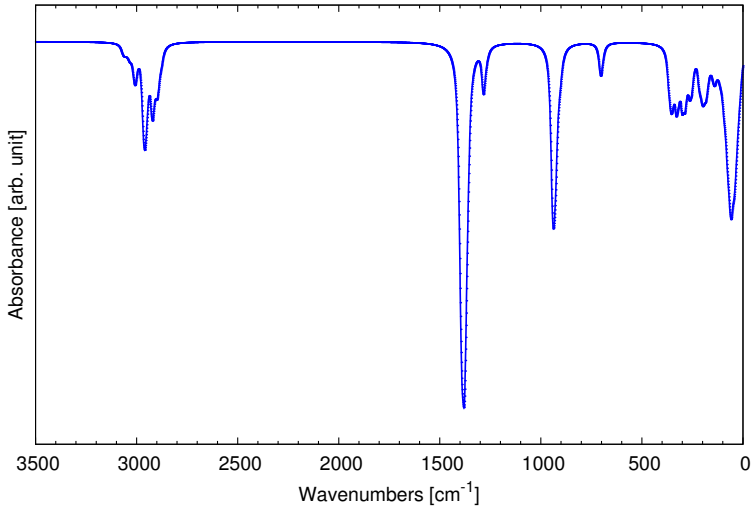

(a)

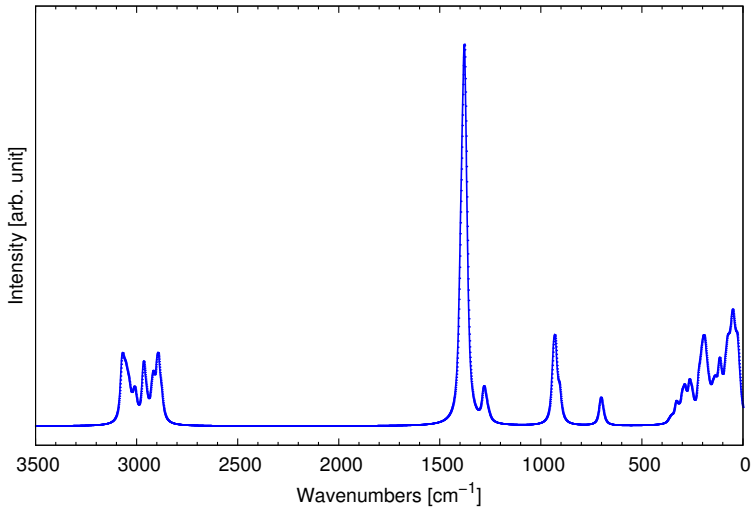

(b)

Figure 7.8: Comparison of the analytically calculated IR (top) and Raman (bottom) spectra of $Au_{20}(S\text{-}CH_3)_{16}$ at the VWN/DZVP/GEN-A2 level of theory.

The vibrational modes corresponding to the gold core are located below 100 cm^{-1}, whereas the peaks in the region between 250 and 350 cm^{-1} correspond to the stretching of the superficial gold and sulfur atoms. The peak at 700 cm^{-1} is assigned to C-S stretching, whereas the peak at 900 cm^{-1} corresponds to a methyl rocking vibration mode. The peak appearing between 1250 to 1300 cm^{-1} is assigned to symmetric CH_3 bending, whereas the most intense peak for both spectra, located between 1350 and 1450 cm^{-1} is assigned to the methyl twisting. The region between 2800 and 3000 cm^{-1} can be assigned to the symmetric C-H stretching and the region between 3000 and 3100 corresponds to modes assigned to asymmetric C-H stretching. The calculation of the Hessian matrix took around 6 hours to be completed. As a single-point SCF energy for this system can be obtained in around 210 seconds with the used computational settings here, an estimate for the finite-difference Hessian matrix calculation is approximately 42 hours. This means that the analytic approach is about 6 times faster than its finite-difference counterpart.

In order to show the efficiency of the analytic second-order energy-derivatives for a medium-sized nanocluster the optimization of the tert-butylbenzenethiolate-protected gold cluster $Au_{36}(S\text{-}C_6H_4t\text{-}Bu)_{16}$ was also performed. The structure of this system is depicted in Figure 7.9. The resulting size of the cluster is approximately 2.63 nm—about the double of the previous cluster, with a core size of 1.01 nm. Each sulfur atom is, similar to the $Au_{20}(S\text{-}CH_3)_{16}$, connected to two superficial gold atoms with an average bond length of 2.33 Å.

To perform this structure optimization an initial analytic Hessian matrix was calculated. The parallel run was performed on 96 Intel Xeon X5675 @ 3.07 GHz processors with 4 GB of RAM. The methodology employed was the same as for the $Au_{20}(S\text{-}CH_3)_{16}$ cluster, with the exception of an adaptive grid with 10^{-8} a.u. grid tolerance. The calculation of the analytic Hessian matrix took around 7 days. As the single-point SCF energy calculation for this system needs 90 minutes, an estimate for the finite-difference Hessian matrix calculation is approximately 212 days. This means that the analytic approach is about 28 times faster than its finite-difference counterpart.

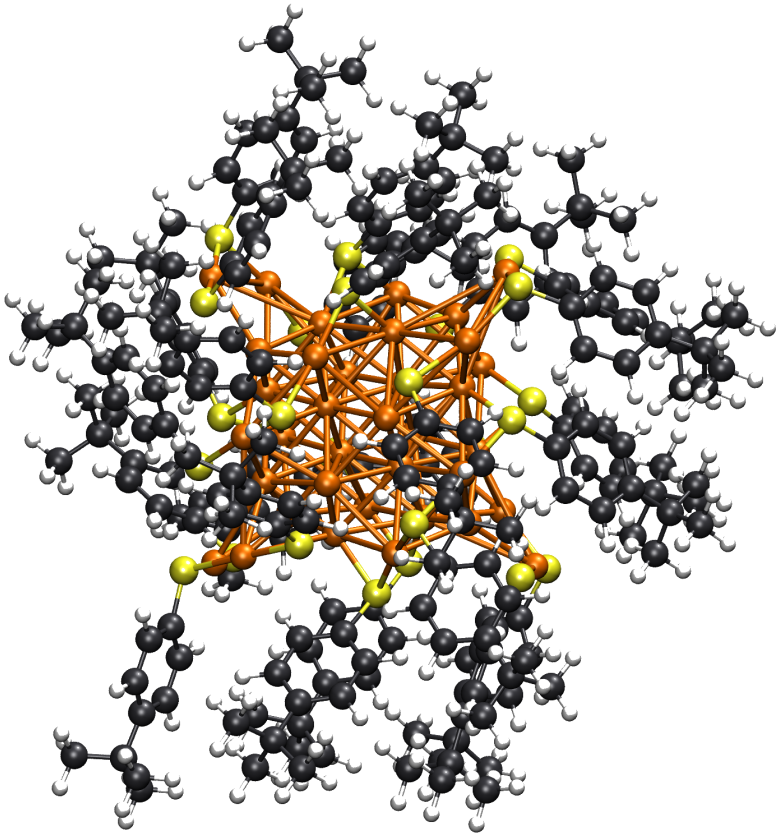

Figure 7.9: Optimized structure of the thiolate-protected $Au_{36}(S\text{-}C_6H_4t\text{-}Bu)_{16}$

It is evident that the finite-difference Hessian matrix calculations have become prohibitive for 612 atoms at the level of theory presented (about 7 000 basis functions, 12 500 auxiliary-functions and 180 ECP shells). Thus, if structure optimizations and vibrational analyses for systems of the size of the $Au_{279}(SR)_{84}$ nanocluster are performed, the analytic second-order ADFT-energy derivative is the method of choice to perform those calculations in reasonable times.

7.3 Endohedral Uranium Fullerenes

Already in 1985 it was proposed that fullerene cages could confine atoms or even small molecules in their interior. These structures have attracted special attention as a new class of technologically relevant materials [186]. The metal-containing fullerenes, more commonly called endohedral metallofullerenes (EMFs), have been attracting wide interest all over the world over the past two decades [217–219]. An interesting but difficult task in the study of EMFs is the structure determination of these systems, due to the large number of possible isomers that must be considered for a certain fullerene. Here, the combination of experimental IR and Raman spectroscopy with DFT calculations of molecular structures and vibrational spectra has proven already valuable for reliable structure elucidation of EMFs [220, 221]. In addition, Raman spectra are also useful tools for determining the metallofullerene symmetry and metal-cage bond strength [222]. In order to demonstrate the usefulness of our methodology in this respect, the harmonic vibrational frequencies as well as IR and Raman intensities were calculated for two isomers of $U_2@C_{80}$. The structures studied here are the result of an extensive search for minimum structures [223, 224] by exploring the potential energy surface using Born-Oppenheimer meta-molecular dynamics in which the atomic weights of uranium atoms are artificially reduced. Note that this does not alter the potential energy surface but greatly enhances the explored area in a given time period. This search yielded two isomers which are energetically very similar, but geometrically different. We will label them here as S_1 and S_2, respectively. Their optimized geometries are depicted in Figure 7.10. As the IR and Raman spectroscopy are techniques sensitive enough to distinguish geometrically different structures, the theoretical calculation can be used to characterize a determined structure by comparing with an experimental spectrum.

For the theoretical studies of these systems, the structure optimizations were performed without any symmetry constraint. Although these systems are not as large as the giant fullerenes, or the tert-butylbenzenethiolate-protected gold cluster, the SCF energy calculation requires many iterations to reach the convergence criteria. Thus, the use of the analytic

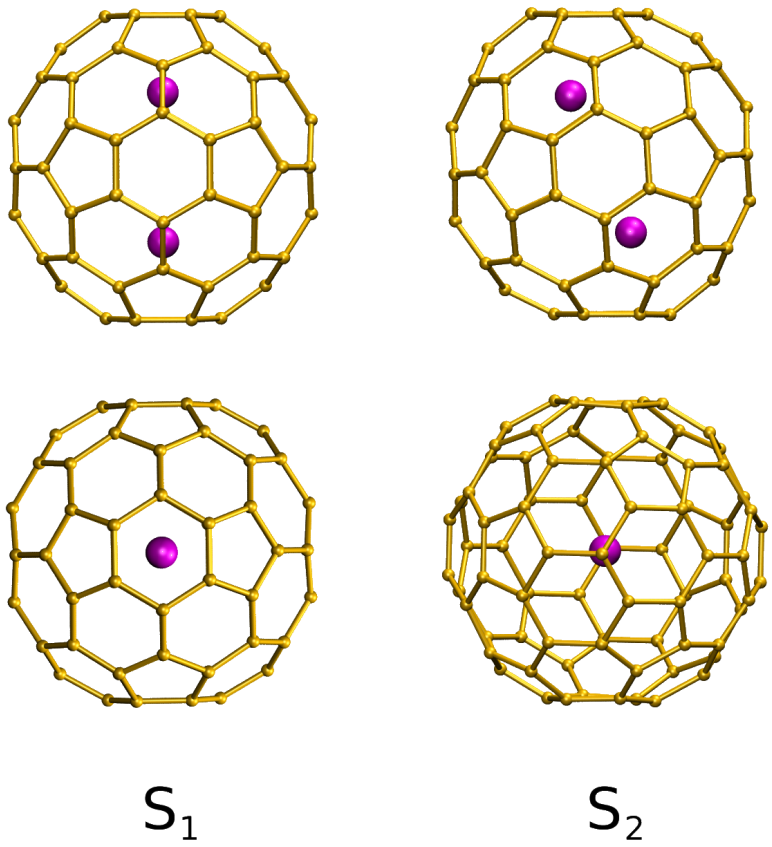

Figure 7.10: Perspective drawings showing the relative orientations of the optimized structures of S_1 (left) and S_2 (right). The first row shows an orientation where the principal axis lies in the plane of the paper, which passes through the U atoms. The second row shows a top view along the principal axis.

second-order energy-derivatives for the calculation of the vibrational spectra clearly becomes advantageous, as only one SCF calculation is required. These structure optimizations and frequency analyses were performed in parallel on 32 Intel Xeon E5-2650 @ 2.2GHz processors with 4 GB of RAM. The optimization and frequency analysis of the endohedral uranium fullerenes were performed using the GGA PBE [45] exchange-correlation functionals. The SCF energy convergence and auxiliary density convergence [102] were set to 10^{-9} a.u. and 10^{-6} a.u., respectively. For the numerical integration a pruned grid with 99 radial shells and 590 angular points per shell was used [214]. For the carbon atom the all-electron DZVP-GGA basis set was employed, whereas for the uranium atom the Stuttgart-Dresden quasi-

relativistic effective core potential with 32 valence electrons [225–227] and the corresponding valence basis set was used. For the density fitting the automatically-generated GEN-A2* [83] and GEN-A2** [224] auxiliary-function set were used for carbon and uranium, respectively. The unrestricted open-shell ADFT methodology was employed because spin contamination is considered negligible, compared to previously performed restricted open-shell calculations [224]. The ADPT convergence criterion was set to 7×10^{-7}. The HXYZ parallelization scheme was employed, along with the Con-EN algorithm. For all other settings the deMon2k defaults are used in these calculations [154]. The calculation of the analytic Hessian matrix took around 16 hours. As the single-point SCF energy calculation for this system needs about 90 minutes, an estimate for the finite-difference Hessian matrix calculation is approximately 295 hours. This means that the analytic approach is almost 18 times faster than its finite-difference counterpart. The obtained vibrational spectra are depicted in Figure 7.11, where the blue and green solid lines correspond to the isomers S_1 and S_2, respectively.

According to the experimental low-energy Raman spectrum of a sample of $U_2@C_{80}$, for a region between 100 and 600 cm^{-1}, obtained by Echegoyen et al. [228], a set of main peaks are observed at 122, 220 and 232 cm^{-1}. The lowest experimental peak, compared to the theoretical results, can be assigned to a Raman-active U-U stretching mode, whereas the remaining active modes can be assigned to breathing modes of the cage with no involvement of the U atoms. In fact, the remaining peaks observed in the theoretical analysis beyond 200 cm^{-1} are assigned to vibrational modes with practically non-existent U involvement. In order to further verify the previous statement, the IR and Raman spectra of an hexanionic fullerene C_{80}^{6-} cage with an approximate icosahedral symmetry were calculated at the same level of theory as for the $U_2@C_{80}$. The resulting C_{80}^{6-} spectra, corresponding to the red lines in Figure 7.11, are compared with those corresponding to the S_1 and S_2 isomers.

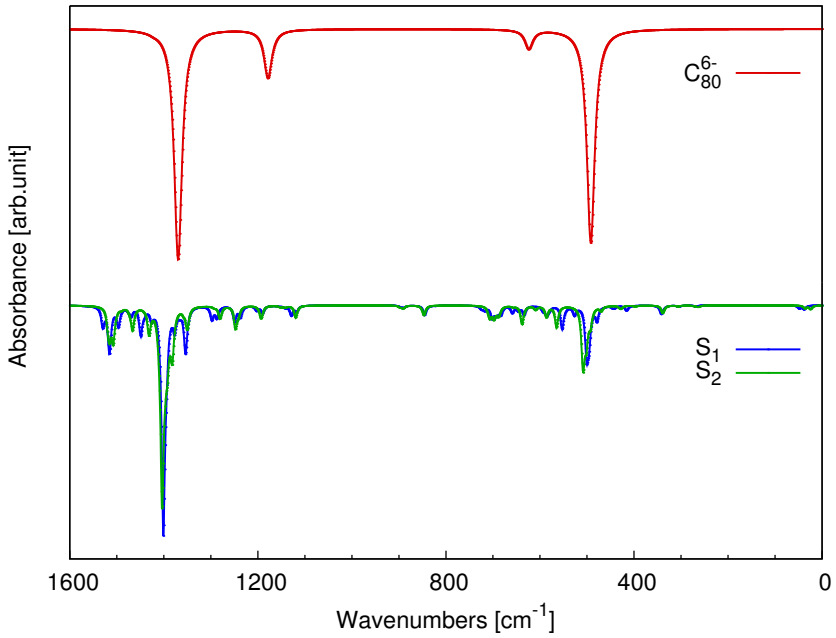

(a)

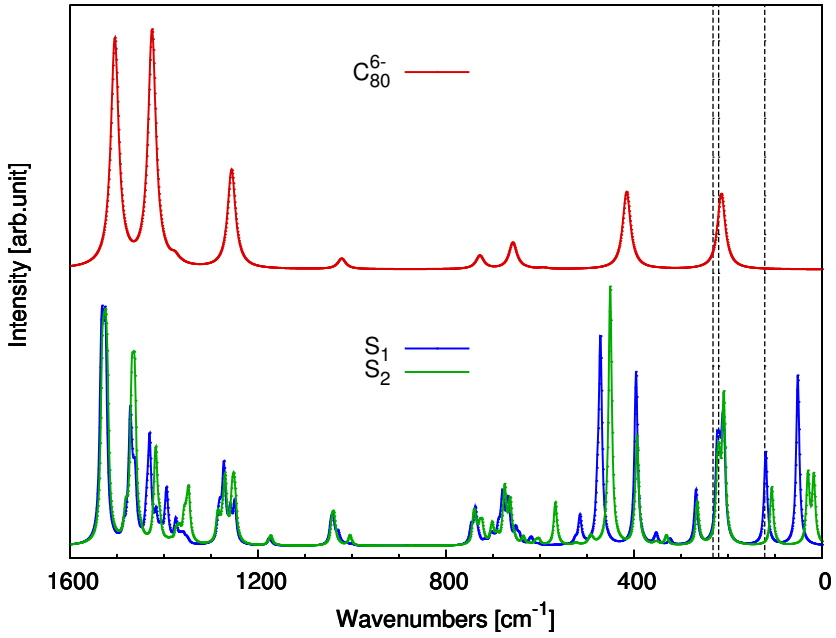

(b)

Figure 7.11: Comparison of the analytic a) IR and b) Raman spectra of S_1 and S_2 isomers with those to the C_{80}^{6-} fullerene. Dashed lines correspond to experimentally observed low-energy Raman spectra of Ref. 228.

As Echegoyen et al. state [228], the formal charge of U inside the fullerene cage is +3, thus, an excess of 6 electrons are transferred from the U dimer to the fullerene cage. The comparison supports the statement that no active modes corresponding to the fullerene cages are present below 200 cm^{-1} in neither IR nor the Raman spectra. Below the reported experimental Raman range, there are Raman-active vibrational modes which, for both S_1 and S_2, can be assigned to uranium-cage interactions where the vibrational mode is analogous to the rotation of the uranium dimer inside the cage. Typically, free (external) rotational modes are expected to have zero frequencies, but due to the confinement and interaction with the fullerene cage these dimer rotations are no longer free. Thus, changes in the total energy and polarizabilities due to the internal rotation of the U dimer are observed, and by consequence, Raman-active modes are seen in the theoretical spectra. The same is also true for the U dimer translational movements, which are IR-active, but their intensities are so weak that they are barely visible. These assignments, with their corresponding relative intensity are presented in Tables 7.1 and 7.2.

Table 7.1: Relative IR and Raman intensities for the S_1 isomer; s: strong, m: medium, w: weak, vw: very weak.

$\tilde{\nu}$ [cm^{-1}]	IR	Raman	Assignment
38.6	vw	-	U-U translation
48.9	vw	-	U-U translation
51.7	-	s	U-U rotation
51.8	-	s	U-U rotation
120.1	-	m	U-U stretching
144.7	vw	-	U-U translation
208.8	-	s	Cage breathing
212.1	-	s	Cage breathing
218.4	-	s	Cage breathing
223.6	-	s	Cage breathing

Table 7.2: Relative IR and Raman intensities for the S_2 isomer; s: strong, m: medium, w: weak, vw: very weak.

$\tilde{\nu}$ [cm^{-1}]	IR	Raman	Assignment
17.8	-	m	U-U rotation
25.0	vw	-	U-U translation
30.2	-	m	U-U rotation
36.9	vw	-	U-U translation
107.2	-	m	U-U stretching
140.2	vw	-	U-U translation
208.5	-	s	Cage breathing
210.0	-	s	Cage breathing
218.8	-	s	Cage breathing
222.6	-	s	Cage breathing

These tables show that the vibrational modes corresponding to the rotational-like modes are almost degenerate in the S_1 isomer, whereas for the S_2 system, degeneracy is broken by the U-U translation-like modes inside the fullerene cage. The comparison of the IR spectra of both S_1 and S_2 isomers (Figure 7.11) presents two important aspects. First, they are very similar throughout the frequency range. Second, the translational-like IR-active modes are so weak that they are barely visible. Thus, the IR spectra cannot provide enough information to distinguish one isomer from another. On the other hand, the Raman spectra could distinguish experimentally one isomer from the other. The single (degenerate) peak corresponding to the rotation-like U-U modes in S_1 isomer has a stronger intensity compared to the double (non-degenerate) modes in S_2. Besides, these intensities are easily visible compared to those of the IR spectra. This finding can be confirmed by very low frequency Raman spectra.

Chapter 8

CONCLUSIONS AND PERSPECTIVES

In this thesis the working equations for the analytic calculation of second-order ADFT-energy derivatives and their efficient serial and parallel implementation have been presented. In the context of ADPT response explicit low-scaling formulas for the calculation of the first-order perturbed density matrix employing the Eirola-Nevanlinna algorithm are derived. As a result, harmonic IR and Raman spectra calculations within the framework of ADFT through ADPT have become accessible. The extension of this approach to the unrestricted and restricted open-shell methodology is rather straightforward and was also implemented into deMon2k.

Serial benchmark calculations of frequency analyses of linear alkane chains demonstrate the improved computational performance of the analytic second-order derivative implementation with respect to their numerical finite-difference counterparts. This performance improvement increases monotonically with increasing degrees of freedom, i.e., with increasing system size.

The increased computational performance is also found in the different parallelization schemes discussed in this work. These parallel implementations, in combination with the conventional and direct variants of the Eirola-Nevanlinna algorithm, permit efficient analytic second-order energy-derivative calculations on a large variety of different computational architectures, ranging from single desktop machines to high performance computer architectures. In this respect it is worthwhile to highlight a general trend observed in the discussed applications. The computational performance improvement due to analytic second-order

energy-derivatives is largest for systems with SCF convergence problems. Marked examples are the discussed endohedral metallofullerenes and the thiolate-protected Au_{36}(S-C_6H_4-t-Bu)$_{16}$ where speed-up factors of 20 to 30 with respect to finite-difference methods are found. These factors are expected to improve even further as these systems increase in size. Note also that the calculation of reliable vibrational spectra demands high quality density matrix and density fitting coefficients, i.e., a well converged single-point SCF solution. Thus, a tightening of the SCF convergence criteria and grid tolerances for the numerical integration of the exchange-correlation contributions as well as for the semi-numerical calculation of pseudopotential integrals [229] is always encouraged.

We also have shown that the calculation of harmonic IR and Raman spectra using analytic second-order ADFT-energy derivatives can produce in essence the same results as four-center Kohn-Sham methods, albeit with dramatically reduced computational demand in CPU time and allocatable memory. Therefore, the methodology proposed here is particularly useful for larger systems where the finite-difference ADFT approach becomes impractical due to prohibitive CPU times. Even though harmonic IR frequencies are very useful for the characterization of the most intense peaks in an experimental spectra, their accuracy is still not sufficient for an ab-initio assignment of experimental spectrum. To this end anharmonic corrections must be included. A possible approach in this direction represents the so-called vibrational self-consistent (VSCF) field method [230–233] that has been used with good success to go beyond the harmonic approximation. This method solves the vibrational Schrödinger equation in mass-weighted normal coordinates by proposing a Hartree product ansatz which leads to single-mode VSCF equations. The major computational difficulty arises from the evaluation of multidimensional integrals which depend upon as many vibrational modes as are coupled in the scheme [234]. The use of third- and fourth-order electronic energy derivatives are useful to detect mode coupling terms which may be expected to give a sizable contribution to the resulting vibrational frequencies [235]. A further extension employs Møller–Plesset perturbation theory in a fashion analogous to its use in electronic structure problems and is called vibrational perturbation theory (VPT). Here the nuclear Hamiltonian contains harmonic and anharmonic terms [236] which depend on third-

and fourth-order derivatives of the energy with respect to the nuclear coordinates. If the anharmonic terms are assumed to be small in comparison to the harmonic ones they may be treated as perturbations and the application of Rayleigh-Schrödinger perturbation theory yields a sequence of vibrational perturbation levels (VPTn, n=1,2,3..) [237]. Thus, in all cases it is clear that third- and fourth-order derivatives of the energy with respect to nuclear coordinates are needed for the calculation of anharmonic vibrational corrections [238]. The analytic evaluation of these derivatives is difficult and can become computationally expensive and numerically challenging because the second-order density matrix derivatives are needed. Particularly, in DFT numerical challenges arise from the third- and fourth-order functional derivatives of the exchange-correlation energy. Therefore, finite-difference methods are usually employed. Their accuracy depends critically on the finite step size employed [236]. Various step sizes have been proposed, from fixed step sizes that range between 0.001 to 0.02 bohr depending on the highest-order derivative information available [239, 240], to adaptive step sizes which are proportional to the reduced mass and harmonic frequencies [241]. Having the evaluation of analytic second-order derivatives at hand, third-order finite-difference derivatives can be computed by the following scheme [242],

$$\frac{\partial^3 E}{\partial R_k \partial R_j \partial R_i} \simeq \frac{1}{2\Delta R_k} \left[\left(\frac{\partial^2 E}{\partial R_j \partial R_i} \right)_{+\Delta R_k} - \left(\frac{\partial^2 E}{\partial R_j \partial R_i} \right)_{-\Delta R_k} \right]. \tag{8.1}$$

Here $(\partial^2 E/\partial R_j \partial R_i)_{\pm \Delta R_k}$ denotes the second-order energy-derivative with respect to nuclear displacements at the nuclear position $R_k \pm \Delta R_k$. Figure 8.1 depicts the grid points used for the finite-difference calculation of third- and fourth-order energy-derivatives. The origin (green) represents the unperturbed coordinates of a molecular system. For the calculation of Eq. (8.1) displacements according to the black dots in Figure 8.1 are performed. At these points SCF calculations must be converged and the corresponding analytic second-order energy-derivatives must be calculated. Note that these steps are independent of each other which permits a simple and efficient parallelization. Thus, for a given molecular system the third-order derivatives can be calculated at a cost comparable to that of $6M$ SCF and analytic Hessian matrix calculations, M being the number of atoms in the system.

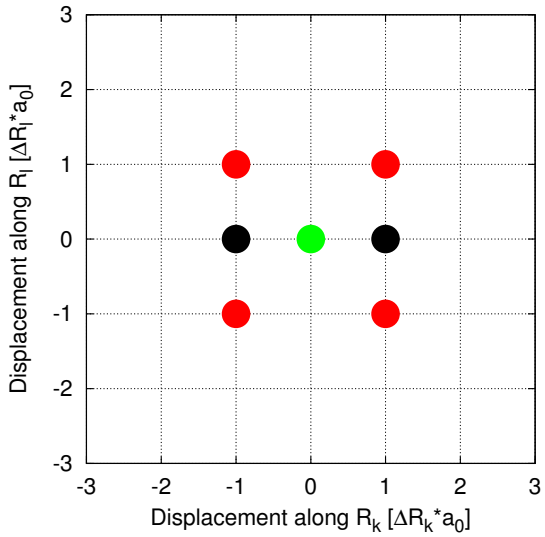

Figure 8.1: Grid points used for the calculation of semi-numerical third- and fourth-order energy-derivatives.

The calculation of the fourth-order electronic energy derivative elements with respect to the same nuclear displacement R_k is straightforward. As Eq. (8.2) shows it only requires the second-order energy-derivatives evaluated at the unperturbed coordinates, i.e., the origin of Figure 8.1 (green dot):

$$\frac{\partial^4 E}{\partial R_k^2 \partial R_j \partial R_i} \simeq \frac{1}{{\Delta R_k}^2} \left[\left(\frac{\partial^2 E}{\partial R_j \partial R_i} \right)_{+\Delta R_k} - 2 \left(\frac{\partial^2 E}{\partial R_j \partial R_i} \right)_{R_0} + \left(\frac{\partial^2 E}{\partial R_j \partial R_i} \right)_{-\Delta R_k} \right]. \tag{8.2}$$

Thus, these derivatives require almost no extra computational effort.

The calculation of fourth-order electronic derivatives with respect to four different displacements require four finite displacements, indicated by the four red dots in Figure 8.1. These derivatives are then calculated as,

$$\frac{\partial^4 E}{\partial R_l \partial R_k \partial R_j \partial R_i} \simeq \frac{1}{4 \Delta R_l \Delta R_k} \left[\left(\frac{\partial^2 E}{\partial R_j \partial R_i} \right)_{+\Delta R_l, +\Delta R_k} - \left(\frac{\partial^2 E}{\partial R_j \partial R_i} \right)_{+\Delta R_l, -\Delta R_k} - \left(\frac{\partial^2 E}{\partial R_j \partial R_i} \right)_{-\Delta R_l, +\Delta R_k} + \left(\frac{\partial^2 E}{\partial R_j \partial R_i} \right)_{-\Delta R_l, -\Delta R_k} \right]. \tag{8.3}$$

Thus, a full set of second-, third- and fourth-order derivatives with respect to nuclear displacements requires $36M^2$ SCF and analytic Hessian matrix calculations. This underlines the importance of a computationally efficient methodology for analytical second-order energy-derivative calculations in the framework of ADFT for the accurate ab-initio simulation of vibrational spectra including anharmonic corrections.

Although ADPT-ADFT theory can provide first-principle calculation of response properties with systems up to around thousand atoms [139], a frequency analysis of a protein in water is still computationally unfeasible with a QM-only methodology. For such systems with many thousands of atoms, hybrid quantum mechanical (QM) and molecular mechanics (MM) methodologies must be used. In such methods the studied system is partitioned into two parts, the QM subsystem (in our previous example, the protein), which could be treated with ADFT, and the embedding environment (the water) which can be described with molecular mechanics methods [243]. As the energy expression for QM/MM is already available in the framework of ADFT [244], analytic second-order derivatives could in principle be calculated. Such a Hessian matrix, schematically depicted in Figure 8.2, can be separated into three main regions: a QM-MM, a QM-QM and a MM-MM block. Whereas the calculation of the QM-QM and MM-MM blocks is rather straightforward the QM-MM block needs some considerations.

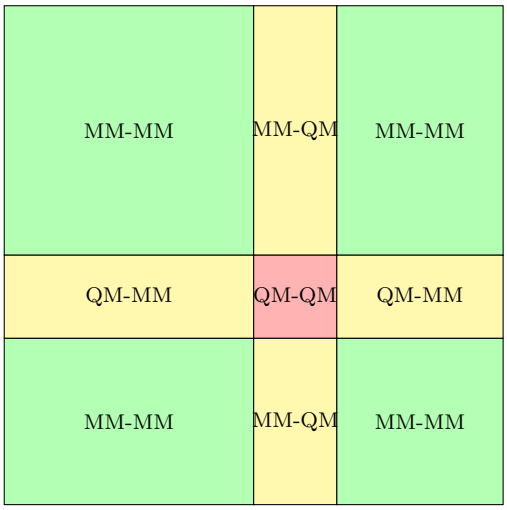

Figure 8.2: Hessian matrix structure for a QM/MM system.

There are two general types of contributions to this block that originate from the introduced MM atoms. The first arises from the mechanical interaction energy between the QM and MM systems. In our QM/MM implementation this term is expressed by a Lennard-Jones potential. Thus, the corresponding second-order derivatives can be straightforward analytically calculated. The second contribution corresponds to the electrostatic interaction between the QM electrons and the MM point charges. This implies the calculation of perturbed density matrix elements, $\mathbf{P}^{(\lambda)}$, for each corresponding MM degree of freedom. It is expected to be the principal bottleneck for the analytic Hessian calculation of a QM/MM system. Therefore, the ADPT equations must also be solved for all MM degrees of freedom. However, the response equation system will have important simplifications due to the fact that there are no basis functions on the MM atoms. These simplifications have been already explored in the framework of conventional DFT/MM calculations for the corresponding CPKS response equations [245, 246]. Despite these improvements such calculations are still prohibitive for large systems, including enzymes. Thus, a similar derivation of second-order ADFT-energy derivatives within the QM/MM framework is expected to be a useful tool to evaluate frequencies and infrared intensities of biological systems.

Appendix A

Perturbation-Dependent Analytic GGA Exchange-Correlation Integrals

The calculation of analytic GGA exchange-correlation contributions [12] is crucial in order to obtain numerically stable and computationally efficient expressions for the calculation of vibrational harmonic frequencies in ADFT. There are several stages in our derivation where exchange-correlation contributions appear. One is the second-order ADFT-energy derivative, Eq. (4.20), in which the following exchange-correlation terms appear:

$$\sum_{\bar{k}} x_{\bar{k}}^{(\eta)} \left\langle \bar{k}^{(\lambda)} \middle| v_{xc}\left[\tilde{\rho}\right] \right\rangle \;\; ; \;\; \sum_{\bar{k}} x_{\bar{k}} \left\langle \bar{k}^{(\lambda\eta)} \middle| v_{xc}\left[\tilde{\rho}\right] \right\rangle \;\; ; \;\; \sum_{\bar{k},\bar{l}} x_{\bar{k}} x_{\bar{l}}^{(\eta)} \left\langle \bar{k}^{(\lambda)} \middle| f_{xc}\left[\tilde{\rho}\right] \middle| \bar{l} \right\rangle \;\; ; \tag{A.1}$$
$$\sum_{\bar{k},\bar{l}} x_{\bar{k}} x_{\bar{l}} \left\langle \bar{k}^{(\lambda)} \middle| f_{xc}\left[\tilde{\rho}\right] \middle| \bar{l}^{(\eta)} \right\rangle .$$

Another stage is the calculation of the perturbed exchange-correlation fitting coefficients, Eq. (5.38), in which the following exchange-correlation terms appear:

$$\sum_{\bar{l}} G_{\bar{k}\bar{l}}^{-1} \left\langle \bar{l}^{(\lambda)} \middle| v_{xc}\left[\tilde{\rho}\right] \right\rangle \;\; ; \;\; \sum_{\bar{l},\bar{m}} G_{\bar{k}\bar{l}}^{-1} \left\langle \bar{l} \middle| f_{xc}\left[\tilde{\rho}\right] \middle| \bar{m} \right\rangle x_{\bar{m}}^{(\lambda)} \;\; ; \;\; \sum_{\bar{l},\bar{m}} G_{\bar{k}\bar{l}}^{-1} \left\langle \bar{l} \middle| f_{xc}\left[\tilde{\rho}\right] \middle| \bar{m}^{(\lambda)} \right\rangle x_{\bar{m}}. \tag{A.2}$$

In the following section we discuss the calculation of the following individual terms using perturbation-dependent basis and auxiliary-functions:

$$\left\langle \bar{k}^{(\lambda)} \middle| v_{xc}\left[\tilde{\rho}\right] \right\rangle , \tag{A.3}$$

$$\left\langle \bar{k}^{(\lambda\eta)} \middle| v_{xc}\left[\tilde{\rho}\right] \right\rangle , \tag{A.4}$$

$$\sum_{\bar{l}} x_{\bar{l}}^{(\eta)} \left\langle \bar{k}^{(\lambda)} \right| f_{xc}\left[\tilde{\rho}\right] \left| \bar{l} \right\rangle, \tag{A.5}$$

$$\sum_{\bar{l}} x_{\bar{l}} \left\langle \bar{k}^{(\lambda)} \right| f_{xc}\left[\tilde{\rho}\right] \left| \bar{l}^{(\eta)} \right\rangle, \tag{A.6}$$

$$\sum_{\bar{l}} x_{\bar{l}}^{(\lambda)} \left\langle \bar{k} \right| f_{xc}\left[\tilde{\rho}\right] \left| \bar{l} \right\rangle, \tag{A.7}$$

$$\sum_{\bar{l}} x_{\bar{l}} \left\langle \bar{k} \right| f_{xc}\left[\tilde{\rho}\right] \left| \bar{l}^{(\lambda)} \right\rangle. \tag{A.8}$$

A.1 Exchange-Correlation Potential Integrals

Throughout this discussion, we assume that the exchange-correlation energy is expressed by the GGA. In the ADFT framework, the functionals in this class depend not only on the auxiliary density but also on its gradient, here expressed through the quantity,

$$\tilde{\gamma} = \vec{\nabla}\tilde{\rho}(\mathbf{r}) \cdot \vec{\nabla}\tilde{\rho}(\mathbf{r}) = \left| \vec{\nabla}\tilde{\rho}(\mathbf{r}) \right|^2. \tag{A.9}$$

The GGA exchange-correlation energy in the framework of ADFT is expressed as,

$$E_{xc}[\tilde{\rho}, \tilde{\gamma}] = \int e_{xc}(\tilde{\rho}, \tilde{\gamma}) \; d\mathbf{r}. \tag{A.10}$$

The functional derivative of $E_{xc}[\tilde{\rho}, \tilde{\gamma}]$ defines the GGA exchange–correlation potential and is given by,

$$v_{xc}[\tilde{\rho}, \tilde{\gamma}](\mathbf{r}) \equiv \frac{\delta E_{xc}[\tilde{\rho}, \tilde{\gamma}]}{\delta \tilde{\rho}(\mathbf{r})} = \frac{\partial e_{xc}(\tilde{\rho}, \tilde{\gamma})}{\partial \tilde{\rho}(\mathbf{r})} - \vec{\nabla} \cdot \frac{\partial e_{xc}(\tilde{\rho}, \tilde{\gamma})}{\partial \vec{\nabla}\tilde{\rho}(\mathbf{r})}. \tag{A.11}$$

Note that $\partial e_{xc}/\partial\vec{\nabla}\tilde{\rho}$ represents a common shorthand notation for a derivative of a scalar quantity, $e_{xc}(\tilde{\rho}, \tilde{\gamma})$, with respect to the three components $\partial\tilde{\rho}(\mathbf{r})/\partial x$, $\partial\tilde{\rho}(\mathbf{r})/\partial y$ and $\partial\tilde{\rho}(\mathbf{r})/\partial z$. Therefore, the derivative $\partial e_{xc}/\partial\vec{\nabla}\tilde{\rho}$ is a Euclidean vector with three components,

$$\frac{\partial e_{xc}}{\partial \vec{\nabla}\tilde{\rho}} = \left(\frac{\partial e_{xc}}{\partial \tilde{\rho}^{(x)}}, \frac{\partial e_{xc}}{\partial \tilde{\rho}^{(y)}}, \frac{\partial e_{xc}}{\partial \tilde{\rho}^{(z)}} \right), \tag{A.12}$$

with,

$$\tilde{\rho}^{(x)} = \frac{\partial \tilde{\rho}(\mathbf{r})}{\partial x} \;\; ; \;\; \tilde{\rho}^{(y)} = \frac{\partial \tilde{\rho}(\mathbf{r})}{\partial y} \;\; ; \;\; \tilde{\rho}^{(z)} = \frac{\partial \tilde{\rho}(\mathbf{r})}{\partial z}. \tag{A.13}$$

We now derive "implementation forms" for the exchange-correlation potential integrals, Eq. (A.3) and (A.4). Our aim is to obtain formulations for perturbation-dependent auxiliary-functions that are as close as possible to those already derived for perturbation-independent auxiliary-functions [12]. We start with the substitution of Eq. (A.11) into Eq. (A.3), which yields:

$$\left\langle \bar{k}^{(\lambda)} \middle| v_{xc}[\tilde{\rho}, \tilde{\gamma}] \right\rangle = \int \left[\frac{\partial e_{xc}(\tilde{\rho}, \tilde{\gamma})}{\partial \tilde{\rho}(\mathbf{r})} - \vec{\nabla} \cdot \frac{\partial e_{xc}(\tilde{\rho}, \tilde{\gamma})}{\partial \vec{\nabla} \tilde{\rho}(\mathbf{r})} \right] \bar{k}^{(\lambda)}(\mathbf{r}) \; d\mathbf{r}. \tag{A.14}$$

Integrating by parts the second term of Eq. (A.14), and noting that $\bar{k}^{(\lambda)}$ vanishes at $\pm\infty$, we obtain:

$$\left\langle \bar{k}^{(\lambda)} \middle| v_{xc}[\tilde{\rho}, \tilde{\gamma}] \right\rangle = \int \left[\frac{\partial e_{xc}(\tilde{\rho}, \tilde{\gamma})}{\partial \tilde{\rho}(\mathbf{r})} + \frac{\partial e_{xc}(\tilde{\rho}, \tilde{\gamma})}{\partial \vec{\nabla} \tilde{\rho}(\mathbf{r})} \cdot \vec{\nabla} \right] \bar{k}^{(\lambda)}(\mathbf{r}) \; d\mathbf{r}. \tag{A.15}$$

Applying the chain rule,

$$\frac{\partial e_{xc}(\tilde{\rho}, \tilde{\gamma})}{\partial \vec{\nabla} \tilde{\rho}(\mathbf{r})} = \frac{\partial e_{xc}(\tilde{\rho}, \tilde{\gamma})}{\partial \left| \vec{\nabla} \tilde{\rho}(\mathbf{r}) \right|} \frac{\vec{\nabla} \tilde{\rho}(\mathbf{r})}{\left| \vec{\nabla} \tilde{\rho}(\mathbf{r}) \right|}, \tag{A.16}$$

to the second term in Eq. (A.15) in order to obtain the derivative of $e_{xc}[\tilde{\rho}, \tilde{\gamma}]$ in terms of the rotationally invariant approximate density derivative norm yields the final "implementation form" for the (A.3) integral:

$$\left\langle \bar{k}^{(\lambda)} \middle| v_{xc}[\tilde{\rho}, \tilde{\gamma}] \right\rangle = \int \left[\frac{\partial e_{xc}(\tilde{\rho}, \tilde{\gamma})}{\partial \tilde{\rho}(\mathbf{r})} + \frac{\partial e_{xc}(\tilde{\rho}, \tilde{\gamma})}{\partial \left| \vec{\nabla} \tilde{\rho}(\mathbf{r}) \right|} \frac{\vec{\nabla} \tilde{\rho}(\mathbf{r})}{\left| \vec{\nabla} \tilde{\rho}(\mathbf{r}) \right|} \cdot \vec{\nabla} \right] \bar{k}^{(\lambda)}(\mathbf{r}) \; d\mathbf{r}. \tag{A.17}$$

Note the appearance of an auxiliary-function mixed derivative, $\vec{\nabla} \bar{k}^{(\lambda)}(\mathbf{r})$, with respect to nuclear and electronic coordinates which is the main difference to the equivalent term for

perturbation-independent auxiliary-functions. Due to the use of primitive Hermite-Gaussian auxiliary-functions these mixed derivatives can be straightforward calculated from corresponding derivatives with respect to electron coordinates alone [99]. Following the same argument the "implementation form" for the (A.4) integral is given as,

$$\left\langle \bar{k}^{(\lambda\eta)} \middle| v_{xc}[\tilde{\rho},\tilde{\gamma}] \right\rangle = \int \left[\frac{\partial e_{xc}(\tilde{\rho},\tilde{\gamma})}{\partial \tilde{\rho}(\mathbf{r})} + \frac{\partial e_{xc}(\tilde{\rho},\tilde{\gamma})}{\partial \left|\vec{\nabla}\tilde{\rho}(\mathbf{r})\right|} \frac{\vec{\nabla}\tilde{\rho}(\mathbf{r})}{\left|\vec{\nabla}\tilde{\rho}(\mathbf{r})\right|} \cdot \vec{\nabla} \right] \bar{k}^{(\lambda\eta)} \, d\mathbf{r}. \tag{A.18}$$

The third-order auxiliary-function mixed derivatives, $\vec{\nabla}\bar{k}^{(\lambda\eta)}(\mathbf{r})$, can be calculated as described above, i.e., as derivatives with respect to electron coordinates alone.

A.2 Exchange-Correlation Kernel Integrals

For the evaluation of the integral sums (A.5), (A.6), (A.7) and (A.8) the exchange-correlation kernel, which is the functional derivative of the exchange-correlation potential, is needed. Generally, the exchange-correlation potential is a functional at coordinate $\mathbf{r}$ that might vary by a density change at a different point $\mathbf{r}'$. Therefore, we obtain for its derivative,

$$\frac{\partial v_{xc}[\tilde{\rho},\tilde{\gamma}](\mathbf{r})}{\partial \lambda} = \int \frac{\delta v_{xc}[\tilde{\rho},\tilde{\gamma}](\mathbf{r})}{\delta \tilde{\rho}(\mathbf{r}')} \frac{\partial \tilde{\rho}(\mathbf{r}')}{\partial \lambda} \, d\mathbf{r}'. \tag{A.19}$$

However, due to the semi-local nature of GGA potentials, i.e., $v_{xc}[\tilde{\rho},\tilde{\gamma}](\mathbf{r})$ is only a function of $\tilde{\rho}(\mathbf{r})$ and its derivatives at this position, the functional derivative in Eq. (A.19) is given by [247],

$$\frac{\delta v_{xc}[\tilde{\rho},\tilde{\gamma}](\mathbf{r})}{\delta \tilde{\rho}(\mathbf{r}')} = \delta(\mathbf{r}-\mathbf{r}') \frac{d v_{xc}[\tilde{\rho},\tilde{\gamma}](\mathbf{r})}{d \tilde{\rho}(\mathbf{r}')}. \tag{A.20}$$

Expanding the differential in Eq. (A.20) for a GGA functional yields:

$$\frac{\delta v_{xc}[\tilde{\rho},\tilde{\gamma}](\mathbf{r})}{\delta \tilde{\rho}(\mathbf{r}')} = \delta(\mathbf{r}-\mathbf{r}') \left[\frac{\partial v_{xc}[\tilde{\rho},\tilde{\gamma}](\mathbf{r})}{\partial \tilde{\rho}(\mathbf{r}')} + \frac{\partial v_{xc}[\tilde{\rho},\tilde{\gamma}](\mathbf{r})}{\partial \vec{\nabla}'\tilde{\rho}(\mathbf{r}')} \cdot \frac{\partial \vec{\nabla}'\tilde{\rho}(\mathbf{r}')}{\partial \tilde{\rho}(\mathbf{r}')} \right]. \tag{A.21}$$

The last term of Eq. (A.21) can be expressed as,

$$\begin{aligned}\frac{\partial\vec{\nabla}'\tilde{\rho}(\mathbf{r}')}{\partial\tilde{\rho}(\mathbf{r}')} =& \frac{\partial}{\partial\tilde{\rho}(\mathbf{r}')}\left(\frac{\partial}{\partial x'}\tilde{\rho}(\mathbf{r}'),\frac{\partial}{\partial y'}\tilde{\rho}(\mathbf{r}'),\frac{\partial}{\partial z'}\tilde{\rho}(\mathbf{r}')\right)\\ =& \left(\frac{\partial}{\partial x'}\frac{\partial\tilde{\rho}(\mathbf{r}')}{\partial\tilde{\rho}(\mathbf{r}')},\frac{\partial}{\partial y'}\frac{\partial\tilde{\rho}(\mathbf{r}')}{\partial\tilde{\rho}(\mathbf{r}')},\frac{\partial}{\partial z'}\frac{\partial\tilde{\rho}(\mathbf{r}')}{\partial\tilde{\rho}(\mathbf{r}')}\right) = \vec{\nabla}'. \end{aligned} \tag{A.22}$$

Therefore, the GGA exchange-correlation potential derivative takes the form:

$$\frac{\delta v_{xc}[\tilde{\rho},\tilde{\gamma}](\mathbf{r})}{\delta\tilde{\rho}(\mathbf{r}')} = \delta(\mathbf{r}-\mathbf{r}')\left[\frac{\partial v_{xc}[\tilde{\rho},\tilde{\gamma}](\mathbf{r})}{\partial\tilde{\rho}(\mathbf{r}')} + \frac{\partial v_{xc}[\tilde{\rho},\tilde{\gamma}](\mathbf{r})}{\partial\vec{\nabla}'\tilde{\rho}(\mathbf{r}')}\cdot\vec{\nabla}'\right] = f_{xc}[\tilde{\rho},\tilde{\gamma}](\mathbf{r},\mathbf{r}'). \tag{A.23}$$

With this form for the ADFT GGA exchange-correlation kernel, $f_{xc}[\tilde{\rho},\tilde{\gamma}](\mathbf{r},\mathbf{r}')$, we now turn to the evaluation of the integral sums. Because of their structural similarities, we will only discuss in detail Eq. (A.5) which is expressed as,

$$\begin{aligned} S \equiv& \sum_{\bar{l}} x_{\bar{l}}^{(\eta)} \left\langle \bar{k}^{(\lambda)}\right| f_{xc}[\tilde{\rho},\tilde{\gamma}] \left|\bar{l}\right\rangle = \\ & \sum_{\bar{l}} x_{\bar{l}}^{(\eta)} \iint \bar{k}^{(\lambda)}(\mathbf{r})\ \delta(\mathbf{r}-\mathbf{r}')\left[\frac{\partial v_{xc}[\tilde{\rho},\tilde{\gamma}](\mathbf{r})}{\partial\tilde{\rho}(\mathbf{r}')} + \frac{\partial v_{xc}[\tilde{\rho},\tilde{\gamma}](\mathbf{r})}{\partial\vec{\nabla}'\tilde{\rho}(\mathbf{r}')}\cdot\vec{\nabla}'\right]\bar{l}(\mathbf{r}')\ d\mathbf{r}\ d\mathbf{r}'. \end{aligned} \tag{A.24}$$

To ease the notation we introduce the differential $d\mathbf{u}' = \delta(\mathbf{r}-\mathbf{r}')\ d\mathbf{r}'$:

$$S = \sum_{\bar{l}} x_{\bar{l}}^{(\eta)} \iint \bar{k}^{(\lambda)}(\mathbf{r})\left[\frac{\partial v_{xc}[\tilde{\rho},\tilde{\gamma}](\mathbf{r})}{\partial\tilde{\rho}(\mathbf{r}')} + \frac{\partial v_{xc}[\tilde{\rho},\tilde{\gamma}](\mathbf{r})}{\partial\vec{\nabla}'\tilde{\rho}(\mathbf{r}')}\cdot\vec{\nabla}'\right]\bar{l}(\mathbf{r}')\ d\mathbf{r}\ d\mathbf{u}'. \tag{A.25}$$

This expression can be expanded into two terms,

$$\begin{aligned} S =& \sum_{\bar{l}} x_{\bar{l}}^{(\eta)} \iint \bar{k}^{(\lambda)}(\mathbf{r})\left[\frac{\partial v_{xc}[\tilde{\rho},\tilde{\gamma}](\mathbf{r})}{\partial\tilde{\rho}(\mathbf{r}')}\right]\bar{l}(\mathbf{r}')\ d\mathbf{r}\ d\mathbf{u}' + \\ & \sum_{\bar{l}} x_{\bar{l}}^{(\eta)} \iint \bar{k}^{(\lambda)}(\mathbf{r})\left[\frac{\partial v_{xc}[\tilde{\rho},\tilde{\gamma}](\mathbf{r})}{\partial\vec{\nabla}'\tilde{\rho}(\mathbf{r})}\cdot\vec{\nabla}'\right]\bar{l}(\mathbf{r}')\ d\mathbf{r}\ d\mathbf{u}'. \end{aligned} \tag{A.26}$$

Reordering the integrands,

$$S = \sum_{\bar{l}} x_{\bar{l}}^{(\eta)} \iint \bar{l}(\mathbf{r}') \left[\frac{\partial v_{xc}[\tilde{\rho}, \tilde{\gamma}](\mathbf{r})}{\partial \tilde{\rho}(\mathbf{r}')} \right] \bar{k}^{(\lambda)}(\mathbf{r}) \; d\mathbf{r} \; d\mathbf{u}' + \sum_{\bar{l}} x_{\bar{l}}^{(\eta)} \iint \vec{\nabla}' \; \bar{l}(\mathbf{r}') \cdot \left[\frac{\partial v_{xc}[\tilde{\rho}, \tilde{\gamma}](\mathbf{r})}{\partial \vec{\nabla}' \tilde{\rho}(\mathbf{r}')} \right] \bar{k}^{(\lambda)}(\mathbf{r}) \; d\mathbf{r} \; d\mathbf{u}', \tag{A.27}$$

and expanding the exchange-correlation potential according to Eq. (A.11) yields the following explicit form for the (A.5) integral sum,

$$\begin{aligned} S = & \sum_{\bar{l}} x_{\bar{l}}^{(\eta)} \iint \bar{l}(\mathbf{r}') \left[\frac{\partial^2 e_{xc}[\tilde{\rho}, \tilde{\gamma}]}{\partial \tilde{\rho}(\mathbf{r}') \partial \tilde{\rho}(\mathbf{r})} \right] \bar{k}^{(\lambda)}(\mathbf{r}) \; d\mathbf{r} \; d\mathbf{u}' - \\ & \sum_{\bar{l}} x_{\bar{l}}^{(\eta)} \int \bar{l}(\mathbf{r}') \frac{\partial}{\partial \tilde{\rho}(\mathbf{r}')} \left[\int \vec{\nabla} \cdot \frac{\partial e_{xc}[\tilde{\rho}, \tilde{\gamma}]}{\partial \vec{\nabla} \tilde{\rho}(\mathbf{r})} \; \bar{k}^{(\lambda)}(\mathbf{r}) \; d\mathbf{r} \right] d\mathbf{u}' + \\ & \sum_{\bar{l}} x_{\bar{l}}^{(\eta)} \int \vec{\nabla}' \bar{l}(\mathbf{r}') \cdot \frac{\partial}{\partial \vec{\nabla}' \tilde{\rho}(\mathbf{r}')} \left[\int \frac{\partial e_{xc}[\tilde{\rho}, \tilde{\gamma}]}{\partial \tilde{\rho}(\mathbf{r})} \; \bar{k}^{(\lambda)}(\mathbf{r}) \; d\mathbf{r} \right] d\mathbf{u}' - \\ & \sum_{\bar{l}} x_{\bar{l}}^{(\eta)} \int \vec{\nabla}' \bar{l}(\mathbf{r}') \cdot \frac{\partial}{\partial \vec{\nabla}' \tilde{\rho}(\mathbf{r}')} \left[\int \vec{\nabla} \cdot \frac{\partial e_{xc}[\tilde{\rho}, \tilde{\gamma}]}{\partial \vec{\nabla} \tilde{\rho}(\mathbf{r})} \; \bar{k}^{(\lambda)}(\mathbf{r}) \; d\mathbf{r} \right] d\mathbf{u}' \equiv \\ & s_a + s_b + s_c + s_d. \end{aligned} \tag{A.28}$$

By applying the $d\mathbf{u}'$ differential with the variable collapse according to the Dirac delta function the term s_a turns into its "implementation form",

$$s_a = \sum_{\bar{l}} x_{\bar{l}}^{(\eta)} \int \bar{l}(\mathbf{r}) \left[\frac{\partial^2 e_{xc}[\tilde{\rho}, \tilde{\gamma}]}{\partial \tilde{\rho}(\mathbf{r}) \partial \tilde{\rho}(\mathbf{r})} \right] \bar{k}^{(\lambda)}(\mathbf{r}) \; d\mathbf{r}. \tag{A.29}$$

Integration by parts of the second term of Eq. (A.28), s_b, assuming that the $\bar{k}(\mathbf{r})$ derivatives vanish at $\pm\infty$, yields:

$$s_b = \sum_{\bar{l}} x_{\bar{l}}^{(\eta)} \int \bar{l}(\mathbf{r}') \frac{\partial}{\partial \tilde{\rho}(\mathbf{r}')} \left[\int \frac{\partial e_{xc}[\tilde{\rho}, \tilde{\gamma}]}{\partial \vec{\nabla} \tilde{\rho}(\mathbf{r})} \cdot \vec{\nabla} \bar{k}^{(\lambda)}(\mathbf{r}) \; d\mathbf{r} \right] d\mathbf{u}'. \tag{A.30}$$

To proceed further,we collapse the variables according to the Dirac delta function as,

$$s_b = \sum_{\bar{l}} x_{\bar{l}}^{(\eta)} \int \bar{l}(\mathbf{r}) \; \frac{\partial}{\partial \tilde{\rho}(\mathbf{r})} \frac{\partial e_{xc}[\tilde{\rho}, \tilde{\gamma}]}{\partial \vec{\nabla} \tilde{\rho}(\mathbf{r})} \cdot \vec{\nabla} \bar{k}^{(\lambda)}(\mathbf{r}) \; d\mathbf{r}. \tag{A.31}$$

By applying the chain rule, Eq. (A.16), the expression can be rewritten as,

$$s_b = \sum_{\bar{l}} x_{\bar{l}}^{(\eta)} \int \bar{l}(\mathbf{r}) \; \frac{\partial}{\partial \tilde{\rho}(\mathbf{r})} \left[\frac{\partial e_{xc}[\tilde{\rho}, \tilde{\gamma}]}{\partial \left| \vec{\nabla} \tilde{\rho}(\mathbf{r}) \right|} \frac{\vec{\nabla} \tilde{\rho}(\mathbf{r})}{\left| \vec{\nabla} \tilde{\rho}(\mathbf{r}) \right|} \right] \cdot \vec{\nabla} \bar{k}^{(\lambda)}(\mathbf{r}) \; d\mathbf{r}. \tag{A.32}$$

Finally, s_b is expressed in the "implementation form" as,

$$s_b = \sum_{\bar{l}} x_{\bar{l}}^{(\eta)} \int \bar{l}(\mathbf{r}) \; \frac{\partial^2 e_{xc}[\tilde{\rho}, \tilde{\gamma}]}{\partial \tilde{\rho}(\mathbf{r}) \partial \left| \vec{\nabla} \tilde{\rho}(\mathbf{r}) \right|} \frac{\vec{\nabla} \tilde{\rho}(\mathbf{r})}{\left| \vec{\nabla} \tilde{\rho}(\mathbf{r}) \right|} \cdot \vec{\nabla} \bar{k}^{(\lambda)}(\mathbf{r}) \; d\mathbf{r}. \tag{A.33}$$

For the third term of Eq. (A.28), s_c, the variable collapse due to the $d\mathbf{u}'$ differential results in the following expression:

$$s_c = \sum_{\bar{l}} x_{\bar{l}}^{(\eta)} \int \vec{\nabla} \bar{l}(\mathbf{r}) \cdot \frac{\partial^2 e_{xc}[\tilde{\rho}, \tilde{\gamma}]}{\partial \vec{\nabla} \tilde{\rho}(\mathbf{r}) \partial \tilde{\rho}(\mathbf{r})} \; \bar{k}^{(\lambda)}(\mathbf{r}) \; d\mathbf{r}. \tag{A.34}$$

The application of the chain rule, Eq. (A.16), yields the "implementation form" for the s_c term,

$$s_c = \sum_{\bar{l}} x_{\bar{l}}^{(\eta)} \int \vec{\nabla} \bar{l}(\mathbf{r}) \cdot \frac{\vec{\nabla} \tilde{\rho}(\mathbf{r})}{\left| \vec{\nabla} \tilde{\rho}(\mathbf{r}) \right|} \; \frac{\partial^2 e_{xc}[\tilde{\rho}, \tilde{\gamma}]}{\partial \tilde{\rho}(\mathbf{r}) \partial \left| \vec{\nabla} \tilde{\rho}(\mathbf{r}) \right|} \; \bar{k}^{(\lambda)}(\mathbf{r}) \; d\mathbf{r}. \tag{A.35}$$

For the last term of Eq. (A.28), s_d, the integration by parts of the inner integral, again assuming that the auxiliary-function derivative vanishes at $\pm\infty$, yields:

$$s_d = \sum_{\bar{l}} x_{\bar{l}}^{(\eta)} \int \vec{\nabla}' \bar{l}(\mathbf{r}') \cdot \frac{\partial}{\partial \vec{\nabla}' \tilde{\rho}(\mathbf{r}')} \left[\int \frac{\partial e_{xc}[\tilde{\rho}, \tilde{\gamma}]}{\partial \vec{\nabla} \tilde{\rho}(\mathbf{r})} \cdot \vec{\nabla} \bar{k}^{(\lambda)}(\mathbf{r}) \; d\mathbf{r} \right] d\mathbf{u}'. \tag{A.36}$$

After applying the chain rule, Eq. (A.16), we obtain,

$$s_d = \sum_{\bar{l}} x_{\bar{l}}^{(\eta)} \int \vec{\nabla}' \bar{l}(\mathbf{r}') \cdot \frac{\partial}{\partial \vec{\nabla}' \tilde{\rho}(\mathbf{r}')} \left[\int \frac{\partial e_{xc}[\tilde{\rho}, \tilde{\gamma}]}{\partial \left| \vec{\nabla} \tilde{\rho}(\mathbf{r}) \right|} \frac{\vec{\nabla} \tilde{\rho}(\mathbf{r})}{\left| \vec{\nabla} \tilde{\rho}(\mathbf{r}) \right|} \cdot \vec{\nabla} \bar{k}^{(\lambda)}(\mathbf{r}) \, d\mathbf{r} \right] d\mathbf{u}'. \tag{A.37}$$

Applying the $d\mathbf{u}'$ differential with the variable collapse according to the Dirac delta function then yields:

$$s_d = \sum_{\bar{l}} x_{\bar{l}}^{(\eta)} \int \vec{\nabla} \bar{l}(\mathbf{r}) \cdot \frac{\partial}{\partial \vec{\nabla} \tilde{\rho}(\mathbf{r})} \left[\frac{\partial e_{xc}[\tilde{\rho}, \tilde{\gamma}]}{\partial \left| \vec{\nabla} \tilde{\rho}(\mathbf{r}) \right|} \frac{\vec{\nabla} \tilde{\rho}(\mathbf{r})}{\left| \vec{\nabla} \tilde{\rho}(\mathbf{r}) \right|} \cdot \vec{\nabla} \bar{k}^{(\lambda)}(\mathbf{r}) \right] d\mathbf{r}. \tag{A.38}$$

In this case the outer (partial) differentiation generates two terms due to the product in the inner integral. Thus we find:

$$\begin{aligned} s_d = & \sum_{\bar{l}} x_{\bar{l}}^{(\eta)} \int \vec{\nabla} \bar{l}(\mathbf{r}) \cdot \frac{\partial^2 e_{xc}[\tilde{\rho}, \tilde{\gamma}]}{\partial \vec{\nabla} \tilde{\rho}(\mathbf{r}) \partial \left| \vec{\nabla} \tilde{\rho}(\mathbf{r}) \right|} \left(\frac{\vec{\nabla} \tilde{\rho}(\mathbf{r})}{\left| \vec{\nabla} \tilde{\rho}(\mathbf{r}) \right|} \cdot \vec{\nabla} \bar{k}^{(\lambda)}(\mathbf{r}) \right) d\mathbf{r} + \\ & \sum_{\bar{l}} x_{\bar{l}}^{(\eta)} \int \vec{\nabla} \bar{l}(\mathbf{r}) \cdot \frac{\partial e_{xc}[\tilde{\rho}, \tilde{\gamma}]}{\partial \left| \vec{\nabla} \tilde{\rho}(\mathbf{r}) \right|} \frac{\partial}{\partial \vec{\nabla} \tilde{\rho}(\mathbf{r})} \left(\frac{\vec{\nabla} \tilde{\rho}(\mathbf{r})}{\left| \vec{\nabla} \tilde{\rho}(\mathbf{r}) \right|} \cdot \vec{\nabla} \bar{k}^{(\lambda)}(\mathbf{r}) \right) d\mathbf{r}, \\ = & \; s_{d_a} + s_{d_b}. \end{aligned} \tag{A.39}$$

After interchanging the differentiation in the first term of Eq. (A.39) and applying the chain rule, Eq. (A.16), we obtain:

$$s_{d_a} = \sum_{\bar{l}} x_{\bar{l}}^{(\eta)} \int \vec{\nabla} \bar{l}(\mathbf{r}) \cdot \frac{\partial^2 e_{xc}[\tilde{\rho}, \tilde{\gamma}]}{\partial \left| \vec{\nabla} \tilde{\rho}(\mathbf{r}) \right|^2} \frac{\vec{\nabla} \tilde{\rho}(\mathbf{r})}{\left| \vec{\nabla} \tilde{\rho}(\mathbf{r}) \right|} \left(\frac{\vec{\nabla} \tilde{\rho}(\mathbf{r})}{\left| \vec{\nabla} \tilde{\rho}(\mathbf{r}) \right|} \cdot \vec{\nabla} \bar{k}^{(\lambda)}(\mathbf{r}) \right) d\mathbf{r}. \tag{A.40}$$

Rearranging Eq. (A.40) according to the scalar product yields the final "implementation form" for the s_{d_a} term,

$$s_{d_a} = \sum_{\bar{l}} x_{\bar{l}}^{(\eta)} \int \left(\frac{\vec{\nabla} \bar{l}(\mathbf{r}) \cdot \vec{\nabla} \tilde{\rho}(\mathbf{r})}{\left| \vec{\nabla} \tilde{\rho}(\mathbf{r}) \right|} \right) \left(\frac{\vec{\nabla} \tilde{\rho}(\mathbf{r}) \cdot \vec{\nabla} \bar{k}^{(\lambda)}(\mathbf{r})}{\left| \vec{\nabla} \tilde{\rho}(\mathbf{r}) \right|} \right) \frac{\partial^2 e_{xc}[\tilde{\rho}, \tilde{\gamma}]}{\partial \left| \vec{\nabla} \tilde{\rho}(\mathbf{r}) \right|^2} \, d\mathbf{r}. \tag{A.41}$$

For the evaluation of the s_{d_b} term in Eq. (A.39) we employ the following expansion:

$$\frac{\partial}{\partial\vec{\nabla}\tilde{\rho}(\mathbf{r})}\left(\frac{\nabla\tilde{\rho}(\mathbf{r})\cdot\vec{\nabla}\bar{k}^{(\lambda)}}{\left|\vec{\nabla}\tilde{\rho}(\mathbf{r})\right|}\right)=\frac{\vec{\nabla}\bar{k}^{(\lambda)}(\mathbf{r})}{\left|\vec{\nabla}\tilde{\rho}(\mathbf{r})\right|}-\left(\vec{\nabla}\tilde{\rho}(\mathbf{r})\cdot\vec{\nabla}\bar{k}^{(\lambda)}(\mathbf{r})\right)\frac{\vec{\nabla}\tilde{\rho}(\mathbf{r})}{\left|\vec{\nabla}\tilde{\rho}(\mathbf{r})\right|^{3}}. \tag{A.42}$$

A detailed derivation of Eq. (A.42) is given in the appendix of Ref. 12. By substituting Eq. (A.42) into the s_{d_b} term we find:

$$s_{d_b}=\sum_{\bar{l}}x_{\bar{l}}^{(\eta)}\int\vec{\nabla}\bar{l}(\mathbf{r})\cdot\frac{\partial e_{xc}[\tilde{\rho},\tilde{\gamma}]}{\partial\left|\vec{\nabla}\tilde{\rho}(\mathbf{r})\right|}\left(\frac{\vec{\nabla}\bar{k}^{(\lambda)}(\mathbf{r})}{\left|\vec{\nabla}\tilde{\rho}(\mathbf{r})\right|}-\left(\vec{\nabla}\tilde{\rho}(\mathbf{r})\cdot\vec{\nabla}\bar{k}^{(\lambda)}(\mathbf{r})\right)\frac{\vec{\nabla}\tilde{\rho}(\mathbf{r})}{\left|\vec{\nabla}\tilde{\rho}(\mathbf{r})\right|^{3}}\right)d\mathbf{r}. \tag{A.43}$$

The expansion and rearrangement of Eq. (A.43) yield the following "implementation form" for s_{d_b},

$$\begin{aligned}s_{d_b}=&\sum_{\bar{l}}x_{\bar{l}}^{(\eta)}\int\frac{\partial e_{xc}[\tilde{\rho},\tilde{\gamma}]}{\partial\left|\vec{\nabla}\tilde{\rho}(\mathbf{r})\right|}\left(\frac{\vec{\nabla}\bar{l}(\mathbf{r})\cdot\vec{\nabla}\bar{k}^{(\lambda)}(\mathbf{r})}{\left|\vec{\nabla}\tilde{\rho}(\mathbf{r})\right|}\right)d\mathbf{r}\;-\\&\sum_{\bar{l}}x_{\bar{l}}^{(\eta)}\int\frac{\partial e_{xc}[\tilde{\rho},\tilde{\gamma}]}{\partial\left|\vec{\nabla}\tilde{\rho}(\mathbf{r})\right|}\left(\vec{\nabla}\tilde{\rho}(\mathbf{r})\cdot\vec{\nabla}\bar{k}^{(\lambda)}(\mathbf{r})\right)\left(\frac{\vec{\nabla}\bar{l}(\mathbf{r})\cdot\vec{\nabla}\tilde{\rho}(\mathbf{r})}{\left|\vec{\nabla}\tilde{\rho}(\mathbf{r})\right|^{3}}\right)d\mathbf{r}.\end{aligned} \tag{A.44}$$

Thus, we find as final "implementation form" for s_d,

$$\begin{aligned}s_d=&\sum_{\bar{l}}x_{\bar{l}}^{(\eta)}\int\left(\frac{\vec{\nabla}\bar{l}(\mathbf{r})\cdot\vec{\nabla}\tilde{\rho}(\mathbf{r})}{\left|\vec{\nabla}\tilde{\rho}(\mathbf{r})\right|}\right)\left(\frac{\vec{\nabla}\tilde{\rho}(\mathbf{r})\cdot\vec{\nabla}\bar{k}^{(\lambda)}(\mathbf{r})}{\left|\vec{\nabla}\tilde{\rho}(\mathbf{r})\right|}\right)\frac{\partial^2 e_{xc}[\tilde{\rho},\tilde{\gamma}]}{\partial\left|\vec{\nabla}\tilde{\rho}(\mathbf{r})\right|^{2}}\,d\mathbf{r}\;+\\&\sum_{\bar{l}}x_{\bar{l}}^{(\eta)}\int\frac{\partial e_{xc}[\tilde{\rho},\tilde{\gamma}]}{\partial\left|\vec{\nabla}\tilde{\rho}(\mathbf{r})\right|}\left(\frac{\vec{\nabla}\bar{l}(\mathbf{r})\cdot\vec{\nabla}\bar{k}^{(\lambda)}(\mathbf{r})}{\left|\vec{\nabla}\tilde{\rho}(\mathbf{r})\right|}\right)d\mathbf{r}\;-\\&\sum_{\bar{l}}x_{\bar{l}}^{(\eta)}\int\frac{\partial e_{xc}[\tilde{\rho},\tilde{\gamma}]}{\partial\left|\vec{\nabla}\tilde{\rho}(\mathbf{r})\right|}\left(\vec{\nabla}\tilde{\rho}(\mathbf{r})\cdot\vec{\nabla}\bar{k}^{(\lambda)}(\mathbf{r})\right)\left(\frac{\vec{\nabla}\bar{l}(\mathbf{r})\cdot\vec{\nabla}\tilde{\rho}(\mathbf{r})}{\left|\vec{\nabla}\tilde{\rho}(\mathbf{r})\right|^{3}}\right)d\mathbf{r}.\end{aligned} \tag{A.45}$$

We now give the explicit formulation of the "implementation forms" for the integral sums (A.5) to (A.8).

"Implementation form" of integral sum (A.5):

$$\begin{aligned}
\sum_{\bar{l}} x_{\bar{l}}^{(\eta)} \left\langle \bar{k}^{(\lambda)} \right| f_{xc}\left[\tilde{\rho}\right] \left| \bar{l} \right\rangle = & \sum_{\bar{l}} x_{\bar{l}}^{(\eta)} \int \bar{l}(\mathbf{r}) \left[\frac{\partial^2 e_{xc}[\tilde{\rho},\tilde{\gamma}]}{\partial\tilde{\rho}(\mathbf{r})\partial\tilde{\rho}(\mathbf{r})} \right] \bar{k}^{(\lambda)}(\mathbf{r})\, d\mathbf{r} + \\
& \sum_{\bar{l}} x_{\bar{l}}^{(\eta)} \int \bar{l}(\mathbf{r})\, \frac{\partial^2 e_{xc}[\tilde{\rho},\tilde{\gamma}]}{\partial\tilde{\rho}(\mathbf{r})\partial \left|\vec{\nabla}\tilde{\rho}(\mathbf{r})\right|} \frac{\vec{\nabla}\tilde{\rho}(\mathbf{r})}{\left|\vec{\nabla}\tilde{\rho}(\mathbf{r})\right|} \cdot \vec{\nabla}\bar{k}^{(\lambda)}(\mathbf{r})\, d\mathbf{r} + \\
& \sum_{\bar{l}} x_{\bar{l}}^{(\eta)} \int \vec{\nabla}\bar{l}(\mathbf{r}) \cdot \frac{\vec{\nabla}\tilde{\rho}(\mathbf{r})}{\left|\vec{\nabla}\tilde{\rho}(\mathbf{r})\right|}\, \frac{\partial^2 e_{xc}[\tilde{\rho},\tilde{\gamma}]}{\partial\tilde{\rho}(\mathbf{r})\partial \left|\vec{\nabla}\tilde{\rho}(\mathbf{r})\right|} \bar{k}^{(\lambda)}(\mathbf{r})\, d\mathbf{r} + \\
& \sum_{\bar{l}} x_{\bar{l}}^{(\eta)} \int \left(\frac{\vec{\nabla}\bar{l}(\mathbf{r}) \cdot \vec{\nabla}\tilde{\rho}(\mathbf{r})}{\left|\vec{\nabla}\tilde{\rho}(\mathbf{r})\right|} \right) \left(\frac{\vec{\nabla}\tilde{\rho}(\mathbf{r}) \cdot \vec{\nabla}\bar{k}^{(\lambda)}(\mathbf{r})}{\left|\vec{\nabla}\tilde{\rho}(\mathbf{r})\right|} \right) \frac{\partial^2 e_{xc}[\tilde{\rho},\tilde{\gamma}]}{\partial \left|\vec{\nabla}\tilde{\rho}(\mathbf{r})\right|^2}\, d\mathbf{r} + \\
& \sum_{\bar{l}} x_{\bar{l}}^{(\eta)} \int \frac{\partial e_{xc}[\tilde{\rho},\tilde{\gamma}]}{\partial \left|\vec{\nabla}\tilde{\rho}(\mathbf{r})\right|} \left(\frac{\vec{\nabla}\bar{l}(\mathbf{r}) \cdot \vec{\nabla}\bar{k}^{(\lambda)}(\mathbf{r})}{\left|\vec{\nabla}\tilde{\rho}(\mathbf{r})\right|} \right) d\mathbf{r} - \\
& \sum_{\bar{l}} x_{\bar{l}}^{(\eta)} \int \frac{\partial e_{xc}[\tilde{\rho},\tilde{\gamma}]}{\partial \left|\vec{\nabla}\tilde{\rho}(\mathbf{r})\right|} \left(\vec{\nabla}\tilde{\rho}(\mathbf{r}) \cdot \vec{\nabla}\bar{k}^{(\lambda)}(\mathbf{r}) \right) \left(\frac{\vec{\nabla}\bar{l}(\mathbf{r}) \cdot \vec{\nabla}\tilde{\rho}(\mathbf{r})}{\left|\vec{\nabla}\tilde{\rho}(\mathbf{r})\right|^3} \right) d\mathbf{r}.
\end{aligned} \tag{A.46}$$

"Implementation form" of integral sum (A.6):

$$\begin{aligned}
\sum_{\bar{l}} x_{\bar{l}} \left\langle \bar{k}^{(\lambda)} \right| f_{xc}\left[\tilde{\rho}\right] \left| \bar{l}^{(\eta)} \right\rangle = & \sum_{\bar{l}} x_{\bar{l}} \int \bar{l}^{(\eta)}(\mathbf{r}) \left[\frac{\partial^2 e_{xc}[\tilde{\rho},\tilde{\gamma}]}{\partial\tilde{\rho}(\mathbf{r})\partial\tilde{\rho}(\mathbf{r})} \right] \bar{k}^{(\lambda)}(\mathbf{r}) d\mathbf{r} + \\
& \sum_{\bar{l}} x_{\bar{l}} \int \bar{l}^{(\eta)}(\mathbf{r}) \frac{\partial^2 e_{xc}[\tilde{\rho},\tilde{\gamma}]}{\partial\tilde{\rho}(\mathbf{r})\partial \left|\vec{\nabla}\tilde{\rho}(\mathbf{r})\right|} \frac{\vec{\nabla}\tilde{\rho}(\mathbf{r})}{\left|\vec{\nabla}\tilde{\rho}(\mathbf{r})\right|} \cdot \vec{\nabla}\bar{k}^{(\lambda)}(\mathbf{r})\, d\mathbf{r} + \\
& \sum_{\bar{l}} x_{\bar{l}} \int \vec{\nabla}\bar{l}^{(\eta)}(\mathbf{r}) \cdot \frac{\vec{\nabla}\tilde{\rho}(\mathbf{r})}{\left|\vec{\nabla}\tilde{\rho}(\mathbf{r})\right|}\, \frac{\partial^2 e_{xc}[\tilde{\rho},\tilde{\gamma}]}{\partial\tilde{\rho}(\mathbf{r})\partial \left|\vec{\nabla}\tilde{\rho}(\mathbf{r})\right|} \bar{k}^{(\lambda)}(\mathbf{r})\, d\mathbf{r} + \\
& \sum_{\bar{l}} x_{\bar{l}} \int \left(\frac{\vec{\nabla}\bar{l}^{(\eta)}(\mathbf{r}) \cdot \vec{\nabla}\tilde{\rho}(\mathbf{r})}{\left|\vec{\nabla}\tilde{\rho}(\mathbf{r})\right|} \right) \left(\frac{\vec{\nabla}\tilde{\rho}(\mathbf{r}) \cdot \vec{\nabla}\bar{k}^{(\lambda)}(\mathbf{r})}{\left|\vec{\nabla}\tilde{\rho}(\mathbf{r})\right|} \right) \frac{\partial^2 e_{xc}[\tilde{\rho},\tilde{\gamma}]}{\partial \left|\vec{\nabla}\tilde{\rho}(\mathbf{r})\right|^2}\, d\mathbf{r} + \\
& \sum_{\bar{l}} x_{\bar{l}} \int \frac{\partial e_{xc}[\tilde{\rho},\tilde{\gamma}]}{\partial \left|\vec{\nabla}\tilde{\rho}(\mathbf{r})\right|} \left(\frac{\vec{\nabla}\bar{l}^{(\eta)}(\mathbf{r}) \cdot \vec{\nabla}\bar{k}^{(\lambda)}(\mathbf{r})}{\left|\vec{\nabla}\tilde{\rho}(\mathbf{r})\right|} \right) d\mathbf{r} -
\end{aligned}$$

$$\sum_{\bar{l}} x_{\bar{l}} \int \frac{\partial e_{xc}[\tilde{\rho},\tilde{\gamma}]}{\partial \left|\vec{\nabla}\tilde{\rho}(\mathbf{r})\right|} \left(\vec{\nabla}\tilde{\rho}(\mathbf{r}) \cdot \vec{\nabla}\bar{k}^{(\lambda)}(\mathbf{r})\right) \left(\frac{\vec{\nabla}\bar{l}^{(\eta)}(\mathbf{r}) \cdot \vec{\nabla}\tilde{\rho}(\mathbf{r})}{\left|\vec{\nabla}\tilde{\rho}(\mathbf{r})\right|^3}\right) d\mathbf{r}. \tag{A.47}$$

"Implementation form" of integral sum (A.7):

$$\begin{aligned}
\sum_{\bar{l}} x_{\bar{l}}^{(\lambda)} \left\langle \bar{k}\right| f_{xc}\left[\tilde{\rho}\right] \left|\bar{l}\right\rangle = & \sum_{\bar{l}} x_{\bar{l}}^{(\lambda)} \int \bar{l}(\mathbf{r}) \left[\frac{\partial^2 e_{xc}[\tilde{\rho},\tilde{\gamma}]}{\partial\tilde{\rho}(\mathbf{r})\partial\tilde{\rho}(\mathbf{r})}\right] \bar{k}(\mathbf{r})\ d\mathbf{r} + \\
& \sum_{\bar{l}} x_{\bar{l}}^{(\lambda)} \int \bar{l}(\mathbf{r}) \frac{\partial^2 e_{xc}[\tilde{\rho},\tilde{\gamma}]}{\partial\tilde{\rho}(\mathbf{r})\partial\left|\vec{\nabla}\tilde{\rho}(\mathbf{r})\right|} \frac{\vec{\nabla}\tilde{\rho}(\mathbf{r})}{\left|\vec{\nabla}\tilde{\rho}(\mathbf{r})\right|} \cdot \vec{\nabla}\bar{k}(\mathbf{r})\ d\mathbf{r} + \\
& \sum_{\bar{l}} x_{\bar{l}}^{(\lambda)} \int \vec{\nabla}\bar{l}(\mathbf{r}) \cdot \frac{\vec{\nabla}\tilde{\rho}(\mathbf{r})}{\left|\vec{\nabla}\tilde{\rho}(\mathbf{r})\right|} \frac{\partial^2 e_{xc}[\tilde{\rho},\tilde{\gamma}]}{\partial\tilde{\rho}(\mathbf{r})\partial\left|\vec{\nabla}\tilde{\rho}(\mathbf{r})\right|} \bar{k}(\mathbf{r})\ d\mathbf{r} + \\
& \sum_{\bar{l}} x_{\bar{l}}^{(\lambda)} \int \left(\frac{\vec{\nabla}\bar{l}(\mathbf{r}) \cdot \vec{\nabla}\tilde{\rho}(\mathbf{r})}{\left|\vec{\nabla}\tilde{\rho}(\mathbf{r})\right|}\right) \left(\frac{\vec{\nabla}\tilde{\rho}(\mathbf{r}) \cdot \vec{\nabla}\bar{k}(\mathbf{r})}{\left|\vec{\nabla}\tilde{\rho}(\mathbf{r})\right|}\right) \frac{\partial^2 e_{xc}[\tilde{\rho},\tilde{\gamma}]}{\partial\left|\vec{\nabla}\tilde{\rho}(\mathbf{r})\right|^2}\ d\mathbf{r} + \\
& \sum_{\bar{l}} x_{\bar{l}}^{(\lambda)} \int \frac{\partial e_{xc}[\tilde{\rho},\tilde{\gamma}]}{\partial\left|\vec{\nabla}\tilde{\rho}(\mathbf{r})\right|} \left(\frac{\vec{\nabla}\bar{l}(\mathbf{r}) \cdot \vec{\nabla}\bar{k}(\mathbf{r})}{\left|\vec{\nabla}\tilde{\rho}(\mathbf{r})\right|}\right)\ d\mathbf{r} - \\
& \sum_{\bar{l}} x_{\bar{l}}^{(\lambda)} \int \frac{\partial e_{xc}[\tilde{\rho},\tilde{\gamma}]}{\partial\left|\vec{\nabla}\tilde{\rho}(\mathbf{r})\right|} \left(\vec{\nabla}\tilde{\rho}(\mathbf{r}) \cdot \vec{\nabla}\bar{k}(\mathbf{r})\right) \left(\frac{\vec{\nabla}\bar{l}(\mathbf{r}) \cdot \vec{\nabla}\tilde{\rho}(\mathbf{r})}{\left|\vec{\nabla}\tilde{\rho}(\mathbf{r})\right|^3}\right) d\mathbf{r}.
\end{aligned} \tag{A.48}$$

"Implementation form" of integral sum (A.8),

$$\begin{aligned}
\sum_{\bar{l}} x_{\bar{l}} \left\langle \bar{k}\right| f_{xc}\left[\tilde{\rho}\right] \left|\bar{l}^{(\lambda)}\right\rangle = & \sum_{\bar{l}} x_{\bar{l}} \int \bar{l}^{(\lambda)}(\mathbf{r}) \left[\frac{\partial^2 e_{xc}[\tilde{\rho},\tilde{\gamma}]}{\partial\tilde{\rho}(\mathbf{r})\partial\tilde{\rho}(\mathbf{r})}\right] \bar{k}(\mathbf{r})\ d\mathbf{r} + \\
& \sum_{\bar{l}} x_{\bar{l}} \int \bar{l}^{(\lambda)}(\mathbf{r}) \frac{\partial^2 e_{xc}[\tilde{\rho},\tilde{\gamma}]}{\partial\tilde{\rho}(\mathbf{r})\partial\left|\vec{\nabla}\tilde{\rho}(\mathbf{r})\right|} \frac{\vec{\nabla}\tilde{\rho}(\mathbf{r})}{\left|\vec{\nabla}\tilde{\rho}(\mathbf{r})\right|} \cdot \vec{\nabla}\bar{k}(\mathbf{r})\ d\mathbf{r} + \\
& \sum_{\bar{l}} x_{\bar{l}} \int \vec{\nabla}\bar{l}^{(\lambda)}(\mathbf{r}) \cdot \frac{\vec{\nabla}\tilde{\rho}(\mathbf{r})}{\left|\vec{\nabla}\tilde{\rho}(\mathbf{r})\right|} \frac{\partial^2 e_{xc}[\tilde{\rho},\tilde{\gamma}]}{\partial\tilde{\rho}(\mathbf{r})\partial\left|\vec{\nabla}\tilde{\rho}(\mathbf{r})\right|} \bar{k}(\mathbf{r})\ d\mathbf{r} + \\
& \sum_{\bar{l}} x_{\bar{l}} \int \left(\frac{\vec{\nabla}\bar{l}^{(\lambda)}(\mathbf{r}) \cdot \vec{\nabla}\tilde{\rho}(\mathbf{r})}{\left|\vec{\nabla}\tilde{\rho}(\mathbf{r})\right|}\right) \left(\frac{\vec{\nabla}\tilde{\rho}(\mathbf{r}) \cdot \vec{\nabla}\bar{k}(\mathbf{r})}{\left|\vec{\nabla}\tilde{\rho}(\mathbf{r})\right|}\right) \frac{\partial^2 e_{xc}[\tilde{\rho},\tilde{\gamma}]}{\partial\left|\vec{\nabla}\tilde{\rho}(\mathbf{r})\right|^2}\ d\mathbf{r} +
\end{aligned}$$

$$\sum_{\bar{l}} x_{\bar{l}} \int \frac{\partial e_{xc}[\tilde{\rho},\tilde{\gamma}]}{\partial \left|\vec{\nabla}\tilde{\rho}(\mathbf{r})\right|} \left(\frac{\vec{\nabla}\bar{l}^{(\lambda)}(\mathbf{r}) \cdot \vec{\nabla}\bar{k}(\mathbf{r})}{\left|\vec{\nabla}\tilde{\rho}(\mathbf{r})\right|} \right) d\mathbf{r} \; -$$

$$\sum_{\bar{l}} x_{\bar{l}} \int \frac{\partial e_{xc}[\tilde{\rho},\tilde{\gamma}]}{\partial \left|\vec{\nabla}\tilde{\rho}(\mathbf{r})\right|} \left(\vec{\nabla}\tilde{\rho}(\mathbf{r}) \cdot \vec{\nabla}\bar{k}(\mathbf{r}) \right) \left(\frac{\vec{\nabla}\bar{l}^{(\lambda)}(\mathbf{r}) \cdot \vec{\nabla}\tilde{\rho}(\mathbf{r})}{\left|\vec{\nabla}\tilde{\rho}(\mathbf{r})\right|^3} \right) d\mathbf{r}. \quad \text{(A.49)}$$

These are the generic working equations for the calculation of GGA exchange–correlation integrals needed for the analytical calculation of second-order ADFT-energy derivatives. The first- and second-order derivatives of $e_{xc}(\tilde{\rho},\tilde{\gamma})$ are specific for each GGA functional. They are the same as for perturbation-independent basis and auxiliary-functions.

Appendix B

Perturbed Energy-Weighted Density Matrix Calculation

The perturbed energy-weighted density matrix, $\mathbf{W}^{(\lambda)}$, is needed for the calculation of analytic second-order energy-derivatives. It can be calculated in two different ways, both of them originate from the Kohn-Sham equations,

$$\sum_{v} K_{\mu\nu} c_{\nu i} = \sum_{v} S_{\mu\nu} c_{\nu i} \epsilon_i. \tag{B.1}$$

Multiplication of Eq. (B.1) by $c_{\sigma i}$ and summation over all occupied MOs yields:

$$\sum_{\nu} \sum_{i}^{occ} K_{\mu\nu} c_{\nu i} c_{\sigma i} = \sum_{\nu} \sum_{i}^{occ} S_{\mu\nu} c_{\nu i} c_{\sigma i} \epsilon_i. \tag{B.2}$$

To proceed, we now introduce the (closed-shell) density matrix, Eq. (3.4), on the left-hand side of Eq. (B.2) and the (closed-shell) energy-weighted density matrix, Eq. (4.15), on the right-hand side of Eq. (B.2). Thus, we obtain,

$$\sum_{\nu} K_{\mu\nu} P_{\nu\sigma} = \sum_{\nu} S_{\mu\nu} W_{\nu\sigma}. \tag{B.3}$$

Differentiation of Eq. (B.3) with respect to the perturbation parameter λ yields:

$$\sum_{\nu} K^{(\lambda)}_{\mu\nu} P_{\nu\sigma} + \sum_{\nu} K_{\mu\nu} P^{(\lambda)}_{\nu\sigma} = \sum_{\nu} S^{(\lambda)}_{\mu\nu} W_{\nu\sigma} + \sum_{\nu} S_{\mu\nu} W^{(\lambda)}_{\nu\sigma}. \tag{B.4}$$

From this equation we find as explicit expression for the energy-weighted density matrix derivative,

$$\mathbf{W}^{(\lambda)} = \mathbf{S}^{-1}\left(\mathbf{K}^{(\lambda)}\mathbf{P} + \mathbf{K}\mathbf{P}^{(\lambda)} - \mathbf{S}^{(\lambda)}\mathbf{W}\right). \tag{B.5}$$

In our experience Eq. (B.5) is prone to numerical instabilities due to the overlap matrix inversion. Therefore, an alternative for the calculation of the perturbed energy-weighted density matrix avoiding the inversion of the overlap matrix, is presented. We start again from Eq. (B.1) but now multiplying from left by $c_{\mu j}$ and sum over all basis functions:

$$\sum_{\mu,\nu} c_{\mu j} K_{\mu\nu} c_{\nu i} = \sum_{\mu,\nu} c_{\mu j} S_{\mu\nu} c_{\nu i} \epsilon_i. \tag{B.6}$$

To proceed, we employ the orthogonality constraint, Eq. (2.24), on the right-hand side of Eq. (B.6), yielding:

$$\sum_{\mu,\nu} c_{\mu j} K_{\mu\nu} c_{\nu i} = \delta_{ji}\epsilon_i. \tag{B.7}$$

By multiplication of $c_{\mu j}$ from left and $c_{\nu i}$ from right and summation over all occupied MOs on both sides of Eq. (B.7) we obtain:

$$\sum_{i,j}^{occ}\sum_{\mu,\nu} c_{\sigma j} c_{\mu j} K_{\mu\nu} c_{\nu i} c_{\tau i} = \sum_{i,j}^{occ} c_{\sigma j}\delta_{ji}\epsilon_i c_{\tau i} = \sum_{i}^{occ} c_{\sigma i}\epsilon_i c_{\tau i}. \tag{B.8}$$

The introduction of the (closed-shell) energy-weighted density matrix, Eq. (4.15) on the right-hand side of Eq. (B.8), and the (closed-shell) density matrix, Eq. (3.4), on the left-hand side of Eq. (B.8) yields:

$$\frac{1}{2}\mathbf{PKP} = \mathbf{W}. \tag{B.9}$$

From the differentiation of Eq. (B.9) with respect to the perturbation parameter λ the explicit expression for the energy-weighted density matrix derivative is obtained:

$$\frac{1}{2}\left(\mathbf{P}^{(\lambda)}\mathbf{K}\mathbf{P} + \mathbf{P}\mathbf{K}^{(\lambda)}\mathbf{P} + \mathbf{P}\mathbf{K}\mathbf{P}^{(\lambda)}\right) = \mathbf{W}^{(\lambda)}. \tag{B.10}$$

Even when the evaluation of Eq. (B.10) requires 6 matrix-matrix multiplications for each perturbation, this expression does not need the overlap matrix nor its inverse, thus, the numerical instabilities associated with the inversion of the overlap matrix are circumvented.

Appendix C

Unrestricted Self-Consistent Perturbation Theory

This appendix extends the results of section 5.1 to open-shell systems. The appearing $\mathbf{R}$ matrices can be closed-shell or open-shell density matrices. In the latter case they are marked with a spin-specific superscript σ that can be either α or β. By generalization of Eq. (5.33) the perturbed density matrix, with n being the occupation number of the MOs, is given by,

$$\breve{\mathbf{R}}^{(\lambda)} = n\breve{\mathbf{\Pi}}^{(\lambda)} = n(\breve{\mathbf{\Pi}}^{(\lambda)}_{ou} + \breve{\mathbf{\Pi}}^{(\lambda)}_{uo} + \breve{\mathbf{\Pi}}^{(\lambda)}_{oo}), \tag{C.1}$$

$$\breve{\mathbf{R}}^{(\lambda)} = n\left(\sum_{i}^{occ}\sum_{a}^{uno}\breve{\mathbf{c}}_i\frac{\mathcal{K}^{(\lambda)}_{ia} - \epsilon_i\mathcal{S}^{(\lambda)}_{ia}}{\epsilon_i - \epsilon_a}\breve{\mathbf{c}}_a^{\mathrm{T}} + \sum_{i}^{occ}\sum_{a}^{uno}\breve{\mathbf{c}}_a\frac{\mathcal{K}^{(\lambda)}_{ia} - \epsilon_i\mathcal{S}^{(\lambda)}_{ia}}{\epsilon_i - \epsilon_a}\breve{\mathbf{c}}_i^{\mathrm{T}} - \breve{\mathbf{S}}^{(\lambda)}_{oo}\right). \tag{C.2}$$

Back-transformation to the non-orthogonal basis by $\mathbf{R}^{(\lambda)} = \mathbf{S^{-1/2}}\breve{\mathbf{R}}^{(\lambda)}\mathbf{S^{-1/2}}$ yields:

$$\mathbf{R}^{(\lambda)} = n\left(\sum_{i}^{occ}\sum_{a}^{uno}\mathbf{c}_i\frac{\mathcal{K}^{(\lambda)}_{ia} - \epsilon_i\mathcal{S}^{(\lambda)}_{ia}}{\epsilon_i - \epsilon_a}\mathbf{c}_a^{\mathrm{T}} + \sum_{i}^{occ}\sum_{a}^{uno}\mathbf{c}_a\frac{\mathcal{K}^{(\lambda)}_{ia} - \epsilon_i\mathcal{S}^{(\lambda)}_{ia}}{\epsilon_i - \epsilon_a}\mathbf{c}_i^{\mathrm{T}} - \mathbf{R}\mathbf{S}^{(\lambda)}\mathbf{R}\right). \tag{C.3}$$

For open-shell systems, the occupation number is $n = 1$ for each spin-orbital. Therefore, the perturbed spin-density matrices are given by:

$$R^{(\lambda),\sigma}_{\mu\nu} = \sum_{i}^{occ}\sum_{a}^{uno}\frac{\mathcal{K}^{(\lambda),\sigma}_{ia} - \epsilon^{\sigma}_i\mathcal{S}^{(\lambda),\sigma}_{ia}}{\epsilon^{\sigma}_i - \epsilon^{\sigma}_a}\left(c^{\sigma}_{\mu i}c^{\sigma}_{\nu a} + c^{\sigma}_{\mu a}c^{\sigma}_{\nu i}\right) - \sum_{\sigma,\tau}R^{\sigma}_{\mu\sigma}S^{(\lambda)}_{\sigma\tau}R^{\sigma}_{\tau\nu}. \tag{C.4}$$

Appendix D

Unrestricted ADPT Equation System

This appendix extends the results of section 5.2 to open-shell systems where the total electronic density is given by the sum of the α and β spin densities,

$$\rho(\mathbf{r}) = \rho^{\alpha}(\mathbf{r}) + \rho^{\beta}(\mathbf{r}). \tag{D.1}$$

We assume that the same separation in α and β spin densities also holds for the approximate density,

$$\tilde{\rho}(\mathbf{r}) = \tilde{\rho}^{\alpha}(\mathbf{r}) + \tilde{\rho}^{\beta}(\mathbf{r}) = \sum_{\bar{k}} \left(x_{\bar{k}}^{\alpha} + x_{\bar{k}}^{\beta} \right) \bar{k}(\mathbf{r}). \tag{D.2}$$

The $x_{\bar{k}}^{\alpha}$ and $x_{\bar{k}}^{\beta}$ are spin-polarized fitting coefficients which are obtained from separate spin-dependent fitting equations (3.27). The fitting of the total density remains variational. The spin-polarized density matrix elements are given by,

$$R_{\mu\nu}^{\sigma} = \sum_{i}^{occ_{\sigma}} c_{\mu i}^{\sigma} c_{\nu i}^{\sigma}. \tag{D.3}$$

Similar to the unrestricted Hartree-Fock methodology [62], two sets of Kohn-Sham equations are obtained. The corresponding spin-polarized ADFT Kohn-Sham matrix elements are given by,

$$K_{\mu\nu}^{\sigma} = H_{\mu\nu} + \sum_{\bar{k}} \left\langle \mu\nu \,\|\, \bar{k} \right\rangle \left(x_{\bar{k}} + z_{\bar{k}}^{\sigma} \right). \tag{D.4}$$

The ADPT equations are derived by starting from Eq. (C.4) and following the same procedure as in section 5.2 using the corresponding spin-polarized matrices and MOs. Therefore, the open-shell perturbed Kohn-Sham matrix elements, assuming perturbation-dependent basis and auxiliary-functions, have the form:

$$K_{\mu\nu}^{(\lambda),\sigma} = H_{\mu\nu}^{(\lambda)} + \sum_{\bar{k}} \left\langle \mu\nu \,\|\, \bar{k} \right\rangle^{(\lambda)} (x_{\bar{k}} + z_{\bar{k}}^{\sigma}) + \sum_{\bar{k}} \left\langle \mu\nu \,\|\, \bar{k} \right\rangle \left(x_{\bar{k}}^{(\lambda)} + z_{\bar{k}}^{(\lambda),\sigma} \right). \tag{D.5}$$

The perturbed spin-polarized exchange-correlation coefficients are given by,

$$z_{\bar{k}}^{(\lambda),\sigma} = \sum_{\bar{l}} G_{\bar{k}\bar{l}}^{-1} \left\langle \bar{l}^{(\lambda)} \middle| v_{xc}^{\sigma}[\tilde{\rho}] \right\rangle - \sum_{\bar{l},\bar{m}} G_{\bar{k}\bar{l}}^{-1} G_{\bar{l}\bar{m}}^{(\lambda)} z_{\bar{m}}^{\sigma} + \sum_{\bar{l}} G_{\bar{k}\bar{l}}^{-1} \left\langle \bar{l} \middle| v_{xc}^{(\lambda),\sigma}[\tilde{\rho}] \right\rangle. \tag{D.6}$$

The spin-polarized exchange-correlation potential appearing here is defined as,

$$v_{xc}^{\sigma}[\tilde{\rho}](\mathbf{r}') \equiv \frac{\delta E_{xc}[\tilde{\rho}]}{\delta \tilde{\rho}^{\sigma}(\mathbf{r}')}. \tag{D.7}$$

Since $v_{xc}^{\sigma}[\tilde{\rho}]$ is a functional of $\tilde{\rho}^{\alpha}(\mathbf{r})$ and $\tilde{\rho}^{\beta}(\mathbf{r})$, the derivative of $v_{xc}[\tilde{\rho}]$ with respect to the perturbation parameter λ generates two terms:

$$\frac{\partial v_{xc}^{\sigma}[\tilde{\rho}](\mathbf{r})}{\partial \lambda} = \int \frac{\delta v_{xc}^{\sigma}[\tilde{\rho}](\mathbf{r})}{\delta \tilde{\rho}^{\alpha}(\mathbf{r}')} \frac{\partial \tilde{\rho}^{\alpha}(\mathbf{r}')}{\partial \lambda} \, d\mathbf{r}' + \int \frac{\delta v_{xc}^{\sigma}[\tilde{\rho}](\mathbf{r})}{\delta \tilde{\rho}^{\beta}(\mathbf{r}')} \frac{\partial \tilde{\rho}^{\beta}(\mathbf{r}')}{\partial \lambda} \, d\mathbf{r}'. \tag{D.8}$$

At this point it is convenient to introduce the spin-polarized exchange-correlation kernel as,

$$f_{xc}^{\sigma\tau}[\tilde{\rho}](\mathbf{r}, \mathbf{r}') = \frac{\delta v_{xc}^{\sigma}[\tilde{\rho}](\mathbf{r})}{\delta \tilde{\rho}^{\tau}(\mathbf{r}')}. \tag{D.9}$$

Note that this kernel depends on two spins indicated by the superscripts σ and τ. By inserting Eq. (D.8) and (D.9) into Eq. (D.6) we obtain the following expression for the perturbed

spin-polarized exchange-correlation coefficients:

$$z_{\bar{k}}^{(\lambda),\sigma} = \sum_{\bar{l}} G_{\bar{k}\bar{l}}^{-1} \left\langle \bar{l}^{(\lambda)} \middle| v_{xc}^{\sigma}[\tilde{\rho}] \right\rangle - \sum_{\bar{l},\bar{m}} G_{\bar{k}\bar{l}}^{-1} G_{\bar{l}\bar{m}}^{(\lambda)} z_{\bar{m}}^{\sigma} + \sum_{\bar{l},\bar{m}} \sum_{\tau}^{\alpha,\beta} G_{\bar{k}\bar{l}}^{-1} \left\langle \bar{l} \right| f_{xc}^{\sigma\tau}[\tilde{\rho}] \left| \bar{m} \right\rangle x_{\bar{m}}^{(\lambda),\tau} + \sum_{\bar{l},\bar{m}} \sum_{\tau}^{\alpha,\beta} G_{\bar{k}\bar{l}}^{-1} \left\langle \bar{l}^{(\lambda)} \right| f_{xc}^{\sigma\tau}[\tilde{\rho}] \left| \bar{m}^{(\lambda)} \right\rangle x_{\bar{m}}^{\tau}. \tag{D.10}$$

Following the same argumentation as in section 5.2 the unrestricted ADPT equation system is obtained as:

$$\begin{bmatrix} \frac{\mathbf{1}}{\mathbf{2}}\mathbf{G} - \mathbf{A}^{\alpha}\ (\mathbf{E} + \mathbf{F}^{\alpha\alpha}) & -\mathbf{A}^{\alpha} - \mathbf{A}^{\alpha}\ \mathbf{F}^{\alpha\beta} \\ -\mathbf{A}^{\beta} - \mathbf{A}^{\beta}\ \mathbf{F}^{\beta\alpha} & \frac{\mathbf{1}}{\mathbf{2}}\mathbf{G} - \mathbf{A}^{\beta}\ (\mathbf{E} + \mathbf{F}^{\beta\beta}) \end{bmatrix} \begin{bmatrix} \mathbf{x}^{(\lambda),\alpha} \\ \mathbf{x}^{(\lambda),\beta} \end{bmatrix} = \begin{bmatrix} \mathbf{b}^{(\lambda),\alpha} \\ \mathbf{b}^{(\lambda),\beta} \end{bmatrix}. \tag{D.11}$$

Compared to the implementation of the closed-shell ADPT equations, Eq. (5.46), the unrestricted ADPT equation system, Eq. (D.11), requires the calculation and storage of two spin-dependent Coulomb response matrices, $\mathbf{A}^{\alpha}$ and $\mathbf{A}^{\beta}$, three spin-dependent Kernel matrices, $\mathbf{F}^{\alpha\alpha}$, $\mathbf{F}^{\beta\beta}$ and $\mathbf{F}^{\alpha\beta}$, and the complete open-shell response matrix of size 4 ($N_{aux} \times N_{aux}$). Despite the higher storage requirements, by following the same implementation described in Section 5.4, the RAM memory requirements for the open-shell ADPT Eirola-Nevannlina algorithm, compared to the closed-shell scheme, is only marginally increased, as only the working vectors of size N_{aux} are doubled. Thus, the limiting factor to calculate an open-shell system of a certain size is the hard disk storage available.

Bibliography

[1] P. Hohenberg and W. Kohn. Inhomogeneous electron gas. *Phys. Rev.* 136:B864, 1964.

[2] M. Head-Gordon and E. Artacho. Chemistry on the computer. *Phys. Today* 61(4):58, 2008.

[3] W. Kohn and L. J. Sham. Self-consistent equations including exchange and correlation effects. *Phys. Rev.* 140:A1133, 1965.

[4] R. Fournier. Second and third derivatives of the linear combination of Gaussian type orbitals-local spin density energy. *J. Chem. Phys.* 92:5422, 1990.

[5] A. Komornicki and G. Fitzgerald. Molecular gradients and Hessians implemented in density functional theory. *J. Chem. Phys.* 98:1398, 1993.

[6] S. M. Colwell, C. W. Murray, N. C. Handy, and R. D. Amos. The determination of hyperpolarisabilities using density functional theory. *Chem. Phys. Lett.* 210:261, 1993.

[7] F. Furche and R. Ahlrichs. Adiabatic time-dependent density functional methods for excited state properties. *J. Chem. Phys.* 117:7433, 2002.

[8] P. Pulay. Analytical derivatives, forces, force constants, molecular geometries, and related response properties in electronic structure theory. *Wiley Interdisciplinary Reviews: Computational Molecular Science* 4:169, 2014.

[9] J. Carmona-Espíndola, R. Flores-Moreno, and A. M. Köster. Time-dependent auxiliary density perturbation theory. *J. Chem. Phys.* 133:084102, 2010.

[10] J. Carmona-Espíndola, R. Flores-Moreno, and A. M. Köster. Static and dynamic first hyperpolarizabilities from time-dependent auxiliary density perturbation theory. *Int. J. Quantum Chem.* 112:3461, 2012.

[11] D. Mejía-Rodríguez, R. I. Delgado-Venegas, P. Calaminici, and A. M. Köster. Robust and efficient auxiliary density perturbation theory calculations. *J. Chem. Theory Comput.* 11:1493, 2015.

[12] B. Zuñiga-Gutierrez and A. M. Köster. Analytical GGA exchange-correlation kernel calculation in auxiliary density functional theory. *Mol. Phys.* 114:1026, 2016.

[13] R. Flores-Moreno, J. Melin, J. V. Ortiz, and G. Merino. Efficient evaluation of analytic Fukui functions. *J. Chem. Phys.* 129:224105, 2008.

[14] E. Schrödinger. Quantisierung als Eigenwertproblem (Erste Mitteilung). *Ann. Physik* 79:361, 1926.

[15] E. Schrödinger. Quantisierung als Eigenwertproblem (Zweite Mitteilung). *Ann. Physik* 79:489, 1926.

[16] E. Schrödinger. Quantisierung als Eigenwertproblem (Dritte Mitteilung). *Ann. Physik* 80:437, 1926.

[17] E. Schrödinger. Quantisierung als Eigenwertproblem (Vierte Mitteilung). *Ann. Physik* 81:109, 1926.

[18] E. Schrödinger. An undulatory theory of the mechanics of atoms and molecules. *Phys. Rev.* 28(6):1049, 1926.

[19] M. Born and R. Oppenheimer. Zur Quantentheorie der Molekeln. *Ann. Physik* 389(20):457, 1927.

[20] S. Epstein. *The variation method in quantum chemistry* volume 33. Elsevier, 2012.

[21] C. Eckart. The theory and calculation of screening constants. *Phys. Rev.* 36(5):878, 1930.

[22] R. K. Nesbet. *Variational principles and methods in theoretical physics and chemistry.* Cambridge University Press, 2004.

[23] D. A. McQuarrie. *Quantum chemistry.* University Science Books, 2008.

[24] M. Born. The statistical interpretation of quantum mechanics. Nobel Lecture, 1954.

[25] J. Itatani, J. Levesque, D. Zeidler, H. Niikura, H. Pépin, J. Kieffer, P. B. Corkum, and D. M. Villeneuve. Tomographic imaging of molecular orbitals. *Nature* 432(7019):867, 2004.

[26] A. Scrinzi, M. Y. Ivanov, R. Kienberger, and D. M. Villeneuve. Attosecond physics. *J. Phys. B: At. Mol. Opt. Phys.* 39(1):R1, 2005.

[27] J. S. Lundeen, B. Sutherland, A. Patel, C. Stewart, and C. Bamber. Direct measurement of the quantum wavefunction. *Nature* 474(7350):188, 2011.

[28] J. C. Slater. A simplification of the Hartree-Fock method. *Phys. Rev.* 81:385, 1951.

[29] J. C. Slater and K. H. Johnson. Self-consistent-field Xα cluster method for polyatomic molecules and solids. *Phys. Rev. B* 5:844, 1972.

[30] L. H. Thomas. The calculation of atomic fields. *Math. Proc. Cambridge Phil. Soc.* 23(5):542, 1927.

[31] E. Fermi. Un metodo statistico per la determinazione di alcune priorieta dell'atome. *Rend. Accad. Naz. Lincei* 6(602):32, 1927.

[32] P. Dirac. Note on exchange phenomena in the Thomas atom. *Math. Proc. Camb. Phil. Soc* 26:376, 1930.

[33] O. Gunnarsson and B. I. Lundqvist. Exchange and correlation in atoms, molecules, and solids by the spin-density-functional formalism. *Phys. Rev. B* 13(10):4274, 1976.

[34] P. W. Ayers and R. G. Parr. Is it impossible to find the universal density functional? Or is it just well-hidden? *Indian Journal of Chemistry* 53:929–931, 2014.

[35] K. Capelle. A bird's-eye view of density-functional theory. *Brazilian Journal of Physics* 36(4A):1318, 2006.

[36] J. C Slater. The theory of complex spectra. *Phys. Rev.* 34(10):1293, 1929.

[37] A. D Becke. Perspective: Fifty years of density-functional theory in chemical physics. *J. Chem. Phys.* 140(18):18A301, 2014.

[38] J. P. Perdew, K. Schmidt, V. Van Doren, C. Van Alsenoy, and P. Geerlings. Jacob's ladder of density functional approximations for the exchange-correlation energy. In *AIP Conference Proceedings* volume 577, page 1, 2001.

[39] J. P. Perdew, A. Ruzsinszky, J. Tao, V. N Staroverov, G. E. Scuseria, and G. I. Csonka. Prescription for the design and selection of density functional approximations: More constraint satisfaction with fewer fits. *J. Chem. Phys.* 123(6):62201, 2005.

[40] S. H. Vosko, L. Wilk, and M. Nusair. Accurate spin-dependent electron liquid correlation energies for local spin density calculations: A critical analysis. *Can. J. Phys.* 58:1200, 1980.

[41] A. D. Becke. Density-functional exchange-energy approximation with correct asymptotic behavior. *Phys. Rev. A* 38(6):3098, 1988.

[42] R. Colle and O. Salvetti. Approximate calculation of the correlation energy for the closed shells. *Theoretical Chemistry Accounts: Theory, Computation, and Modeling (Theoretica Chimica Acta)* 37(4):329, 1975.

[43] R. Colle and O. Salvetti. A general method for approximating the electronic correlation energy in molecules and solids. *J. Chem. Phys.* 79(3):1404, 1983.

[44] C. Lee, W. Yang, and R. G. Parr. Development of the Colle-Salvetti correlation-energy formula into a functional of the electron density. *Phys. Rev. B* 37(2):785, 1988.

[45] J. P. Perdew, K. Burke, and M. Ernzerhof. Generalized gradient approximation made simple. *Phys. Rev. Lett.* 77:3865, 1996.

[46] J. Tao, J. P. Perdew, V. N. Staroverov, and G. E. Scuseria. Climbing the density functional ladder: Nonempirical meta-generalized gradient approximation designed for molecules and solids. *Phys. Rev. Lett.* 91(14):146401, 2003.

[47] J. Sun, A. Ruzsinszky, and J. P. Perdew. Strongly constrained and appropriately normed semilocal density functional. *Phys. Rev. Lett.* 115:036402, 2015.

[48] D. Mejía-Rodríguez, X. Huang, J. Martín del Campo, and A. M. Köster. Chapter four – Hybrid functionals with variationally fitted exact exchange. *Adv. Quantum Chem.* 71:41, 2015.

[49] Z. Ul-Haq and J. D. Madura. *Frontiers in Computational Chemistry: Volume 2: Computer Applications for Drug Design and Biomolecular Systems.* Elsevier, 2015.

[50] A. D. Becke. Density-functional thermochemistry. III. The role of exact exchange. *J. Chem. Phys.* 98:5648, 1993.

[51] T. Yanai, D. P. Tew, and N. C. Handy. A new hybrid exchange-correlation functional using the Coulomb-attenuating method (CAM-B3LYP). *Chem. Phys. Lett.* 393:51, 2004.

[52] R. Baer, E. Livshits, and U. Salzner. Tuned range-separated hybrids in density functional theory. *Annu. Rev. Phys. Chem.* 61:85–109, 2010.

[53] D. Mejía-Rodríguez and A. M. Köster. Robust and efficient variational fitting of Fock exchange. *J. Chem. Phys.* 141:124114, 2014.

[54] M. Ernzerhof. Construction of the adiabatic connection. *Chem. Phys. Lett.* 263:499, 1996.

[55] Y. Zhao, B. J. Lynch, and D. G. Truhlar. Doubly hybrid meta DFT: New multi-coefficient correlation and density functional methods for thermochemistry and thermochemical kinetics. *J. Phys. Chem. A* 108:4786, 2004.

[56] S. Grimme. Semiempirical hybrid density functional with perturbative second-order correlation. *J. Chem. Phys.* 124:034108, 2006.

[57] J. Toulouse, K. Sharkas, E. Brémond, and C. Adamo. Communication: Rationale for a new class of double-hybrid approximations in density-functional theory. *J. Chem. Phys.* 135:101102, 2011.

[58] E. Brémond and C. Adamo. Seeking for parameter-free double-hybrid functionals: The PBE0-DH model. *J. Chem. Phys.* 135(2):024106, 2011.

[59] E. Brémond, J. C. Sancho-García, A. J. Pérez-Jiménez, and C. Adamo. Communication: Double-hybrid functionals from adiabatic-connection: The QIDH model. *J. Chem. Phys.* 141:031101, 2014.

[60] E. Bremond, I. Ciofini, J. C. Sancho-García, and C. Adamo. Nonempirical double-hybrid functionals: An effective tool for chemists. *Acc. Chem. Research* 49:1503, 2016.

[61] C. C. J. Roothaan. Self-consistent field theory for open shells of electronic systems. *Rev. Mod. Phys.* 32(2):179, 1960.

[62] J. A. Pople and R. K. Nesbet. Self-consistent orbitals for radicals. *J. Chem. Phys.* 22(3):571, 1954.

[63] J. S. Binkley, J. A. Pople, and P.A. Dobosh. The calculation of spin-restricted single-determinant wavefunctions. *Mole. Phys.* 28(6):1423, 1974.

[64] S. F. Boys. Electronic wave functions I. A general method of calculation for the stationary states of any molecular system. In *Proc. R. Soc. Lon. A* volume 200, page 542, 1950.

[65] J. Andzelm and E. Wimmer. Density functional Gaussian-type-orbital approach to molecular geometries, vibrations, and reaction energies. *J. Chem. Phys.* 96:1280, 1992.

[66] C. C. J. Roothaan. New developments in molecular orbital theory. *Reviews of Modern Physics* 23:69, 1951.

[67] G. G. Hall. The molecular orbital theory of chemical valency. A method of calculating ionization potentials. *Proceedings of the Royal Society of London Series* 205:541, 1951.

[68] R. E. Stratmann, G. E. Scuseria, and M. J. Frisch. Achieving linear scaling in exchange-correlation density functional quadratures. *Chem. Phys. Lett.* 257:213, 1996.

[69] G. E. Scuseria. Linear scaling density functional calculations with Gaussian orbitals. *J. Phys. Chem. A* 103:4782–4790, 1999.

[70] B. I. Dunlap, J. W. D. Conolly, and J. R. Sabin. On some approximations in applications of Xα theory. *J. Chem. Phys.* 71:3396, 1979.

[71] B. I. Dunlap, J. W. D. Conolly, and J. R. Sabin. On first-row diatomic molecules and local density models. *J. Chem. Phys.* 71:4993, 1979.

[72] J. W. Mintmire and B. I. Dunlap. Fitting the Coulomb potential variationally in linear-combination-of-atomic-orbitals density-functional calculations. *Phys. Rev. A* 25:88, 1982.

[73] J. W. Mintmire, J. R. Sabin, and S. B. Trickey. Local-density-functional methods in two-dimensionally periodic systems. Hydrogen and beryllium monolayers. *Phys. Rev. B* 26(4):1743, 1982.

[74] H. Sambe and R. H. Felton. A new computational approach to Slater's SCF-Xα equation. *J. Chem. Phys.* 62(3):1122, 1975.

[75] M. Feyereisen, G. Fitzgerald, and A. Komornicki. Use of approximate integrals in ab initio theory. An application in MP2 energy calculations. *Chem. Phys. Lett.* 208(5):359, 1993.

[76] O. Vahtras, J. Almlöf, and M. W. Feyereisen. Integral approximations for LCAO-SCF calculations. *Chem. Phys. Lett.* 213(5):514, 1993.

[77] R. Ahlrichs. Efficient evaluation of three-center two-electron integrals over Gaussian functions. *Phys. Chem. Chem. Phys.* 6(22):5119, 2004.

[78] M. J. Frisch, G. W. Trucks, H. B. Schlegel, G. E. Scuseria, M. A. Robb, J. R. Cheeseman, G. Scalmani, V. Barone, G. A. Petersson, H. Nakatsuji, X. Li, M. Caricato, A. Marenich, J. Bloino, B. G. Janesko, R. Gomperts, B. Mennucci, H. P. Hratchian, J. V. Ortiz, A. F. Izmaylov, J. L. Sonnenberg, D. Williams-Young, F. Ding, F. Lipparini, F. Egidi, J. Goings, B. Peng, A. Petrone, T. Henderson, D. Ranasinghe, V. G. Zakrzewski, J. Gao, N. Rega, G. Zheng, W. Liang, M. Hada, M. Ehara, K. Toyota, R. Fukuda, J. Hasegawa, M. Ishida, T. Nakajima, Y. Honda, O. Kitao, H. Nakai, T. Vreven, K. Throssell, J. A. Montgomery, Jr., J. E. Peralta, F. Ogliaro, M. Bearpark, J. J. Heyd, E. Brothers, K. N. Kudin, V. N. Staroverov, T. Keith, R. Kobayashi, J. Normand, K. Raghavachari, A. Rendell, J. C. Burant, S. S. Iyengar, J. Tomasi, M. Cossi, J. M. Millam, M. Klene, C. Adamo, R. Cammi, J. W. Ochterski, R. L. Martin, K. Morokuma, O. Farkas, J. B. Foresman, and D. J. Fox. Gaussian 09 Revision A.02. Gaussian Inc. Wallingford CT 2016.

[79] B. I. Dunlap, N. Rösch, and S. B. Trickey. Variational fitting methods for electronic structure calculations. *Mol. Phys.* 108:3167, 2010.

[80] A. M. Köster, G. Geudtner, P. Calaminici, M. E. Casida, R. Flores-Moreno, G. U. Gamboa, A. Goursot, T. Heine, A. Ipatov, F. Janetzko, J. M. del Campo J. U. Revelez, A. Vela, B. Zuñiga-Gutiérrez, and D. R. Salahub. *deMon2k, version 3.* The deMon Developers: Cinvestav México D. F., 2011.
See: http://www.deMon-software.com.

[81] A. M. Köster. Hermite Gaussian auxiliary functions for the variational fitting of the Coulomb potential in density functional methods. *J. Chem. Phys.* 118:9943, 2003.

[82] A. Álvarez-Ibarra. *Expansión asintótica de integrales moleculares en métodos autoconsistentes de teoría de funcionales de la densidad auxiliar.* PhD thesis, CINVESTAV, 2013.

[83] P. Calaminici, F. Janetzko, A. M. Köster, R. Mejia-Olvera, and B. Zuniga-Gutierrez. Density functional theory optimized basis sets for gradient corrected functionals: $3d$ transition metal systems. *J. Chem. Phys.* 126:044108, 2007.

[84] A. M. Köster. Efficient recursive computation of molecular integrals for density functional methods. *J. Chem. Phys.* 104:4114, 1996.

[85] V. D. Domínguez-Soria, G. Geudtner, J. L. Morales, P. Calaminici, and A. M. Köster. Robust and efficient density fitting. *J. Chem. Phys.* 131:124102, 2009.

[86] R. Fletcher. A new approach to variable metric algorithms. *The Computer Journal* 13(3):317, 1970.

[87] D. F. Shanno. Conditioning of quasi-Newton methods for function minimization. *Mathematics of computation* 24(111):647, 1970.

[88] D. Goldfarb. A family of variable-metric methods derived by variational means. *Mathematics of computation* 24(109):23, 1970.

[89] A. Alvarez-Ibarra and A. M. Köster. Double asymptotic expansion of three-center electronic repulsion integrals. *J. Chem. Phys.* 139:024102, 2013.

[90] A. Alvarez-Ibarra, A. M. Kôster, R. Zhang, and D. R. Salahub. Asymptotic expansion for electrostatic embedding integrals in QM/MM calculations. *J. Chem. Theory Comput.* 8(11):4232, 2012.

[91] E. J. Baerends, D. E. Ellis, and P. Ros. Self-consistent molecular Hartree-Fock-Slater calculations I. The computational procedure. *Chem. Phys.* 2(1):41, 1973.

[92] M. E. Casida, C. Daul, A. Goursot, A. M. Köster, L. G. M. Pettersson, E. Proynov, A. St-Amant, D. R. Salahub, H. Duarte, N. Godbout, J. Guan, C. Jamorski, M. Leboeuf, V. Malkin, O. Malkina, F. Sim, and A. Vela. *deMon-KS, version 3.5.* deMon Software, Montréal, 1996.

[93] S. B. Trickey, J. A. Alford, and J. C. Boetgger. Methods and implementation of robust, high-precision Gaussian Basis DFT calculations for periodic systems: the GTOFF Code. *Computational materials science* 15:171, 2004.

[94] L. Versluis and T. Ziegler. The determination of molecular structures by density functional theory. The evaluation of analytical energy gradients by numerical integration. *J. Chem. Phys.* 88:322, 1988.

[95] S. Gusarov, T. Ziegler, and A. Kovalenko. Self-consistent combination of the three-dimensional RISM theory of molecular solvation with analytical gradients and the Amsterdam density functional package. *J. Phys. Chem. A* 110(18):6083, 2006.

[96] D. N. Laikov. Fast evaluation of density functional exchange-correlation terms using the expansion of the electron density in auxiliary basis sets. *Chem. Phys. Lett.* 281:151, 1997.

[97] A. M. Köster. Entwicklung einer lcgto-dichtefunktionalmethode mit hilfsfunktionen. Habilitation thesis, Universität Hannover, 1998.

[98] J. U. Reveles. *Geometry Optimization in LCGTO-DFT Methods with Auxiliary Functions.* PhD thesis, CINVESTAV, 2004.

[99] A. M. Köster, J. U. Reveles, and J. Martin del Campo. Calculation of exchange-correlation potentials with auxiliary function densities. *J. Chem. Phys.* 121:3417, 2004.

[100] A. M. Köster, R. Flores-Moreno, J. U. Reveles, and J. Martin del Campo. Efficient and reliable numerical integration of exchange-correlation energies and potentials. *J. Chem. Phys.* 121:681, 2004.

[101] U. Birkenheuer, A. B. Gordienko, V. A. Nasluzov, M. K. Fuchs-Rohr, and N. Rösch. Model density approach to the Kohn-Sham problem: Efficient extension of the density fitting technique. *Int. J. Quantum Chem.* 102:743, 2005.

[102] A. M. Köster, J. Martin del Campo, F. Janetzko, and B. Zuniga-Gutierrez. A MinMax self-consistent-field approach for auxiliary density functional theory. *J. Chem. Phys.* 130:114106, 2009.

[103] S. B. Trickey. Private communication to A. M. Köster (unpublished).

[104] B. G. Johnson and D. A. Holder. A Generalized Formulation of Density Functional Theory with Auxiliary Basis Sets. In *The J-Matrix Method* page 311. Springer, 2008.

[105] P. Pulay. Convergence acceleration of iterative sequences. The case of SCF iteration. *Chem. Phys. Lett.* 73(2):393, 1980.

[106] P. Pulay. Improved SCF convergence acceleration. *J. Comp. Chem.* 3(4):556, 1982.

[107] C. L. Lawson, R. J. Hanson, D. R. Kincaid, and F. T. Krogh. Basic linear algebra subprograms for Fortran usage. *ACM Trans. Math. Softw.* 5:308, 1979.

[108] J. J. Dongarra, J. Du Croz, I. S. Duff, S. Hammarling, and R. J. Hanson. An extended set of FORTRAN basic linear algebra subprograms. *ACM Trans. Math. Softw.* 14:1, 1988.

[109] J. J. Dongarra, J. Du Croz, I. S. Duff, S. Hammarling, and R. J. Hanson. An extended set of FORTRAN basic linear algebra subprograms: Model implementation and test programs. *ACM Trans. Math. Softw.* 14:18, 1988.

[110] J. J. Dongarra, J. Du Croz, I. S. Duff, and S. Hammarling. A set of level 3 basic linear algebra subprograms. *ACM Trans. Math. Softw.* 16:1, 1990.

[111] Algorithm 679: A set of level 3 basic linear algebra subprograms: model implementation and test programs. *ACM Trans. Math. Softw.* 16:18, 1990.

[112] E. Anderson, Z. Bai, C. Bischof, S. Blackford, J. Demmel, J. Dongarra, J. Du-Croz, A. Greenbaum, S. Hammarling, A. McKenney, and D. Sorensen. *LAPACK Users' Guide*. Society for Industrial and Applied Mathematics, Philadelphia, PA, third edition, 1999.

[113] A. Dalgarno and A. L. Stewart. On the perturbation theory of small disturbances. In *Proceedings of the Royal Society of London A: Mathematical, Physical and Engineering Sciences* volume 238, page 269, 1956.

[114] P. Pulay. Ab initio calculation of force constants and equilibrium geometries in polyatomic molecules: I. Theory. *Mol. Phys.* 17:197, 1969.

[115] P. Pulay. Direct use of the gradient for investigating molecular energy surfaces. In Schaefer H. F., editor, *Applications of electronic structure theory. Modern Theoretical Chemistry* volume 4, pages 153–185. Springer, 1977.

[116] M. Krack and A. M. Köster. An adaptive numerical integrator for molecular integrals. *J. Chem. Phys.* 108:3226, 1998.

[117] J. Carmona-Espíndola. *Teoría de la Densidad Auxiliar Perturbada Dependiente del Tiempo: Desarrollo, Implementación y Aplicaciones*. PhD thesis, CINVESTAV, 2012.

[118] J. Almlöf and P. R. Taylor. Molecular properties from perturbation theory: A unified treatment of energy derivatives. *International Journal of Quantum Chemistry* 27(6):743, 1985.

[119] A. Komornicki and J. W. McIver. An efficient ab-initio method for computing infrared and Raman intensities: Application to ethylene. *J. Chem. Phys.* 70:2014, 1979.

[120] J. Gerratt and I. M. Mills. Force constants and dipole-moment derivatives of molecules from perturbed Hartree-Fock calculations. I. *J. Chem. Phys.* 49(4):1719, 1968.

[121] J. A. Pople, R. Krishnan, H. B. Schlegel, and J. S. Binkley. Derivative studies in Hartree-Fock and Møller-Plesset theories. *International Journal of Quantum Chemistry* 16(S13):225, 1979.

[122] S. P. Karna and M. Dupuis. Frequency dependent nonlinear optical properties of molecules: Formulation and implementation in the HONDO program. *J. Comp. Chem.* 12(4):487, 1991.

[123] A. M. Lee and S. M. Colwell. The determination of hyperpolarizabilities using density functional theory with nonlocal functionals. *J. Chem. Phys.* 101(11):9704, 1994.

[124] A. M. N. Niklasson and V. Weber. Linear scaling density matrix perturbation theory for basis-set-dependent quantum response calculations: An orthogonal formulation. *J. Chem. Phys.* 127(6):064105, 2007.

[125] M. Kobayashi, T. Touma, and H. Nakai. Dynamic hyperpolarizability calculations of large systems: The linear-scaling divide-and-conquer approach. *J. Chem. Phys.* 136(8):084108, 2012.

[126] T. Kjærgaard, P. Jørgensen, J. Olsen, S. Coriani, and T. Helgaker. Hartree-Fock and Kohn-Sham time-dependent response theory in a second-quantization atomic-orbital formalism suitable for linear scaling. *J. Chem. Phys.* 129(5):054106, 2008.

[127] M. Beer and C. Ochsenfeld. Efficient linear-scaling calculation of response properties: Density matrix-based Laplace-transformed coupled-perturbed self-consistent field theory, 2008.

[128] P. Sałek, S. Høst, L. Thøgersen, P.l Jørgensen, P. Manninen, J. Olsen, B. Jansík, S. Reine, F. Pawłowski, E. Tellgren, et al. Linear-scaling implementation of molecular electronic self-consistent field theory. *J. Chem. Phys.* 126(11):114110, 2007.

[129] C. Ochsenfeld and M. Head-Gordon. A reformulation of the coupled perturbed self-consistent field equations entirely within a local atomic orbital density matrix-based scheme. *Chem. Phys. Lett.* 270(5):399, 1997.

[130] T. Janowski, K. Wolinski, and P. Pulay. Efficient calculation of the density response function from generalized polarizabilities. *Theo. Chem. Acc.* 135(1):6, 2016.

[131] J. Kussmann, A. Luenser, M. Beer, and C. Ochsenfeld. A reduced-scaling density matrix-based method for the computation of the vibrational Hessian matrix at the self-consistent field level. *J. Chem. Phys.* 142:094101, 2015.

[132] S. V. Shedge, S. Pal, and A. M. Köster. Validation and application of auxiliary density perturbation theory and non-iterative approximation to coupled-perturbed Kohn-Sham approach for calculation of dipole-quadrupole polarizability. *Chem. Phys. Lett.* 510:185, 2011.

[133] B. I. Dunlap and I. V. Schweigert. Self-consistent, constrained linear-combination-of-atomic-potentials approach to quantum mechanics. *J. Chem. Phys.* 134(4):044122, 2011.

[134] S. V. Shedge, J. Carmona-Espindola, S. Pal, and A. M. Köster. Comparison of the auxiliary density perturbation theory and the noniterative approximation to the coupled perturbed Kohn-Sham method: Case study of the polarizabilities of disubstituted azoarene molecules. *J. Phys. Chem. A* 114(6):2357, 2010.

[135] K. B. Sophy, S. V. Shedge, and S. Pal. Noniterative density functional response approach: Application to nonlinear optical properties of p-nitroaniline and its methyl-substituted derivatives. *J. Phys. Chem. A* 112(44):11266, 2008.

[136] K. B. Sophy and S. Pal. Density functional response approach for the linear and nonlinear electric properties of molecules. *J. Chem. Phys.* 118(24):10861, 2003.

[137] R. Flores-Moreno and A. M. Köster. Auxiliary density perturbation theory. *J. Chem. Phys.* 128:134105, 2008.

[138] R. Flores Moreno. *Derivadas Analíticas en Métodos LCGTO-DFT Empleando Pseudo-Potenciales y Funciones Auxiliares*. PhD thesis, CINVESTAV, 2006.

[139] R. I. Delgado-Venegas, D. Mejía-Rodríguez, R. Flores-Moreno, P. Calaminici, and A. M. Köster. Analytic second derivatives from auxiliary density perturbation theory. *J. Chem. Phys.* 145(22):224103, 2016.

[140] J. L. Dodds, R. McWeeny, and A. J. Sadlej. Self-consistent perturbation theory: Generalization for perturbation-dependent non-orthogonal basis set. *Mol. Phys.* 34:1779, 1977.

[141] R. McWeeny. *Methods of Molecular Quantum Mechanics*. Academic Press, London, 2 edition, 2001.

[142] G. Diercksen and R. McWeeny. Self-consistent perturbation theory. I. General formulation and some applications. *J. Chem. Phys.* 44(9):3554, 1966.

[143] R. McWeeny and G. Diercksen. Self-consistent perturbation theory II. Extension to open shells. *J. Chem. Phys.* 49(11):4852, 1968.

[144] J. L. Dodds, R. McWeeny, W. T. Raynes, and J. P. Riley. SCF theory for multiple perturbations. *Molecular Physics* 33(3):611, 1977.

[145] P. O. Löwdin. On the non-orthogonality problem connected with the use of atomic wave functions in the theory of molecules and crystals. *J. Chem. Phys.* 18:365, 1950.

[146] A. Szabo and N. S. Ostlund. *Modern Quantum Chemistry: Intro to Advanced Electronic Structure Theory*. Dover publications Inc., Mineola, 1996.

[147] R. McWeeny. Perturbation theory for the Fock-Dirac density matrix. *Phys. Rev.* 126(3):1028, 1962.

[148] A. Neumaier. Solving ill-conditioned and singular linear systems: A tutorial on regularization. *SIAM review* 40:636, 1998.

[149] T. Eirola and O. Nevanlinna. Accelerating with rank-one updates. *Linear Algebra and its Applications* 121:511, 1989.

[150] U. M. Yang and K. A. Gallivan. A new family of preconditioned iterative solvers for nonsymmetric linear systems. *Applied Numerical Mathematics* 19:287, 1995.

[151] D. Mejía-Rodríguez. *Low-Order Scaling Methods for Auxiliary Density Functional Theory*. PhD thesis, CINVESTAV, 2015.

[152] G. Geudtner, F. Janetzko, A. M. Köster, A. Vela, and P. Calaminici. Parallelization of the deMon2k code. *J. Comp. Chem.* 27:483, 2006.

[153] N. Godbout, D. R. Salahub, J. Andzelm, and E. Wimmer. Optimization of Gaussian-type basis sets for local spin density functional calculations. Part I. Boron through neon, optimization technique and validation. *Can. J. Phys.* 70:560, 1992.

[154] See: www.demon-software.com/public_html/support/htmlug. *deMon2k User's Guide.*

[155] P. Calaminici, V. D. Domínguez-Soria, G. Geudtner, E. Hernández-Marín, and A. M. Köster. Parallelization of three-center electron repulsion integrals. *Theo. Chem. Acc.* 115(4):221, 2006.

[156] D. Culler, R. Karp, D. Patterson, A. Sahay, K. E. Schauser, E. Santos, R. Subramonian, and T. Von Eicken. LogP: Towards a realistic model of parallel computation. In *ACM Sigplan Notices* volume 28, page 1, 1993.

[157] Kenneth Levenberg. A method for the solution of certain non-linear problems in least squares. *Quarterly of applied mathematics* 2(2):164, 1944.

[158] D. W. Marquardt. An algorithm for least-squares estimation of nonlinear parameters. *Journal of the society for Industrial and Applied Mathematics* 11:431, 1963.

[159] R. Fletcher. *Practical methods of optimization. Vol. 1, Unconstrained optimization* volume 1. 1980.

[160] J. M. del Campo. *Exploring Chemical Reactivity with Auxiliary Density Functional Theory.* PhD thesis, CINVESTAV, 2008.

[161] J. Nocedal and S. J. Wright. *Numerical optimization.* Springer-Verlag, 1999.

[162] C. G. Broyden. The convergence of a class of double-rank minimization algorithms 1. general considerations. *IMA Journal of Applied Mathematics* 6(1):76, 1970.

[163] J. M. del Campo and A. M. Köster. The importance of step control in optimization methods. *Croatica Chemica Acta* 82(1):283, 2009.

[164] T. H. Fischer and J. Almlöf. General methods for geometry and wave function optimization. *The Journal of Physical Chemistry* 96(24):9768, 1992.

[165] R. Lindh, A. Bernhardsson, G. Karlström, and P. Malmqvist. On the use of a Hessian model function in molecular geometry optimizations. *Chem. Phys. Lett.* 241(4):423, 1995.

[166] J. Baker, A. Kessi, and B. Delley. The generation and use of delocalized internal coordinates in geometry optimization. *J. Chem. Phys.* 105(1):192, 1996.

[167] J. M. Bofill. Updated Hessian matrix and the restricted step method for locating transition structures. *J. Comp. Chem.* 15(1):1, 1994.

[168] P. Culot, G. Dive, V. H. Nguyen, and J. M. Ghuysen. A quasi-Newton algorithm for first-order saddle-point location. *Theo. Chim. Acta* 82:189, 1992.

[169] K. Fukui. The path of chemical reactions-the IRC approach. *Acc. Chem. Res.* 14(12):363, 1981.

[170] A. Ghysels, V. Van Speybroeck, E. Pauwels, S. Catak, B. R. Brooks, D. Van Neck, and M. Waroquier. Comparative study of various normal mode analysis techniques based on partial Hessians. *J. Comp. Chem.* 31(5):994, 2010.

[171] I. N Levine, D. H. Busch, and H. Shull. *Quantum Chemistry* volume 6. Pearson Prentice Hall Upper Saddle River, NJ, 2009.

[172] W. Cheney and D. Kincaid. *Linear algebra: Theory and applications* volume 110. The Australian Mathematical Society, 2009.

[173] K. P. Lawley. *Advances in Chemical Physics, Volume 67: AB INITIO Methods in Quantum Chemistry II* volume 142. John Wiley & Sons, 2009.

[174] J. Neugebauer, M. Reiher, C. Kind, and B. A. Hess. Quantum chemical calculation of vibrational spectra of large molecules-Raman and IR spectra for buckminsterfullerene. *J. Comp. Chem.* 23(9):895, 2002.

[175] E. B. Wilson, J. C. Decius, and P. C. Cross. *Molecular vibrations: The theory of infrared and Raman vibrational spectra*. Courier Corporation, 2012.

[176] H. Hellmann. *Einführung in die Quantenchemie*. Franz Deuticke, Leipzig, 1937.

[177] R. P. Feynman. Forces in molecules. *Phys. Rev.* 56:340, 1939.

[178] S. P. S. Porto. Angular dependence and depolarization ratio of the Raman effect. *J. Opt. Soc. Am.* 56:1585, 1966.

[179] C. D. Allemand. Depolarization ratio measurements in Raman spectrometry. *Applied Spectroscopy* 24:348, 1970.

[180] F. Siebert and P. Hildebrandt. Theory of infrared absorption and Raman spectroscopy. *Vibrational Spectroscopy in Life Science* page 11, 2008.

[181] G. Placzek. Intensität und Polarisation der Ramanschen Streustrahlung mehratomiger Moleküle. *Z. Phys.* 70:84, 1931.

[182] D. P. Strommen. Specific values of the depolarization ratio in Raman spectroscopy: Their origins and significance. *J. Chem. Educ* 69:803, 1992.

[183] D. A. Long. *The Raman effect: a unified treatment of the theory of Raman scattering by molecules*. Wiley, 2002.

[184] S. S. Andrews. Using rotational averaging to calculate the bulk response of isotropic and anisotropic samples from molecular parameters. *J. Chem. Educ* 81(6):877, 2004.

[185] P. W. Fowler and D. E. Manolopoulos. *An atlas of fullerenes.* Courier Corporation, 2006.

[186] H. W. Kroto, J. R. Heath, S. C. O'Brien, R. F. Curl, and R. E. Smalley. C_{60}: Buckminsterfullerene. *Nature* 318(6042):162, 1985.

[187] H. K. H. Lee, A. M. Telford, J. A. Rohr, M. F. Wyatt, B. Rice, J. Wu, A. de Castro Maciel, S. M. Tuladhar, E. Speller, J. McGettrick, J. R. Searle, S. Pont, T. Watson, T. Kirchartz, J. R. Durrant, W. C. Tsoi, J. Nelson, and Z. Li. The role of fullerenes in the environmental stability of polymer: Fullerene solar cells. *Energy & Environmental Science* 11:417, 2018.

[188] L. Echegoyen, N. Chen, S. Fortier, W. Cai, J. Murillo, and M. Gomez. Uranium-based endohedral fullerenes: Mono-, di-metallic and cluster compounds. In *Meeting Abstracts* number 9, page 791. The Electrochemical Society, 2018.

[189] Y. Matsuo, H. Okada, and H. Ueno. Introduction to endohedral fullerenes with the C_{60} cage. In *Endohedral Lithium-containing Fullerenes.* Springer, 2017.

[190] J. Goclon, K. Winkler, and J. T. Margraf. Theoretical investigation of interactions between palladium and fullerene in polymer. *RSC Advances* 7(4):2202, 2017.

[191] F. Calvo, E. Yurtsever, and A. Tekin. Physisorption of H_2 on fullerenes and the solvation of C_{60} by hydrogen clusters at finite temperature: A theoretical assessment. *J. Phys. Chem. A* 122:2792, 2018.

[192] H. W. Kroto and K. McKay. The formation of quasi-icosahedral spiral shell carbon particles. *Nature* 331(6154):328, 1988.

[193] P. Schwerdtfeger, L. Wirz, and J. Avery. Program fullerene: a software package for constructing and analyzing structures of regular fullerenes. *J. Comp. Chem.* 34(17):1508, 2013.

[194] Patrizia Calaminici, Gerald Geudtner, and Andreas M. Köster. First-principle calculations of large fullerenes. *J. Chem. Theory Comput.* 5:29, 2009.

[195] F. Janetzko, A. M. Köster, and D. R. Salahub. Development of the cyclic cluster model formalism for Kohn-Sham auxiliary density functional theory methods. *J. Chem. Phys.* 128:024102, 2008.

[196] P. P. Shanbogh and N. G. Sundaram. Fullerenes revisited. *Resonance* 20:123, 2015.

[197] D. S. Bethune, G. Meijer, W. C. Tang, H. J. Rosen, W. G. Golden, H. Seki, C. A. Brown, and M. S. de Vries. Vibrational Raman and infrared spectra of chromatographically separated C_{60} and C_{70} fullerene clusters. *Chem. Phys. Lett.* 179(1-2):181, 1991.

[198] R. Jin. Atomically precise metal nanoclusters: stable sizes and optical properties. *Nanoscale* 7(5):1549, 2015.

[199] H. Qian, M. Zhu, Z. Wu, and R. Jin. Quantum sized gold nanoclusters with atomic precision. *Acc. Chem. Res.* 45(9):1470, 2012.

[200] P. Maity, S. Xie, M. Yamauchi, and T. Tsukuda. Stabilized gold clusters: From isolation toward controlled synthesis. *Nanoscale* 4(14):4027, 2012.

[201] D. Jiang. The expanding universe of thiolated gold nanoclusters and beyond. *Nanoscale* 5(16):7149, 2013.

[202] S. Knoppe and T. Verbiest. Resonance enhancement of nonlinear optical scattering in monolayer-protected gold clusters. *J. Am. Chem. Soc.* 139(42):14853, 2017.

[203] K. G. Stamplecoskie, G. Yousefalizadeh, L. Gozdzialski, and H. Ramsay. Photovoltaics as an experimental tool for determining frontier orbital energies and photocatalytic activity of thiol protected gold clusters. *J. Phys. Chem. C,* Just Accepted 2018.

[204] R. Itteboina, U. D. Madhuri, P. Ghosal, M. Kannan, T. K. Sau, T. Tsukuda, and S. Bhardwaj. Efficient one-pot synthesis and pH-dependent tuning of photoluminescence and stability of $Au_{18}(SC_2H_4CO_2H)_{14}$ cluster. *J. Phys. Chem. A* 122(5):1228, 2018.

[205] X. Hu, Y. Zheng, J. Zhou, D. Fang, H. Jiang, and X. Wang. Silver-assisted thiolate ligand exchange induced photoluminescent boost of gold nanoclusters for selective imaging of intracellular glutathione. *Chem. Mater.* 30(6):1947, 2018.

[206] M. Zhu, E. Lanni, N. Garg, M. E. Bier, and R. Jin. Kinetically controlled, high-yield synthesis of Au_{25} clusters. *J. Am. Chem. Soc.* 130(4):1138, 2008.

[207] Z. Wu, J. Suhan, and R. Jin. One-pot synthesis of atomically monodisperse, thiol-functionalized Au_{25} nanoclusters. *J. Mater. Chem.* 19(5):622, 2009.

[208] H. Qian and R. Jin. Controlling nanoparticles with atomic precision: the case of $Au_{144}(SCH_2CH_2Ph)_{60}$. *Nano Lett.* 9(12):4083, 2009.

[209] B. Kumar, Y. Niihori, W. Kurashige, and Y. Negishi. Controlled thiolate-protected gold and alloy clusters. In *Descriptive Inorganic Chemistry Researches of Metal Compounds*. InTech, 2017.

[210] A. C. Templeton, W. P. Wuelfing, and R. W. Murray. Monolayer-protected cluster molecules. *Acc. Chem. Res.* 33(1):27, 2000.

[211] M. C. Daniel and D. Astruc. Gold nanoparticles: assembly, supramolecular chemistry, quantum-size-related properties, and applications toward biology, catalysis, and nanotechnology. *Chem. Rev.* 104(1):293, 2004.

[212] Y. Negishi, K. Nobusada, and T. Tsukuda. Glutathione-protected gold clusters revisited: Bridging the gap between gold (I)-thiolate complexes and thiolate-protected gold nanocrystals. *J. Am. Chem. Soc.* 127(14):5261–5270, 2005.

[213] N. A. Sakthivel, M. Stener, L. Sementa, A. Fortunelli, G. Ramakrishna, and A. Dass. $Au_{279}(SR)_{84}$: The smallest gold thiolate nanocrystal that is metallic and the birth of plasmon. *J. Phys. Chem. Lett.* 9:1295, 2018.

[214] P. M. W. Gill, B. G. Johnson, and J. A. Pople. A standard grid for density functional calculations. *Chem. Phys. Lett.* 209:506, 1993.

[215] D. Figgen, K. A. Peterson, M. Dolg, and H. Stoll. Energy-consistent pseudopotentials and correlation consistent basis sets for the 5*d* elements Hf-Pt. *J. Chem. Phys.* 130(16):164108, 2009.

[216] G. A. Bishea and M. D. Morse. Spectroscopic studies of jet-cooled AgAu and Au_2. *J. Chem. Phys.* 95(8):5646–5659, 1991.

[217] H. Shinohara. Endohedral metallofullerenes. *Reports on Progress in Physics* 63(6):843, 2000.

[218] A. A. Popov, S. Yang, and Lo. Dunsch. Endohedral fullerenes. *Chem. Rev* 113(8):5989, 2013.

[219] X. Lu, L. Echegoyen, A. L Balch, S. Nagase, and T. Akasaka. *Endohedral Metallofullerenes: Basics and Applications.* CRC Press, 2014.

[220] A. A. Popov, M. Krause, S. Yang, J. Wong, and L. Dunsch. C_{78} cage isomerism defined by trimetallic nitride cluster size: a computational and vibrational spectroscopic study. *J. Phys. Chem. B* 111(13):3363, 2007.

[221] S. Yang, A. A. Popov, and L. Dunsch. Violating the isolated pentagon rule (IPR): The endohedral non-IPR C_{70} cage of $Sc_3N@C_{70}$. *Angewandte Chemie Int. Ed.* 46(8):1256, 2007.

[222] J. Zhang, M. Ge, X. Miao, S. Li, C. Hao, and X. Jia. The computational vibrational and ultraviolet spectra study of endohedral dimetallofullerene $La_2@$ C_{80}. *J. Comput. Theor. Nanosci.* 6(2):459, 2009.

[223] S. E. Pérez-Figueroa. *Structures and stabilities of endohedral fullerenes containing lanthanides and actinides. In preparation.* PhD thesis, CINVESTAV, 2018.

[224] S. E. Pérez-Figueroa. Private communication.

[225] W. Küchle, M. Dolg, H. Stoll, and H. Preuss. Energy-adjusted pseudopotentials for the actinides. Parameter sets and test calculations for thorium and thorium monoxide. *J. Chem. Phys.* 100:7535, 1994.

[226] X. Cao, M. Dolg, and H. Stoll. Valence basis sets for relativistic energy-consistent small-core actinide pseudopotentials. *J. Chem. Phys.* 118:487, 2003.

[227] X. Cao and M. Dolg. Segmented contraction scheme for small-core actinide pseudopotential basis sets. *J. Mol. Struct. (Theochem)* 673:203, 2004.

[228] X. Zhang, Y. Wang, R. Morales-Martínez, J. Zhong, C. de Graaf, A. Rodríguez-Fortea, J. M. Poblet, L. Echegoyen, L. Feng, and N. Chen. U_2@Ih(7)-C_{80}: Crystallographic characterization of a long-sought dimetallic actinide endohedral fullerene. *J. Am. Chem. Soc.* 140(11):3907, 2018.

[229] R. Flores-Moreno, R. J. Alvarez-Mendez, A. Vela, and A. M. Köster. Half-numerical evaluation of pseudopotential integrals. *J. Comp. Chem.* 27(9):1009, 2006.

[230] J. M. Bowman. Self-consistent field energies and wavefunctions for coupled oscillators. *J. Chem. Phys.* 68:608, 1978.

[231] G. D. Carney, L. L. Sprandel, and C. W. Kern. Variational approaches to vibration-rotation spectroscopy for polyatomic molecules. *Advances in Chemical Physics* 37:305, 2007.

[232] M. Cohen, S. Greita, and R. P. McEarchran. Approximate and exact quantum mechanical energies and eigenfunctions for a system of coupled oscillators. *Chem. Phys. Lett.* 60(3):445, 1979.

[233] R. B. Gerber and M. A. Ratner. A semiclassical self-consistent field (SC-SCF) approximation for eigenvalues of coupled-vibration systems. *Chem. Phys. Lett.* 68:195, 1979.

[234] G. M. Chaban, J. O. Jung, and R. B. Gerber. Ab initio calculation of anharmonic vibrational states of polyatomic systems: Electronic structure combined with vibrational self-consistent field. *J. Chem. Phys.* 111(5):1823, 1999.

[235] P. Seidler, T. Kaga, K. Yagi, O. Christiansen, and K. Hirao. On the coupling strength in potential energy surfaces for vibrational calculations. *Chem. Phys. Lett.* 483:138, 2009.

[236] Y. Lin, A. T. B. Gilbert, and P. M. W. Gill. Calculating molecular vibrational spectra beyond the harmonic approximation. *Theor. Chem. Acc.* 120:23, 2008.

[237] L. S. Norris, M. A. Ratner, A. E. Roitberg, and R. B. Gerber. Møller-plesset perturbation theory applied to vibrational problems. *J. Chem. Phys.* 105(24):11261, 1996.

[238] C. Stein. *Highly Accurate Spectroscopic Parameters from Ab Initio Calculations: The Interstellar Molecules I-C_3H^+ and C_4*. Springer, 2016.

[239] A. G. Császár. Anharmonic molecular force fields. *Enc. Comp. Chem.* 1998.

[240] P. Åstrand, K. Ruud, and P. R. Taylor. Calculation of the vibrational wave function of polyatomic molecules. *J. Chem. Phys.* 112(6):2655, 2000.

[241] A. D. Boese, W. Klopper, and J. M. L. Martin. Anharmonic force fields and thermodynamic functions using density functional theory. *Mol. Phys.* 103(6):863, 2005.

[242] F. W. J. Olver. *NIST Handbook of Mathematical Functions Hardback and CD-ROM*. Cambridge University Press, 2010.

[243] G. Groenhof. Introduction to QM/MM simulations. In *Bio. Sim.* page 43. Springer, 2013.

[244] D. R. Salahub, S. Y. Noskov, B. Lev, R. Zhang, V. Ngo, A. Goursot, P. Calaminici, A. M. Köster, A. Alvarez-Ibarra, D. Mejía-Rodríguez, and et al. QM/MM calculations with deMon2k. *Molecules* 20(3):4780, 2015.

[245] Q. Cui and M. Karplus. Molecular properties from combined QM/MM methods I. Analytical second derivative and vibrational calculations. *J. Chem. Phys.* 112(3):1133, 2000.

[246] Q. Cui and M. Karplus. Molecular properties from combined QM/MM methods II. Chemical shifts in large molecules. *J. Phys. Chem. B* 104(15):3721, 2000.

[247] R.G. Parr and W. Yang. *Density-Functional Theory of Atoms and Molecules*. Oxford University Press, New York, NY, 1989.